8-1-2002

Implementation of a Digital Signal Processor (DSP) Based Space Vector Control of AC Induction Motor Drives

Koby Asirvatham

IMPLEMENTATION OF A DIGITAL SIGNAL PROCESSOR (DSP) BASED
SPACE VECTOR CONTROL OF AC INDUCTION MOTOR DRIVES

by

Koby Asirvatham
Bachelor of Science, University of Idaho, 1995

A Thesis

Submitted to the Graduate Faculty

of the

University of North Dakota

in partial fulfillment of the requirements

for the degree of

Master of Science

Grand Forks, North Dakota
August 2002

This thesis, submitted by Koby Asirvatham in partial fulfillment for the Degree of Master of Science from the University of North Dakota, has been read by the Faculty Advisory Committee under whom the work has been done and is hereby approved.

_____
(Chairperson)

_____

_____

_____

This thesis meets the standards for appearance, conforms to the style and format requirements of the Graduate School of the University of North Dakota, and is hereby approved.

_____
Dean of the Graduate School

_____
June 3, 2002
Date

ii

PERMISSION

Title   Implementation of a Digital Signal Processor (DSP) Based Space Vector Control of AC Induction Motor Drives

Department Electrical Engineering

Degree   Master of Science

In presenting this thesis in partial fulfillment of the requirements for a graduate degree from the University of North Dakota, I agree that the library of this University shall make it freely available for inspection. I further agree that permission for extensive copying for scholarly purposes may be granted by the professor who supervised my thesis work or, in his absence, by the chairperson of the department or the Dean of the Graduate School. It is understood that any copying or publication or other use of this thesis or part thereof for financial gain shall not be allowed without my written permission. It is also understood that due recognition shall be given myself and the University of North Dakota in any scholarly use which may be made of any material in my thesis.

Signature   _Kelly_

Date   _05/29/02_

iii

TABLE OF CONTENTS

LIST OF ILLUSTRATIONS

LIST OF TABLES

ACKOWLEDGEMENTS

First of all, I am grateful to my thesis advisor, Dr. Hossein Salehfar for his guidance, support and stimulating suggestions. His purchasing of the state-of-the-art power electronics hardware and software improved my research skills and prepared me for future challenges. I am thankful to my committee members, Dr Arthur R. Miles and Dr. Mohammad Khavanin for their helpful comments and suggestions, and their willingness to be my committee members.

I am also indebted to Professor Arnold Johnson for giving me an opportunity to study at UND. Many thanks to my close friends, classmates, and professors, who have made learning more fun than ever. Last but not least, I am forever indebted to my parents who have encouraged and inspired me all along in my academic endeavors.

ABSTRACT

The inverters transfer energy from a DC source to a controlled process in the form of pulse trains, using semiconductor switches which are turned on and off at fast repetition rates. This thesis explains in depth how these pulse trains synthesize sine waves. AC waveform generation techniques such as the square wave and Pulse Width Modulation (PWM) are compared in terms of their harmonic elimination capability and fundamental gain control. Various PWM techniques such as bipolar switching, unipolar switching, selective harmonic elimination switching and Space Vector PWM (SVPWM) switching are analyzed and compared in terms of their ability to control harmonic distortion (THD), minimize switching losses, control fundamental gain and maximize DC bus utilization capacity. The selective harmonic elimination technique is covered in depth including a technique that utilizes a neural network controller to remove a selected set of harmonics. This thesis focuses on Space Vector PWM (SVPWM) technique since it has many advantages over other conventional methods such as sine wave PWM. Thus, the SVPWM theory and experimental analysis is presented in depth. The SVPWM technique was realized using the state-of-the-art power electronics hardware and Digital Signal Processing (DSP) software. The experimental procedure and harmonics analysis of the DSP based SVPWM output waveforms and inverter output voltages and currents are presented. The experiments were carried out using power electronics development modules

such as the Texas Instrument's TMS320LF2407 DSK (eZdsp), Digital Motor Controller (DMC1500), and the VisSim™/TI C2000 Rapid Prototyper software package and a three-phase AC induction motor. The VisSim™/TI C2000 Rapid Prototyper was extensively used to model an AC induction motor control sub-system that generates real time SVPWM waveforms to control a three-phase induction motor. The AC induction motor control sub-system was implemented using the principle of constant Volts/Hertz (V/Hz) profile. Several measurements and observations of the phase-voltages, line-voltages and phase currents were made to observe the quality of the power produced using the SVPWM technique. The SVPWM waveforms were simulated using MATLAB™ software and the VisSim™/TI C2000 Rapid Prototyper software. These simulated SVPWM waveforms were compared with the DSP generated SVPWM waveforms and the inverter output. The completed project will give the user the ability to use the VisSim™/TI C2000 Rapid Prototyper software to generate SVPWM waveform and power the DSP controller (eZdsp), interface the DMC1500 (inverter) with the eZdsp and control a three-phase induction motor. An extension of the conventional three-phase SVPWM to higher order phase systems is reviewed. An overview of the principle of sensorless variable speed three-phase AC motor drives with closed-loop speed control is included.

CHAPTER 1

INTRODUCTION

In electrical engineering, an inverter is a device for converting Direct Current (DC) electricity into Alternating Current (AC) electricity. The quality of the AC current, voltage, and frequency that the inverter produces determines the types of appliances and equipment it can operate. The three basic types of inverter waveforms are sine wave, quasi sine wave and square-wave (which looks the least like a sine-wave) [79]. These waveforms are shown in Figure 1.1 [81]. Quasi sine wave inverters can operate most devices except
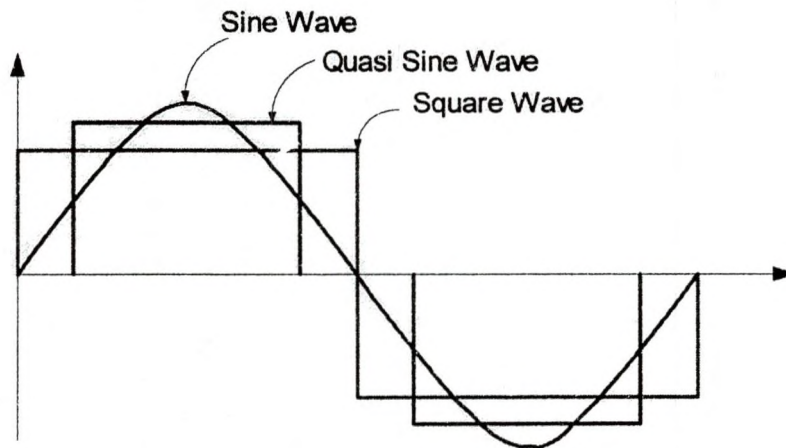
Figure 1.1: Three Basic Types of Inverter Waveforms

those most sensitive to harmonics, such as laser printers, computers and waveform sensitive audio equipment. Square-wave inverters, whose waveform is rich in harmonics, are mostly suitable for heat devices.

Harmonics are more of a concern now than ever before, because of the ever-increasing use of non-linear loads. These loads draw current in a non-sinusoidal fashion creating harmonics. High frequency currents travel on the outer edge of the conductors (skin effect) creating heat. The generated heat can cause conductors to heat up and motors and transformers to fail. The heat sometimes causes circuit breakers to trip. The cables carrying harmonic current also behave like an antenna, propagating spurious emission that can broadcast over a distance. These emissions can induce voltages, currents or crosstalk on adjacent cables, which is potentially dangerous to equipment and personnel [65]. The risk of automated processes breaking down is very likely. Because of these negative effects, harmonics are a nuisance to the user and the designer as well, so they should be kept to a minimum.

1.1 Square Wave Inverter

A square waveform is composed of a fundamental component plus an infinite number of odd harmonic multiples. These harmonic multiples are high in amplitude and are close to the fundamental component. They are always present at the output of the inverter and would create EMI (Electromagnetic Interference) problems to other systems and contribute to the distortion of the inverter output voltage. Some of the undesirable effects harmonic currents have in the distribution system are heating of magnetic devices, parasitic ground currents, higher energy costs, failure of power factor correction capacitors, high frequency fields that can introduce interference into telephone lines and corrupt data in adjacent data lines, stray magnetic fields, and also the triplen harmonics

that produce higher than expected neutral current [91]. The presence of the third and fifth harmonics alone can contribute more than thirty percent to the THD (Total Harmonic Distortion). What makes it worse is the existence of the third and fifth harmonics in the vicinity of the fundamental component (f_1). Therefore for the square wave voltage waveform to be of practical use, it has to go through an elaborate multistage filtering to produce a pure sinusoidal output voltage [2]. The filtering tasks required of these filters are complicated, expensive and contribute to the overall size and cost of the inverter.

Chapter two presents an analysis of the square wave inverter. Before the availability of power switching devices, the first-generation inverters generated sine waves by first generating square waves followed by a massive multi-stage low-pass filtering (harmonic traps) to recover the fundamental frequency component [2]. A harmonic trap is a tuned low-pass filter that gives near infinite attenuation at a designed trap frequency [85]. In a quasi sine wave inverter the third harmonic is absent, however the fifth and subsequent harmonics still require laborious filtering as in the square wave case.

1.2 Pulse Width Modulation (PWM)

Researchers have long been looking for cost effective ways to control harmonics. In recent years, advancements in power semiconductors and microprocessor technologies and the use of Digital Signal Processors (DSP) in motor control have revolutionized dramatically the technique of harmonic control. The availability of the high speed switching devices such as MOSFETs, IGBTs and SCRs has made high switching frequency PWM and selective switching

harmonic elimination PWM possible. For example, in a typical PWM waveform shown in Figure 1.2, switching at angles, $\alpha = 23.62°$ and $\beta = 33.3°$ generates a pulse train in which the third and fifth harmonics (the most difficult to filter due to their high content, and their nearness to the fundamental frequency) can be eliminated [2]. The elimination of the third and fifth harmonics causes the
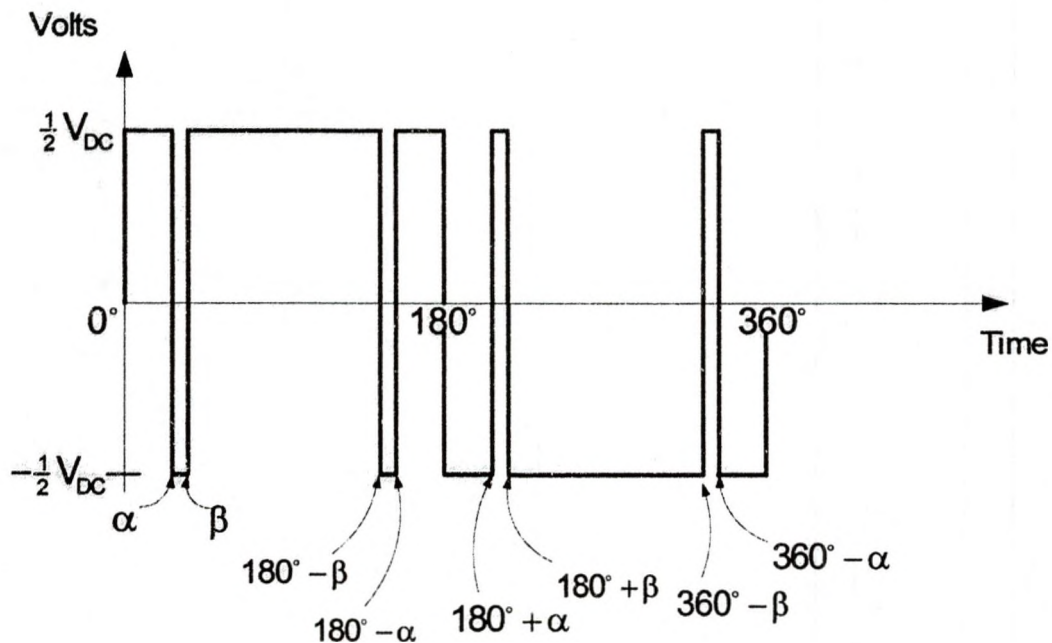
Figure 1.2: A Typical PWM Waveform

amplitude of subsequent higher order harmonics such as seventh and ninth to increase. However, these harmonics are far above the fundamental component so they can easily be filtered out with a low pass filter. Increasing the number of switching angles, α and β increases the number of pulses per cycle, resulting in more harmonics being eliminated. However, increasing the number of switching angles contributes to higher switching losses and attenuation in the fundamental component amplitude. Switching power converters offer the flexibility to regulate both the frequency and the magnitude of the fundamental voltage and current

applied to a motor. Consequently improved efficiency and performance are achieved by these motor drives with less generated noises. The switching technologies have moved the harmonics to the high side of the frequency spectra where the higher order harmonics are easily filtered out with a single, high bandwidth low pass filter. This means that fewer components, such as capacitors and inductors are needed to implement this filter which contributes to lower cost and the size of the inverter.

There is another relatively new PWM technique called the Space Vector PWM (SVPWM) method which has become very popular in three-phase motor applications [23]. This method of generating three-phase sine waves is based on a rotating space vector in the complex plane. The rotating vector at each position in the complex plane is approximated by a sequential application of time-based space vectors, which generate the necessary PWM pulses to turn on and turn off the power transistors.

The power that the inverter uses to drive a motor is controlled by the Pulse Width Modulated (PWM) signals applied to the gates of power transistors. The PWM signals are a series of pulses with constant frequency but of variable duty ratio. In every PWM period there is a single pulse of constant amplitude but the pulse's width varies from period to period according to the modulating signal. Applying these pulses to the power transistor gate will cause the turn on and turn off durations of the power transistor to vary in each switching period.

In Chapter 2 the advantages and disadvantages of square wave switching technique are analyzed. Chapter 3 presents analysis of the principle of sine

wave PWM switching technique, which includes selective harmonic elimination technique and the implementation of the selective harmonic elimination technique using a neural network controller. Chapter 4 presents the famous space vector pulse width modulation (SVPWM) theory in detail, and Chapter 5 and 6 present a complete experimental setup and analysis of an AC induction motor control sub-system using the SVPWM method. In chapters 5 and 6, the VisSim^{TM}/TI C2000 Rapid Prototyper is used to model an AC Induction Motor Control sub-system. The DSP controller (TMS320LF2407 DSK), Digital Motor Controller (DMC1500) and VisSim^{TM}/TI C2000 rapid prototyper software is put together to run a three-phase AC induction motor. Several measurements and observations of phase voltages, phase currents, line voltages and the associated harmonics are made at the DSP output and the motor input. These experimental waveforms are compared with theoretical (VisSim^{TM} & MATLAB^{TM}) and real time (DSP) waveforms.

CHAPTER 2

SQUARE WAVE INVERTERS

Modulation is the process of turning transistors on and off rapidly so as to produce the net effect of an average voltage [86]. For example, if an inverter with a bus voltage of V_{DC} is on 50% of the time, then the results would be a square wave with an average output voltage of zero. Modulation allows a power transistor to control much more power than a linear (unmodulated) power stage. This is why almost all industrial servo controllers use modulated power stages [86]. The weakness of modulation is the creation of electrical noise caused by rapid voltage transitions during switching. This chapter looks at the square wave voltage source inverter and its noisy waveform apart from the switching noise. The output of the square waveform is analyzed to see what its advantages and disadvantages are.

2.1 Square Wave Output

A simple voltage source inverter circuit is shown in Figure 2.1. The switches S_1 and S_2 represent the power transistor switches that connect the bus voltage to the inverter output. This design essentially consists of switches S_1 and S_2, that switch on and off alternately. When S_1 opens then S_2 closes and the corresponding inverter output is, $V_{a0} = -\frac{1}{2}V_{DC}$. When S_1 closes then S_2 opens and the corresponding inverter output is, $V_{a0} = +\frac{1}{2}V_{DC}$. Alternately closing S_1 and
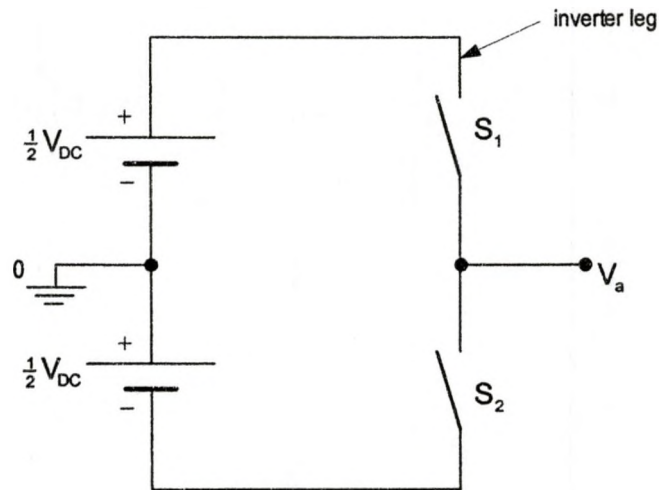
Figure 2.1: One-leg Inverter Single-phase Switching Circuit

S_2 fifty percent of the time creates a square waveform. The resulting square voltage waveform and its corresponding frequency spectra are shown in Figures 2.2 and 2.3, respectively. When both switches are closed, $V_{a0} = 0$. This situation (i.e., both switches closed) is called "short through". Therefore only one switch should be closed at any time to get an output.
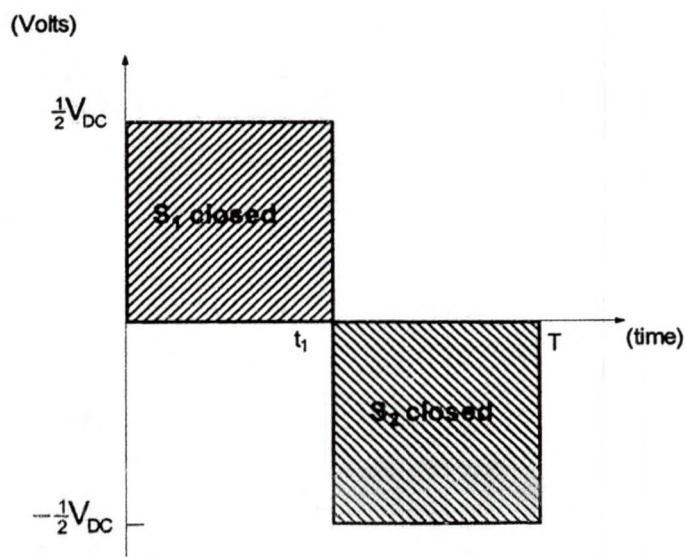
Figure 2.2: Square Wave
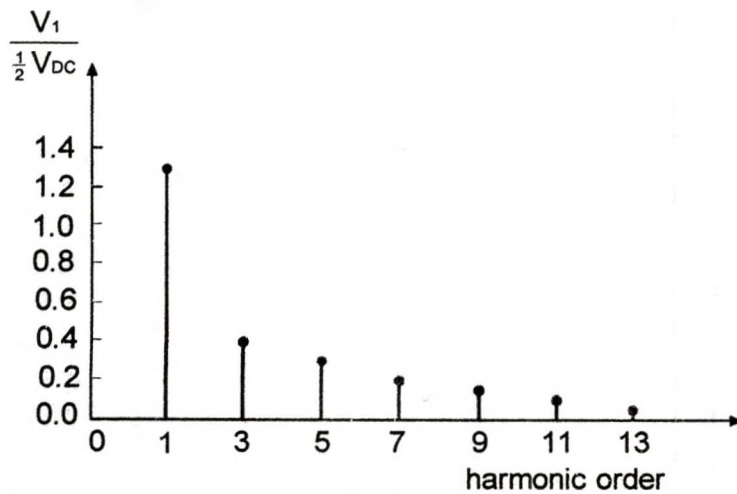
Figure 2.3. Square Wave Harmonic Spectra

It was mentioned earlier that a square wave is a waveform that is composed of a fundamental frequency component plus an infinite number of odd harmonics multiples. From a Fourier series analysis the total output voltage of the square wave can be expressed as [87]:

$$V_0(\omega_0 t) = \frac{4}{\pi}\left(\frac{V_{DC}}{2}\right)\left[\sin(\omega_0 t) + \frac{1}{3}\sin(3\omega_0 t) + \frac{1}{5}\sin(5\omega_0 t) + ...\right] \qquad (2.1)$$

where the maximum amplitude of the fundamental frequency voltage is [9]:

$$V_1 = \frac{4}{\pi}\left(\frac{V_{DC}}{2}\right) = 1.273\left(\frac{V_{DC}}{2}\right) \qquad (2.2)$$

As can be seen from equation (2.2), the square wave inverter has a very high level of fundamental frequency component amplitude. However, the square wave's high fundamental frequency component amplitude can be seriously distorted by the presence of high content odd harmonic multiples, especially the third and fifth harmonic components. The large magnitudes of the third and fifth harmonic components, coupled with their closeness to the fundamental

frequency component, make it difficult to implement a low pass filter. The duty ratio of the square wave is fixed so the average output voltage of the square wave generator is only controllable by adjusting the DC bus voltage level. The advantage is that the square wave switching inverter circuit is simple. Only two switchings per period are required to generate the square waveform. This is a big saving of switching losses for very high power applications.

The objective of an inverter is to accept a DC source input and generate an AC fundamental frequency output, making efficient use of the available DC power and create the least harmonics possible. The quality of the AC output voltage or current can be described by the Total Harmonic Distortion (THD). The THD gives the quality of all the non-fundamental frequency components present at the output. Assuming no DC component is present at the output voltage, the THD for the first three terms in equation (2.1) is.

$$ \text{THD} = \frac{\sqrt{\sum_{n=2}^{\infty} V_{n,RMS}^2}}{V_{1,RMS}} = \frac{\sqrt{\left(\frac{1}{3}\right)^2 + \left(\frac{1}{5}\right)^2 + \left(\frac{1}{7}\right)^2 + \ldots}}{1} = 0.41 \Rightarrow 41\% \qquad (2.3) $$

In the simplest approach, switching the inverter circuit on and off for an equal interval results in a square waveform. This type of inverter has a high harmonic distortion (50%) and a low efficiency (60% to 80%). A square wave inverter often cannot properly power the electronic equipment and motors tend to run hotter [54]. AC induction motors draw a substantial current surge on startup. They really prefer sine-waves to square-waves and may overheat on the latter [55].

Square Wave inverters are satisfactorily used for loads which are either resistive elements or incandescent lighting but they can be a source of

overheating and inefficiencies when used to energize transformers and electric motors. The harmonic-rich square wave may cause interference or over heating of electrical appliances. For example, induction motors are said to be very noisy on a square wave powered inverter. Some induction motors may not work at all and some seldom develop their full power [53]. It was mentioned the square waveform has a high harmonic distortion. However, if switches are turned on and off several times in a cycle with variable duty ratios, an improved harmonic profile may be achieved [25]. This technique is called Pulse Width Modulation (PWM). The next section describes how this is done.

CHAPTER 3

SINE WAVE PULSE WIDTH MODULATION (PWM) SWITCHING

PWM voltage source inverters control the output voltage by varying the on-times of the switches controlling the widths of the pulses in the modulating time period [56]. By varying the times the pulses are on and transistors are conducting, the switching frequency can be increased or decreased. Also, by changing the width of the pulses, the average voltage to the motor can also be increased or decreased [92]. The basics of PWM techniques are described here. The harmonic elimination technique is analyzed and the application of a neural network controller in the harmonic elimination technique is reviewed. In general Pulse Width Modulation (PWM) refers to a method of carrying information on a train of pulses; the information being encoded is the width of the pulses. Both the output fundamental voltage and frequency are controlled in the inverter by Pulse Width Modulation[60]. The sine wave PWM process is a technique of AC (fundamental frequency) waveform generation from a DC supply source by comparing a modulating signal (the desired sine wave) with a high frequency triangular waveform (the carrier wave whose frequency is the switching frequency of the inverter). Unlike in the square waveform generation process where the pulses' widths are fixed, the PWM waveform pulse widths are continuously changed to produce a desired output. The resulting PWM waveform is a high frequency pulse train of constant amplitude and frequency

12

(period), but with a variable pulse width as a function of time. The width of the

pulse is controlled by the modulating (desired sine wave) signal's amplitude. The

sine wave can be generated by varying the width of the pulses. The frequency at

which the
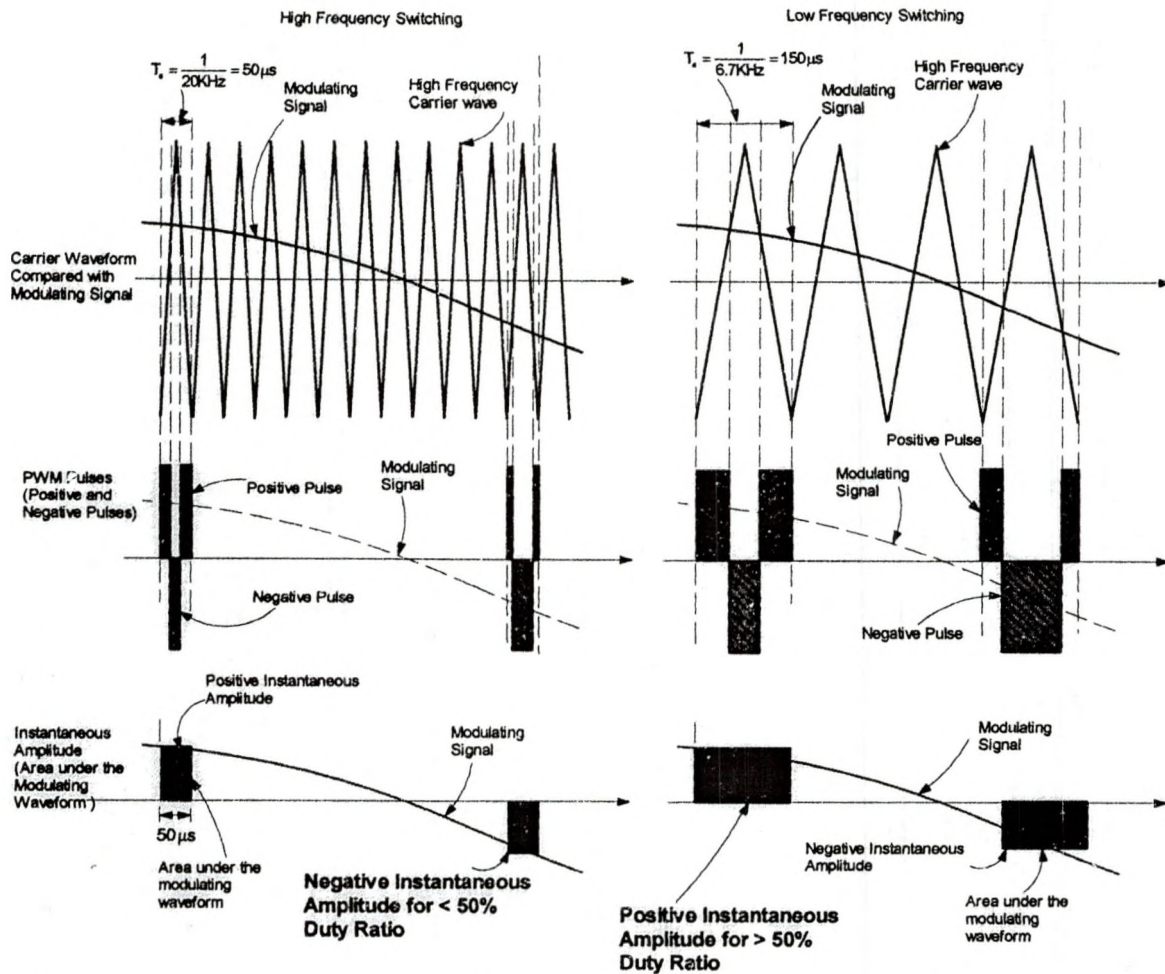
Figure 3.1: Pulse Average Value = "Instantaneous Amplitude"

transistors are turned on and off is called switching frequency. The higher the

switching frequency the better the reproduction of the desired sine wave [61].

Changing the pulse width allows the average voltage output for the duration

of the pulse to be varied linearly from 0 Volts (pulse width equivalent to 50% duty

ratio), to either positive (pulse width equivalent to more than 50% duty ratio) or

negative (pulse width equivalent to less than 50% duty ratio) [59]. This is
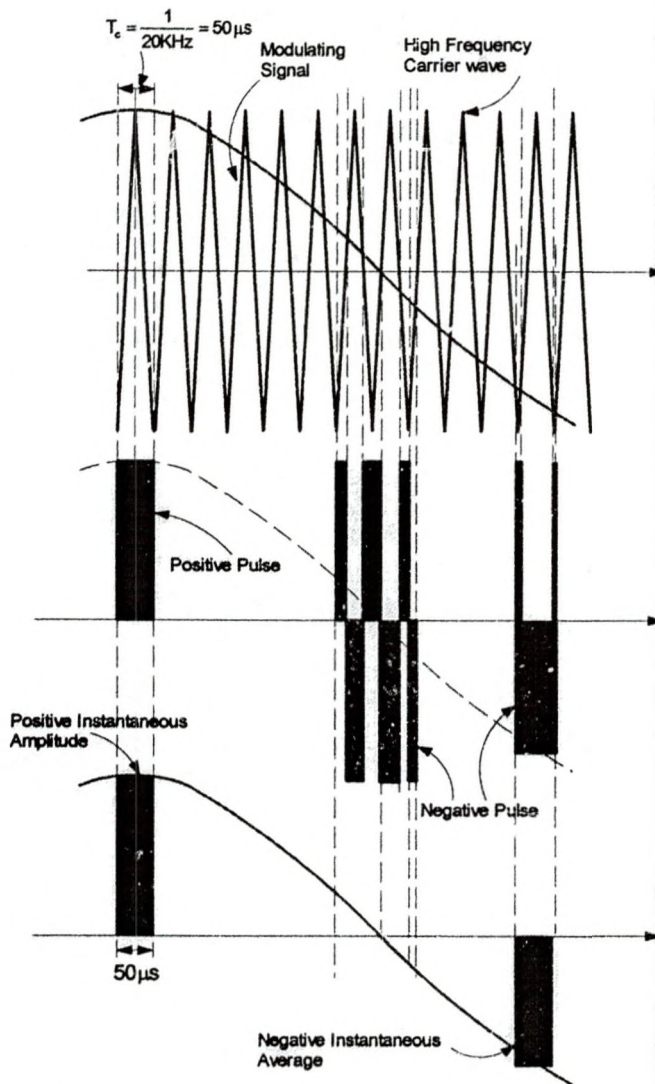
Figure 3.2: Pulse Average Value Equals "Instantaneous Amplitude"
For a Maximum Modulation Index

illustrated in Figures 3.1. Figure 3.2 shows the "instantaneous amplitude"

for a maximum modulation Index.

Figures 3.1 and 3.2 show a few random switching periods for two modulating

waveforms of different amplitude. Every switching period generates negative

and positive pulses of constant amplitude whose average values are equal to the average area under the sine wave. The pulse's width is modulated by the modulating waveform's amplitude. For a switching frequency (f_s) of 20KHz the switching period (T_s) is 50 µsec. Usually T_s is so small compared to the modulating waveform's period (T_{PWM}) that the average area under the sine wave curve can be considered as "instantaneous amplitude". Therefore the average area under the sine wave is its amplitude at every T_s. By integrating the "instantaneous amplitudes" using a low pass filter the replica of the modulating waveform (desired sine wave) is recovered. In reference [9] the "instantaneous amplitude" is termed "instantaneous average"

Thus, the switching pulses create a waveform that contains a replica of the modulating (desired) waveform in its low frequency components, with the higher frequency components being at frequencies close to the carrier (switching) frequency [25]. High frequency harmonics are generated by the fast transitions in the waveform, and low frequency harmonics are generated by slower changes to the fundamental sine wave [64]. The PWM process does not change the RMS value of the AC voltage waveform. It is still equal to the DC bus voltage, hence the total harmonic distortion is not affected by the PWM process. The harmonic components are merely shifted to the higher frequency range and are automatically filtered due to inductances in the AC system [25]. The filtering action recovers the fundamental frequency waveform by integrating the area under the curve. PWM switching is a special high frequency switching technique that eliminates the dominant lower order harmonics of the square waveform

shown in Figure 2.3, and converts them to higher order harmonics and allows control over the inverter average output voltage from within a controller.

3.1 Sine Wave PWM Technique

Figure 3.3 shows a comparator circuit used for generating a PWM pulse train [69]. Generation of the desired sine wave output voltage is achieved by comparing the modulating signal (desired sine wave) with a high-frequency triangular carrier wave. Depending on whether the modulating signal voltage is larger or smallerthan the carrier waveform, either the positive or negative DC bus voltage is applied at the output. Over one switching time period, the average of the positive and negative DC bus voltages applied to the load is proportional to the amplitude of the modulating signal (assumed constant) in that period [25].
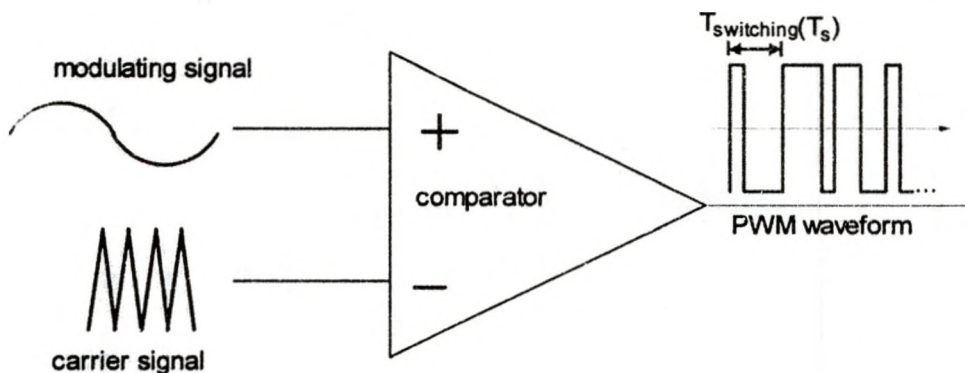
Figure 3.3: A Simple Comparator Circuit for Generating PWM Pulse Train

Figure 3.4 elaborates on a classical example of the PWM waveform generation technique. It shows the modulating signal (V_{ref}) compared with a high frequency triangular wave called the carrier signal (V_c). The duty ratio of the PWM waveform is modulated by V_{ref}, which has the desired fundamental frequency component (f_1) and its amplitude (V_1). Referring to the inverter circuit in Figure 3.4, whenever $V_{ref} > V_c$ the comparator produces a pulse. This pulse

Waveform

T_s V_{ref}

V_c

Comparator
ouput switching
pulses

PWM waveform - pre-filtered
(pole voltage)

Inverter ouput
prior to filter

$\frac{1}{2}V_{DC}$

$-\frac{1}{2}V_{DC}$

(a) Comparator Output

110V AC

V_{DC}

$\frac{1}{2}V_{DC}$

S_1

$\frac{1}{2}V_{DC}$

S_2

$V_{a0} = +\frac{1}{2}V_{DC}$

$+o$

V_a

$-o$

$V_{a0} = -\frac{1}{2}V_{DC}$

Gate Driver

PWM Signal Output
Controller

PC
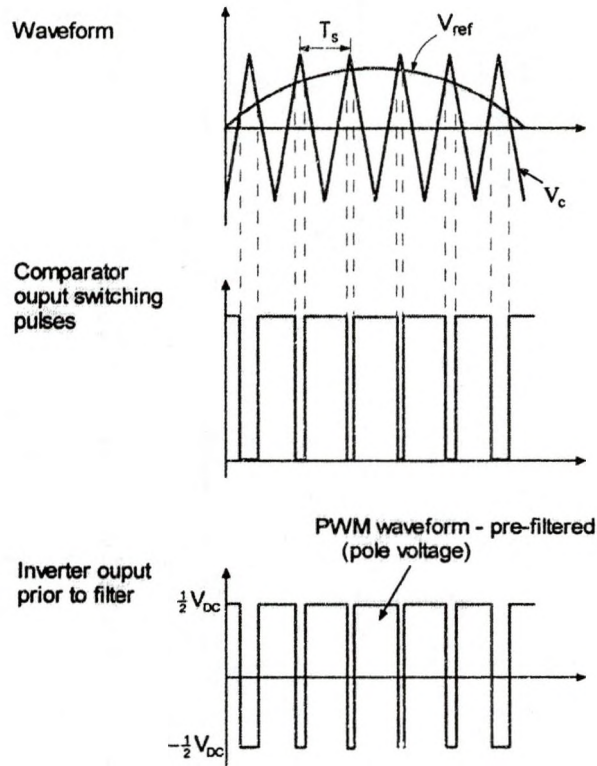
Parallel
Port
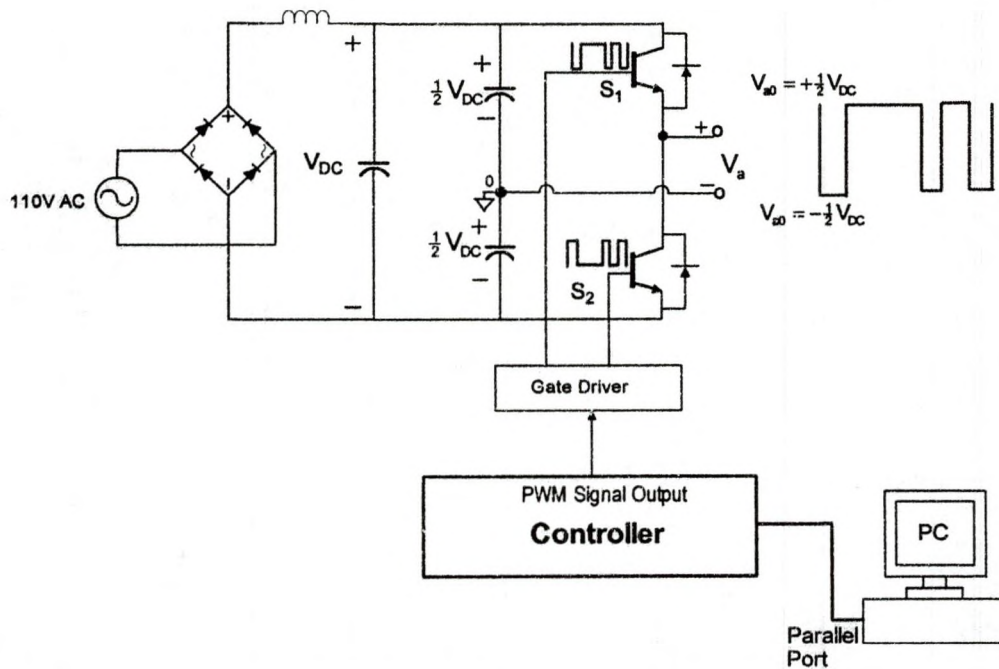
(b) An Overall Structure of a PWM Inverter Circuit

Figure 3.4: Sine Wave Pulse Width Modulation and An Inverter Circuit

will turn S_1 on and S_2 off producing an inverter output of $\frac{1}{2}V_{DC}$, otherwise it will turn S_1 off and S_2 on producing an inverter output of $-\frac{1}{2}V_{DC}$. This is illustrated in Figure 3.4. In Figures 3.1 and 3.2, V_{ref} which is the modulating waveform, carries in it the magnitude and frequency of the desired fundamental output waveform V_1. The switching frequency f_s at which the inverter switches is established by the frequency of V_c. The amplitude modulation index (m_a), the frequency modulation index (m_f) and the duty ratio (D) are defined to be

$$m_a = \frac{|V_{ref}|}{|V_c|}$$

$$m_f = \frac{f_s}{f_{ref}} \qquad (3.1)$$

$$D = \frac{t_{on}}{T_s}$$

where $|V_{ref}|$ is the peak amplitude of the modulating waveform, f_{ref} is the desired frequency of the modulating waveform, $|V_c|$ is the peak amplitude of the carrier waveform (constant) and t_{on} is the on time of the switch S_1. D, the duty ratio, is controlled by both the amplitude and the frequency of the reference modulating signal. These relationships are valid for $0 \le m_a \le 1$[9]. Frequency modulation (m_f) is related to the harmonic number. From Figure 3.4 the pulse rate or the switching frequency is defined by

$$f_s = \frac{1}{T_s} \qquad (3.2)$$

Generally for $0 \le m_a \le 1$ the main harmonic locations of the inverter output voltage are defined by

$$f_n = nm_f \tag{3.3}$$

where n is even or odd integer depending on the value of m_f used. The average voltage seen by the inverter load is equal to:

$$V_{avg} = DV_{ref} \tag{3.4}$$

Reducing t_{on} reduces V_{avg}. PWM switching also widens the gap between wanted and unwanted frequency components, provides nearly a fundamental sinusoid wave at the output and allows controllability from within the inverter. Disadvantages such as high stresses on switching devices, creation of new harmonics and attenuation of the wanted fundamental frequency output are some areas that require an in depth research effort [2].

3.2 Fundamental Frequency Component Generation

Figure 3.5 illustrates the PWM technique further. To understand how the PWM waveform is related to the desired fundamental frequency output, consider the high frequency triangular waveform V_c with frequency f_s and switching time period T_s, and a modulating signal V_{ref} with the frequency f_{ref} and modulating time period T_{PWM}. As mentioned earlier, if $f_s \gg f_{ref}$ then V_{ref} appears to be constant in the switching time period T_s. Therefore the average amplitude of the modulating signal can be considered to be constant during the "narrow" switching time period T_s. It was shown in Figures 3.1 and 3.2, with this assumption, the average voltage applied to the load during the switching period T_s is proportional to the amplitude of the modulating signal alone.

$$V_{ref} = (V_{avg})_{out} \tag{3.5}$$

Therefore the pole voltage (V_{a0}) or the inverter output voltage (shown in Figure
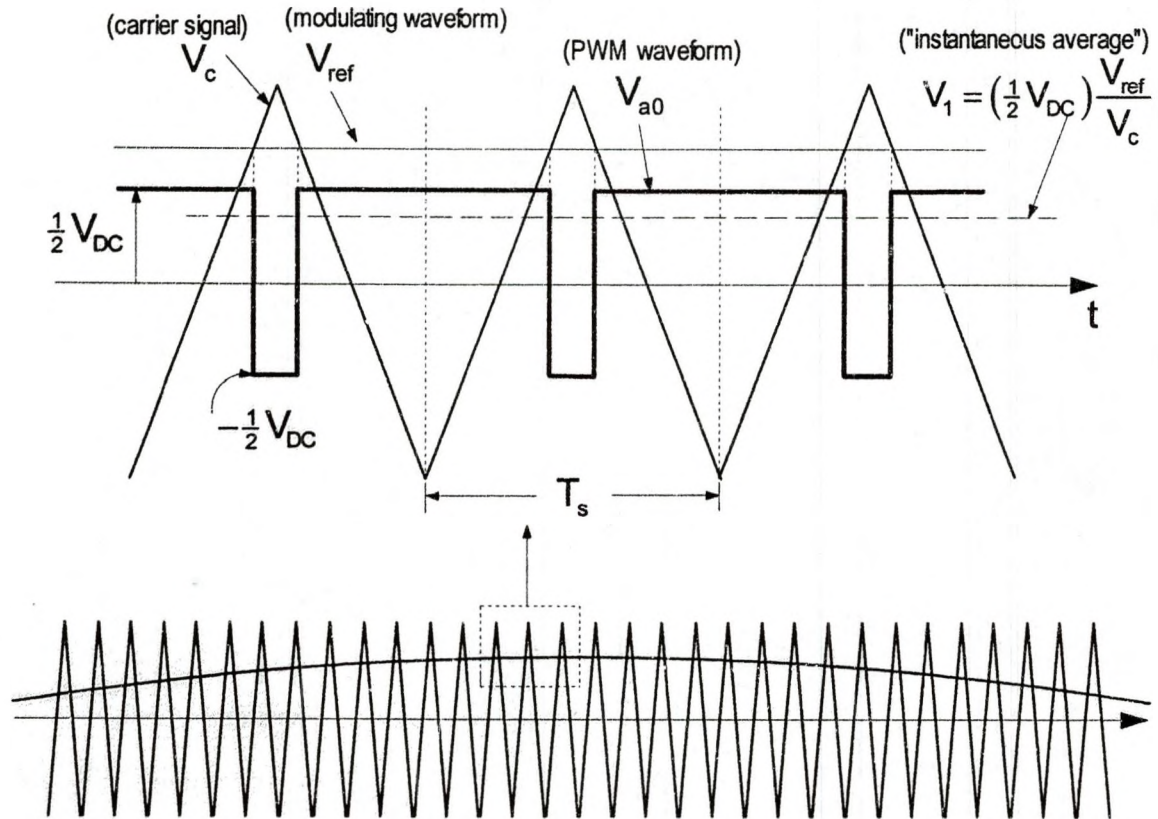
Figure 3.5: Pulse Width Modulation Technique

3.4) averaged over one switching time period (T_s) is the fundamental frequency component of V_{a0} in that switching time period,

$$V_1 = (V_{avg})_{out} \tag{3.6}$$

where the average output voltage in that time period can be calculated as

$$\left(V_{avg}\right)_{out} = \left(\frac{V_{DC}}{2}\right)\frac{t_{on}}{T_s} = \left(\frac{V_{DC}}{2}\right)D \tag{3.7}$$

From Figure 3.6, using the principle of similar triangles it can be shown that

$$\frac{t_{on}}{T_s} = \frac{t_2}{t_1} = \frac{V_{ref}}{V_c} \tag{3.8}$$

Substituting equations (3.7) and (3.8) into equation (3.6), the fundamental frequency output voltage V_1 is expressed as:

$$V_1 = \left(\frac{V_{DC}}{2}\right)\frac{V_{ref}}{V_c} \qquad V_{ref} \leq V_c \qquad\qquad (3.9)$$
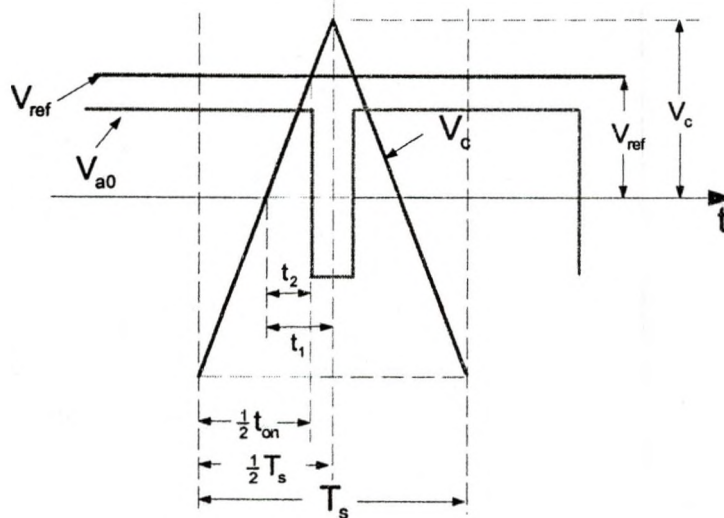
Figure 3.6: Expression for Duty Ratio

Equation 3.9 is termed as "instantaneous amplitude". The "instantaneous amplitude" is the fundamental frequency component of the pulse (V_{a0}) during the switching time period (T_s) [9]. The fundamental frequency component V_1 is shown in dashed line in Figure 3.5. V_{ref} appears to be constant in every switching time period (T_s) but its magnitude changes from one cycle to another depending on where V_c intersects V_{ref}. Therefore the ratio $\frac{V_{ref}}{V_c}$ varies from one T_s to the next T_s. Thus, the "instantaneous amplitude" value also varies accordingly. When the "instantaneous amplitude" of every switching time period (T_s) is traced over the entire modulating signal time period (T_{PWM}) the result is the fundamental frequency component output V_1, which is a sinusoidal replica of V_{ref}. In Figure 3.5, V_1 appears to be lower than V_{ref} because $|V_{ref}| < |V_c|$ in this

example. The ratio of these two quantities controls the pulse width and thus, the fundamental frequency component output V_1.

The following discussion shows the relationship between V_{ref}, V_c, V_1 and V_{DC} (source voltage). The modulating waveform (V_{ref}) contains the desired fundamental frequency component (V_1). Therefore V_{ref} can be expressed as

$$V_{ref} = \left|V_{ref}\right| \sin \omega_{ref} t = \left|V_{r}\right| \sin \omega_1 t \qquad (3.10)$$

where $\left|V_{ref}\right|$ is the peak amplitude of the modulating waveform. Substituting equation (3.10) into equation (3.9) gives the fundamental frequency component as:

$$V_1 = \frac{\left|V_{ref}\right|}{\left|V_c\right|}\left(\frac{V_{DC}}{2}\right)\sin \omega_1 t = m_a \left(\frac{V_{DC}}{2}\right)\sin \omega_1 t \quad \text{for } m_a \leq 1.0 \qquad (3.11)$$

and the amplitude of the fundamental-frequency component of the output voltage as:

$$\left|V_1\right| = m_a\left(\frac{V_{DC}}{2}\right) \quad \text{for } m_a \leq 1.0 \qquad (3.12)$$

which is linearly proportional to m_a, for $m_a \leq 1$. Therefore the modulation index (m_a) has absolute control over the average inverter output voltage. The switching frequency components (high frequency components) created by sine wave PWM process are located as defined by equation (3.3). This means that even after the harmonic elimination process, the RMS value of the AC output voltage waveform is still the same as the input DC voltage. Therefore the total harmonic distortion (THD) is not affected by the PWM process [25]. The PWM process simply shifts the harmonic components to a higher end of the frequency

spectra where they are filtered out.

3.3 Determining Switching Instances

In this section, the PWM techniques are elaborated further to show how the switching instances are determined. Switching instances are determined based on the concept of equation (3.5). Consider the arbitrary n^{th} pulse of the PWM waveform generated by the intersection of carrier signal (V_c) and modulating signal (V_{ref}), as shown in Figure 3.7. The switching pulses that control the turn on and the turn off intervals of the transistors in an inverter circuit generate an area in each switching period equal to the area under the modulating signal bounded by angles θ_{lead} and θ_{trail} [4]. The area under the modulating signal over the interval ϕ_c is divided into two equal intervals ($\frac{1}{2}\phi_c$), as shown by the shaded areas. Similarly the nth pulse is divided over the same intervals as shown by the shaded areas. The left-half area (A_{refL}) under the modulating signal is shaded darker than the right-half area (A_{refR}). A_{refL}, with β_n and $\beta_n - \frac{1}{2}\phi$ as upper and lower limits, corresponds to the left half pulse area, A_{PWML}. A_{refR} with $\beta_n + \frac{1}{2}\phi$ and β_n as upper and lower limits corresponds to the right half pulse area, A_{PWMR}. Applying the concept in equation in (3.5) that says that the average area under the modulating signal (V_{ref}) is equal to the average pulse area. Therefore the area under the modulating signal and the pulse area can be equated as follows

$$A_{refL} = A_{PWML} \tag{3.13}$$

$$A_{refR} = A_{PWMR} \tag{3.14}$$
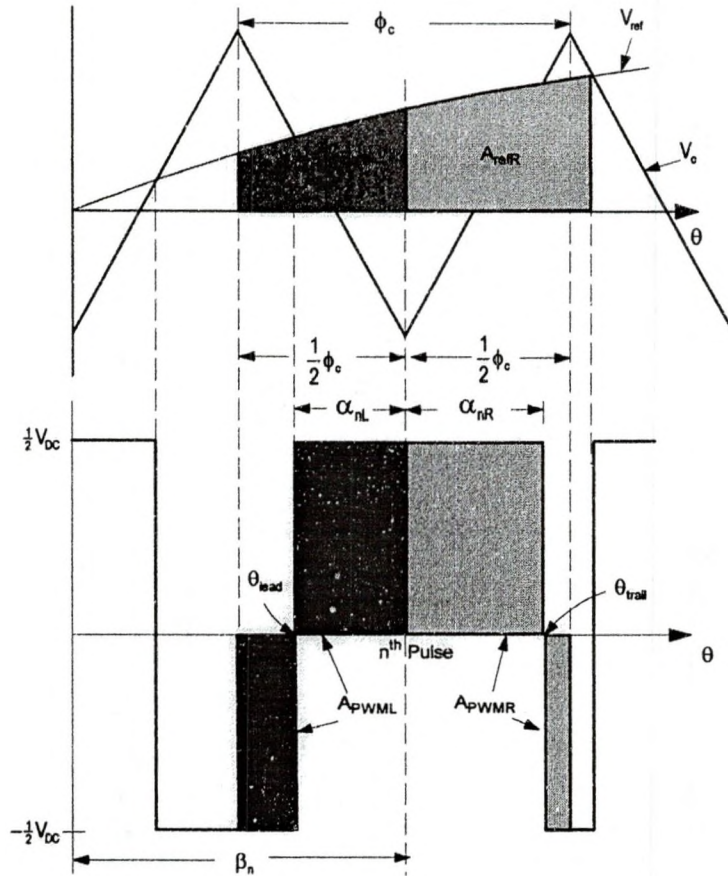
Figure 3.7: An Arbitrary n^{th} Pulse

The left side area, A_{refL} can be represented by the integral

$$A_{refL} = \int_{\beta_n - \frac{1}{2}\phi_c}^{\beta_n} V_{ref} \sin\theta \, d\theta = V_{ref}\left[\cos\left(\beta_n - \frac{\phi_c}{2}\right) - \cos\beta_n\right] \tag{3.15}$$

Using the identity

$$\cos u - \cos v = -2\sin\left(\frac{u+v}{2}\right)\sin\left(\frac{u-v}{2}\right) \tag{3.16}$$

the equation (3.15) can be written as

$$A_{refL} = 2V_{ref}\sin\left(\frac{\phi_c}{4}\right)\sin\left(\beta_n - \frac{\phi_c}{4}\right) \tag{3.17}$$

Since $\sin\phi_c$ is approximately ϕ_c for very small ϕ_c, the equation (3.17) reduces to

$$A_{refL} = \frac{1}{2}\phi_c V_{ref}\sin\left(\beta_n - \frac{\phi_c}{4}\right) \tag{3.18}$$

Similar equation derived for A_{refR} is

$$A_{refR} = \frac{1}{2}\phi_c V_{ref}\sin\left(\beta_n + \frac{\phi_c}{4}\right) \tag{3.19}$$

The left half pulse-area is calculated as

$$A_{PWML} = \left(\tfrac{1}{2}V_{DC}\right)\left[\alpha_{nL} - \left(\frac{\phi_c}{2} - \alpha_{nL}\right)\right] = \left(\tfrac{1}{2}V_{DC}\right)\left[2\alpha_{nL} - \frac{\phi_c}{2}\right] \tag{3.20}$$

and the right half pulse area is

$$A_{PWMR} = \left(\tfrac{1}{2}V_{DC}\right)\left[\alpha_{nR} - \left(\frac{\phi_c}{2} - \alpha_{nR}\right)\right] = \left(\tfrac{1}{2}V_{DC}\right)\left[2\alpha_{nR} - \frac{\phi_c}{2}\right] \tag{3.21}$$

To derive the switching instant of the leading edge of the pulse, let

$$\begin{aligned} A_{refL} &= A_{PWML} \\ \frac{1}{2}\phi_c V_{ref}\sin\left(\beta_n - \frac{\phi_c}{4}\right) &= \left(\tfrac{1}{2}V_{DC}\right)\left[2\alpha_{nL} - \frac{\phi_c}{2}\right] \end{aligned} \tag{3.22}$$

Solving for α_{nL} gives

$$\alpha_{nL} = \frac{\phi_c}{4}\left[1 + \frac{V_{ref}}{\tfrac{1}{2}V_{DC}}\sin\left(\beta_n - \frac{\phi_c}{4}\right)\right] \tag{3.23}$$

A similar derivation for the trailing edge of the pulse gives

$$A_{refR} = A_{PWLR} \tag{3.24}$$

$$\alpha_{nR} = \frac{\phi_c}{4}\left[1 + \frac{V_{ref}}{\tfrac{1}{2}V_{DC}}\sin\left(\beta_n + \frac{\phi_c}{4}\right)\right] \tag{3.25}$$

The switching angle of the nth pulse leading edge is

$$\theta_{lead} = \beta_n - \alpha_{nL} \tag{3.26}$$

and the switching angle of the nth pulse trailing edge is

$$\theta_{trail} = \beta_n + \alpha_{nR} \tag{3.27}$$

In equations (3.23) and (3.25), α_{nL} and α_{nR} are not equal, as can be seen from Figure 3.7 because this is an asymmetric pulse. In symmetric pulses, the positive pulse widths α_{nL} and α_{nR} are the same[4].

$$\alpha_{nL} = \alpha_{nR} = \alpha_n = \frac{\phi_c}{4}\left[1 + \frac{V_{ref}}{\frac{1}{2}V_{DC}}\sin\beta_n\right] \tag{3.28}$$

3.4 Bipolar PWM Switching

The bipolar PWM switching technique is the same as that illustrated in Figure 3.4. It is now elaborated in Figure 3.8. In bipolar PWM switching the pulses are positive and negative for the entire cycle of the modulating signal. As can be seen from Figure 3.8, the bipolar switching pulses jump between $-\frac{1}{2}V_{DC}$ and $+\frac{1}{2}V_{DC}$ throughout the entire period of the modulating signal. That is, whenever $V_c > V_{ref}$ the inverter output voltage (pole voltage) is, $-\frac{1}{2}V_{DC}$ and whenever $V_{ref} > V_c$ the inverter output voltage (pole voltage) is $+\frac{1}{2}V_{DC}$. Figure 3.9 shows the bipolar PWM waveform harmonic spectra. The main harmonics are located at integer multiples of the frequency index (m_f) with sidebands clustered around them. It can be seen from the frequency spectra that the bipolar PWM waveform's fundamental frequency gain is 0.8, which corresponds to $m_a = 0.8$, where m_a is the amplitude modulation index.
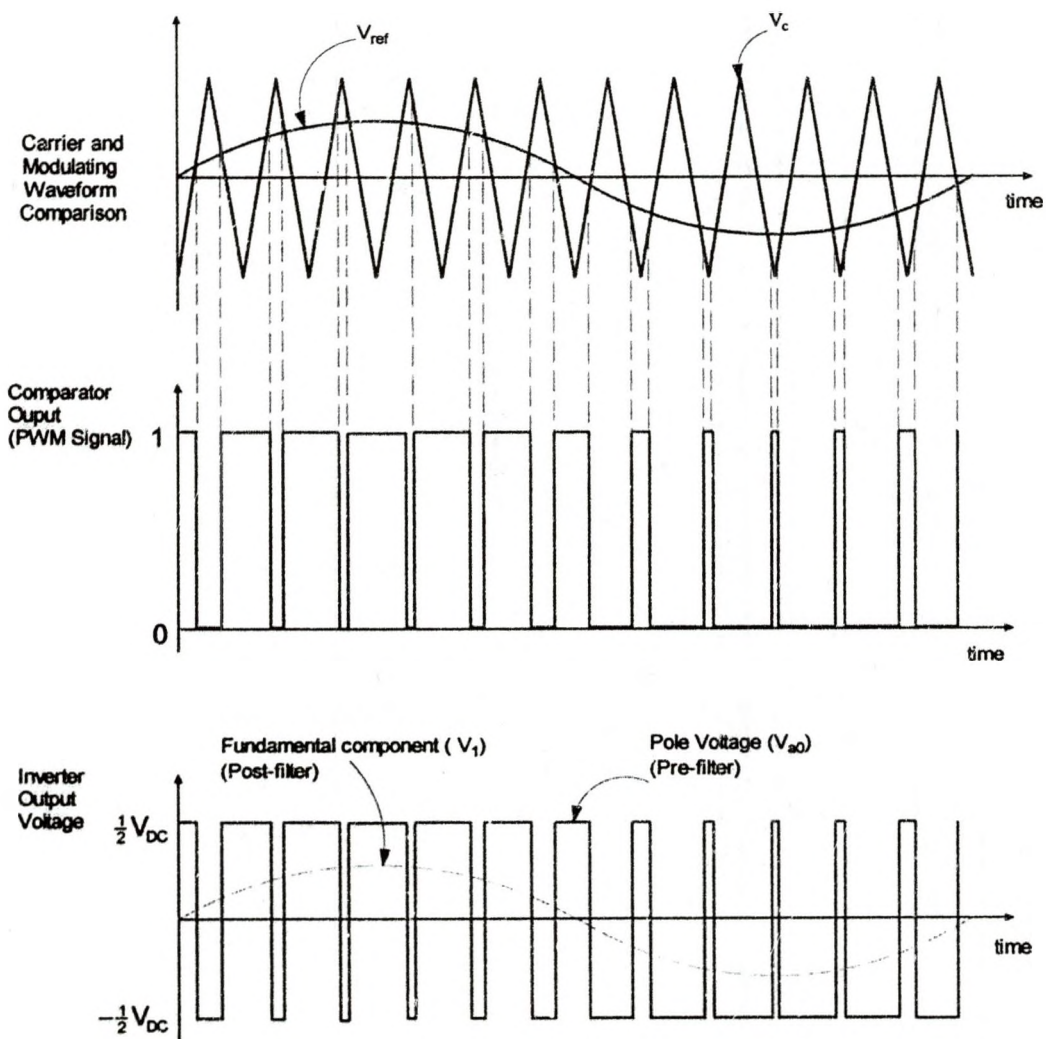
Figure 3.8: Sine Wave-Bipolar PWM Switching
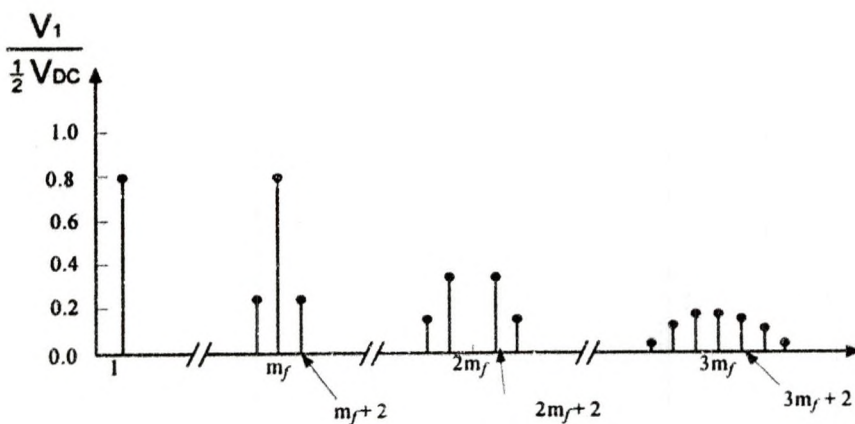
Figure 3.9: Bipolar Harmonics Spectrum

3.5 Unipolar PWM Switching

In unipolar PWM switching, two complementary bipolar PWM waveforms, V_{a01} and V_{a02}, the pole voltages are generated as shown in Figure 3.10. The unipolar PWM waveform then is obtained by taking the difference between V_{a01} and V_{a02}. It can be seen from the unipolar PWM waveform shown in Figure 3.10 that the pole voltage pulses are positive for the positive half cycle of the modulating signal and negative for the negative half cycle of the modulating signal. Two modulating signals, V_{ref1} and V_{ref2} are required to generate complementary pole voltages V_{a01} and V_{a02}. Since two modulating signals are used for each PWM period, the switching frequency of unipolar PWM switching is twice the bipolar PWM switching frequency. In unipolar PWM technique the modulating signal is sampled twice that of the bipolar PWM technique. The advantage is that doubling the switching frequency helps eliminate the harmonics at and around the odd switching frequency index, m_f. This is evident from comparing the bipolar and unipolar PWM waveforms' spectra in Figures 3.9 and 3.11 [9]. The harmonic clusters around odd m_f's have disappeared from the unipolar PWM spectra. However, operation at high frequency results in higher switching losses and higher switching stresses caused by the circuit parasitics (stray inductance, junction capacitance)[66]. In addition, high speed switching transistors are costly.
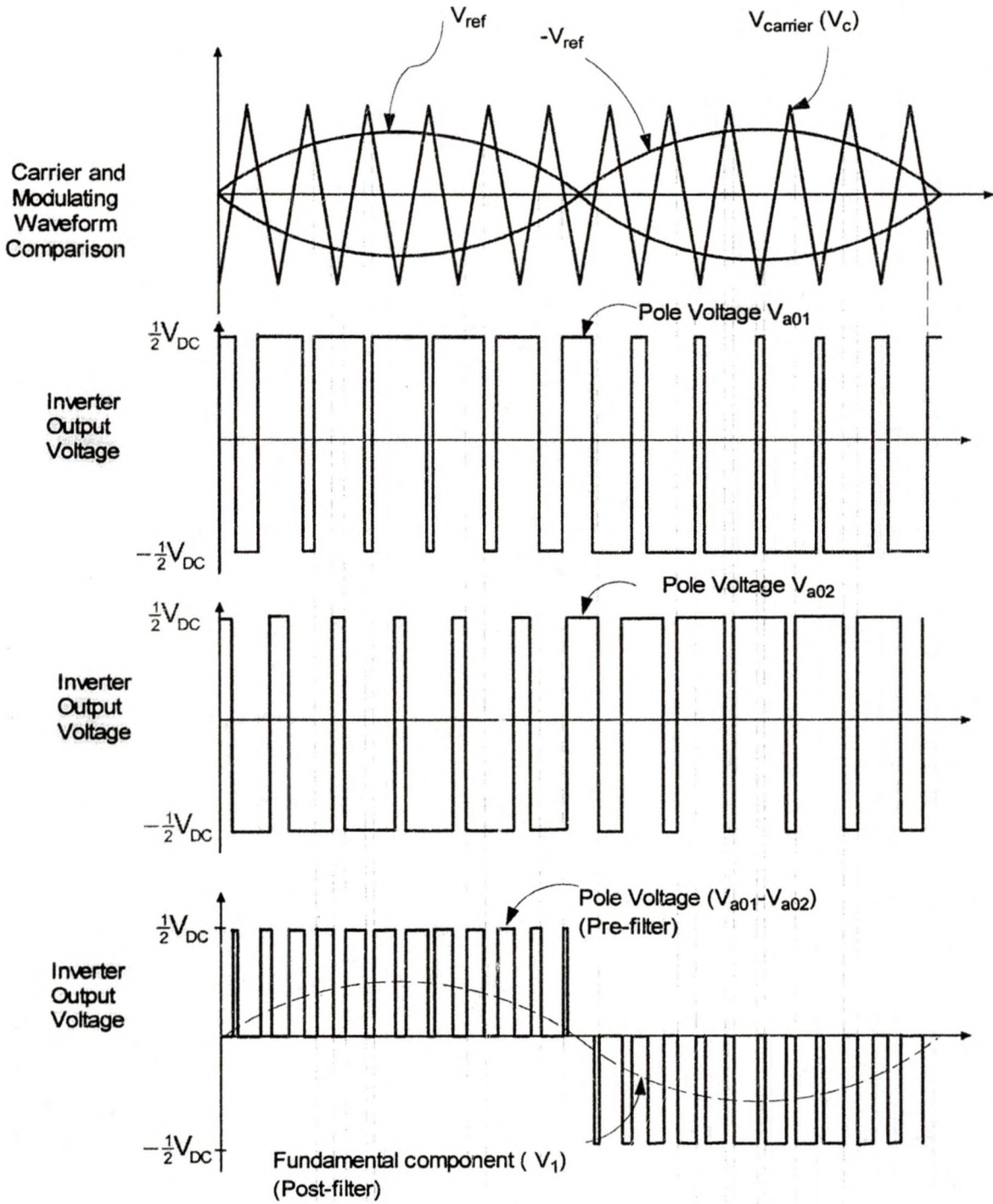
Figure 3.10: Unipolar PWM Switching
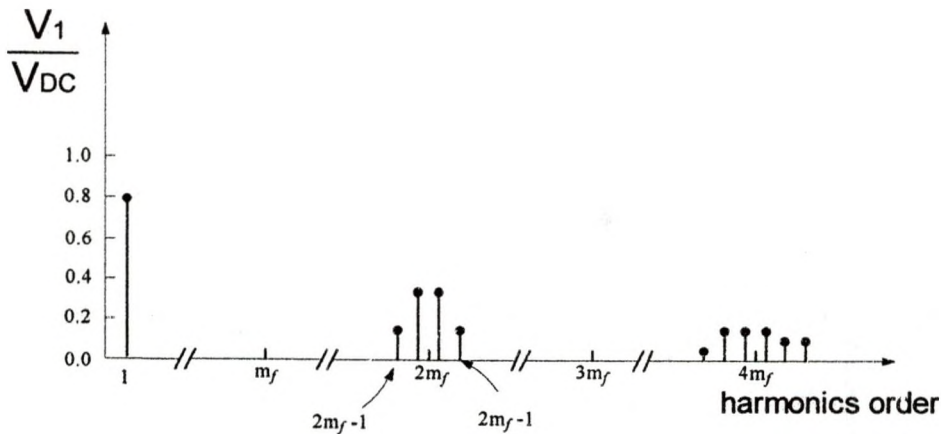
Figure 3.11: Unipolar Harmonic Spectra

3.6 Higher Frequency Switching Issues

Figure 3.12 illustrates a typical power loss characteristic across a power

transistor switch. During switching, the current cannot drop to zero instantly.

Therefore current decreases gradually and voltage increases with a finite shape.

Therefore, during commutation the power is not zero. The energy dissipated

through the junction during commutation is represented by the area under the

power curve [67]. There is a finite time during the transitions where devices are

conducting a significant amount of current while a large voltage is applied across

them. Thus, there is a significant amount of energy dissipation across the

switches. This energy loss increases with increasing frequency. At high

frequencies, high dv/dt and di/dt induce voltage and current oscillations in

parasitic capacitors and inductors during switching transitions. These oscillations

result in higher peak currents and voltages in the devices and thus the switching

losses increase [66]. These oscillations also generate EMI noise, which can

interfere with the operation of other circuits. When a transistor switch is turned

Power: P(t)=V(t)i(t)

Current :i(t)

Voltage:V(t)

The power is not zero in
this region unless the
voltage is zero
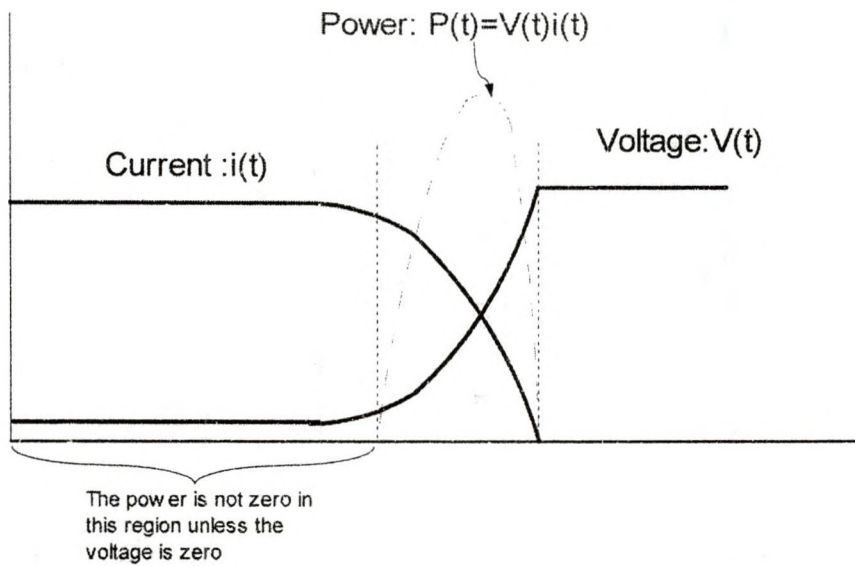
Figure 3.12: Switching Power Losses

on while having a voltage across it, the energy stored in the parasitic capacitance

across the switch is dissipated across the switching junction. This loss increases

with the frequency and is proportional to the square of the voltage across the

device before turn-on.

3.7 Benefits Of Higher Switching Frequencies

High switching frequency PWM approximates the desired sinusoidal modulating

waveform more closely than the lower switching frequencies.   Figure 3.13

compares the quality of the fundamental waveforms produced by low switching

frequency, high switching frequency and very high switching frequency sine wave

PWM.   At very high switching frequencies (Figure 3.13 (c)) the fundamental

waveform is smoother.   For lower switching frequencies, more distorted

fundamental waveforms are produced, as indicated by the Figures 3.13 (a) and

3.13 (b). Ideally at very high switching frequencies, a pure sine wave can be

produced. When motors are connected to AC drives, they produce audible noise

if the switching frequency is limited within the audio range frequency (1–3 KHz).
However, with higher switching frequencies (> 3 KHz) there is less of the
annoying "whine" that was associated with motors operated by the earlier
generation of AC drives [68].

(a) Low Switching Frequency

(b) High Switching Frequency

(c) Very High Switching Frequency (Ideal)
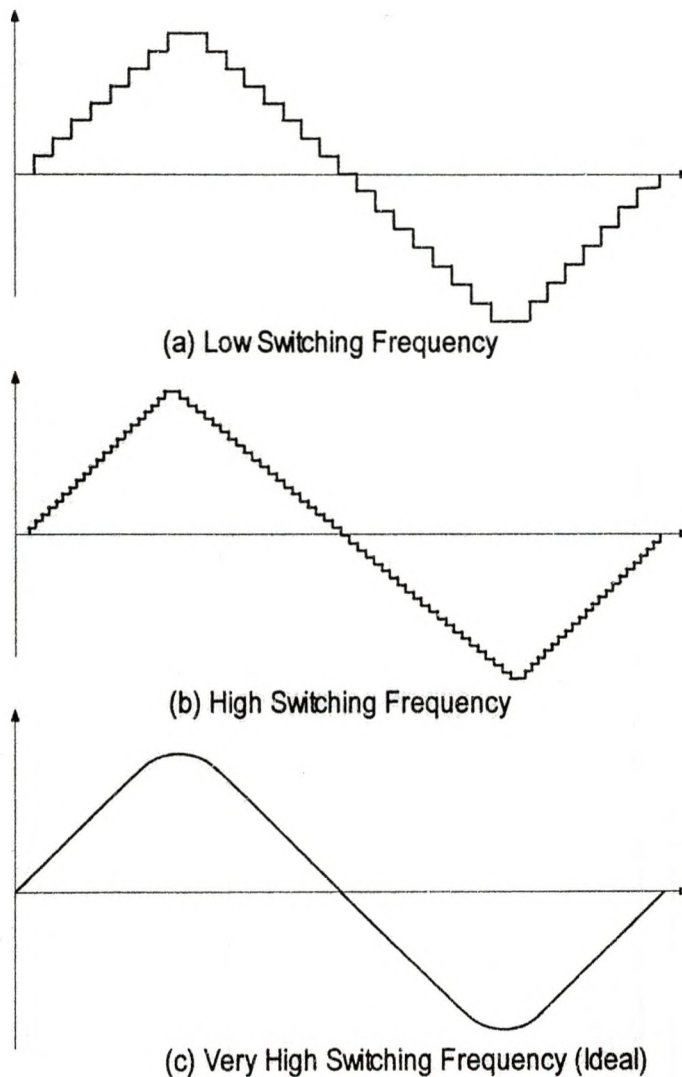
Figure 3.13: Low and High Frequency PWM Switching PWM Waveforms

3.8 Selective Harmonic Elimination PWM

There is another type of PWM switching technique called the harmonic elimination PWM. To implement the PWM techniques discussed in the previous section, high switching frequencies are needed. The switching angles are determined by the intersecting points of the carrier signal and the modulating signal. The result is a series of pulses that contain the fundamental frequency component
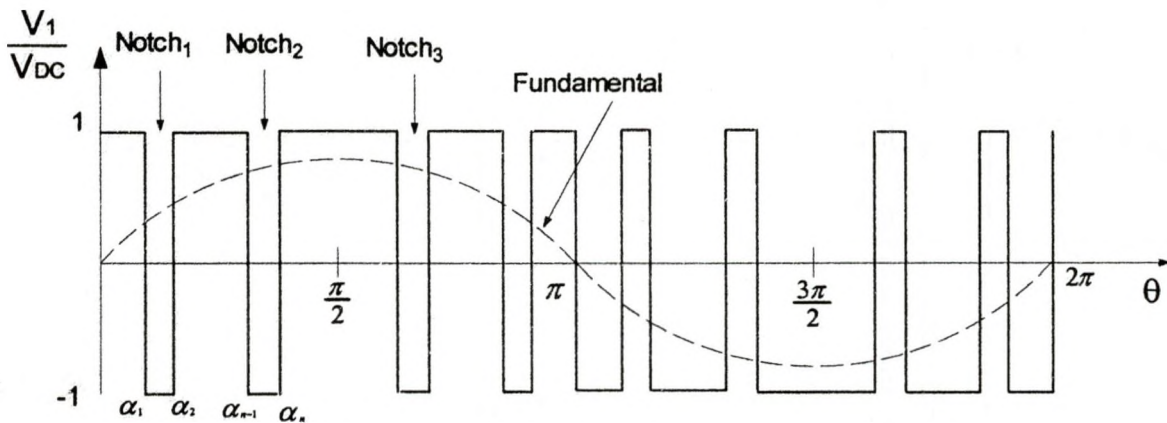
Figure 3.14: Programmed Harmonic Elimination

superimposed on the high frequency switching harmonics. The selective harmonic elimination method is a low frequency switching technique. In the selective harmonic elimination method there is no need for high switching frequency carrier signals to determine the switching frequency. This method eliminates the need for high switching frequencies by incorporating a set of pre-calculated switching angles. These switching angles are solved for by using a set of Fourier series equations. For example, Figure 3.14 shows a PWM waveform with notches formed by some switching angles(α_1, α_2...α_{n-1}.). Certain

harmonics can be eliminated if these switching angles are properly selected based on some predetermined calculations. In this case, the waveform in Figure 3.14 has an odd half-wave symmetry. Therefore only odd harmonics exist [9]. The Fourier coefficients of the waveform (with odd-function symmetry) are [10]:

$$a_0 = \frac{1}{2\pi} \int_0^{2\pi} f(\theta) d\theta = 0$$

$$a_k = \frac{2}{2\pi} \int_0^{2\pi} f(\theta) \sin(k\theta_0) d\theta = 0 \tag{3.29}$$

$$b_k = \frac{2}{2\pi} \int_0^{2\pi} f(\theta) \sin(k\theta_0) d\theta \neq 0$$

Using the quarter wave symmetry simplifies the task of evaluating the Fourier coefficients and thus b_k reduces to

$$b_k = \frac{8}{2\pi} \int_0^{\pi/2} f(\theta) \sin(k\theta) d\theta \quad \text{for k odd}$$

$$b_k = \frac{4}{\pi} \left[\int_0^{\alpha_1} (V_{DC}) \sin(k\theta) d\theta - \int_{\alpha_1}^{\alpha_2} (V_{DC}) \sin(k\theta) d\theta + \int_{\alpha_2}^{\alpha_3} (V_{DC}) \sin(k\theta) d\theta - \ldots + (-1)^n \int_{\alpha_n}^{\frac{\pi}{2}} (V_{DC}) \sin(k\theta) d\theta \right]$$

$$b_k = \frac{4(V_{DC})}{\pi} \left[\int_0^{\alpha_1} \sin(k\theta) d\theta - \int_{\alpha_1}^{\alpha_2} \sin(k\theta) d\theta + \int_{\alpha_2}^{\alpha_3} \sin(k\theta) d\theta - \ldots + (-1)^n \int_{\alpha_n}^{\frac{\pi}{2}} \sin(k\theta) d\theta \right]$$

$$= \frac{4(V_{DC})}{\pi} \left[1 - 2\cos(k\alpha_1) + 2\cos(k\alpha_2) - 2\cos(k\alpha_3) + \ldots + (-1)^n 2\cos(k\alpha_n) \right]$$

$$\tag{3.30}$$

Therefore, for a voltage waveform with odd and half-wave symmetries and n notches per quarter cycle, the Fourier series ($V(\alpha)$) with peak magnitude of the harmonic components, including the fundamental is given by

$$V(\alpha) = \sum_{k=odd}^{\infty} V_k \sin k\theta_0$$

$$V_1 = \frac{4(V_{DC})}{\pi}\left[1 - 2\cos(\alpha_1) + 2\cos(\alpha_2) - 2\cos(\alpha_3) + \ldots + (-1)^n 2\cos(\alpha_n)\right]$$

$$V_3 = \frac{4(V_{DC})}{3\pi}\left[1 - 2\cos(3\alpha_1) + 2\cos(3\alpha_2) - 2\cos(3\alpha_3) + \ldots + (-1)^n 2\cos(3\alpha_n)\right]$$

.

.

. $\qquad\qquad\qquad\qquad\qquad\qquad\qquad\qquad\qquad\qquad\qquad$ (3.31)

$$V_k = \frac{4(V_{DC})}{k\pi}\left[1 - 2\cos(k\alpha_1) + 2\cos(k\alpha_2) - 2\cos(k\alpha_3) + \ldots + (-1)^n 2\cos(k\alpha_n)\right]$$

Where V_k is the magnitude of the kth harmonic and α_n is the nth primary switching angle. There are several control (harmonic and fundamental components) options possible [25]. One of the control options is that n selected harmonics can be eliminated. Another control option may be to eliminate n-1 odd harmonics and obtain a desired fundamental component amplitude. For instance, to eliminate the third and fifth harmonics and to obtain a certain fundamental voltage amplitude, three switching angles α_1, α_2 and α_3, per quarter-cycle are required. From equation (3.31), the three equations needed to solve for the switching angles of the notches are:

$$V_1 = \frac{4(V_{DC})}{\pi}\left[1 - 2\cos(\alpha_1) + 2\cos(\alpha_2) - 2\cos(\alpha_3)\right] = V_{1max}$$

$$V_3 = \frac{4(V_{DC})}{3\pi}\left[1 - 2\cos(3\alpha_1) + 2\cos(3\alpha_2) - 2\cos(3\alpha_3)\right] = 0 \qquad (3.32)$$

$$V_5 = \frac{4(V_{DC})}{5\pi}\left[1 - 2\cos(5\alpha_1) + 2\cos(5\alpha_2) - 2\cos(5\alpha_3)\right] = 0$$

V_1 is set to some desired value V_{1max} and $V_3 = V_5 = 0$ because the third and fifth harmonics need to be eliminated. To solve for the three switching angles (α_1, α_2,

α_3), the Newton-Raphson method can be applied to equation (3.32) [8].

Figure 3.15 shows the typical notched waveform of one of the phases of a three-phase system. This waveform has seven pulses over one fundamental period. This corresponds to seven switchings of the inverter in a PWM period. In comparison to the square waveform, the switching frequency of the waveform in Figure 3.15 is seven times higher. Therefore notching increases the switching
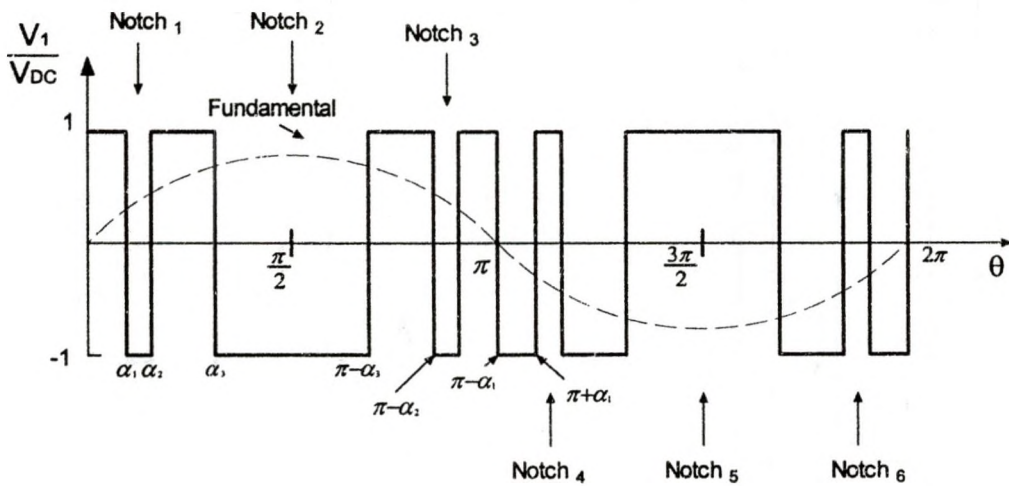
Figure 3.15: Harmonic Elimination and Fundamental Frequency Control

frequency and thereby lowers the fundamental frequency amplitude. It can be shown that the fifth and seventh harmonic elimination (triplen harmonics not included) results in a lower available maximum fundamental frequency output voltage [12], compared to that of the square wave shown in equation (2.2)

$$V_1 = 1.188 \left(\tfrac{1}{2} V_{DC} \right) \tag{3.33}$$

The relationship between notch angle and the percentage of the maximum fundamental frequency output voltage amplitude is shown in Figure 3.16 [12]. Figure 3.16 serves as a guide for a combination of conduction angles that can be used without losing much of the needed fundamental frequency output voltage

amplitude. This technique eliminates the unwanted lower order harmonics without the need for a very high speed switching. Here the switches are switched at a lower speed. As many harmonics as needed can be eliminated by this method. However to implement this, VLSI circuits and microcontrollers are required [9]. The calculations required to determine the switching angles are
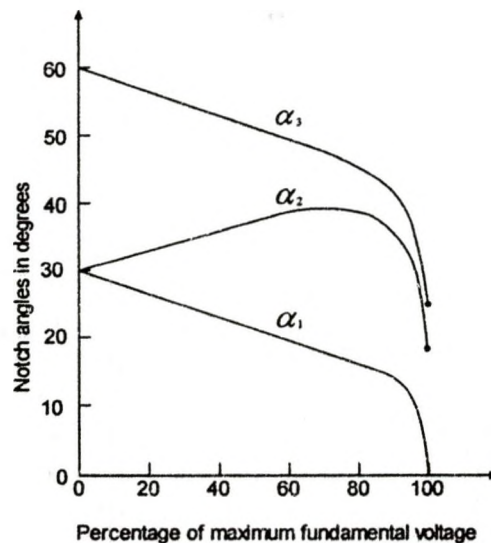
Figure 3.16: Relationship Between Notch Angle and Percentage of Maximum Fundamental Voltage

very involved and it is difficult to implement the harmonic elimination PWM online because of computation power and memory requirements. The programmed harmonic elimination technique combines both square-wave switching and PWM techniques to control the output voltage and eliminate a selected set of harmonics. The next section discusses how this concept is implemented using a neural network controller.

3.9 Optimal PWM-Sigmoid And Piecewise Artificial Neural Network

This technique utilizes an Artificial Neural Network controller to remove the selected harmonics and control the fundamental frequency and ut voltage of a

three-phase inverter. Figure 3.17 shows the overall structure of the inverter. The
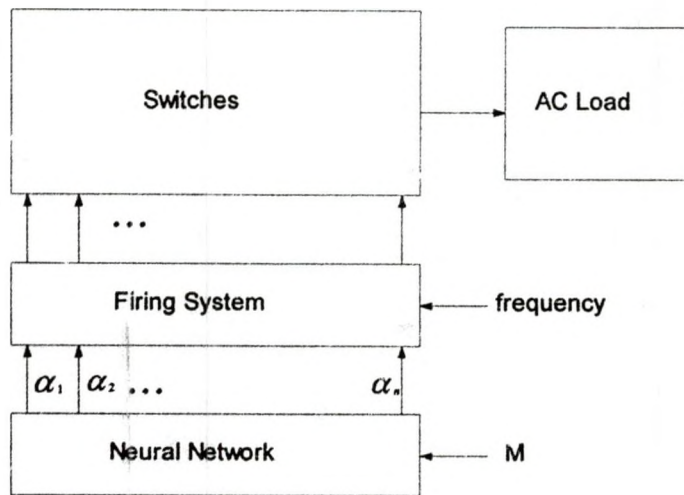
Figure 3.17: The Overall Structure of Neural Network Powered Inverter

use of nonlinear (sigmoid) and piecewise-linear neuron characteristic transfer

functions is compared. Figure 3.18 shows the PWM waveform for selective

harmonic elimination. In Figure 3.18, the switching angles α_1, α_2, α_3 and α_4 per

quarter cycle of the fundamental frequency output can be adjusted to eliminate

lower order harmonics. This scheme allows the chosen harmonics in the PWM

waveform to be removed with the lowest possible number of switching actions
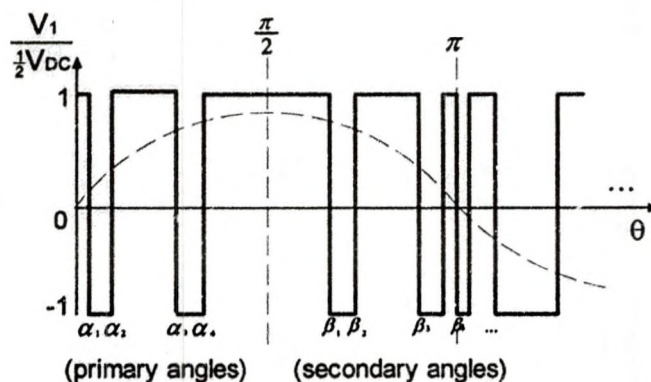
Figure 3.18: PWM Waveform for Selective Harmonic Elimination

[1]. As mentioned before, the magnitude of harmonics for a PWM waveform

with odd and half wave symmetries, and n switching actions per quarter cycle of fundamental frequency is given by equation (3.34), which is the same as equation (3.31).

$$h_1 = \frac{4V_{DC}}{\pi}\left(1 - 2\cos(\alpha_1) + 2\cos(\alpha_2) - 2\cos(\alpha_3) + ... + (-1)^n 2\cos(\alpha_n)\right)$$

$$h_3 = \frac{4V_{DC}}{3\pi}\left(1 - 2\cos(3\alpha_1) + 2\cos(3\alpha_2) - 2\cos(3\alpha_3) + ... + (-1)^n 2\cos(3\alpha_n)\right)$$

$$\cdot$$
$$\cdot$$
$$\cdot$$

(3.34)

$$h_k = \frac{4V_{DC}}{k\pi}\left(1 - 2\cos(k\alpha_1) + 2\cos(k\alpha_2) - 2\cos(k\alpha_3) + ... + (-1)^n 2\cos(k\alpha_n)\right)$$

Optimization of the output signal depends on the value of h_1 (the desired fundamental output voltage) which may change and the required α's and β's need to be recalculated on line. New values of h_1 need to be solved. Since h_1 is nonlinear, an iterative solution method is required. This requires a fast processor, which has a direct effect on implementation and cost. Usually several values of the modulation index ($M = h_1/V_{DC}$) are tabulated and referenced. A feed-forward neural network uses the M as input values to produce a set of primary switching angles (α's) as shown in figure 3.17. The neural network uses one input neuron M and n output neurons (the switching angles). The neurons have sigmoid characteristics and bias. Equation (3.34) can be solved by Newton-Raphson method off-line for over one hundred values of M [1]. The values of M act as the training set for the network. To ensure convergence, the value of α_n obtained for each M input is fed back as an initial guess for the next M input. Using this method, the off-line solution of equation (3.34) is easy and there is no need to use complicated techniques like the Walsh function method [1].

Figures 3.19 and 3.20 show the harmonic spectra for M=0.5 and M=1. Selected non-triplen harmonics are completely eliminated and the fundamental gain is linearly proportional to M. Hardware implementation using the sigmoid transfer
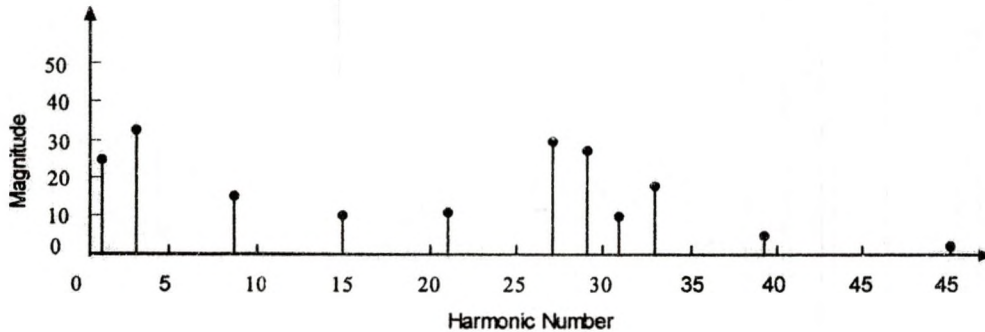
Figure 3.19: Neutral Network Frequency Spectra for M=0.5 Using Sigmoid Transfer Function

function is difficult and costly, because it requires expensive processors and circuit boards. Therefore, sequential processors can be used to emulate the neural network. The sigmoid neuron transfer function requires a time consuming calculation involving the exponential function and division for each neuron and the sequential processors are not powerful enough to handle that. Therefore the nonlinear sigmoid transfer function is replaced with piecewise-linear neuron transfer function. When the piecewise-linear neuron transfer
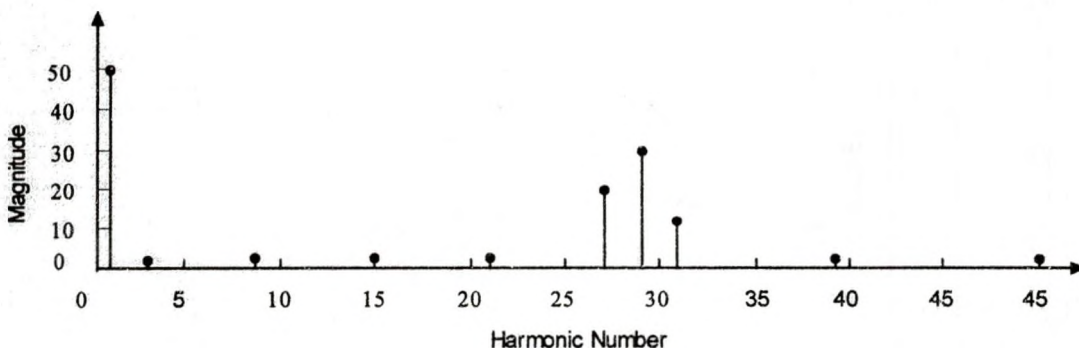
Figure 3.20: Frequency Spectra when M=1, Using Sigmoid Neuron Characteristics Transfer Function for the Artificial Neutral Network Controller

function is used for the neurons with the same weight for the links as in the case of the nonlinear sigmoid neuron transfer function, the α's do not differ much from the previous ones. However the output voltage harmonics are very sensitive to the slight variation of the α's, therefore large magnitude harmonics are present at the output, as shown in Figure 3.21. To solve this problem the piecewise-linear characteristics for
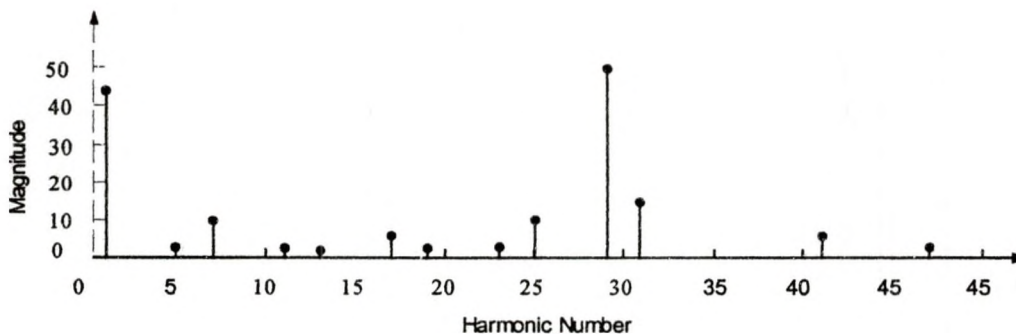
Figure 3.21: Neural Network Frequency Spectra for M=1 Using Piecewise-linear Transfer Function

neurons is used to train the network. The weights of the previous network (with nonlinear neurons) are used as a starting point and the back propagation method
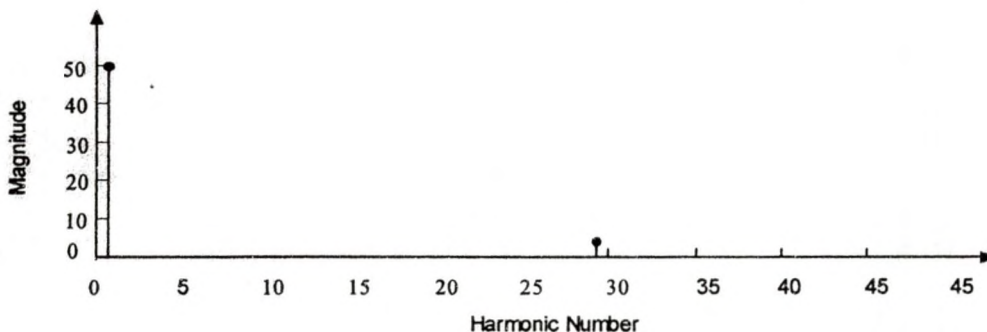
Figure 3.22: Neural Network Frequency Spectra for M=1 Using Piecewise-linear Transfer Function (containing piecewise-linear characteristics for neurons)

ripple [1]. The neural network controller successfully controls the fundamental magnitude of the output and removes the selected harmonics.

CHAPTER 4

SPACE VECTOR PULSE WIDTH MODULATION (SVPWM)

In this chapter the space vector pulse width modulation (SVPWM) technique is presented. Starting from the definition of space vectors, it is illustrated how space vectors are constructed from a three-phase inverter state. For a three-phase inverter, there are eight possible inverter states that can generate eight space vectors. It is shown how these space vectors are combined to approximate a rotating vector in real-time. The rotating vector is a real-time space vector that rotates in the complex plane. This rotating vector is also called the reference vector and represents a three-phase sinusoidal set. The successful application of space vectors requires pre-calculated duty ratios. The duty ratios coupled with a sequential application of the space vectors result in three-phase PWM waveforms. Full mathematical derivation is presented to determine the space vector duty ratios. MATLAB^{TM} simulation are used to verify the duty ratios and the line voltage waveforms. The multi-phase space vector inverter is analyzed and compared with the three phase inverter. The theory of a sensorless three-phase AC motor drive with closed-loop speed control is discussed to illustrate the slip compensation technique using both sensored and sensorless control.

4.1 Resultant Voltage Vector
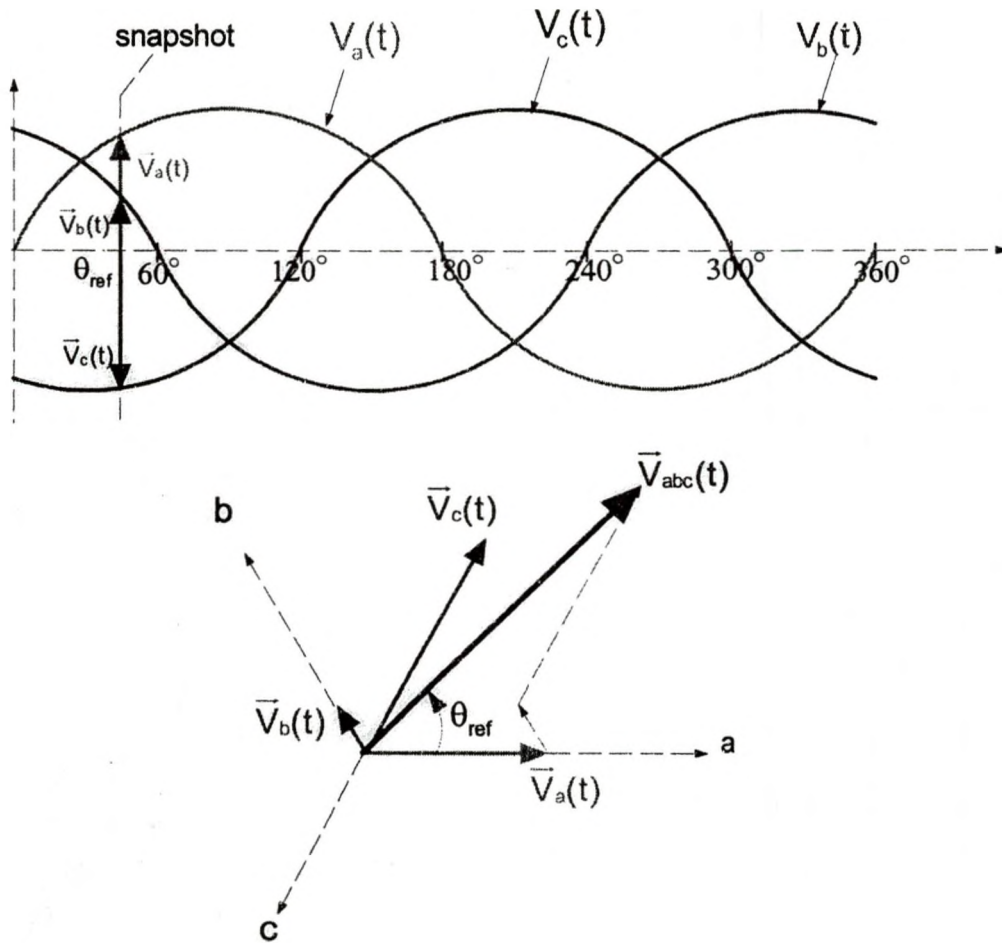
Figure 4.1: Construction of Resultant "Voltage Vector" From a Three-phase Voltage Set

For a three-phase system shown in Figure 4.1 the resultant "voltage vector" $\vec{V}_{abc}(t)$ at snapshot 1 can be constructed using the equation

$$\vec{V}_{abc}(t) = \vec{V}_a(t) + \vec{V}_b(t) + \vec{V}_c(t) \tag{4.1}$$

where

$$\vec{V}_a(t) = V_a(t)$$
$$\vec{V}_b(t) = V_b(t)e^{j120°} \tag{4.2}$$
$$\vec{V}_c(t) = V_c(t)e^{j240°}$$

where $V_a(t), V_b(t)$ and $V_c(t)$ are called the phase components. Combining

equations (4.1) and (4.2), the resultant "voltage vector" can be written as

$$\vec{V}_{abc}(t) \equiv V_a(t) + V_b(t)e^{j120°} + V_c(t)e^{j240°} \tag{4.3}$$

4.2 Space Vector Theory

Given a three-phase balanced voltage set as shown in Figure 4.1 the

phase components $V_a(t)$, $V_b(t)$ and $V_c(t)$ at any point sum up to zero [21].

$$V_a(t) + V_b(t) + V_c(t) = 0 \tag{4.4}$$

The space vector $\vec{V}$ is then defined to be

$$\vec{V} \equiv \tfrac{2}{3}\vec{V}_{abc}(t) = \tfrac{2}{3}[V_a(t) + V_b(t)e^{j120°} + V_c(t)e^{j240°}] \tag{4.5}$$

The construction of the space vector is illustrated in Figure 4.2. From above it

should be noted that the space vectors are defined as the sum of their phase

components multiplied by their respective phase-axis orientation [23]. The result

of this definition is equation (4.5). At any particular instance of time, the phase

components $V_a(t)$, $V_b(t)$ and $V_c(t)$ may have different amplitudes, are spatially

separated by 120° and may differ in sign. The magnitude of a phase component

is a function of time and is proportional to its physical length, as shown by the

snapshot in Figure 4.1. The phase components signs correspond to the

directions they are pointing, up or down, along the time line. In this case $V_a(t)$

and $V_b(t)$ are positive because they are pointing upward, and $V_c(t)$ is negative

because it is pointing downward. At any point in time, they should add up to

zero. At a different point in time, a unique set of phase components combine to

produce a new space vector. Figure 4.3 illustrates the direct transformation,
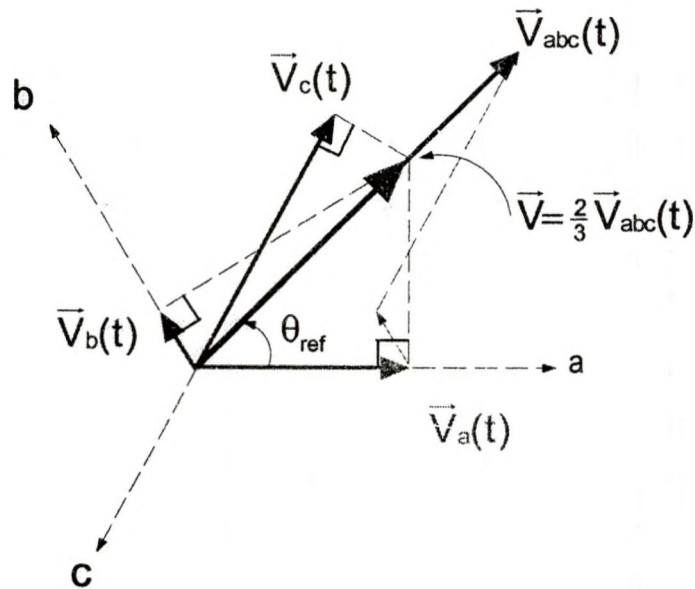
Figure 4.2: Construction of Resultant Space Vector Using Reverse Vector Transformation

which is the orthogonal projection of the voltage vector $\vec{V}_{abc}(t)$ onto the

imaginary-β and the real-α axes in the complex plane. This direct transformation
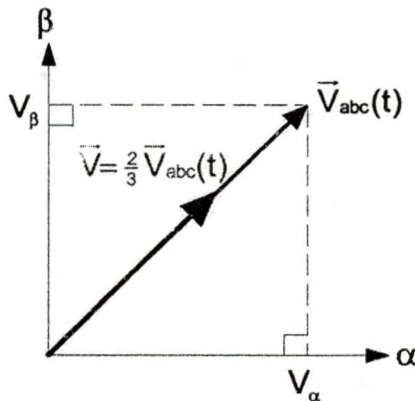
Figure 4.3: Direct Transformation

is called the three-phase to two-phase transformation [18]. Using the direct

transformation, the voltage vector $\vec{V}_{abc}(t)$ can be written in the complex plane as

$$\vec{V}_{abc}(t) = V_\alpha + jV_\beta \qquad (4.6)$$

The opposite of direct transformation is the reverse vector transformation

illustrated in Figure 4.2. The reverse vector transformation can be achieved by projecting $\frac{2}{3}\vec{V}_{abc}(t)$ onto the three axes [22]. Combining equations (4.5) and (4.6), the space vector can be related to the complex plane as

$$\vec{V} = \frac{2}{3}\vec{V}_{abc}(t) = \frac{2}{3}(V_\alpha + jV_\beta) = \frac{2}{3}\left[V_a(t) + \vec{a}V_b(t) + \vec{a}^2V_c(t)\right] \tag{4.7}$$

where $\vec{a} = e^{j120°}$ and $\vec{a}^2 = e^{j240°}$.

4.3 Introduction To Space Vector Modulation (SVPWM)
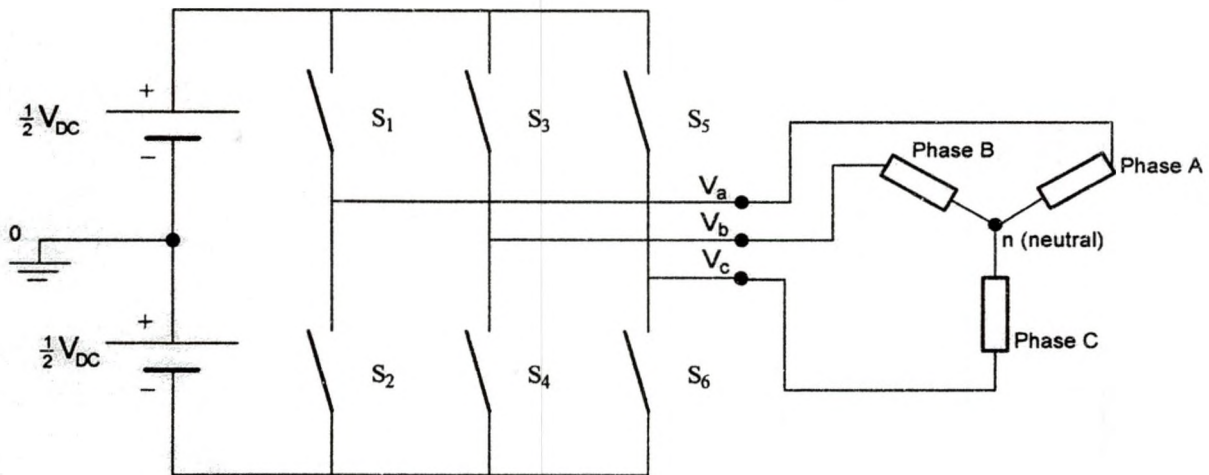
Figure 4.4: Three-phase Inverter with Star Connected Load

A three-phase inverter with the star connected load is shown in Figure 4.4. V_{a0}, V_{b0} and V_{c0} are the inverter output voltages with respect to the return terminal of the DC source voltage marked "0". These voltages are termed as pole voltages or inverter phase voltages. V_{an}, V_{bn} and V_{cn} are the load phase voltages, the inverter output voltages with respect to the floating terminal star-point, n. The difference between any two phase voltages are the line voltages V_{ab}, V_{bc} and V_{ca}. The three-phase SVPWM refers the PWM technique based on the fact that a three-phase quantity could be represented in real-time by a single

vector. During each PWM period, this vector is approximated by using the six

power switches' commutation sequences. A typical PWM duty ratio can be pre-

calculated relating to the requirements of a specific application such as the

minimization of particular harmonics. The resulting PWM pattern is then

periodically applied to the upper and lower switches (S_1, S_2, S_3, S_4, S_5 S_6) of the

three-phase power inverter shown in Figure 4.4. Each switching circuit

configuration generates three independent pole voltages, V_{a0}, V_{b0} and V_{c0}. The

two possible values of pole voltages that can be produced are $-\frac{1}{2}V_{DC}$ and

$+\frac{1}{2}V_{DC}$. For example, when switches S_1, S_4 and S_5 are closed each time, the

corresponding pole voltages are:

$$
\begin{aligned}
V_{a0} &= \tfrac{1}{2}V_{DC} \\
V_{b0} &= -\tfrac{1}{2}V_{DC} \\
V_{c0} &= \tfrac{1}{2}V_{DC}
\end{aligned}
\tag{4.8}
$$

This is one of the eight circuit configurations called operating states of the

inverter or inverter states. On each inverter leg, when one switch is closed then

the other switch must be opened. No two switches on the same leg should be

closed or opened at the same time. When the upper switch is closed on a

particular leg, this situation is denoted by a "1" and if it is open then it is denoted

as a "0". Using this notation, the inverter state in equation (4.8) can be

represented by the notation (101) and the corresponding space vector is denoted

as $\vec{V}_{101}$ or $\vec{V}_6$. There are altogether eight (2^3) possible inverter states. All the

possible pole voltages created by the eight inverter states can be transformed

into eight corresponding space vectors by plugging in the pole voltage values of

S_2, S_4, S_6 - closed

$V_{a0} = -\frac{1}{2}V_{DC} \quad V_{b0} = -\frac{1}{2}V_{DC} \quad V_{c0} = -\frac{1}{2}V_{DC}$

$\vec{V}_0 = \vec{V}_{000} = \frac{2}{3}\left(-\frac{1}{2}V_{DC}e^{j0°} + -\frac{1}{2}V_{DC}e^{j120°} + -\frac{1}{2}V_{DC}e^{j240°}\right) \rightarrow 0$
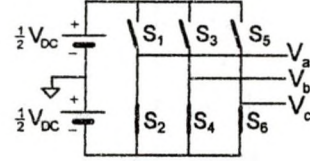
S_1, S_4, S_6 - closed

$V_{a0} = +\frac{1}{2}V_{DC} \quad V_{b0} = -\frac{1}{2}V_{DC} \quad V_{c0} = -\frac{1}{2}V_D$

$\vec{V}_1 = \vec{V}_{100} = \frac{2}{3}\left(+\frac{1}{2}V_{DC}e^{j0°} - \frac{1}{2}V_{DC}e^{j120°} - \frac{1}{2}V_{DC}e^{j240°}\right) \rightarrow \frac{2}{3}V_{DC}$
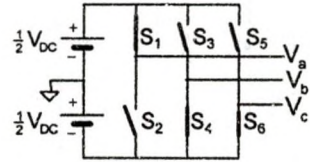
S_1, S_3, S_6 - closed

$V_{a0} = +\frac{1}{2}V_{DC} \quad V_{b0} = +\frac{1}{2}V_{DC} \quad V_{c0} = -\frac{1}{2}V_{DC}$

$\vec{V}_2 = \vec{V}_{110} = \frac{2}{3}\left(+\frac{1}{2}V_{DC}e^{j0°} + \frac{1}{2}V_{DC}e^{j120°} - \frac{1}{2}V_{DC}e^{j240°}\right) \rightarrow \frac{2}{3}V_{DC}e^{j60°}$
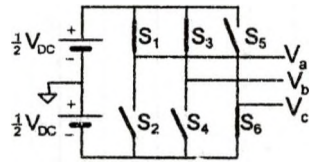
S_2, S_3, S_6 - closed

$V_{a0} = -\frac{1}{2}V_{DC} \quad V_{b0} = +\frac{1}{2}V_{DC} \quad V_{c0} = -\frac{1}{2}V_{DC}$

$\vec{V}_3 = \vec{V}_{010} = \frac{2}{3}\left(-\frac{1}{2}V_{DC}e^{j0°} + \frac{1}{2}V_{DC}e^{j120°} - \frac{1}{2}V_{DC}e^{j240°}\right) \rightarrow \frac{2}{3}V_{DC}e^{j120°}$
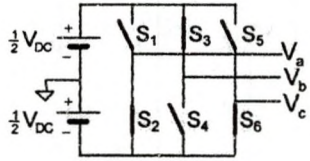
S_2, S_3, S_5 - closed

$V_{a0} = -\frac{1}{2}V_{DC} \quad V_{b0} = +\frac{1}{2}V_{DC} \quad V_{c0} = +\frac{1}{2}V_{DC}$

$\vec{V}_4 = \vec{V}_{011} = \frac{2}{3}\left(-\frac{1}{2}V_{DC}e^{j0°} + \frac{1}{2}V_{DC}e^{j120°} + \frac{1}{2}V_{DC}e^{j240°}\right) \rightarrow \frac{2}{3}V_{DC}e^{j180°}$
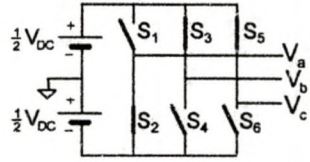
S_2, S_4, S_5 - closed

$V_{a0} = -\frac{1}{2}V_{DC} \quad V_{b0} = -\frac{1}{2}V_{DC} \quad V_{c0} = +\frac{1}{2}V_{DC}$

$\vec{V}_5 = \vec{V}_{001} = \frac{2}{3}\left(-\frac{1}{2}V_{DC}e^{j0°} - \frac{1}{2}V_{DC}e^{j120°} + \frac{1}{2}V_{DC}e^{j240°}\right) \rightarrow \frac{2}{3}V_{DC}e^{j240°}$
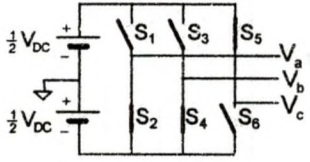
S_1, S_4, S_5 - closed

$V_{a0} = +\frac{1}{2}V_{DC} \quad V_{b0} = -\frac{1}{2}V_{DC} \quad V_{c0} = +\frac{1}{2}V_{DC}$

$\vec{V}_6 = \vec{V}_{101} = \frac{2}{3}\left(+\frac{1}{2}V_{DC}e^{j0°} - \frac{1}{2}V_{DC}e^{j120°} + \frac{1}{2}V_{DC}e^{j240°}\right) \rightarrow \frac{2}{3}V_{DC}e^{j300°}$
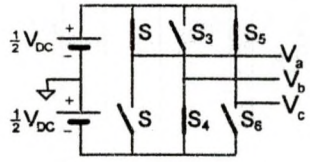
S_1, S_3, S_5 - closed

$V_{a0} = +\frac{1}{2}V_{DC} \quad V_{b0} = +\frac{1}{2}V_{DC} \quad V_{c0} = +\frac{1}{2}V_{DC}$

$\vec{V}_7 = \vec{V}_{111} = \frac{2}{3}\left(+\frac{1}{2}V_{DC}e^{j0°} + \frac{1}{2}V_{DC}e^{j120°} + \frac{1}{2}V_{DC}e^{j240°}\right) \rightarrow 0$
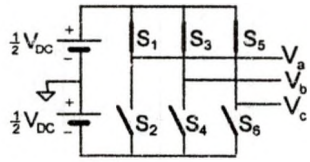
Figure 4.5: Switching States, Pole Voltages and Corresponding Space Vectors

each inverter state into equation (4.5). The resultant eight space vectors are denoted as $\vec{V}_{000}, \vec{V}_{100}, \vec{V}_{110}, \vec{V}_{010}, \vec{V}_{011}, \vec{V}_{001}, \vec{V}_{101}, \vec{V}_{111}$ or $\vec{V}_0, \vec{V}_1, \vec{V}_2, \vec{V}_3, \vec{V}_4, \vec{V}_5, \vec{V}_6, \vec{V}_7$. All the inverter states and space vectors are shown in Figure 4.5. $\vec{V}_0$ and $\vec{V}_7$ are the null-state vectors; they apply zero voltages. $\vec{V}_1, \vec{V}_2, \vec{V}_3, \vec{V}_4, \vec{V}_5, \vec{V}_6$ are the active-state vectors that apply non-zero voltages. Figure 4.6 shows all the eight
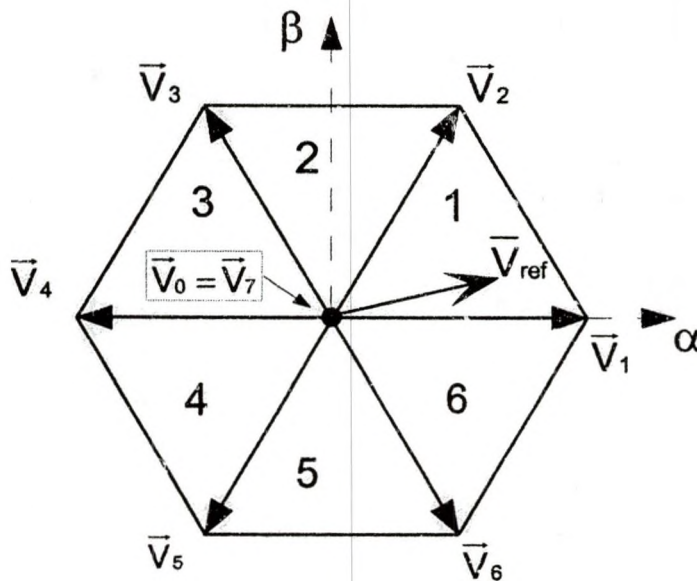
Figure 4.6: Space Vector and Rotating Reference Vector

space vectors plotted on the complex plane. The space vectors take six distinct angles as commanded by the inverter state, forming a hexagon with the null vectors ($\vec{V}_0$ and $\vec{V}_7$) at the center of the hexagon. The hexagon represents the range of all realizable space vectors [17] . It will be shown in later sections that using the space vector modulation process it is possible to realize any arbitrary desired space vector $\vec{V}_{ref}$ that lays within each sector.

4.4 Six-step Mode

The maximum fundamental phase voltage (line-to-neutral voltage) that may be produced by the three-phase inverter for a given DC link voltage (DC bus voltage) occurs under the six-step operation[17]. The six-step operation can be achieved if the space vectors are applied in a certain sequence. For example, if the space vectors are applied in the sequence $\vec{V}_2, \vec{V}_1, \vec{V}_6, \vec{V}_5, \vec{V}_4, \vec{V}_3$, the result will be a six-step line-to-neutral voltage waveform. The following discussion shows the circuit analysis to obtain a six-step voltage waveform The circuit in Figure 4.7 shows one of the eight inverter states and its equivalent circuit schematic. This inverter state corresponds to the space vector $\vec{V}_1$ ($\vec{V}_{100}$) in sector 1.
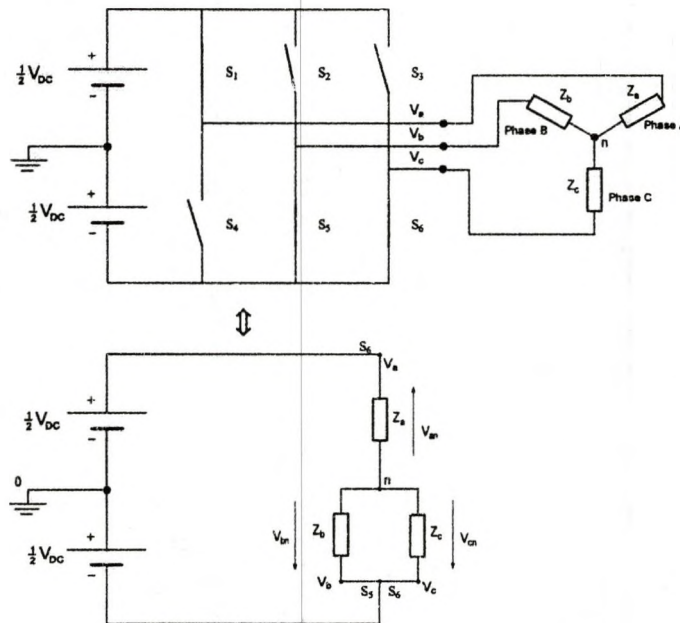
Figure 4.7: Star-Connected Load Step Voltage for Inverter State 100 (space vector $\vec{V}_1$)

Assuming this is a balanced load system then the load phase impedance is

$$Z_a = Z_b = Z_c = Z \tag{4.9}$$

and the equivalent impedance of the parallel loads Z_b and Z_c is

$$Z_{bc} = \frac{Z}{2} \tag{4.10}$$

Using the voltage divider, the load phase voltages V_{an}, V_{bn} and V_{cn} are:

$$V_{an} = \frac{Z_a}{Z_a + Z_{bc}}(V_{DC}) = \frac{Z}{Z + \frac{Z}{2}}(V_{DC}) = Z \cdot \frac{2}{3Z}(V_{DC}) = \frac{2}{3}V_{DC}$$

$$\tag{4.11}$$

$$V_{bn} = V_{cn} = \frac{Z_{bc}}{Z_a + Z_{bc}}(-V_{DC}) = -\frac{\frac{Z}{2}}{Z + \frac{Z}{2}}(V_{DC}) = -\frac{Z}{2} \cdot \frac{2}{3Z}(V_{DC}) = -\frac{1}{3}V_{DC}$$

If similar calculations are carried out for the remaining five active-state space vectors in the other sectors for V_{an}, a six-step waveform for V_{an} would look like the waveform shown in Figure 4.8 (c). The six-step mode waveform is the result of six switching transitions per PWM period and is why this switching scheme is called the six-step operation. Switching frequency harmonics are on the order of $n = 6k \pm 1$ for $k = 1,2,3,...$[14]. The third and multiples of the third (triplens) and even harmonics do not exist. For a circuit system with a floating neutral point and an input voltage source (V_{DC}), the Fourier series of the line-to-neutral voltage ($V_{L-N}(t)$) waveform and its Fourier coefficient ($V_{n,L-N}$) are expressed as:

$$V_{n,L-N}(t) = \sum_{n}^{\infty} V_{n,L-N} \sin(n\omega_0 t)$$

$$V_{n,L-N} = \left| \frac{4V_{DC}}{n\pi}\left[2 + \cos\left(n\frac{\pi}{3}\right) - \cos\left(n\frac{2\pi}{3}\right)\right] \right| \quad \text{for } n = 1,5,7,11,13... \tag{4.12}$$

The Fourier series of the line voltage ($V_{L-L}(t)$) waveform and its Fourier coefficient ($V_{n,L-L}$) are expressed as [14]:

sequence	1	2	3	4	5	6
inverter state	110	100	101	001	011	010
space vector	$\vec{V}_2$	$\vec{V}_1$	$\vec{V}_6$	$\vec{V}_5$	$\vec{V}_4$	$\vec{V}_3$

(a) Three-phase Pole Voltage Waveforms

(b) Line Voltage waveform

V_{an} (fundamental)

V_{an} (six-step voltage waveform)

$V_{max,fo} = \frac{2}{\pi} V_{DC}$

$V_{max,step} = \frac{2}{3} V_{DC}$

(c) Load Phase Waveform (six-step)
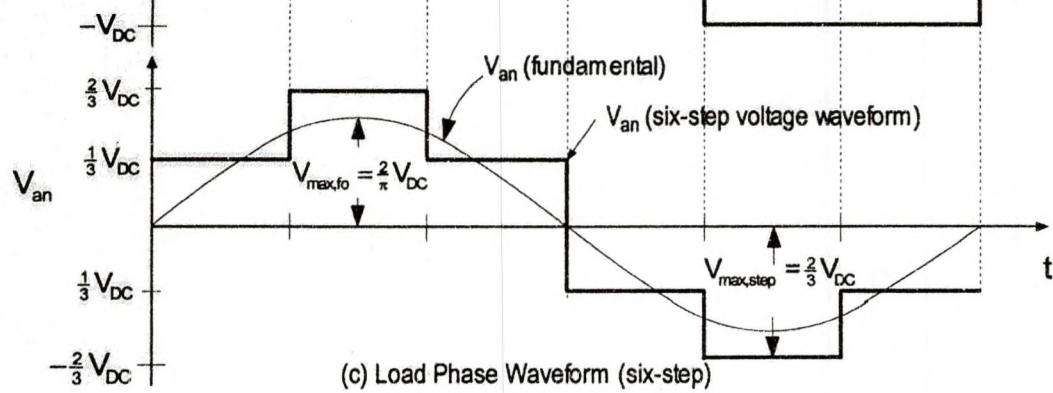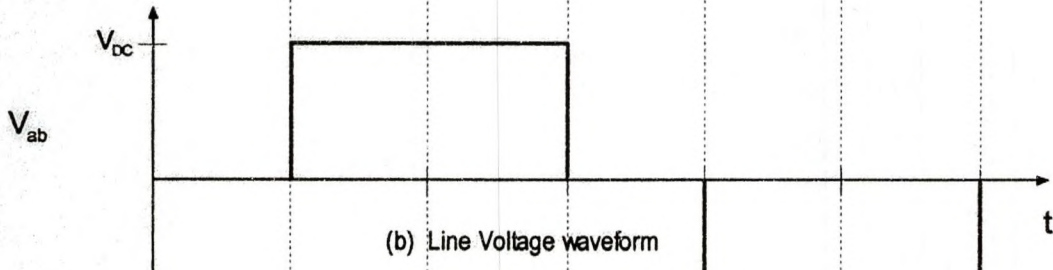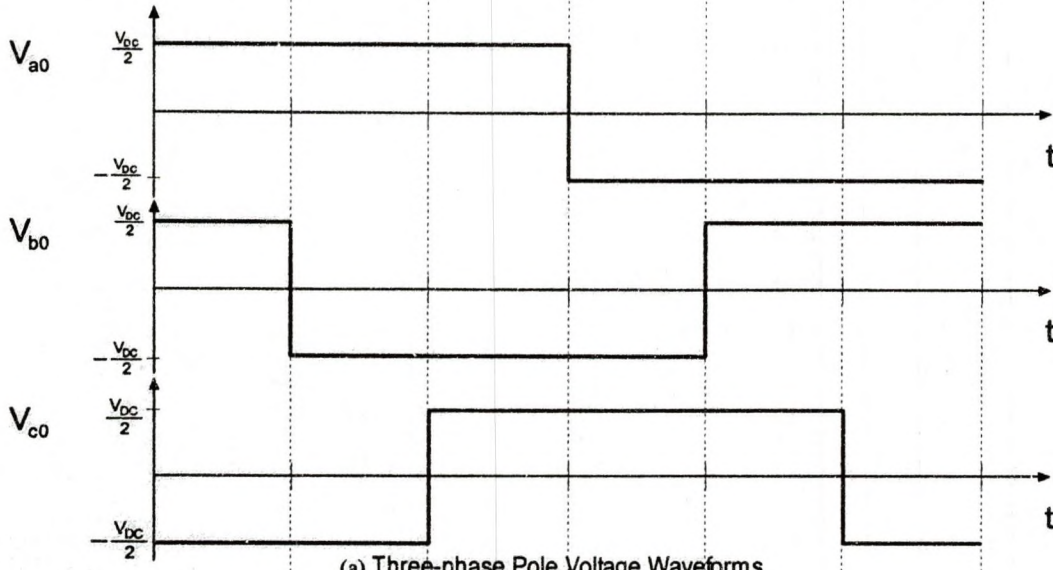
Figure 4.8: Six-step and Fundamental Voltage Waveform on V_{an}

$$V_{L-L}(t) = \sum_{n} V_{n,L-L} \sin(n\omega_0 t)$$

$$V_{n,L-L} = \left| \frac{4V_{DC}}{n\pi} \cos\left(\frac{n\pi}{6}\right) \right| \text{ for } n = 1,5,7,11,13...$$

The maximum realizable fundamental line-to-neutral voltage can be generated under the six-step operation. This maximum realizable fundamental line-to-neutral voltage is the determining factor of a three-phase inverter capability. The maximum fundamental and step voltage amplitudes that can be produced under six-step mode are $\frac{2}{\pi}V_{DC}$ and $\frac{2}{3}V_{DC}$, respectively. These values can be used to determine the voltage utilization capability of various three-phase inverters such as the SVPWM and sine wave PWM. Each step in the waveform represents one inverter state and all the six active-states are used in the six-step mode; within one PWM period. The null-state space vectors are not used in this mode. In this mode the SVPWM is created by generating (within the PWM switching time period (T_{PWM})) a sequence of different inverter states, which correspond to the six-step voltage waveform.

4.5 Space Vector Pulse Width Modulation (SVPWM) Technique

The idea of SVPWM is to generate appropriate space vectors so that any desired vector $\vec{V}_{ref}$ can be approximated within a fundamental period (PWM period in all sectors). Consider $\vec{V}_{ref}$ located in sector 1 of the hexagon shown in Figure 4.6. To approximate $\vec{V}_{ref}$, the space vectors $(\vec{V}_0, \vec{V}_1, \vec{V}_2, \vec{V}_7)$ are applied in the sequence shown in Figure 4.9. Applying these space vectors in this sequence ensures that the transition from one state to the next is performed by switching only one inverter leg [17]. $\vec{V}_{ref}$ can be approximated in a sampling

Sequence: $0 \longrightarrow 1 \longrightarrow 2 \longrightarrow 7 \longrightarrow 2 \longrightarrow 1 \longrightarrow 0$

State: null   active active   null   active active   null

Figure 4.9: Space Vector Sequence in Sector 1

period (Pulse Width Modulation Period in sector 1) by applying $\vec{V}_0$ for a time period T_0, $\vec{V}_1$ for a time period T_1, $\vec{V}_2$ for a time period T_2 and $\vec{V}_7$ for a time period T_7 such that [17]

$$\vec{V}_{ref}.T_{PWM} = \vec{V}_0.T_0 + \vec{V}_1.T_1 + \vec{V}_2.T_2 + \vec{V}_7.T_7 \qquad (4.13)$$

The sequence consists of four space vectors, two of which are the zero-state space vectors. Figure 4.10 illustrates the reference vector ($\vec{V}_{ref}$) approximation process by the projections of $\vec{V}_{ref}$ onto the adjacent space vectors, $\vec{V}_1$ and $\vec{V}_2$. These projections of $\vec{V}_{ref}$ help to determine time scaled adjacent space vectors
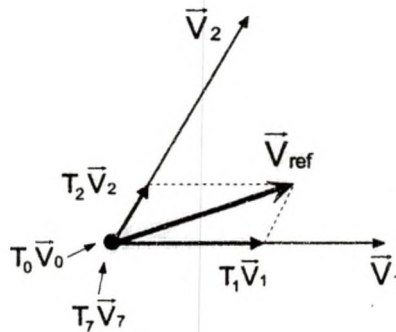
Figure 4.10: Projections of Rotating Vector onto the Adjacent Space Vectors in Sector 1

$T_1\vec{V}_1$ and $T_1\vec{V}_2$ needed to approximate $\vec{V}_{ref}$. By averaging these projections ($T_1\vec{V}_1$ and $T_1\vec{V}_2$) and equating the result to the time averaged reference vector ($T_{PWM}\vec{V}_{ref}$) allows one to determine the space vectors ($\vec{V}_1$ and $\vec{V}_2$) on-times, T_1 and T_2. The null vectors'($\vec{V}_0$ and $\vec{V}_7$), on-times T_0 and T_7 can be determined from [17]

$$T_{PWM} = T_0 + T_1 + T_2 + T_7$$
$$T_{null} = T_0 + T_7 \qquad\qquad\qquad (4.14)$$
$$T_0 = T_7 = \tfrac{1}{2}T_{null}$$

When the reference voltage ($\vec{V}_{ref}$) and the sampling period (T_{PWM}-the period when $\vec{V}_{ref}$ is sampled) are known, it is possible to determine T_1, T_2 and T_{null} [17].

SVPWM is a technique of sinusoidal voltage generation, based on the space vector PWM. This objective is achieved if the $\vec{V}_{ref}$ is approximated instantaneously by a combination of inverter states which correspond to space vectors [21]. It was shown in Figure 4.10 that $\vec{V}_{ref}$ in sector 1 can be approximated by a sequence of time-based space vectors in a sampling period (the period when $\vec{V}_{ref}$ is sampled). In the same way, $\vec{V}_{ref}$ in other sectors can be approximated by other appropriate application of space vectors. When the approximation of the $\vec{V}_{ref}$ is done in all sectors, assuming that it is desired to produce a balanced three-phase sinusoid voltages, then the resultant $\vec{V}_{ref}$ locus is a circle [17]. Therefore, a balanced set of three-phase voltages can be represented by a rotating reference vector ($\vec{V}_{ref}$) of constant magnitude equal to the average value of the combined three-phase voltages, which rotates with an angular velocity of ω_{ref} ($\omega_{ref} = 2\pi f_{ref}$). The reference vector in the complex plane then can be expressed as

$$\vec{V}_{ref} = \left|\vec{V}_{ref}\right| e^{j\omega_{ref}t} = \left|\vec{V}_{ref}\right|(\cos\omega_{ref}t + j\sin\omega_{ref}t) \qquad\qquad (4.15)$$

and the projections of $\vec{V}_{ref}$ on the real and imaginary axis is illustrated in Figure 4.11. With the assumption that the sampling period (sampling $\vec{V}_{ref}$) is sufficiently
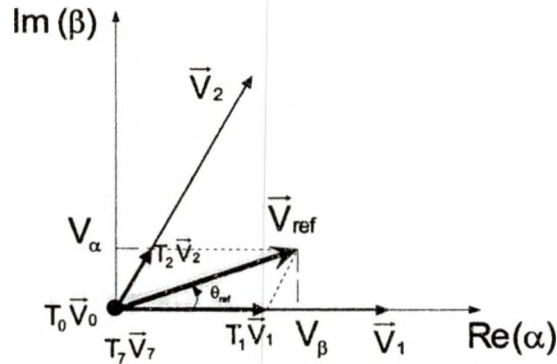
Figure 4.11: Projections of the Rotating Vector in the Complex Plane

small, the average value of the reference space vector ($\vec{V}_{ref,avg}$) can be considered to be approximately constant during this period [17]. The space vector modulation technique is based on the fact that every vector ($\vec{V}_{ref}$) inside each sector of the hexagon can be expressed as a weighted combination of one or more space vectors. Therefore the required $\vec{V}_{ref}$ in sector 1 can be attained by toggling among these four space vectors ($\vec{V}_0, \vec{V}_1, \vec{V}_2, \vec{V}_7$). The key to the space vector modulation is to determine the on-time durations for each of the inverter states or of the space vectors. These times may be calculated by setting the desired average voltage ($\vec{V}_{ref,avg}$) equal to the average of the combination of applied voltages, which are the time averaged space vectors or the inverter states. If the number of sectors is denoted by n then $\vec{V}_n$ and $\vec{V}_{n+1}$ are the two adjacent space vectors with on-times T_n and T_{n+1}. T_0 and T_7 are the total on-times of the null-state space vectors. Assume $\vec{V}_{ref}$ to be the desired space vector in sector n. Then the on-times for each state (how long to apply each space vector) can be calculated from the following relation [17],

$$\vec{V}_{ref,avg} = \left(\vec{V}_0 + \vec{V}_n + \vec{V}_{n+1} + \vec{V}_7\right)_{avg} \qquad (4.16)$$

Equation (4.16) states that within each approximating period (T_{PWM}), the space

vectors, $\vec{V}_0, \vec{V}_n, \vec{V}_{n+1}$ and $\vec{V}_7$ achieve the same average voltage as the

approximated reference vector $\vec{V}_{ref}$. The sequence of application of the space
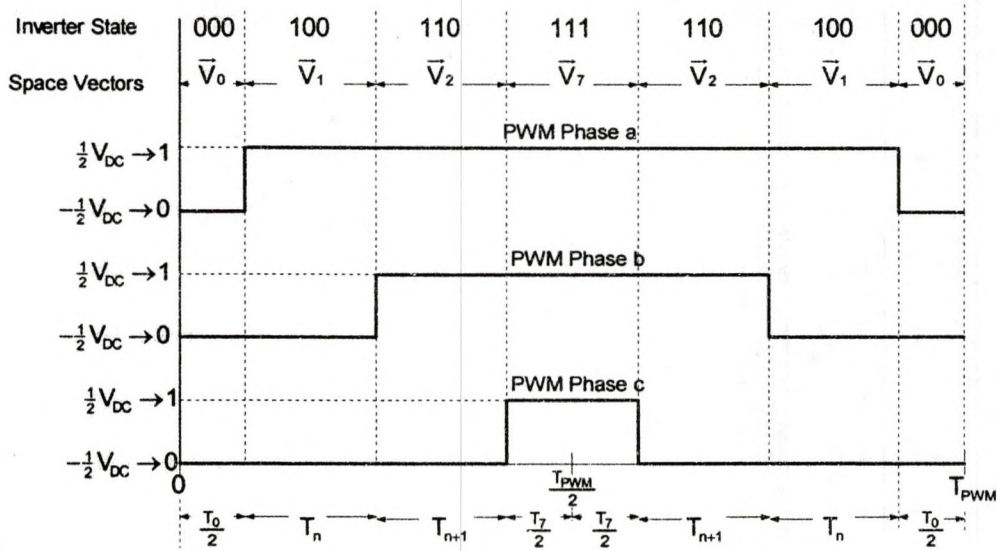
Figure 4.12: PWM Output Signal When the Reference Vector is Sampled in Sector 1

vectors shown in Figure 4.9 is elaborated in Figure 4.12 for n=1. It shows the

sequence and time period of each of the space vectors applied. The next

section will discuss details involved in obtaining the on-times of the active state

space vectors.

4.6 Determination of On-times

As mentioned in the last section, the objective of the SVPWM technique is

to approximate $\vec{V}_{ref}$ (rotating vector) by applying a combination of time averaged

space vectors (inverter states) [27]. To achieve this, for a small sampling time

period ($\vec{V}_{ref}$ approximating period), we let the time averaged inverter output

voltage be equal to the time averaged reference vector ($\vec{V}_{ref,avg}$). Note that the PWM signals in Figure 4.12 are symmetric, thus the on-times are same for the left half and right half of a symmetric PWM signal. Hence, it is sufficient to consider the equation for only one half of the PWM period to determine the on-times of space vectors. Thus, considering the left half of the PWM signal in Figure 4.12, equation (4.16) can be expanded as

$$\frac{1}{\frac{1}{2}T_{PWM}} \int\limits_{0}^{\frac{1}{2}T_{PWM}} \vec{V}_{ref}\, dt = \frac{1}{\frac{1}{2}T_{PWM}} \left(\int\limits_{0}^{\frac{T_0}{2}} \vec{V}_0\, dt + \int\limits_{\frac{T_0}{2}}^{\frac{T_0}{2}+T_n} \vec{V}_n\, dt + \int\limits_{\frac{T_0}{2}+T_n}^{\frac{T_0}{2}+T_n+T_{n+1}} \vec{V}_{n+1}\, dt + \int\limits_{\frac{T_0}{2}+T_n+T_{n+1}}^{\frac{T_{PWM}}{2}} \vec{V}_7\, dt \right) \quad (4.17)$$

From Figure 4.11, the inverter state 000 ($\vec{V}_0$) and 111 ($\vec{V}_7$) apply zero voltage across the load, thus

$$\int\limits_{0}^{\frac{T_0}{2}} \vec{V}_0\, dt = \int\limits_{\frac{T_0}{2}+T_n+T_{n+1}}^{\frac{T_{PWM}}{2}} \vec{V}_7\, dt = 0 \quad (4.18)$$

With the assumption that the sampling period (period when the space vectors are applied in sequence to approximate $\vec{V}_{ref}$) is very small and the change in $\vec{V}_{ref}$ in this "narrow" interval is negligible and the fact that $\vec{V}_n$ and $\vec{V}_{n+1}$ are constant vectors, equation (4.17) reduces to

$$\vec{V}_{ref} = \frac{1}{\frac{1}{2}T_{PWM}} \left[\vec{V}_n.T_n + \vec{V}_{n+1}.T_{n+1} \right] \Rightarrow \vec{V}_{ref}.\frac{T_{PWM}}{2} = \vec{V}_n.T_n + \vec{V}_{n+1}.T_{n+1} \quad (4.19)$$

The null-state on-times for half the PWM period can be calculated from the fact that

$$\frac{1}{2}T_0 + \frac{1}{2}T_7 = \frac{1}{2}T_{PWM} - (T_n + T_{n+1}) \quad (4.20)$$

Next, as shown earlier in Figure 4.5, the six active-state space vectors can be

expressed compactly as

$$\vec{V}_n = \frac{2}{3} V_{DC} e^{j(n-1)60°} \qquad (4.21)$$

where n varies from 1 to 6. From Figure 4.11 $\vec{V}_{ref}$ can be expressed as

$$\vec{V}_{ref} = \left|\vec{V}_{ref}\right| e^{j\omega_{ref}t} = V_\alpha + jV_\beta \qquad (4.22)$$

Inserting equation (4.21) and equation (4.22) into equation (4.19) gives

$$(V_\alpha + jV_\beta)\frac{T_{PWM}}{2} = \frac{2}{3} V_{DC} e^{j(n-1)60°} T_n + \frac{2}{3} V_{DC} e^{j(n+1-1)60°} T_{n+1}$$

$$\frac{V_\alpha T_{PWM}}{2} + j\frac{V_\beta T_{PWM}}{2} = \frac{2}{3} V_{DC}\left[\cos\left((n-1)60°\right) + j\sin\left((n-1)60°\right)\right]T_n \qquad (4.23)$$

$$+ \frac{2}{3} V_{DC}\left[\cos(n60°) + j\sin(n60°)\right]T_{n+1}$$

Separating the real and imaginary parts and equating the corresponding terms from both sides, the above equation can be expressed in matrix form as

$$\begin{bmatrix} V_\alpha \\ V_\beta \end{bmatrix}\frac{T_{PWM}}{2} = \frac{2}{3} V_{DC}\begin{bmatrix} \cos\left[(n-1)60°\right] & \cos(n60°) \\ \sin\left[(n-1)60°\right] & \sin(n60°) \end{bmatrix}\begin{bmatrix} T_n \\ T_{n+1} \end{bmatrix} \qquad (4.24)$$

The Inverse of equation (4.24) gives the expressions for the active-state on-times T_n and T_{n+1}

$$\begin{bmatrix} T_n \\ T_{n+1} \end{bmatrix} = \frac{\sqrt{3}T_{PWM}}{2V_{DC}}\begin{bmatrix} \sin(n60°) & -\cos(n60°) \\ -\sin\left[(n-1)60°\right] & \cos\left[(n-1)60°\right] \end{bmatrix}\begin{bmatrix} V_\alpha \\ V_\beta \end{bmatrix} \qquad (4.25)$$

Substituting the reference vector components

$$V_\alpha = \left|\vec{V}_{ref}\right|\cos\omega_{ref}t$$
$$V_\beta = \left|\vec{V}_{ref}\right|\sin\omega_{ref}t \qquad (4.26)$$

into equation (4.25) gives the on-times in terms of the amplitude of the desired

vector $\left|\vec{V}_{ref}\right|$.

$$\begin{bmatrix} T_n \\ T_{n+1} \end{bmatrix} = \frac{\sqrt{3}T_{PWM}\left|\vec{V}_{ref}\right|}{2V_{DC}} \begin{bmatrix} \sin(n60^\circ) & -\cos(n60^\circ) \\ -\sin\left[(n-1)60^\circ\right] & \cos\left[(n-1)60^\circ\right] \end{bmatrix} \begin{bmatrix} \cos\omega_{ref}t \\ \sin\omega_{ref}t \end{bmatrix} \quad (4.27)$$

where

$$\omega_{ref}t = \theta_{ref} = \tan^{-1}\left(\frac{V_\beta}{V_\alpha}\right) \quad (4.28)$$

is the angle of the rotating vector. The inverter states are usually organized such that only one inverter leg is switched in order to toggle from one state to another state. This is achieved if one PWM cycle (PWM time period) begins with a null-state space vector and ends with another null-state space vector. For example in sector 1 of the hexagon in Figure 4.6 the state sequence could be space vectors in the order $\vec{V}_0\vec{V}_1\vec{V}_2\vec{V}_7\vec{V}_2\vec{V}_1\vec{V}_0$ and in sector 2 it could be of the order $\vec{V}_0\vec{V}_3\vec{V}_2\vec{V}_7\vec{V}_2\vec{V}_3\vec{V}_0$. It should be noted that in the odd sectors the active-state sequence is in ascending-descending order whereas in the even sectors it is in descending-ascending order. The number of commutations per cycle will be minimum if in the odd sectors the active state-sequence is an ascending-descending order as follows

$$\vec{V}_0 \rightarrow \vec{V}_n \rightarrow \vec{V}_{n+1} \rightarrow \vec{V}_7 \rightarrow \vec{V}_{n+1} \rightarrow \vec{V}_n \rightarrow \vec{V}_0$$

and in the even sectors it is a descending-ascending order as follows

$$\vec{V}_0 \rightarrow \vec{V}_{n+1} \rightarrow \vec{V}_n \rightarrow \vec{V}_7 \rightarrow \vec{V}_n \rightarrow \vec{V}_{n+1} \rightarrow \vec{V}_0$$

Applying the space vectors in the above fashion ensures that only one commutation is needed when the inverter changes state. As can be seen from

Figure 4.13 there is only three commutations during each of the $\frac{1}{2}T_{PWM}$ period [24]. During the first $\frac{1}{2}T_{PWM}$ period, the inverter state sequence is 000, 100, 110, 111. For example if the space vector ($\vec{V}_1 \rightarrow \vec{V}_2$) sequence in Figure 4.13
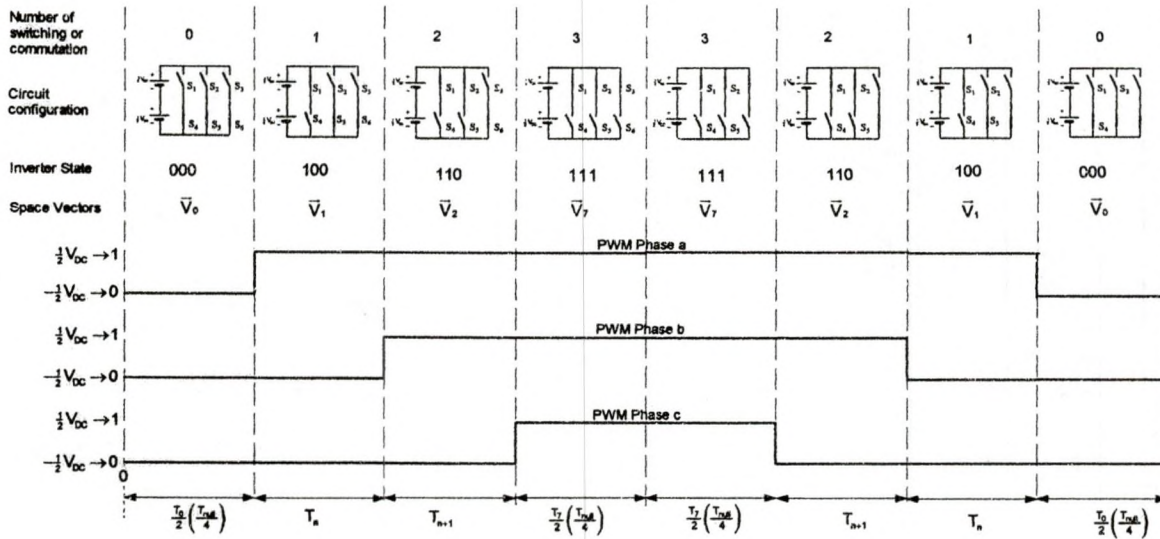
Figure 4.13: Symmetrical PWM Signals and Commutations Per PWM Period in Sector 1

were switched ($\vec{V}_2 \rightarrow \vec{V}_1$) during the first $\frac{1}{2}T_{PWM}$ period, then the corresponding inverter state sequence would be 000, 110, 100, 111. With this choice, the inverter state sequence requires five commutation per $\frac{1}{2}T_{PWM}$ period. Thus, the previous strategy (three commutation per $\frac{1}{2}T_{PWM}$ period) minimizes the number of switching needed (reduce switching frequency) to approximate $\vec{V}_{ref}$ in a PWM period (T_{PWM}) [17]. Therefore, this choice of switching minimizes the current ripple's amplitude at the output [22]. To find the expressions for the active state on times in sector 1, T_1 and T_2 can be evaluated by substituting n=1 in equation (4.27).

$$\begin{bmatrix} T_n \\ T_{n+1} \end{bmatrix} = \frac{\sqrt{3}T_{PWM}|\vec{V}_{ref}|}{2V_{DC}} \begin{bmatrix} \sin(n60°) & -\cos(n60°) \\ -\sin\left[(n-1)60°\right] & \cos\left[(n-1)60°\right] \end{bmatrix} \begin{bmatrix} \cos\omega_{ref}t \\ \sin\omega_{ref}t \end{bmatrix}$$

$$= \frac{\sqrt{3}T_{PWM}|\vec{V}_{ref}|}{2V_{DC}} \begin{bmatrix} \sin(n60°)\cos\omega_{ref}t & - & \cos(n60°)\sin\omega_{ref}t \\ -\sin\left[(n-1)60°\right]\cos\omega_{ref}t & + & \cos\left[(n-1)60°\right]\sin\omega_{ref}t \end{bmatrix}$$

Using the identities sin(x - y) = sinxcosy - cosxsiny and sin(x + y) = sinxcosy + cosxsiny

$$\begin{bmatrix} T_n \\ T_{n+1} \end{bmatrix} = \frac{\sqrt{3}T_{PWM}|\vec{V}_{ref}|}{2V_{DC}} \begin{bmatrix} \sin(n60° - \omega_{ref}t) \\ \sin\left[(n-1)60° + \omega_{ref}t\right] \end{bmatrix}$$

$$\begin{bmatrix} T_1 \\ T_{1+1} \end{bmatrix} = \frac{\sqrt{3}T_{PWM}|\vec{V}_{ref}|}{2V_{DC}} \begin{bmatrix} \sin(60° - \omega_{ref}t) \\ \sin\left[(1-1)60° + \omega_{ref}t\right] \end{bmatrix}$$

$$\begin{bmatrix} T_1 \\ T_2 \end{bmatrix} = \frac{\sqrt{3}T_{PWM}|\vec{V}_{ref}|}{2V_{DC}} \begin{bmatrix} \sin(60° - \omega_{ref}t) \\ \sin\omega_{ref}t \end{bmatrix}$$

$$(4.29)$$

Therefore the average pole voltages over one PWM period can be calculated from the PWM waveforms of Figure 4.13

$$V_{a0}(\omega_{ref}t) = \frac{V_{DC}}{2T_{PWM}}(-\tfrac{T_0}{2} + T_1 + T_2 + T_7 + T_2 + T_1 - \tfrac{T_0}{2})$$

$$V_{b0}(\omega_{ref}t) = \frac{V_{DC}}{2T_{PWM}}(-\tfrac{T_0}{2} - T_1 + T_2 + T_7 + T_2 + T_1 - \tfrac{T_0}{2})$$ $$(4.30)$$

$$V_{c0}(\omega_{ref}t) = \frac{V_{DC}}{2T_{PWM}}(-\tfrac{T_0}{2} - T_1 - T_2 + T_7 - T_2 - T_1 - \tfrac{T_0}{2})$$

As shown in equation (4.14), $T_{null} = T_0 + T_7$. The total null-state time is divided

equally between T_0 and T_7. Therefore substituting $\frac{T_0}{2} = \tfrac{1}{4}T_{null}$, $T_7 = \tfrac{1}{2}T_{null}$ and

substituting for T_1 and T_2 obtained from equation (4.29) gives

$$V_{a0}(\omega_{ref}t) = \frac{V_{DC}}{2T_{PWM}}\left(-\cancel{\tfrac{1}{4}T_{null}} + \frac{\sqrt{3}T_{PWM}|\bar{V}_{ref}|}{2V_{DC}}\sin(60° - \omega_{ref}t) + \frac{\sqrt{3}T_{PWM}|\bar{V}_{ref}|}{2V_{DC}}\sin\omega_{ref}t + \right.$$

$$\left. \cancel{\tfrac{1}{2}T_{null}} + \frac{\sqrt{3}T_{PWM}|\bar{V}_{ref}|}{2V_{DC}}\sin\omega_{ref}t + \frac{\sqrt{3}T_{PWM}|\bar{V}_{ref}|}{2V_{DC}}\sin(60° - \omega_{ref}t) - \cancel{\tfrac{1}{4}T_{null}}\right)$$

$$V_{b0}(\omega_{ref}t) = \frac{V_{DC}}{2T_{PWM}}\left(-\cancel{\tfrac{1}{4}T_{null}} - \frac{\sqrt{3}T_{PWM}|\bar{V}_{ref}|}{2V_{DC}}\sin(60° - \omega_{ref}t) + \frac{\sqrt{3}T_{PWM}|\bar{V}_{ref}|}{2V_{DC}}\sin\omega_{ref}t + \right.$$

$$\left. \cancel{\tfrac{1}{2}T_{null}} + \frac{\sqrt{3}T_{PWM}|\bar{V}_{ref}|}{2V_{DC}}\sin\omega_{ref}t - \frac{\sqrt{3}T_{PWM}|\bar{V}_{ref}|}{2V_{DC}}\sin(60° - \omega_{ref}t) - \cancel{\tfrac{1}{4}T_{null}}\right) \tag{4.31}$$

$$V_{c0}(\omega_{ref}t) = \frac{V_{DC}}{2T_{PWM}}\left(-\cancel{\tfrac{1}{4}T_{null}} - \frac{\sqrt{3}T_{PWM}|\bar{V}_{ref}|}{2V_{DC}}\sin(60° - \omega_{ref}t) - \frac{\sqrt{3}T_{PWM}|\bar{V}_{ref}|}{2V_{DC}}\sin\omega_{ref}t + \right.$$

$$\left. \cancel{\tfrac{1}{2}T_{null}} + \frac{\sqrt{3}T_{PWM}|\bar{V}_{ref}|}{2V_{DC}}\sin\omega_{ref}t - \frac{\sqrt{3}T_{PWM}|\bar{V}_{ref}|}{2V_{DC}}\sin(60° - \omega_{ref}t) - \cancel{\tfrac{1}{4}T_{null}}\right)$$

Simplifying the algebra reduces the above equations to

$$V_{a0}(\omega_{ref}t) = \frac{\sqrt{3}|\bar{V}_{ref}|}{2}\sin(\omega_{ref}t + 60°)$$

$$V_{b0}(\omega_{ref}t) = \frac{3|\bar{V}_{ref}|}{2}\sin(\omega_{ref}t - 60°) \tag{4.32}$$

$$V_{c0}(\omega_{ref}t) = -\frac{\sqrt{3}|\bar{V}_{ref}|}{2}\sin(\omega_{ref}t + 60°)$$

A MATLAB™ plot of the three-phase pole voltages (duty ratios) for $0° \le \omega t \le 360°$ is shown in Figure 4.14. The horizontal axis represents the six intervals corresponding to six sectors of the hexagon of Figure 4.6. The inverter line voltages are obtained as follows:

$$V_{ab}(\omega_{ref}t) = V_{a0}(\omega_{ref}t) - V_{b0}(\omega_{ref}t) = \sqrt{3}|\vec{V}_{ref}|\sin(\omega_{ref}t + 60°)$$

$$V_{bc}(\omega_{ref}t) = V_{ab}(\omega_{ref}t - 120°) \tag{4.33}$$

$$V_{ca}(\omega_{ref}t) = V_{ab}(\omega_{ref}t - 240°)$$

where $0 \le \omega_{ref}t \le 360°$. The MATLAB™ plot of the inverter line-to-line voltages is shown in Figure 4.15.
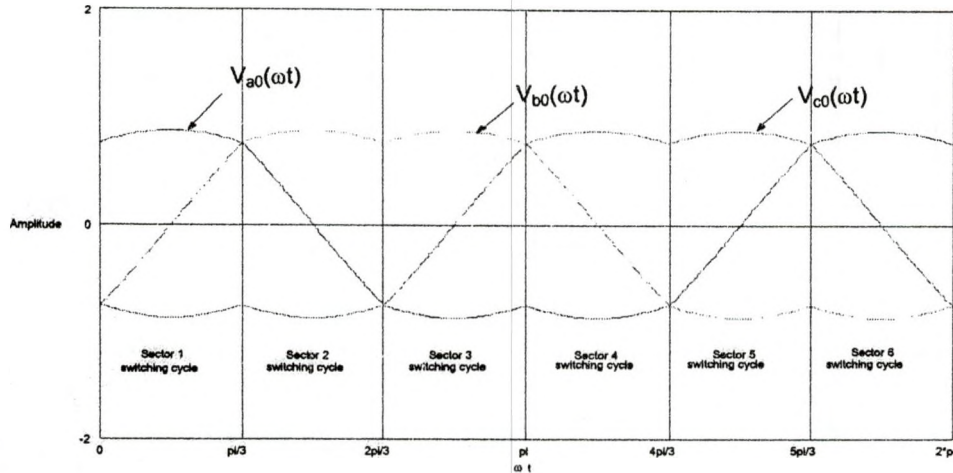
Figure 4.14:Pole Voltages (Duty Ratio) MATLAB™ Plot
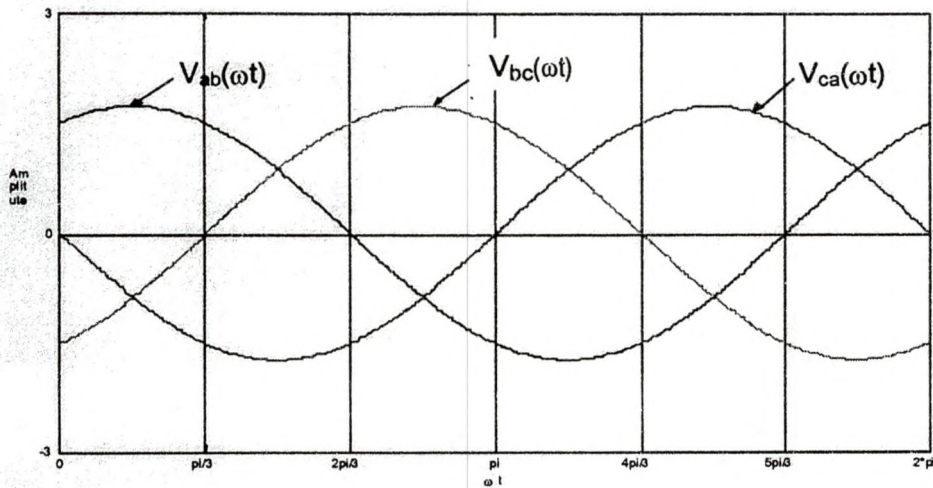
Figure 4.15: Line Voltages MATLAB™ Plot

4.7 Inverter Efficiency

Figure 4.16 illustrates the space vector hexagon with two concentric circles. The smaller circle's radius represents the sine wave PWM maximum achievable reference vector magnitude and the larger circle's radius represents the SVPWM maximum achievable reference vector magnitude. In a sine wave PWM the maximum magnitude of the reference vector is inside of a circle

with a radius of [20]

$$V_{max\,sin} = \frac{V_{DC}}{2} \tag{4.34}$$

In SVPWM it was shown that the length of each space vector is $\frac{2}{3}V_{DC}$. In steady state operation the reference vector magnitude is constant and causes the SVPWM reference vector locus to form a circle with a radius equal to $\left|\vec{V}_{ref}\right|_{max}$ inscribed within the hexagon. The reference vector traces a circular path in the complex plane with an angular velocity ω_{ref}. Each side of the hexagon's midpoint
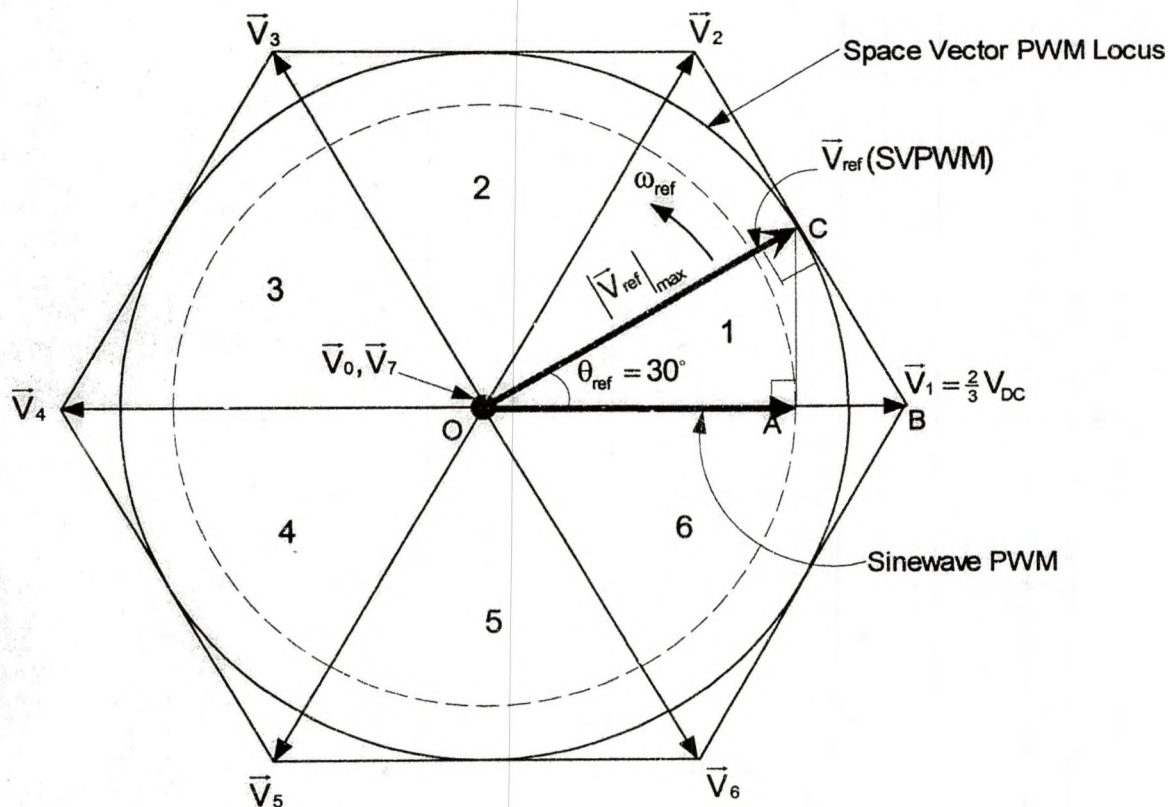
Figure 4.16: Locus of SVPWM vs Locus of Sine Wave PWM

is tangential to the largest circle inscribed in the hexagon. Thus, the largest possible magnitude of reference voltage can be determined from Figure 4.16 as

follows.

$$\cos\theta_{ref} = \frac{OC}{OB} = \frac{\left|\vec{V}_{ref}\right|_{max}}{\left|\vec{V}_1\right|} \tag{4.35}$$

$$\left|\vec{V}_{ref}\right|_{max} = \left|\vec{V}_1\right|\cos30° = \frac{2}{3}V_{DC}\cos30° = \frac{1}{\sqrt{3}}V_{DC}$$

It was noted that the maximum realizable fundamental line-to-neutral voltagewaveform can be generated under the six-step operation. However, this switching strategy is accompanied by a significantly low frequency distortion. From Fourier analysis of equation (4.12) the fundamental frequency voltage amplitude of the six-step waveform is:

$$V_{max\,sixtep} = V_{1,L-N} = \frac{4V_{DC}}{(1)\pi}\cos\left((1)\frac{\pi}{3}\right) = \frac{4V_{DC}}{\pi}\left(\frac{1}{2}\right) = \frac{2V_{DC}}{\pi} \tag{4.36}$$

Therefore the sine wave inverter efficiency compared to the inverter capability in a six-step operation (the maximum fundamental voltage that a three-phase inverter can produce) is:

$$\text{Efficiency} = \frac{V_{max\,sin}}{V_{max\,sixtep}} = \frac{\frac{V_{DC}}{2}}{\frac{2V_{DC}}{\pi}} \times 100\% = 78.5\% \tag{4.37}$$

In general, if the SVPWM process requires generating balanced three-phase line voltages of magnitude $\left|\vec{V}_{ref}\right|$ and frequency ω_{ref} given by [17]:

$$V_{ab}(\omega_{ref}t) = \left|\vec{V}_{ref}\right|\sin(\omega_{ref}t)$$

$$V_{bc}(\omega_{ref}t) = \left|\vec{V}_{ref}\right|\sin(\omega_{ref}t - 120°) \tag{4.38}$$

$$V_{ca}(\omega_{ref}t) = \left|\vec{V}_{ref}\right|\sin(\omega_{ref}t - 240°)$$

then the corresponding rotating vector can be expressed as:

$$\vec{V}_{ref} = \left|\vec{V}_{ref}\right| e^{j\omega_{ref}t} = \left|\vec{V}_{ref}\right|(\cos\omega_{ref}t + j\sin\omega_{ref}t) \tag{4.39}$$

The modulation index is defined as the ratio of the desired peak fundamental frequency magnitude to the highest fundamental frequency output voltage possible in the six step mode (inverter capability)

$$m_a = \frac{\left|\vec{V}_{ref}\right|}{V_{max\,sixstep}} = \frac{\left|\vec{V}_{ref}\right|}{\dfrac{2V_{DC}}{\pi}} = \frac{\pi\left|\vec{V}_{ref}\right|}{2V_{DC}} \tag{4.40}$$

By inserting values for the definition of modulation index into equation (4.40), the corresponding maximum modulation index is

$$m_{a,max} = \frac{\left|\vec{V}_{ref}\right|_{max}}{V_{max,sixstep}} = \frac{\dfrac{1}{\sqrt{3}}V_{DC}}{\dfrac{2}{\pi}V_{DC}} = \frac{\pi}{2\sqrt{3}} = 0.906 \tag{4.41}$$

Therefore the maximum peak fundamental magnitude that may be achieved with the SVPWM technique is 90.6% of the inverter capability compared to sine wave PWM which is 78.5% efficient. The percentage increase in the inverter fundamental frequency output voltage of the SVPWM technique compared to the sine wave PWM technique is

$$\%\,increase = \frac{90.6 - 78.5}{78.5} = 15.4\% \tag{4.42}$$

From equation (4.11) the maximum attainable step voltage (line voltage) in the six-step mode is

$$V_{ab} = V_{an} - V_{bn} = \frac{2}{3}V_{DC} - \left(-\frac{1}{3}V_{DC}\right) = V_{DC} \tag{4.43}$$

From equation (4.40), the reference voltage magnitude can be written as

$$\left|\vec{V}_{ref}\right| = m_a V_{max\,sixstep} = m_a \frac{2V_{DC}}{\pi} \tag{4.44}$$

Where $V_{max\,sixstep}$ is the maximum fundamental frequency output voltage in six-step

mode. Substituting equation (4.44) into equation (4.27) results in

$$\begin{bmatrix} T_n \\ T_{n+1} \end{bmatrix} = \frac{\sqrt{3}m_a T_{PWM}}{\pi} \begin{bmatrix} \sin(n.60°) & -\cos(n.60°) \\ -\sin\left[(n-1).60°\right] & \cos\left[(n-1).60°\right] \end{bmatrix} \begin{bmatrix} \cos\omega_{ref}t \\ \sin\omega_{ref}t \end{bmatrix} \tag{4.45}$$

The switching times computation of the on times does not require the knowledge

of the input voltage source (V_{DC}) but depends only on the desired value of the

modulation index m_a [17].

4.8 Multi-phase Space Vector Inverter Analysis

The purpose of this analysis is to provide a comprehensive investigation of

a multi-leg, multi-phase inverter and propose techniques for its implementation

[31]. Multi-leg, multi-phase inverters are used in special applications. One

example would be where pole-phase modulation is used to control an induction

motor. A three-phase system has 2^3 space vectors. For a n-phase system there

are 2^n space vectors. These space vectors can be divided into $\frac{(n-1)}{2}$ sets which

correspond to the inverter's load circuit configuration. Within each set there

exists a maximum magnitude subset of space vectors. This section presents

several SVPWM techniques that are based on the use of these vectors. For a

practical example a nine-leg, nine-phase inverter circuit shown in Figure 4.17 is

used. Therefore for a nine-phase inverter there are four ($\frac{9-1}{2}$) load equivalent

circuits (four sets) referred to as 4-5 configuration, 3-6 configuration, 2-7

configuration and 1-8 configuration, as shown in Figure 4.18. For a nine- phase

inverter there are 512 (2^9) space vectors. These space vectors can be divided

into subsets {4-5}, {3-6}, {2-7},{1-8}, according to the load configuration shown
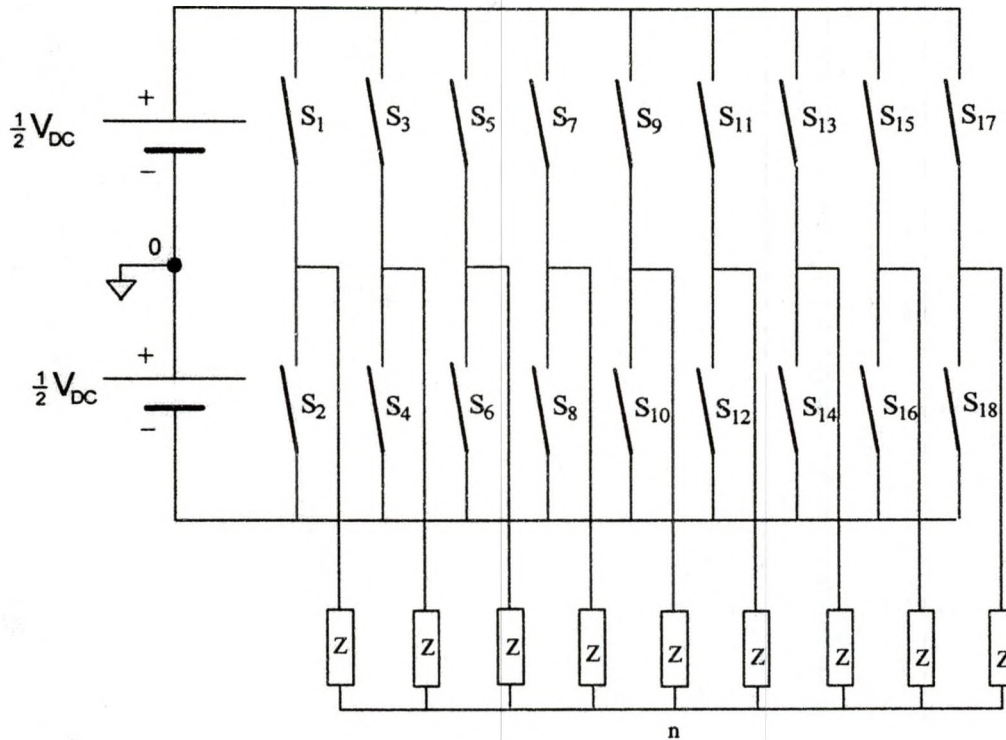
Figure 4.17: Nine-leg Inverter

in Figure 4.18. The four subsets of space vectors generated by the four

equivalent load configurations are shown in Figure 4.19. Each one of these four

equivalent load configurations can be operated to produce a unique eighteen-

step voltage waveform. These waveforms differ in terms of harmonic content

and magnitude of the fundamental component. The resulting fundamental and

harmonic frequency component magnitudes of the four load equivalent circuit

configurations are shown in Table 4.1. Based on the THD figures, the three-

phase inverter is the best. The most inefficient circuit configuration is 1-8 where

more switchings are required to change the voltage level [31].

(a) 4-5 Configuration

(b) 3-6 Configuration

(b) 2-7 Configuration
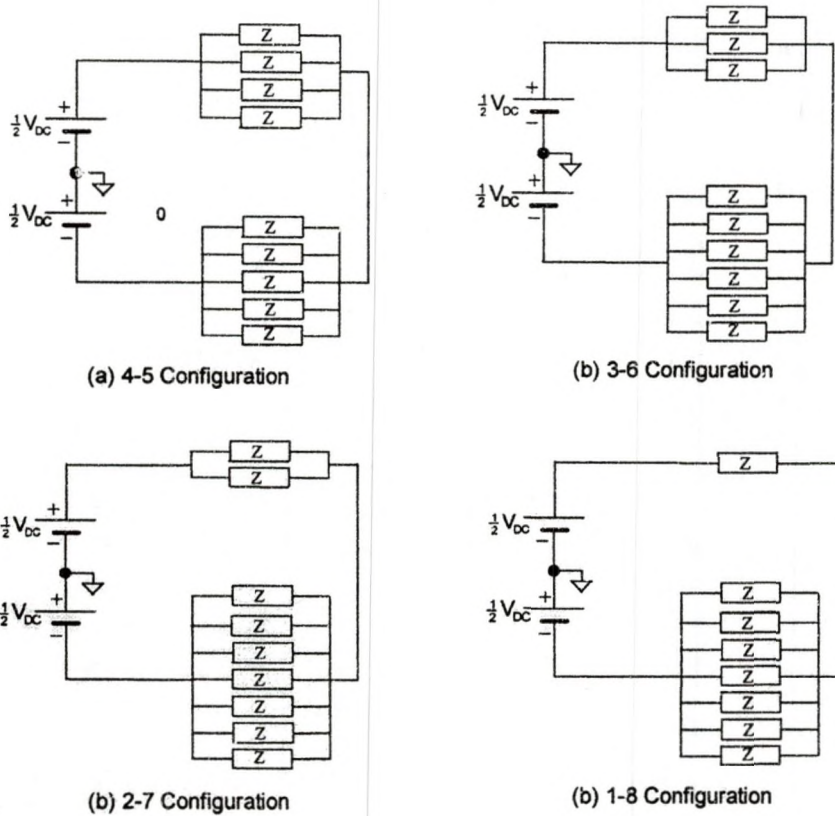
(b) 1-8 Configuration

Figure 4.18: The Four Equivalent Load Configurations of a Nine-Leg Inverter

$\{V_{4-5\ max}\}$

$\{V_{3-6\ max}\}$

$\{V_{2-7\ max}\}$

$\{V_{1-8\ max}\}$
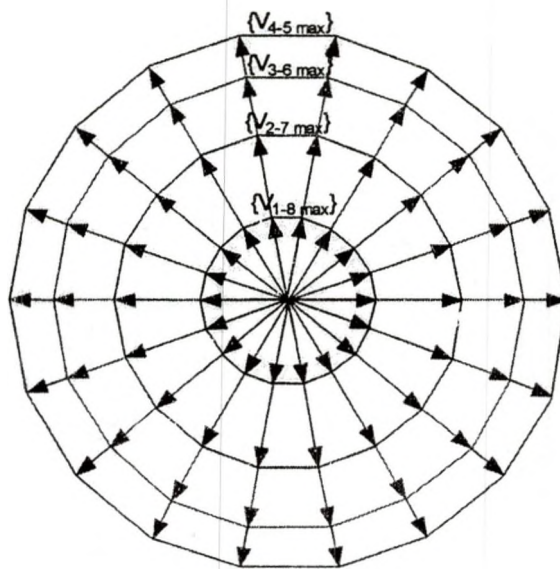
Figure 4.19: The Four Bounding Space Vector Subsets of a Nine-Phase System

Table 4.1 :Harmonic Content of Eighteen-step and Six-step Voltage Waveform

Configuration	f_0	$3f_0$	$5f_0$	$7f_0$	THD
3-phase	0.6366	0	0.1273	0.0909	24.6%
4-5	0.6366	0.2212	0.1273	0.0909	42.6%
3-6	0.5598	0	0.1715	0.2303	26.3%
2-7	0.4155	0.2122	0.0677	0.2619	82.7%
1-8	0.2211	0.2122	0.1951	0.1709	152%

4.9 Extension Of Three-phase SVPWM To n-phase SVPWM

The three-phase SVPWM waveform has a higher DC bus utilization compared to the sine wave PWM waveform. By injecting the third harmonic into the reference voltage signal (the modulating signal), the fundamental frequency component of the phase voltage can be increased [31]. SVPWM is implemented by averaging the time spent by space vectors in adjacent switching states. In Figure 4.11 the reference vector is realized by applying $\vec{V}_0$ for a fraction of time T_0, $\vec{V}_1$ for a fraction of time T_1, $\vec{V}_2$ for a fraction of time T_2, and $\vec{V}_7$ for a fraction of time T_7. The resulting PWM waveforms were shown in Figure 4.12. The disadvantage of using this algorithm is the intensive trigonometric calculations needed. Therefore a method is proposed to simplify the implementation. In this method the third harmonic injection is accomplished by adding a 'voltage offset' to the reference (modulating) voltage signal. This technique requires only addition and multiplication operations therefore can be extended to the n-phase system.

For an n-phase system, the nth harmonic signal is injected by adding the nth harmonic offset to the reference voltage signal . This algorithm is implemented using a DSP processor, a field programmable gate array (FPGA), a nine-phase inverter, and a nine-phase load. The results show that the ninth order harmonic is present in the phase voltages. This harmonic injection increases the fundamental frequency content of the waveform but is filtered in the nine-phase load. However, the fundamental frequency component output is 0.507V whereas for the three-phase system the fundamental frequency component output is 0.577 V with the third harmonic injection. As the number of phases increase, the magnitude of the voltage offset decreases to zero and SVPWM converges to sine wave PWM. Therefore an extension of the conventional three-phase SVPWM to higher order phase systems results in a lower utilization of the DC bus voltage. In order to improve the phase voltage fundamental frequency component in an n-phase system, the following techniques are proposed [31].

Low Order Harmonic Injection

This technique treats the multi-phase system as a sum of lower phase systems. For example in the case of a nine-phase system, the nine-phase system is treated as three three-phase systems displaced by 40°, each producing one-third of the total space vector voltage. The conventional three-phase SVPWM is applied to each of the three systems to realize the voltage command. Lower order harmonic injection allows for the $\sqrt{n}$ order harmonics to be injected into an n-phase system. The result is an increased fundamental

frequency output voltage due to lower order harmonic injection. However $\sqrt{n}$ separate neutrals have to be used because operating with one neutral results in significant phase current harmonic distortion.

SVPWM Using Maximum Subsets

This technique utilizes the fact that a multi-phase system has more than one equivalent load configuration. Along with the zero space vectors, this technique uses only space vectors from a maximum subset (or a combination of maximum subsets) to realize the desired voltage. For example if the space vectors from a maximum subset {4-5} ($\{V_{4\text{-}5\,max}\}$, the eighteen outermost space vectors of Figure 4.19) are used, the result is a greater modulation index but increased harmonic content. If some of the space vectors from a maximum subset {3-6} ($\{V_{3\text{-}6\,max}\}$) are included then the harmonic content is reduced but the modulation index is increased.

Modified SVPWM With Adjusted Zero Space Vectors

Like the previous technique (SVPWM using maximum subsets), the Modified SVPWM with adjusted zero space vectors technique uses only a limited number of switching states, however, it does not necessarily use the zero space vector. Only six switches change states during each PWM period, compared to eighteen switches for the SVPWM schemes such as the extension of three-phase SVPWM to n-phase SVPWM and the SVPWM using maximum subsets. This technique greatly improves switching efficiency.

4.10 Motor Background

The speed of an AC motor depends on the frequency of the input power and the number of poles. The synchronous speed in Revolution Per Minute (RPM) is given by the following equation, where the frequency is in hertz:

$$\text{Synchronous Speed (RPM)} = \frac{120 \times \text{Frequency}}{\text{Poles}} \quad (4.46)$$

It can also be shown that the speed of an AC motor can be varied infinitely by changing the frequency [92]. Therefore with the addition of a Variable Frequency Drive, the speed of the motor can be toggled.

The torque developed in a motor is defined as:

$$\text{Torque} = \text{Force} \times \text{Distance} \quad (4.47)$$

and

$$\text{Force} = kB^2 \quad (4.48)$$

where k is some constant and B is the magnetic field. The magnetic field B is related to the flux (ϕ) and the cross-sectional core area (A) by

$$B = \frac{\phi}{A} \quad (4.49)$$

The flux is defined as

$$\phi = k_s \left(\frac{V}{f}\right) \quad (4.50)$$

where k_s is some constant, V is the inverter fundamental line voltage, and f is the frequency of the inverter fundamental line voltage. Substituting equation (4.49) and (4.50) into equation (4.48) gives

$$\text{Force} = k\left(\frac{\phi}{A}\right)^2 = k\left(\frac{k_s\left(\frac{V}{f}\right)}{A}\right)^2 = k_a\left(\frac{V}{f}\right)^2 \qquad (4.51)$$

Therefore in V/Hz control, the speed of induction motor is controlled by adjusting both the magnitude and frequency of stator voltages in such a way that the air gap flux is always maintained at the desired steady-state level [32].

Volts/Hz Relationship

Equation (4.46) says that the speed of the motor can be changed by changing the frequency. However, frequency is not the only item that must be changed in the motor. Figure 4.20 shows the simplified steady-state equivalent circuit model of an induction motor. In steady state operation the stator resistance, R_s, is assumed to be zero. The total leakage inductance (L_T) is the sum of stator and rotor leakage inductances. Therefore the magnetizing current
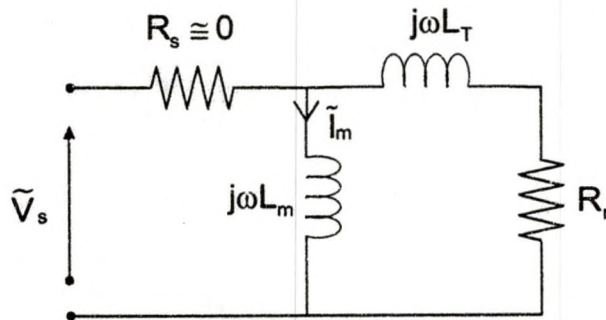
Figure 4.20: Simplified Steady State Equivalent Circuit Model of an Induction Motor

that is responsible for generating the air flux gap can be modelled by the ratio of the stator voltage to frequency. In steady state analysis the corresponding phasor equation is [32].

$$\tilde{I}_m = \frac{\tilde{V}_s}{j\omega L_m} \qquad (4.52)$$

For the motor that is operating in the linear magnetic region, L_m is constant. An expression of equation (4.52), in magnitude form is

$$I_m = \frac{V_s}{\omega L_m} = \frac{V_s}{2\pi f L_m} = K_m \frac{1}{2\pi L_m} \qquad (4.53)$$

where

$$K_m = \frac{V_s}{f} \qquad (4.54)$$

In order to keep K_m constant the ratio of V_s/f must be kept constant at different speeds. For example as the speed increases (frequency increases), the stator voltage (V_s) has to be increased proportionally to maintain the constant V_s/f ratio. The stator voltage frequency represents the synchronous speed (rotating field speed) and not the real motor (rotor) speed. The difference between these two speeds is called slip speed. The slip speed is very small at no load, where the motor speed is close to synchronous speed. As the load increases, the slip speed also increases. Therefore a simple open-loop V_s/f (or V/Hz) system fails to control accurately the speed with the presence of load torque. To rectify this, a slip compensation strategy can be included for speed control. Thus, the result is a closed-loop V/Hz system with a speed sensor as shown in Figure 4.21. A typical V/Hz profile and its basic three speed ranges are shown in Figure 4.22. For the speeds from f_c through f_{rated}, V/Hz are constant. The constant slope represents the air gap flux quantity as shown in equation (4.54). Therefore the speed of the induction motor can be estimated by measuring the stator voltages and stator currents. This type of speed estimator is based on the reactive power Model Reference Adaptive System (MRAS) technique. In this technique the
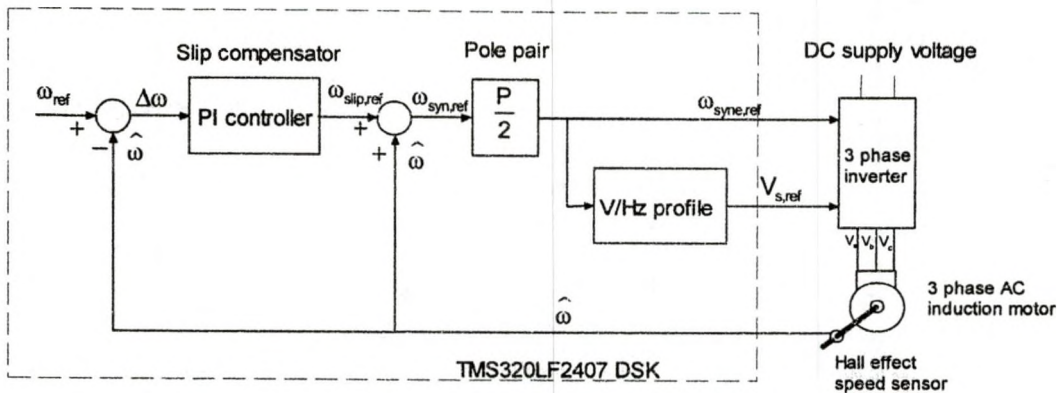
Figure 4.21: Closed-loop V/Hz System With A Speed Sensor
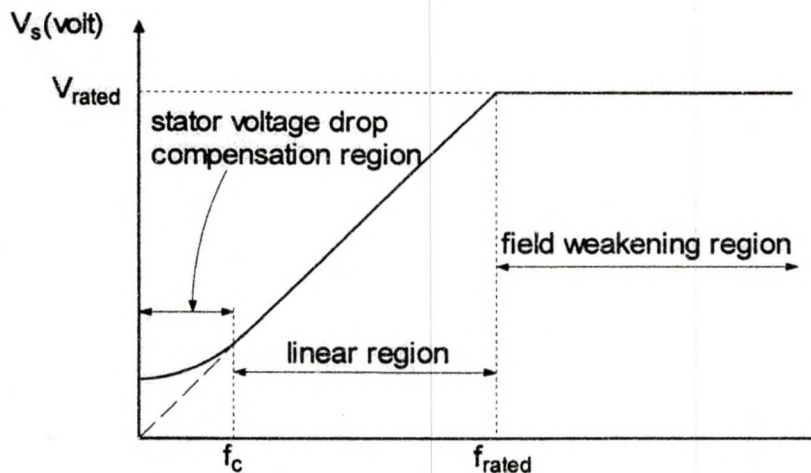
Figure 4.22: Stator Voltage Versus Frequency Profile Under V/Hz Control

required stator voltages and stator currents are measured directly out of the inverter. The stator voltages are indirectly reconstructed from the measured DC-bus voltage and the switching functions. This type of sensorless V/Hz system and closed-loop control using MRAS speed estimator is shown in Figure (4.23) .
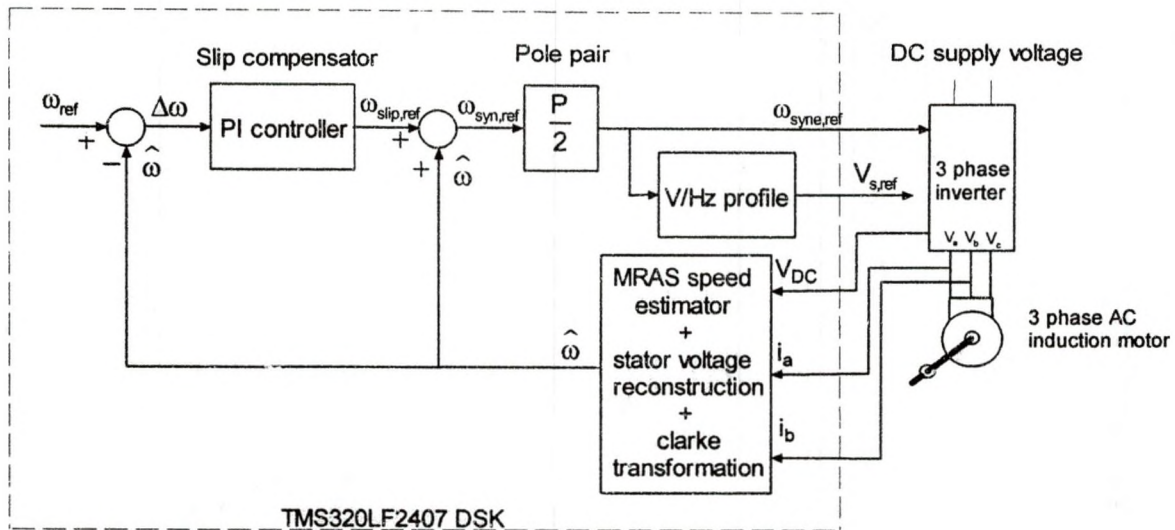
Figure 4.23: A Sensorless V/Hz Closed-Loop Control System

An Overview Of Sensorless Speed Control

Figure 4.24 illustrates the hardware configuration of a sensorless V/Hz system and closed-loop control using MRAS speed estimator. The motor is driven by a voltage source inverter. The TMS320LF2407 DSP that is located on the eZdsp^{TM} (target board) generates six PWM signals that control the power transistors on the DMC 1500 module. Two of the motor phase currents (i_a and i_b) are sensed by the inverter leg resistors and measured by the analog-to-digital converters (ADCs) in TMS320LF2407 DSP. Another ADC channel is used to measure the inverter DC-bus voltage. The DSP calculates the three-phase voltages of the motor based on these three measured parameters. The reactive power MRAS speed estimator module uses the sensed DC voltage and motor phase current inputs to execute speed control without the need of a speed sensor [32].
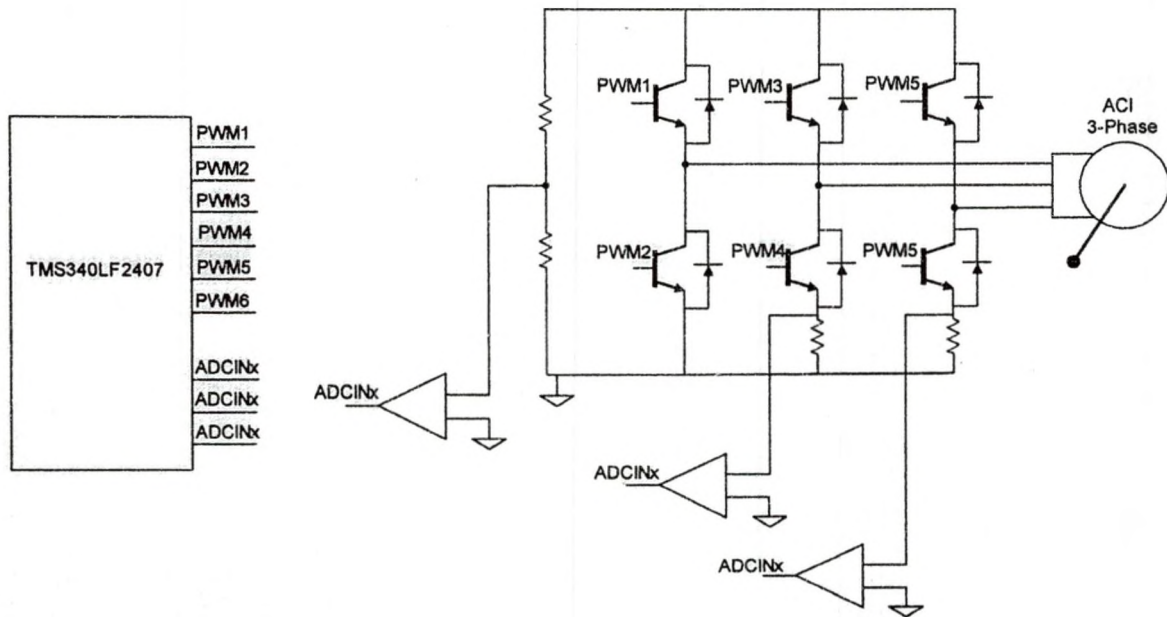
Figure 4.24: A Three-Phase Induction Motor Drive Implementation

CHAPTER 5

SOFTWARE (VisSim™) AND REALTIME (DSP) SIMULATIONS

This chapter presents the experimental procedure, results, analysis, and application of SVPWM in an AC induction motor drive. Experiments were conducted using the commercial development modules such as the DSP controller (eZdsp), Digital Motor Controller (DMC1500), VisSim™/TI C2000 rapid prototyper software package, and a three phase induction motor. VisSim™/TI C2000 rapid prototyper software was used to simulate and generate real-time SVPWM signals [33,34,36,88]. The eZdsp is a development platform based on the Texas Instruments TMS320LF2407 DSP chip, designed and manufactured by Spectrum Digital Incorporated. It was used as a platform to develop and execute the code needed to generate PWM signals. The DMC1500 platform is designed and manufactured by Spectrum Digital Incorporated and utilizes the Texas Instruments eZdsp [43]. This controller board has an AC-to-DC converter that generates a full-wave-rectified and filtered 190-volt DC from an AC supply input of 138V AC at 60 Hz. With proper placement of on-board jumpers, the board can be configured in a voltage doubler mode to generate 320 volts DC if the intended motor application requires the higher voltage [43]. It also has a three-phase power inverter. This power inverter can be configured, with proper placement of jumpers, to drive typical three-phase AC induction motors.

The eZdsp generated PWM signals can be applied to the Digital Motor Controller (DMC1500) to power a three-phase induction motor. SVPWM mathematical expressions that were plotted with MATLAB™ and shown in Figures 4.14 and 4.15 are compared with VisSim™ simulation results. VisSim™ software allows simulation of the power electronic modules by using graphical blocks that represent mathematical functions. The simulation is then converted into a downloadable code file on which the DSP interface block executes on-board the DSP. This feature of VisSim™ makes it possible to validate the behavior of the "simulated" algorithm on the target DSP. The results from DSP controller hardware and the VisSim™ software simulations can be displayed simultaneously in the form of a plot block so they can easily be compared to ensure that their behavior is identical. This ensures that the DSP is feeding the desired signals to the power processor such as the DMC1500. VisSim™ also automatically programs the analog and digital I/Os of the TI TMS320LF2407 (which is a time consuming, tedious task if done manually) [36].

5.1 Volts/Hertz (V/Hz) Profile, Space Vector Generator (SVGEN) and Space Vector PWM (SVPWM)

The VisSim/TI-C2000 Rapid Prototyper includes a "simulation" mode for many of the DMC blocks. The AC induction motor control sub-system has three DMC blocks. These are the Space Vector Generator (SVGEN), Space Vector PWM (SVPWM) and the Volts/Hertz (V/Hz) profile blocks. The compound block shown in Figure 5.1 is composed of these three blocks. These blocks are wired as shown in Figure 5.2. The purposes of these blocks are described as follows:
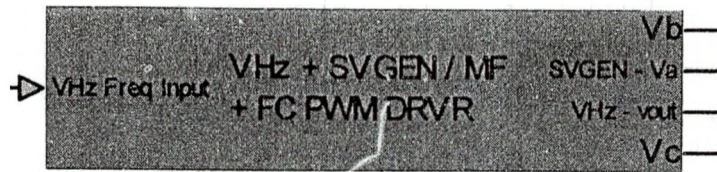
Figure 5.1: Compound Block Composed of TI DMC Blocks
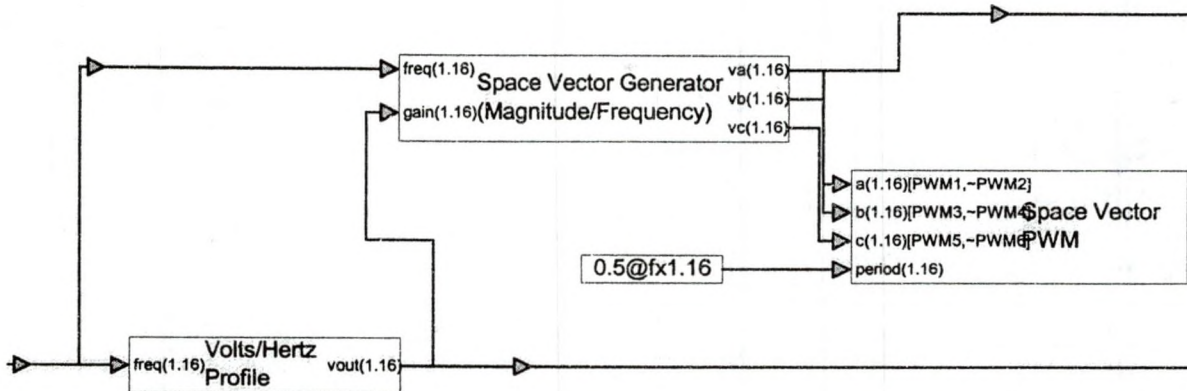
Figure 5.2: SVPWM VisSim™ Model System Block

Volts/Hertz Profile Block

Volts/Hertz profile block shown in Figure 5.3 is a module that generates an output reference voltage for a specific user input frequency, according to the specified Volts/Hertz profile. The user inputs a frequency into the Volts/Hertz profile block as shown in Figure 5.2. The Volts/Hertz profile block then uses this user input frequency to generate a desired reference voltage amplitude, $\left|\vec{V}_{ref}\right|$ so that the constant Volts/Hertz profile is maintained. The Volts/Hertz profile block is a dedicated block that specifies a constant Volts/Hertz profile for various user input frequency [33].

Figure 5.3: Volts/Hertz Profile Block

Space Vector Generator (SVGEN) Block

The Space Vector Generator (SVGEN) block receives the command

inputs $\left|\vec{V}_{ref}\right|$ from the Volts/Hertz profile block and the f_{ref} from the user. These

inputs are the reference vector $\vec{V}_{ref} = \left|\vec{V}_{ref}\right| e^{j\omega_{ref}t}$. The SVGEN block uses $\vec{V}_{ref}$ to

calculate the duty ratio (pole voltage) waveforms shown in MATLAB^{TM} plot

(Figure 4.14). The SVGEN block shown in Figure 5.4 is a module that calculates

the appropriate
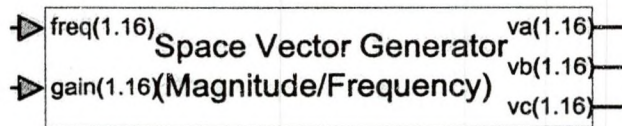
Figure 5.4: Space Vector Generator (Magnitude/Frequency) Block

duty ratios needed to approximate the given $\vec{V}_{ref}$ using the SVPWM technique.

"Freq" and "gain" labeled on the SVGEN block refer to the frequency (f_{ref}) and

amplitude($\left|\vec{V}_{ref}\right|$) of $\vec{V}_{ref}$. "v_a","v_b"and "v_c" refer to the duty ratios (pole voltages)

of PWM1, PWM2 and PWM3.

Space Vector PWM Block

The SVPWM Block shown in Figure 5.5 is a module that uses the

duty ratios (pole voltages such as those in equation (4.30) or (4.32)) from the

SVGEN block and calculates the values for generating PWM outputs (pins 1 – 6).

The SVPWM block basically converts the duty ratio waveforms into PWM

waveforms. These PWM waveforms are the switching pulses shown in Figure

4.13, needed to turn on and turn off the power transistors. PWM outputs 1,3, and

5 control the turn-on and turn-off of the upper power transistors. PWM outputs 2, 4, and 6 control the turn-on and turn-off of the lower power transistors.

```
 ▷ a(1.16)[PWM1,~PWM2]
 ▷ b(1.16)[PWM3,~PWM4]    Space Vector
 ▷ c(1.16)[PWM5,~PWM6]    PWM
 ▷ period(1.16)
```
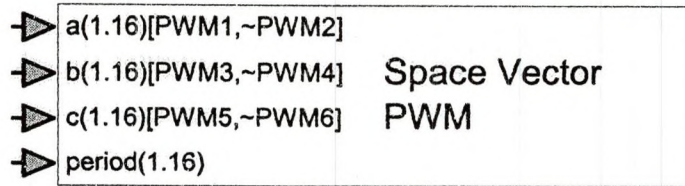
Figure 5.5: Space Vector PWM Block

VisSim[TM] Space Vector Duty Ratio Waveform

Figure 5.6. shows a slider input block followed by convert, compound (TI DMC) and plot block. The V/Hz profile and SVGEN blocks are used to generate the appropriate space vector profile in response to a variation in the slider set point. The desired inverter fundamental output voltage (frequency and amplitude) is dynamically varied using a slider block. A slider block, which is set to produce set points in the range from 0 to 0.8 is connected to a convert block. In this case a slider setpoint of 0.04 is converted into an appropriate data type using a convert block. The converted data is then fed into the compound block which is labeled V/Hz + SVGEN / MF + FC PWM DRVR (TI DMC BLOCKS). The compound block contains the V/Hz profile, SVGEN and SVPWM blocks. The SVPWM block uses the SVGEN block output to generate the appropriate PWM signals. The duty ratio output waveforms of the SVGEN are also connected to analog output ports. One of the three phases (Pole or duty ratio V_a) of the SVGEN and Volts/Hertz profile outputs can be monitored in a plot block as shown in Figure 5.6.

Vary Slider Input | 0.04 | → convert

VHz Freq Input | VHz + SVGEN / MF + FC PWM DRVR | SVGEN - Va | VHz - vout

VisSim Duty Ratio

.009
.007
.005
.003
.001
-.001
-.003
-.005
-.007
-.009
0   .5   1   1.5   2   2.5   3   3.5   4   4.5   5
Time (sec)
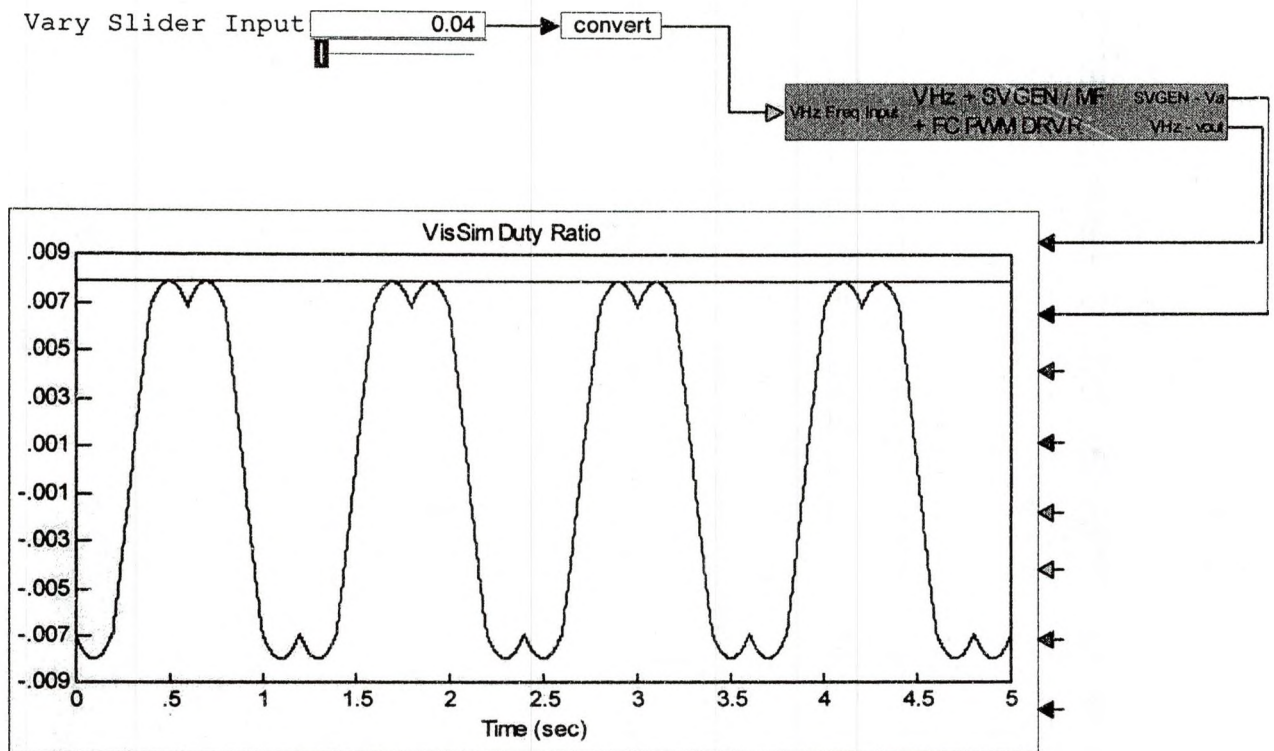
Figure 5.6: VisSim™ Duty Ratio (Pole Voltage) Simulations

The "simulation" mode of VisSim™ allows the DMC blocks (Space Vector Generator, Space Vector PWM and the Volts/Hertz profile blocks) to be executed on the PC host without the need for a DSP target. To test the PC simulation on a DSP target, a DSP interface block is used to download the compiled DMC blocks to the DSP target. VisSim™ automatically generates, compiles and links the code for the DMC blocks. Now the DMC blocks can be executed on-board the DSP—in this case an eZdsp. With this setup the simulated (PC) and compiled version (DSP) of motor control sub-system comprised of V/Hz profile, SVGEN and SVPWM blocks can be run simultaneously and compared using plot blocks, as show in Figure 5.7. The VisSim™ blocks can also be wired to monitor the three-phase duty-ratios (phase voltages) and the line voltage waveforms. Figure

5.8 shows the three-phase duty-ratios and the line voltage waveforms displayed

on the piot block. Apparently the VisSim™ (PC and DSP) generated and
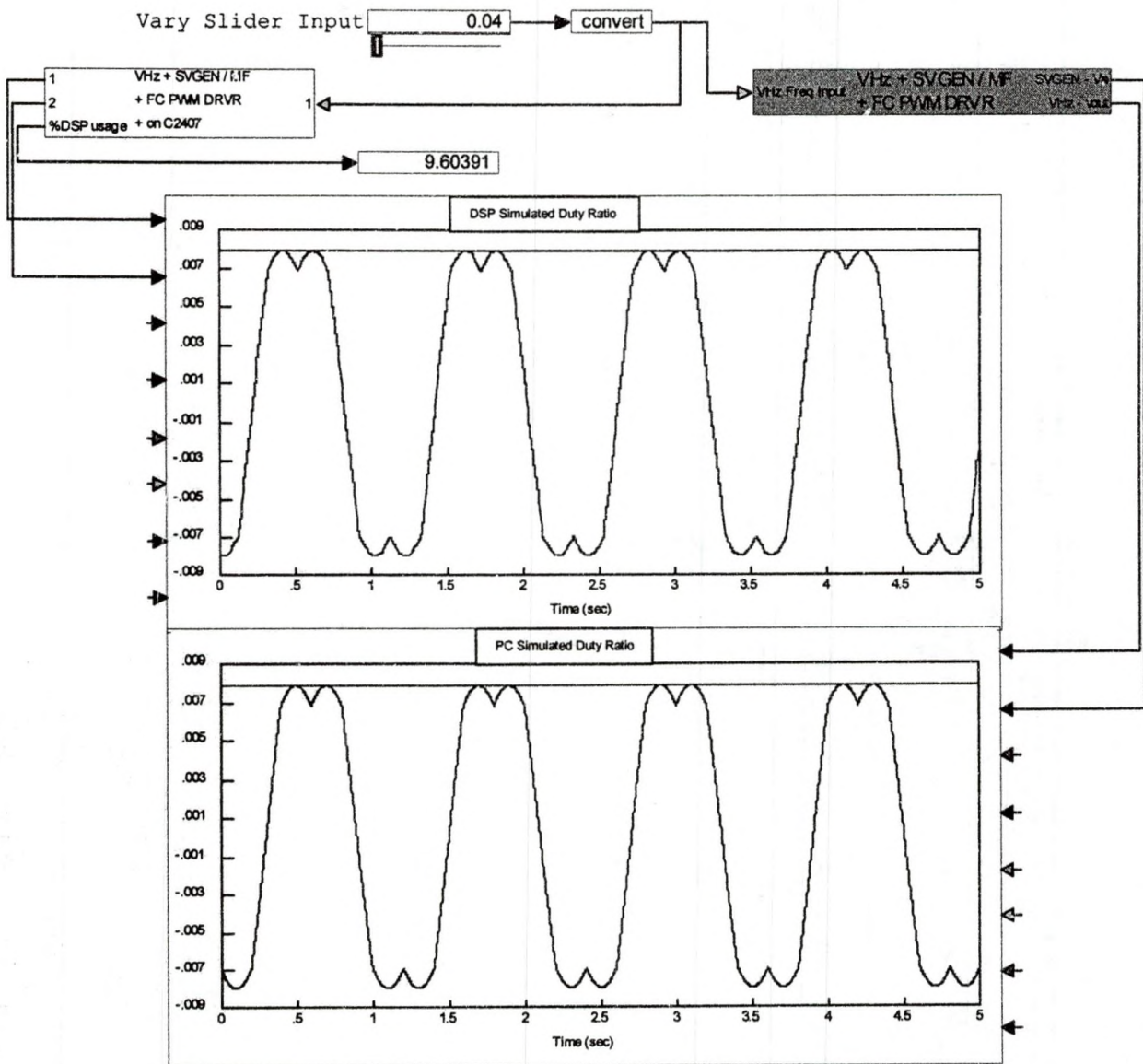
Figure 5.7: DSP and PC Duty Ratio VisSim™ Simulations

MATLAB™ plotted waveforms look identical. The DSP generated waveform

appears to be distorted because there is about 20ms delay imposed by the

communication interface link between the DSP and PC [33].
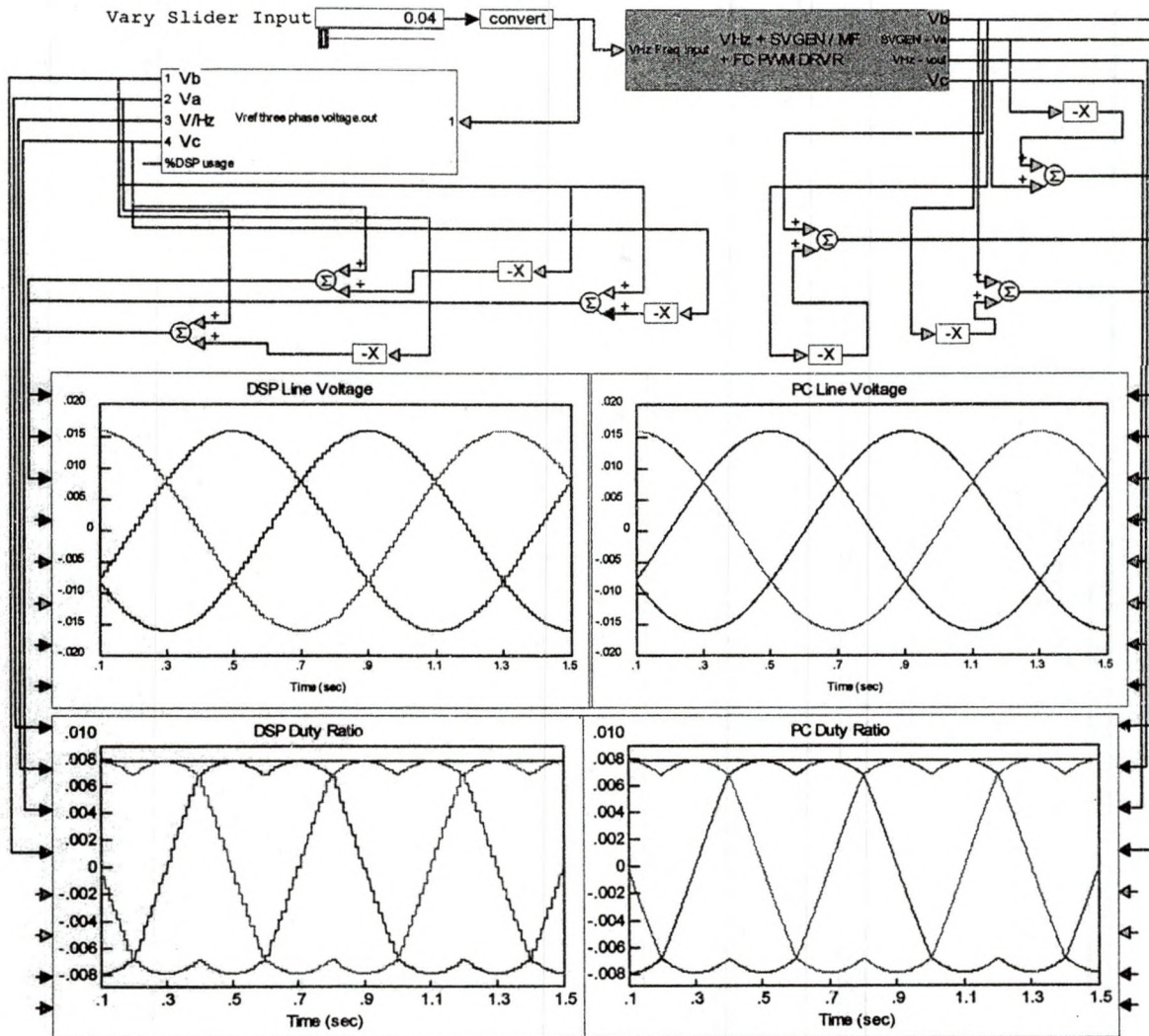
Figure 5.8: DSP and PC Duty Ratio & Line Voltage Simulations

5.2 Rotating Space Vector

The SVPWM for a three-leg voltage source inverter is based on the representation of the three phase quantities as vectors in a two-dimensional α-β plane [29]. As stated in previous chapters, to understand the SVPWM sinusoidal generation process the first thing is to recognize that three phase sinusoidal voltages can be represented by a single rotating vector $\vec{V}_{ref}$ in a complex plane and vice versa, and the rotating vector is composed of α-β components. To practically illustrate this concept, the VisSim™ generated three-phase line-
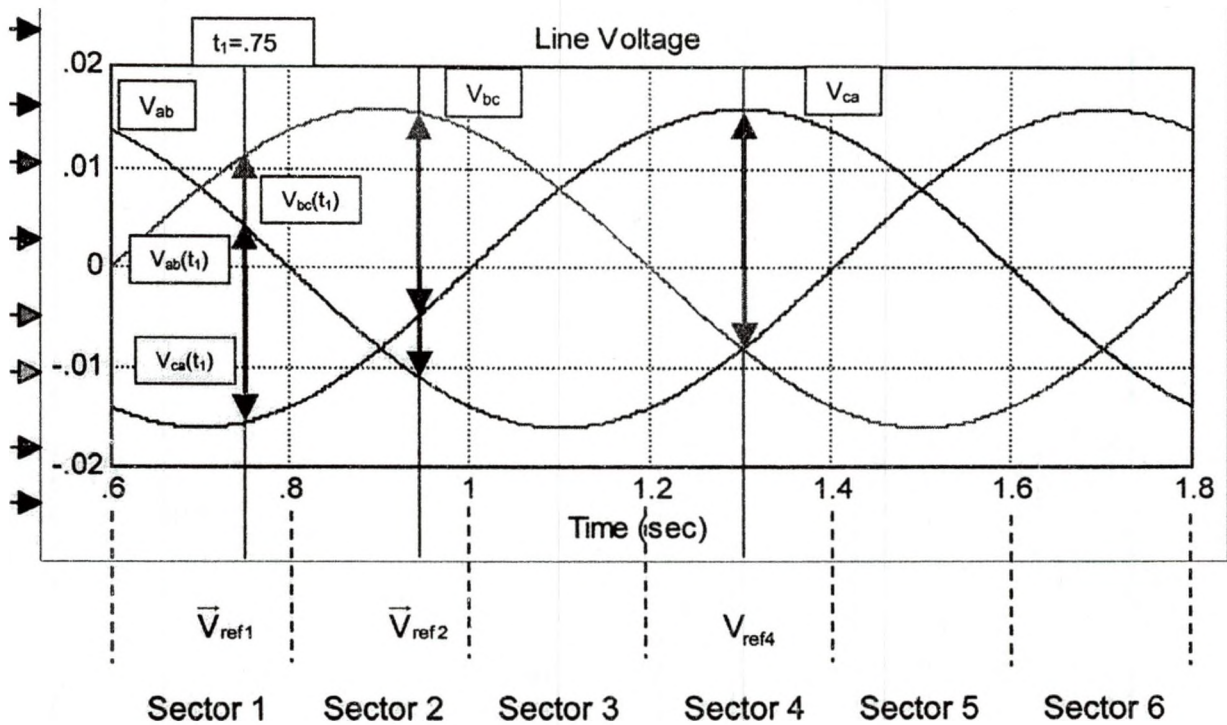
Figure 5.9: VisSim™ Generated Line Voltage Waveforms

voltage waveforms with three snapshots is shown in Figure 5.9. These

waveforms are used to demonstrate how the three-phase quantities in the time

domain can be transformed into a rotating vector in the complex plane. The first

snapshot is taken at $t_1 = .75$ second in the time period $0.6 \leq t \leq 0.8$ second. In

angular terms, $t_1 = .75$ corresponds to $\omega t = 45°$ in the angular period $0 \leq \omega t \leq 60°$.

At $\omega t_1 = 45°$, the phase components $V_{ab}(t_1)$, $V_{bc}(t_1)$ and $V_{ca}(t_1)$ form $\vec{V}_{ref1}$, based

on the definition of a space vector. The construction of $\vec{V}_{ref1}$ is shown in Figure

5.10. Similarly $\vec{V}_{ref2}$ and $\vec{V}_{ref4}$ can be constructed in sector 2 and sector 4,

respectively, as shown in Figure 5.11. It can be seen that the tips of vectors

$\vec{V}_{ref1}$, $\vec{V}_{ref2}$ and $\vec{V}_{ref4}$ are in the path of a circle. If snapshots were taken

continuously for one period, the rotating vector will trace a full circle of constant

radius.
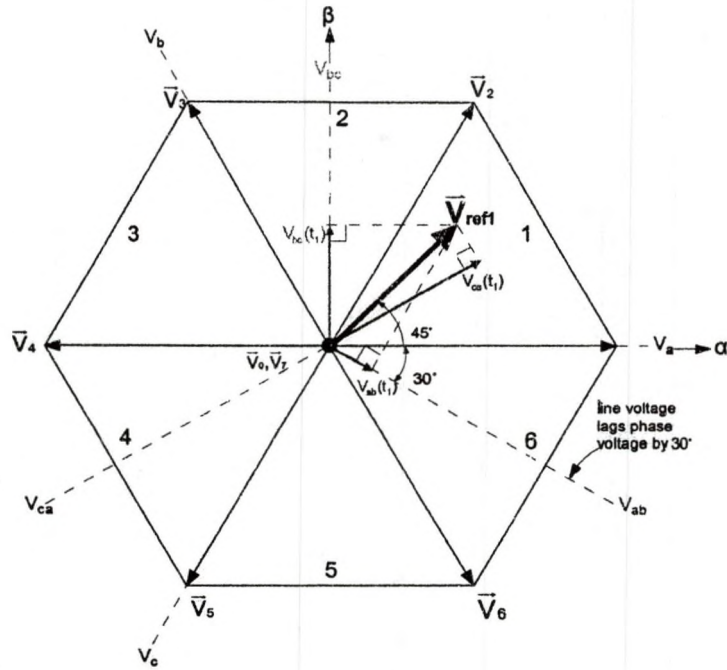
Figure 5.10: Construction of Voltage Vector $\vec{V}_{ref1}$ in Sector 1
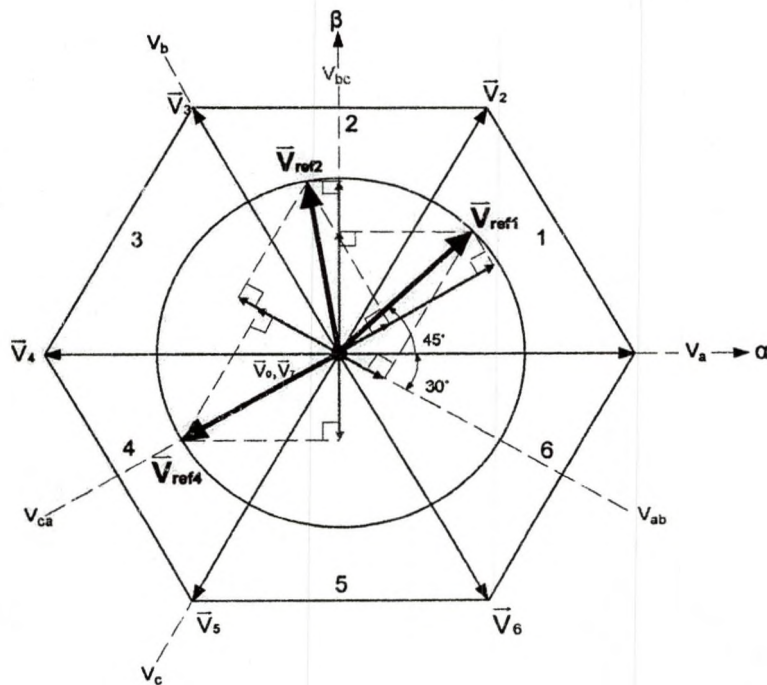
Figure 5.11: Construction of Voltage Vectors $\vec{V}_{ref1}$, $\vec{V}_{ref2}$ and $\vec{V}_{ref4}$

Sampling Rotating Vector
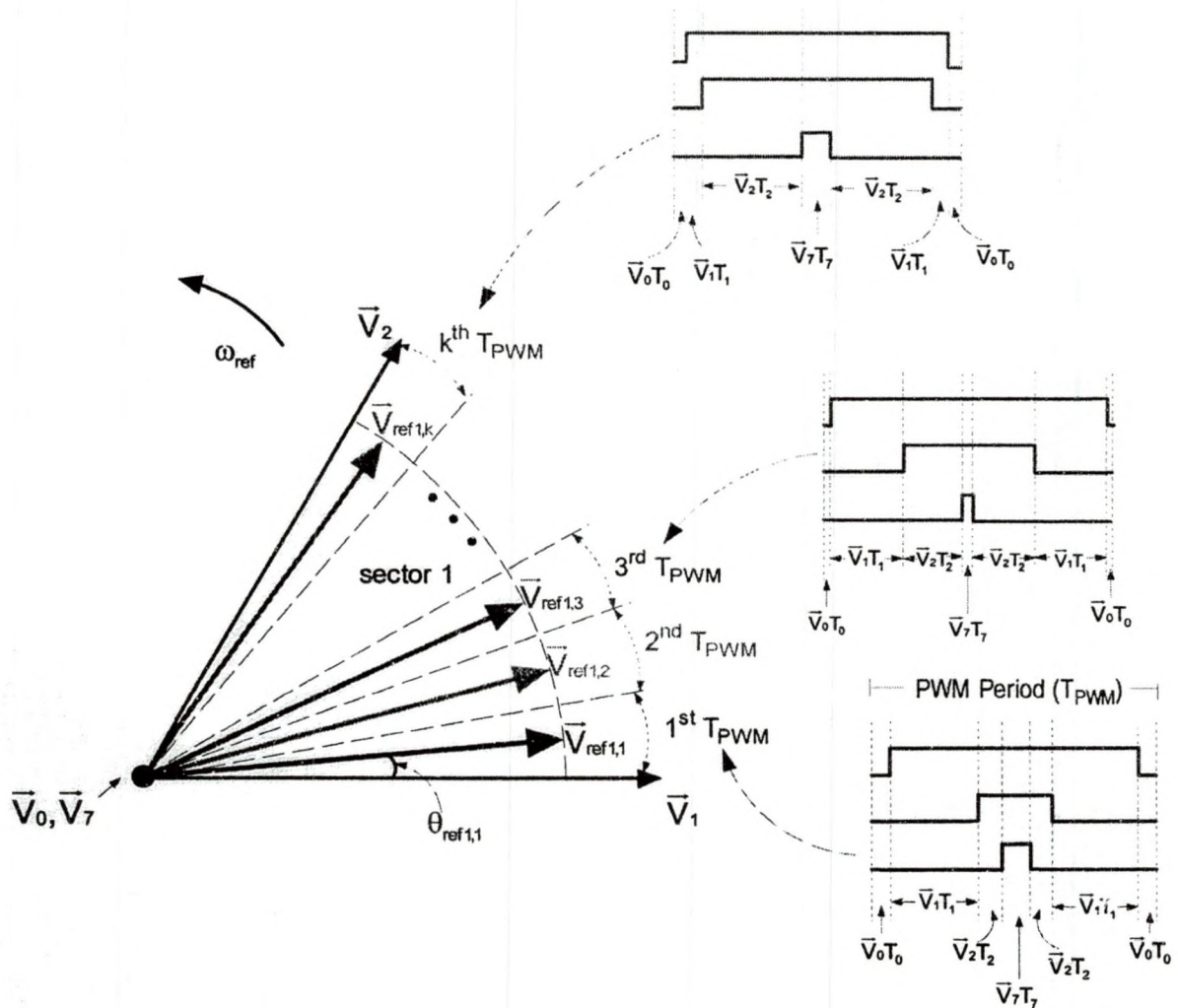
Figure 5.12: Sector Sampling $\vec{V}_{ref1}$ as it Rotates and the Corresponding PWM Waveforms

Figure 5.12 illustrates how the vectors $\vec{V}_{ref1,1}, \vec{V}_{ref1,2} \ldots \vec{V}_{ref1,k}$ are going to be sampled in sector 1 where k is the number of modulation periods (T_{PWM} - PWM period) or sampling periods per sector [35, 45]. As k gets bigger, the number of modulations (sampling) per sector increases. For every rotating vector position ($\vec{V}_{ref1,1}, V_{ref1,2} \ldots V_{ref1,k}$) in sector 1, a unique set of three (phase "a", "b", "c") PWM signals approximate the rotating vector $\vec{V}_{ref1,k}$. This unique set of three-phase PWM signals is the result of the application of time scaled space vectors

$(T_0\vec{V}_0, T_1\vec{V}_1, T_2\vec{V}_2, T_7\vec{V}_7)$. This will be verified from the experimental results in later chapters.

Relationship Between The Rotating Space Vector And The Eight Space Vectors

To determine the relationship between the rotating space vector $(\vec{V}_{ref})$ and the state vectors $(\vec{V}_0, \vec{V}_1 \ldots \vec{V}_n)$, the construction of $\vec{V}_{ref}$ in sector 1 using measured phase components of VisSim^{TM} simulation (line voltages) for a slider set point of 0.2 at $\omega_{ref}t = 45°$ is shown in Figure 5.13. Now the same $\vec{V}_{ref}$ is shown in Figure 5.14 being approximated (sampled) by the time scaled space vectors
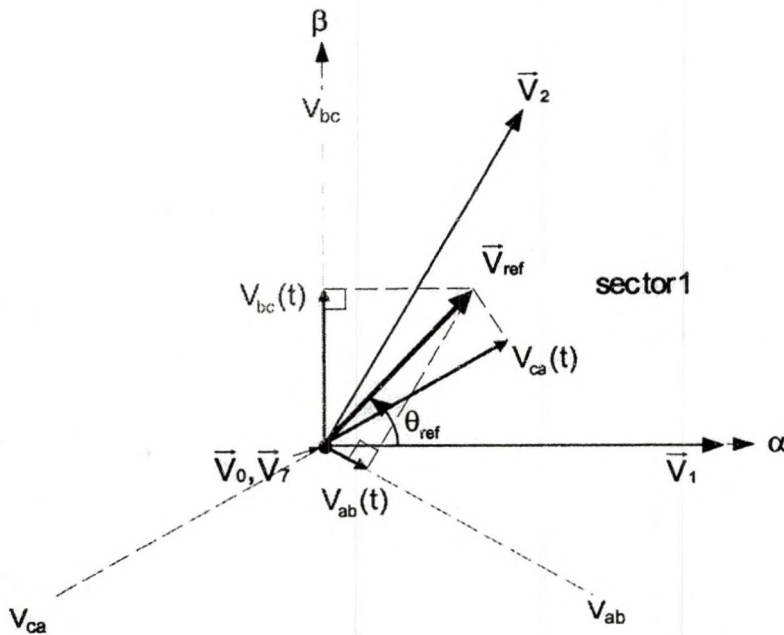
Figure 5.13: Vector Sampling at an Angle θ_{ref} in Sector 1

$(T_0\vec{V}_0, T_1\vec{V}_1, T_2\vec{V}_2, T_7\vec{V}_7)$. During each modulation period, each sampled rotating vector can be expressed using four time scaled space vectors. Therefore, knowing the six switching configurations (inverter states) for each space vector, a time dependent switching sequence can be expressed by equation (4.13) which

is repeated here:

$$\vec{V}_{ref}.T_{PWM} = \vec{V}_0.T_0 + \vec{V}_1.T_1 + \vec{V}_2.T_2 + \vec{V}_7.T_7 \qquad (5.1)$$

The switching time periods (T_0, T_1, T_2, T_7) for the nth sector are then calculated with

the equations that were derived in section 4.6. Figure 5.14 illustrates that $\vec{V}_{ref}$

$$T_1 = \frac{\sqrt{3}T_{PWM}\left|\vec{V}_{ref}\right|}{2V_{DC}}\sin(60° - \omega_{ref}t)$$

$$T_2 = \frac{\sqrt{3}T_{PWM}\left|\vec{V}_{ref}\right|}{2V_{DC}}\sin(\omega_{ref}t) \qquad (5.2)$$

$$T_0 = T_7 = \tfrac{1}{2}\left[T_{PWM} - T_1 - T_2\right]$$
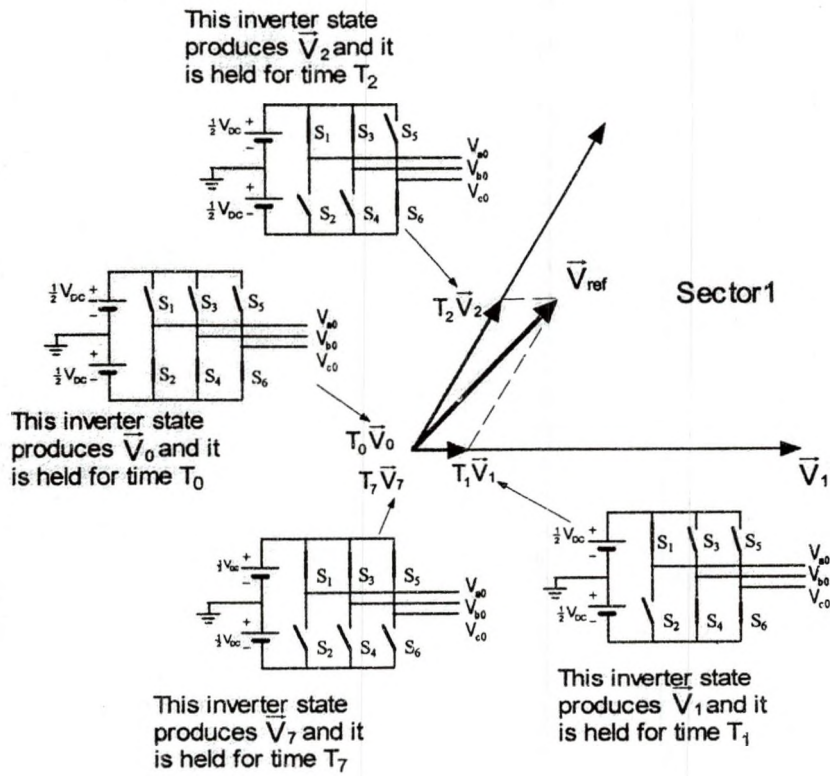
Figure 5.14: $\vec{V}_{ref}$ Sampled by Time Scaled Space Vectors $\vec{V}_0, \vec{V}_1, \vec{V}_2$ and $\vec{V}_7$.

can be approximated in a PWM switching time period by applying $\vec{V}_0$ for a time

T_0, $\vec{V}_1$ for a time T_1, $\vec{V}_2$ for a time T_2 and $\vec{V}_7$ for a time T_7 such that $T_0 + T_1 + T_2$

+ $T_7 = T_{PWM}$. Each space vector $(\vec{V}_0, \vec{V}_1, ..., \vec{V}_7)$ is a result of an inverter state. Inverter state refers to the state of the switches of upper and lower transistors of the inverter. Applying different inverter states in sequence for time periods T_0, T_1, T_2, T_7 results in the PWM waveforms shown in 5.15. Figure 5.15 also shows
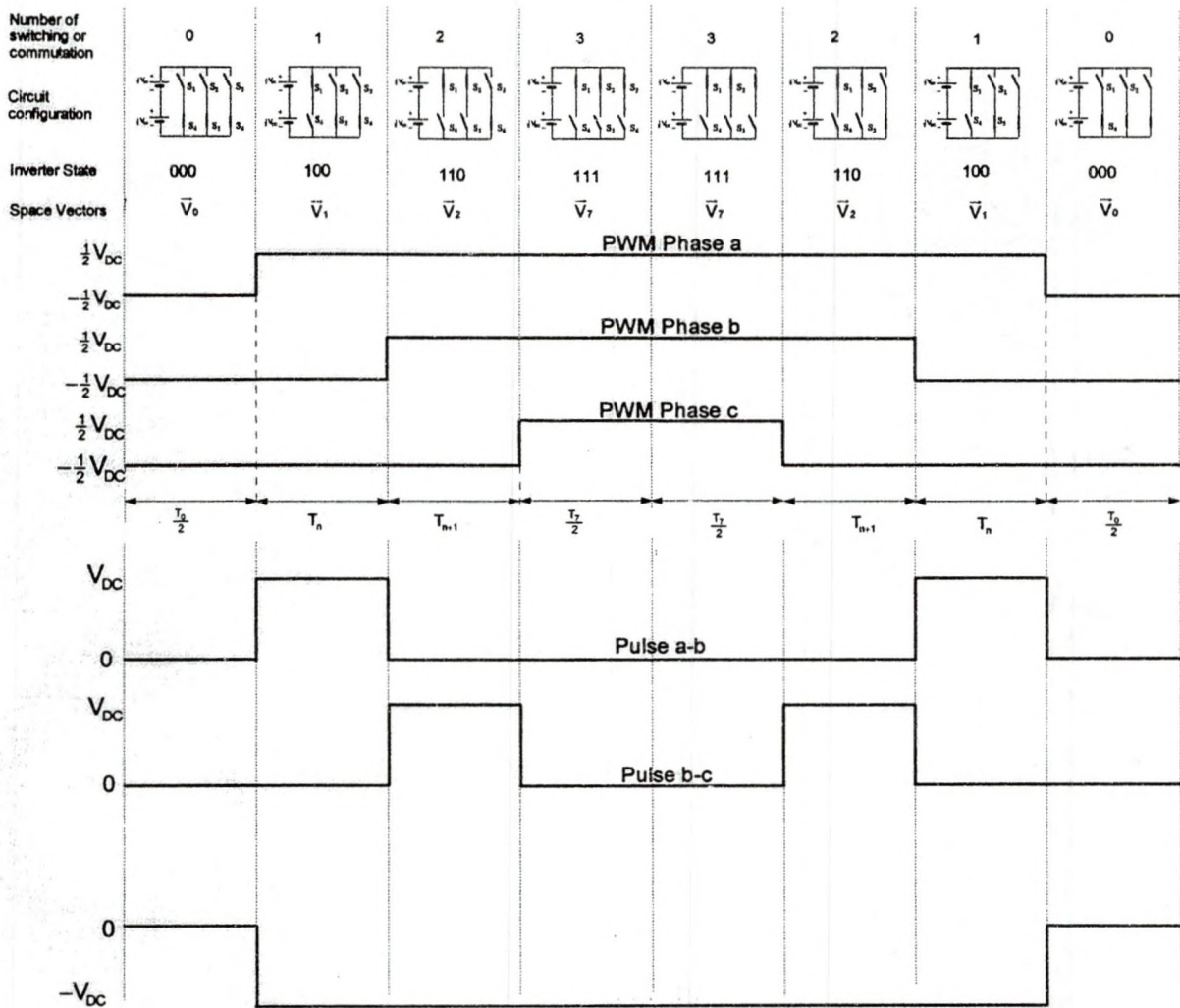
Figure 5.15: Space Vector PWM and its Corresponding Line-to-line Pulses

the corresponding line-to-line pulses. The PWM waveform in real time is a positive pulse train of constant magnitude but with a dynamically varying pulse width. The line-to-line pulses in real-time are a series of negative and positive

pulses with a dynamic pulse width variation. This will also be verified with

experimental results in Chapter 6.

Inverter Circuit Analysis

The following inverter circuit analysis shows the PWM phase and line

pulses corresponding to space vectors $\vec{V}_0, \vec{V}_1, \vec{V}_2$ and $\vec{V}_7$.

Space Vector $\vec{V}_0$

Figure 5.16: Star-Connected Load Step Voltage for Inverter State 000 (Space Vector $\vec{V}_0$)

$$
\begin{aligned}
V_{a0} &= V_{b0} = V_{c0} = -\tfrac{1}{2} V_{DC} \\
V_{an} &= V_{bn} = V_{cn} = 0 \\
V_{ab} &= V_{bc} = V_{ca} = 0
\end{aligned}
\tag{5.3}
$$

Space Vector $\vec{V}_1$

Figure 5.17: Star-Connected Load Step Voltage for Inverter State 100 (space vector $\vec{V}_1$)

$$V_{a0} = \tfrac{1}{2} V_{DC}$$
$$V_{b0} = V_{c0} = -\tfrac{1}{2} V_{DC}$$

(5.4)

$$V_{an} = \frac{Z_a}{Z_a + Z_{bc}}\left(V_{DC}\right) = \frac{Z}{Z + \frac{Z}{2}}\left(V_{DC}\right) = \frac{2Z}{3Z}\left(V_{DC}\right) = \frac{2}{3} V_{DC}$$

(5.5)

$$V_{bn} = V_{cn} = \frac{Z_{bc}}{Z_a + Z_{bc}}\left(-V_{DC}\right) = -\frac{\frac{Z}{2}}{Z + \frac{Z}{2}}\left(V_{DC}\right) = -\frac{Z}{2} \cdot \frac{2}{3Z}\left(V_{DC}\right) = -\frac{1}{3} V_{DC}$$

$$V_{ab} = V_{an} - V_{bn} = V_{DC}$$
$$V_{bc} = V_{bn} - V_{cn} = 0$$
$$V_{ca} = V_{cn} - V_{an} = -V_{DC}$$

(5.6)
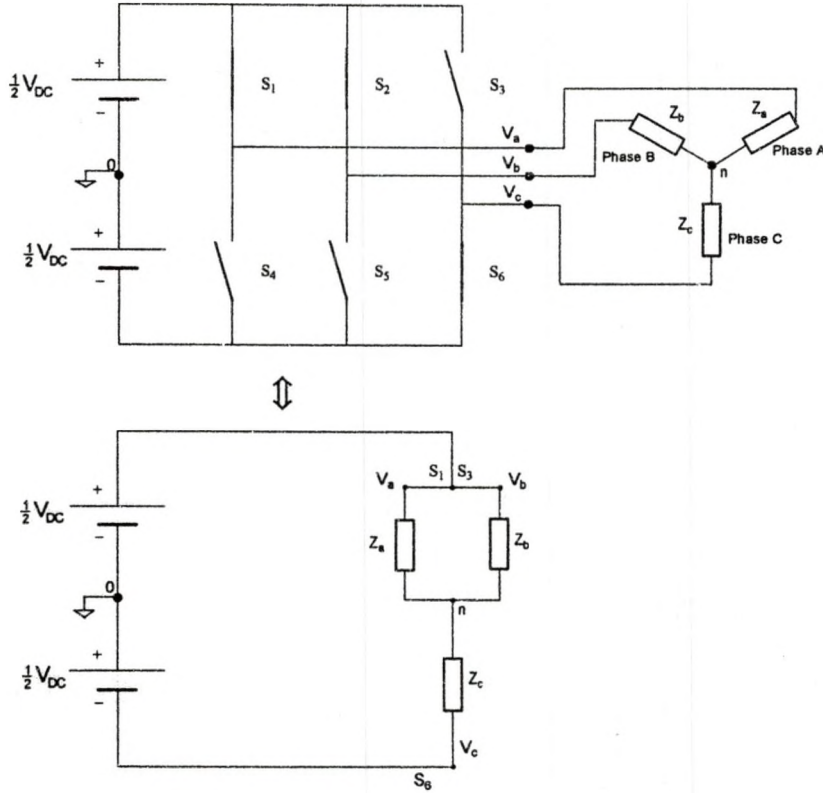
Space Vector $\vec{V}_2$

Figure 5.18: Star-Connected Load Step Voltage for Inverter State 110 (space vector $\vec{V}_2$)

$$V_{a0} = V_{b0} = \tfrac{1}{2}V_{DC}$$
$$V_{c0} = -\tfrac{1}{2}V_{DC} \tag{5.7}$$

$$V_{an} = V_{bn} = \frac{Z_{ab}}{Z_c + Z_{ab}}\left(V_{DC}\right) = \frac{\frac{Z}{2}}{Z + \frac{Z}{2}}\left(V_{DC}\right) = \frac{Z}{2}\frac{2}{3Z}\left(V_{DC}\right) = \tfrac{1}{3}V_{DC}$$

$$V_{cn} = \frac{Z_c}{Z_c + Z_{ab}}\left(-V_{DC}\right) = \frac{Z}{Z + \frac{Z}{2}}\left(-V_{DC}\right) = \frac{2Z}{3Z}\left(-V_{DC}\right) = -\tfrac{2}{3}V_{DC} \tag{5.8}$$

$$V_{ab} = V_{an} - V_{bn} = 0$$
$$V_{bc} = V_{bn} - V_{cn} = V_{DC}$$
$$V_{ca} = V_{cn} - V_{an} = -V_{DC} \tag{5.9}$$
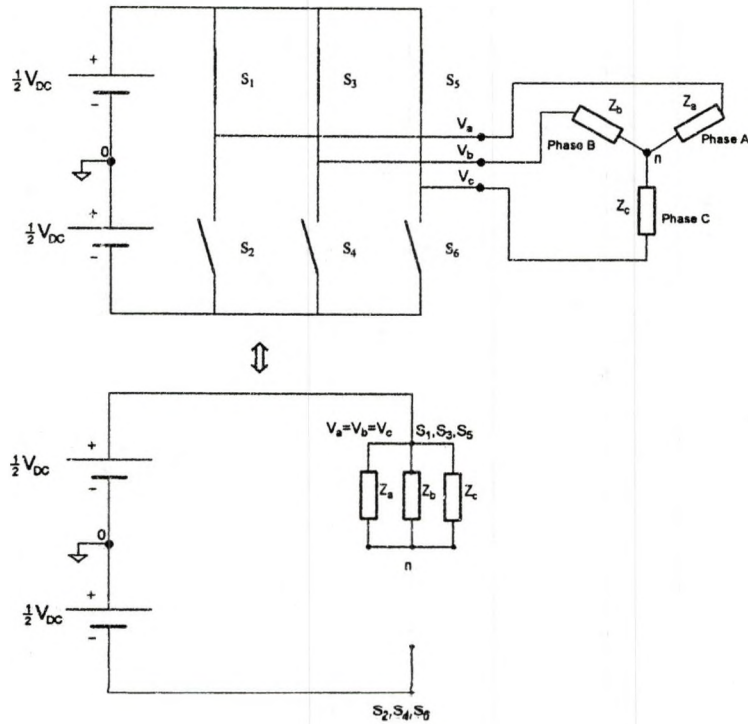
Space Vector $\vec{V}_7$
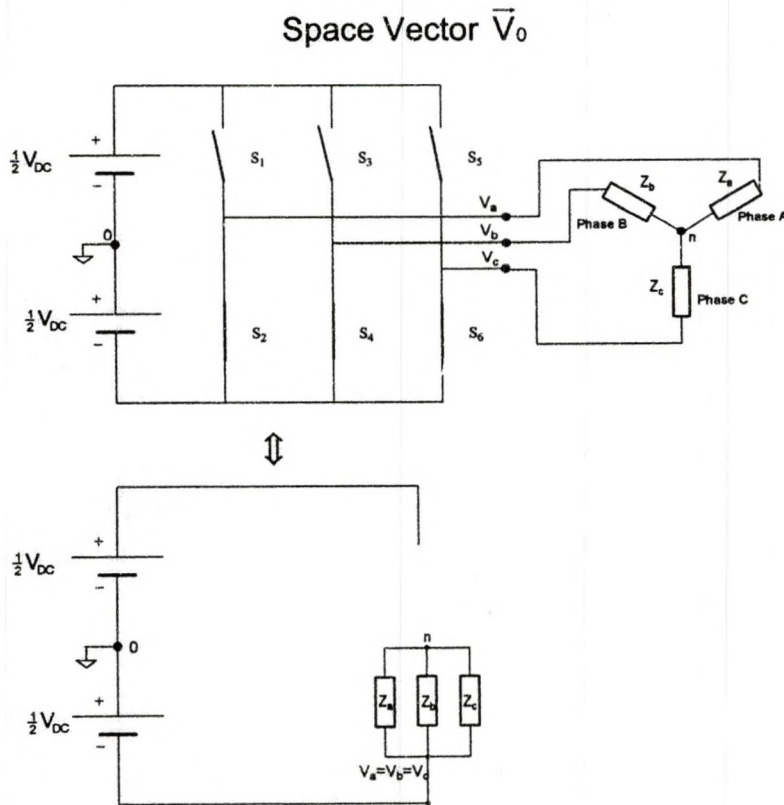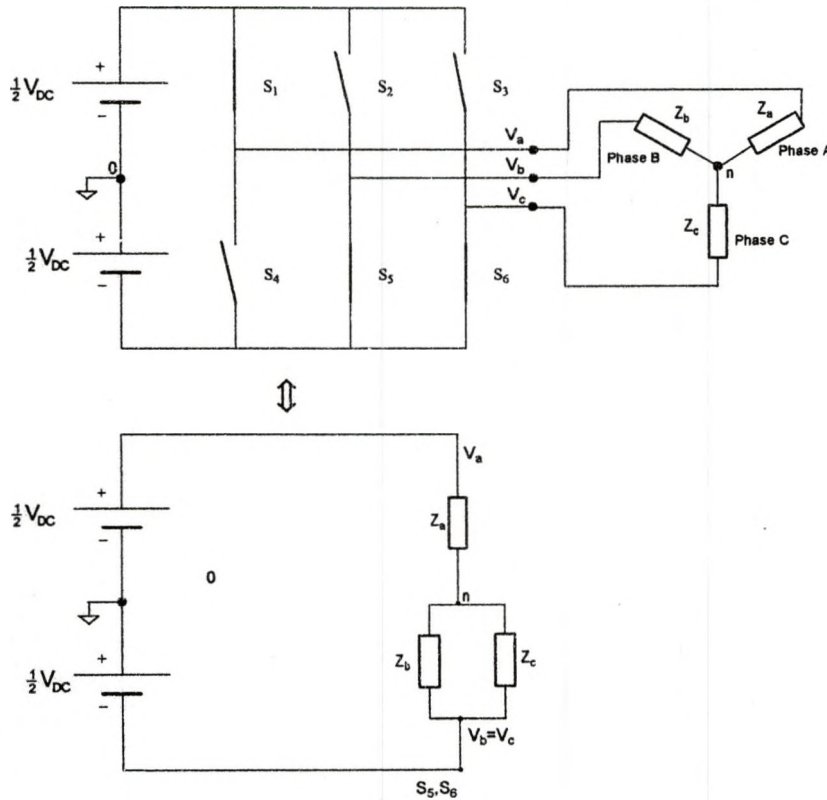

Figure 5.19: Star-Connected Load Step Voltage for Inverter State 111 (space vector $\vec{V}_7$)

$$V_{a0} = V_{b0} = V_{c0} = \tfrac{1}{2}V_{DC}$$
$$V_{an} = V_{bn} = V_{cn} = 0 \tag{5.10}$$
$$V_{ab} = V_{bc} = V_{ca} = 0$$

CHAPTER 6

HARDWARE CONFIGURATION AND EXPERIMENTAL RESULTS

This section covers the experimental analysis of the SVPWM technique and its application to the motor control sub-system mentioned in chapter 5. The eZdsp (DSP controller) was interfaced with the DMC1500 to power a three-phase induction motor. The VisSim^{TM}/TI C2000 rapid prototyper software package was used to model the motor control sub-system and generate codes to execute on the DSP. Only major components in DMC1500 and eZdsp are shown in this setup (Figures 6.1 and 6.2). Details on how to interface eZdsp to DMC1500 can be found in the eZdsp technical reference manual [38] and in the DMC1500 technical reference manual [39].

6.1 Overview Of The DMC1500 And eZdsp

The DMC1500 is the power stage of a Digital Motor Controller development system. The computing engine for the DMC1500 is the eZdsp (DSP controller). The DMC1500 allows development to be done with AC induction, DC Brushless, and Switched Reluctance motors. To accommodate these three types of motors, the DMC1500 has many jumper options and connections. The DMC1500 is intended to be used in a development environment only.

6.2 Experimental Procedure

The overall experimental system consists of the following hardware and

software items as follows.

1. Spectrum Digital DMC1500 drive platform

2. Spectrum Digital TMS320LF2407 DSK platform (eZdsp)

3. Three-phase induction motor, 3/4hp, 2.6 Amps, 208 Volts AC, Emerson, Model P55AZET-220, CAT 2758244.

4. PC with Code Composer(CC) 4.12 and VisSim^{TM} /TI C2000 rapid Prototyper v 4.5g installed;

5. Low Pass Filter/High Pass Filter, Waveteck Rockland, Model 852, Dual HI/LO Filter, IBM 656819A

6. Variable auto transformer (Variac), Tenma Input 117V/ouput 130V

7. Isolation Transformer

A complete list of equipment and pictures of setup can be found in the Appendices.

Measurements At The DSP Controller Output

Prior to applying the PWM signals to the gates of the power transistors, the DSP PWM signal outputs were analyzed to verify the theory and to ensure that the desired PWM signals were being generated by the DSP. Figure 6.1 illustrates one of the experimental setups to view the PWM-Phase "a" (line-to-ground PWM output) output signal at the interface connector (P2). For slider set points 0.4 and 0.8, line-to-ground and line-to-line PWM waveforms were observed with and without low pass filtering.

To run the eZdsp the following steps were required:

1) Turn-on the 5V DC power supply to the eZdsp

2) Run VisSim™/TI C2000 rapid prototyper software program

   (ACIM_TUTORIAL_4_DSP_EZ2407.VSM)

3) Set the slider position to a nominal value of 0.2 and click go

   (Note that the slider set point value of 0.2 is the normalized frequency input).

4) Compare the waveforms from plot blocks display with scopemeter display.

PWM1~PWM2 ---- Phase-V_a PWM1-PWM3 ---- Phase-V_{ab}
PWM3~PWM4 ---- Phase-V_b PWM3-PWM5 ---- Phase-V_{bc}
PWM5~PWM6 ---- Phase-V_c PWM5-PWM1 ---- Phase-V_{ca}
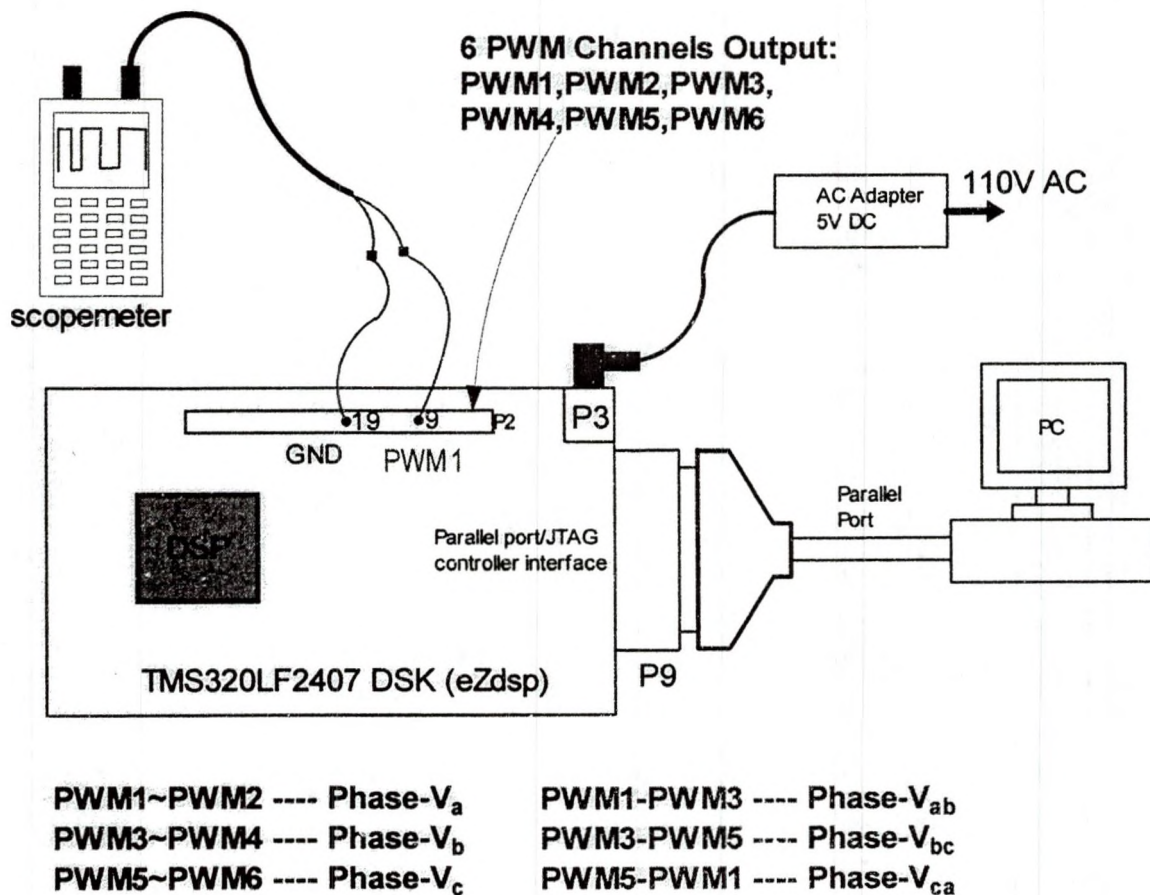
Figure 6.1: eZdsp Connection and Setup to Observe PWM Outputs

Measurements At The Motor Input

After ensuring that the desired PWM signals are produced by the eZdsp, it

was connected to the three-phase motor through the digital motor controller

board (DMC1500) as shown in Figure 6.2. Photos of the hardware and overall

Three-phase induction motor,
3/4hp, 208 Volts AC, 2.6 Amps
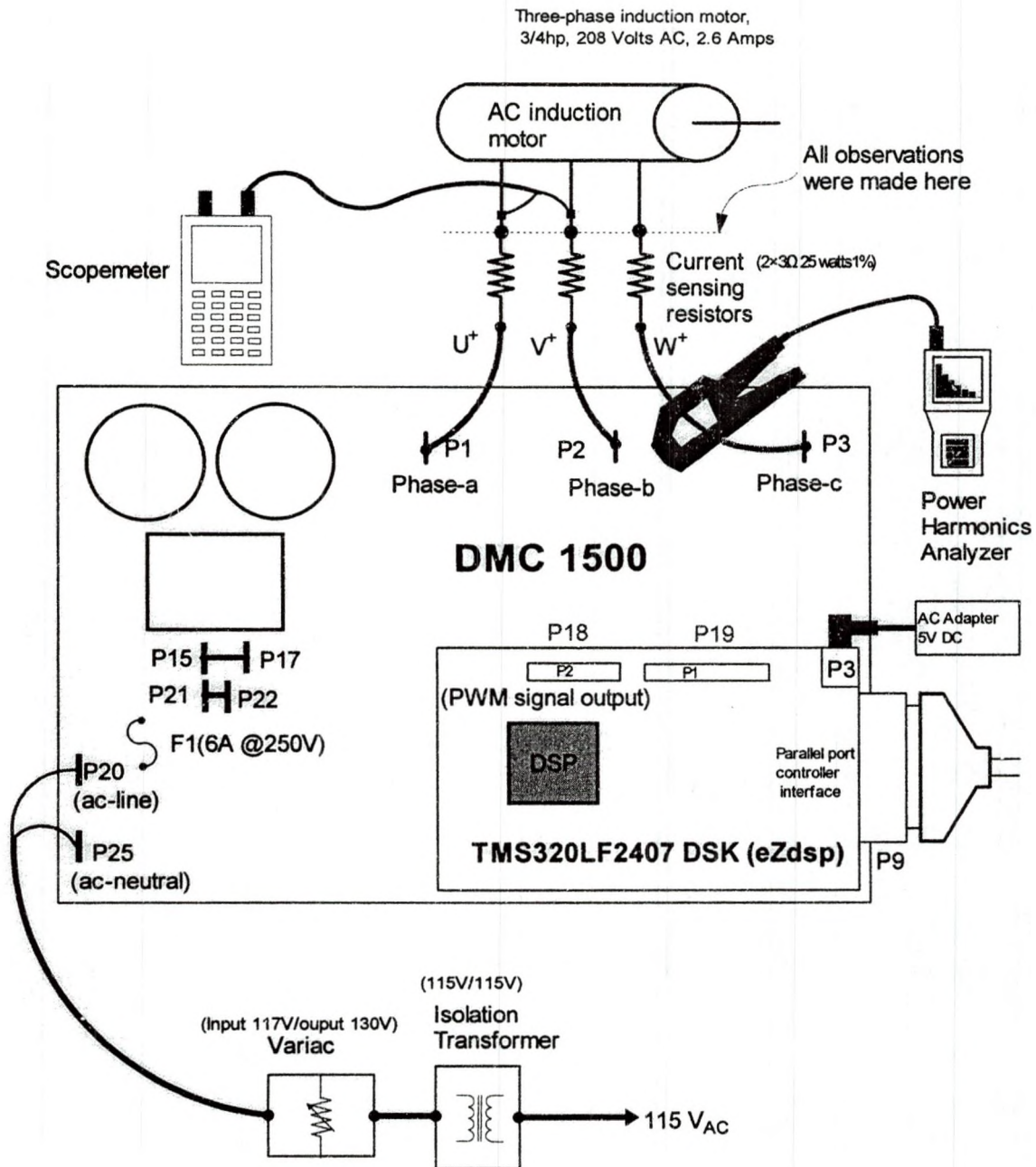
Figure 6.2: eZdsp, DMC Controller and Motor Connection-Experimentation System Setup

system setup are shown in the Appendices. To run the motor the following steps

were required:

1) Turn-on the 5V DC power supply to the eZdsp

2) Run VisSim™/TI C2000 rapid prototyper software program

(ACIM_TUTORIAL_4_DSP_EZ2407.VSM)

3) Set the slider position to a nominal value of 0.2 and click go

4) Turn the variac input until the motor starts to run.

Figure 6.2 illustrates the experimental setup to view the line voltage waveform applied across the motor stator winding. A power harmonic analyzer (Fluke 41) was used to observe the current and voltage harmonics. At slider set-points 0.4 and 0.8 phase current, phase voltage and line voltage waveforms were observed with and without a low pass filter with cut-off frequencies 20Hz, 30Hz, 200Hz, 1.5KHz, 3KHz and 30KHz. The phase current waveforms were also observed by observing the voltage across current sensing resistors and also with a current probe (Fluke 41).

6.3 Results And Discussion

DSP Output Observation Using Fluke 99B Scopemeter

Six PWM signals are distributed through connector P2 to turn on and off the power transistors on the DMC1500. The three-phase signals are PWM1 (PWM signal-phase "a"), PWM3 (PWM signal-phase "b") and PWM5 (PWM signal-phase "c"), whereas PWM2, PWM4 and PWM6 are complementary PWM signals.

The PWM1 signal for a slider set point of 0.2 is shown in Figure 6.3. It can be seen that the amplitude of the pulse train is about 3.44Vp-p at 2 KHz (switching frequency) with a PWM period of 500µsec (1/2KHz).
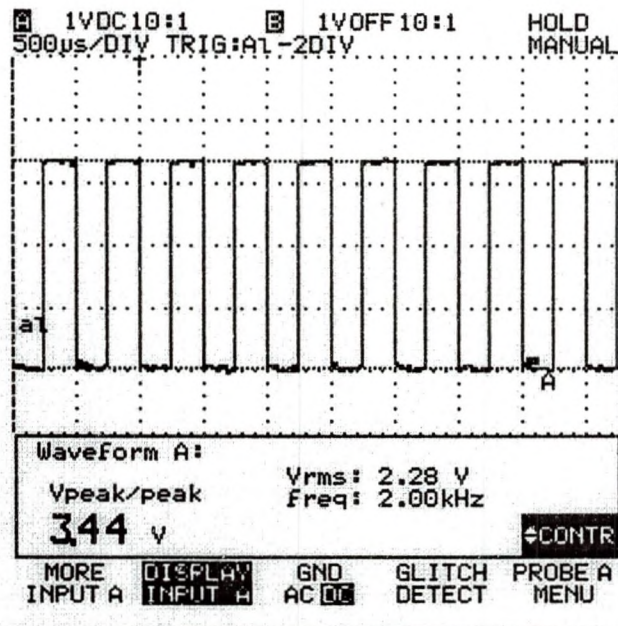
Figure 6.3: DSP PWM1 Signal for a Slider Set point of 0.2

Observed PWM1 and PWM2 waveforms at a slider setpoint of 0.2 is

shown in Figure 6.4. It seems like PWM1 and PWM2 waveforms are

complementary pulses; when PWM1 is high PWM 2 is low and vice versa. This

strategy ensures that no two transistors on the same leg are turned turn on

simultaneously.
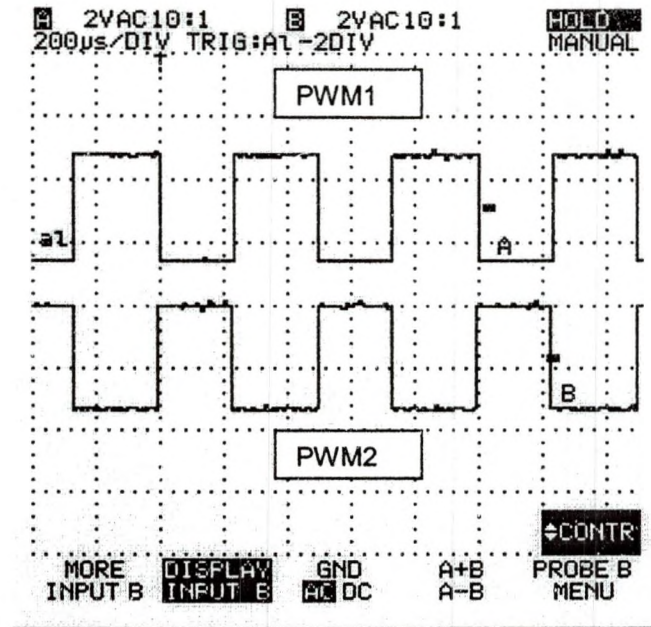
Figure 6.4: DSP PWM1 and PWM2 Signals for a Slider Set point of 0.2

Figure 6.5 shows PWM1 and PWM2 waveforms at a slider set point of 0.8. Increasing the slider set point from 0.2 to 0.8 does not change the frequency or amplitude of the pulse train. The pulses' widths however "swing" wider (i.e., the duty cycle of the switches increases). This implies that these pulses are for switching and controlling the "on" and "off" durations of pulses. PWM1, PWM3 and PWM5 control the turn-on and turn-off intervals of the upper-leg's power transistors and PWM2, PWM4 and PWM6 control the turn-on and turn-off intervals of the lower-leg's power transistors. Increasing the slider set point increases the on-time duration (i.e., the duty ratio) of the power transistor related to PWM1.
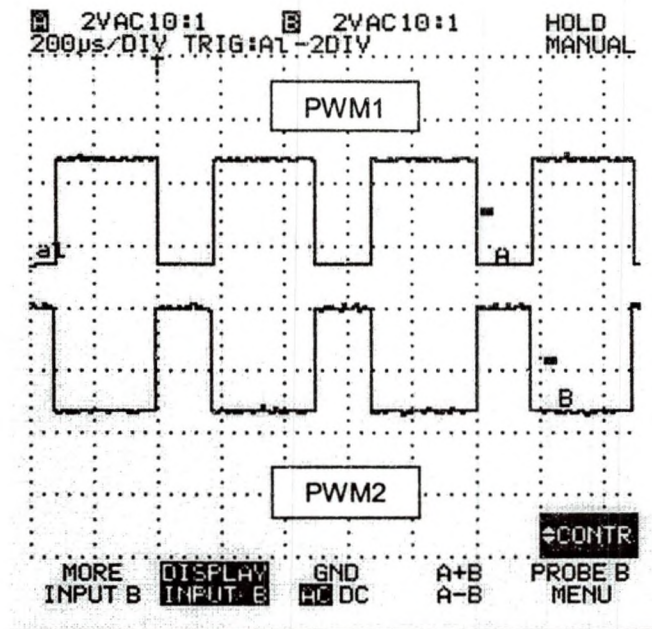
Figure 6.5: DSP PWM1 and PWM2 Signals for a Slider Set Point of 0.8

Figures 6.6, 6.7 and 6.8 display two of the three-phase PWM signals,

(PWM1 and PWM3) taken at three random instances. They resemble the

theoretical PWM waveforms illustrated in Figure 4.13. These three PWM signal

patterns are unique for the three instances because $\vec{V}_{ref}$ has rotated to different

positions. Different positions of $\vec{V}_{ref}$ means different sampling periods and

thereby different PWM signal patterns. This also agrees with the sector sampling

illustration in Figure 5.12.
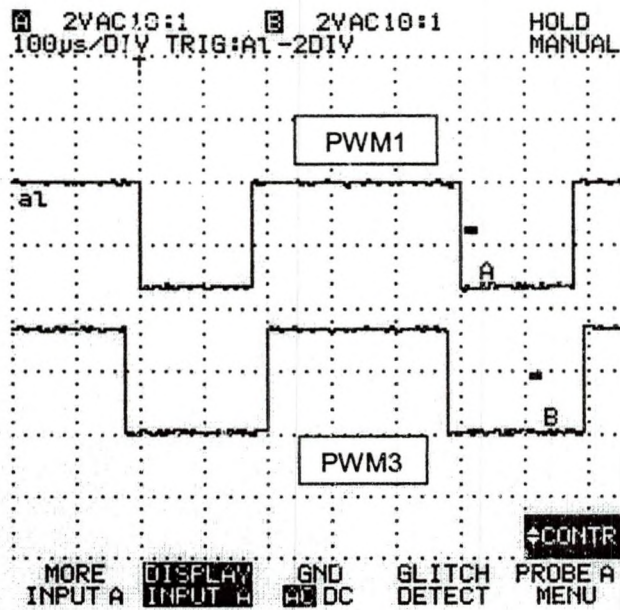
Figure 6.6: DSP PWM1 and PWM3 for a $\overline{V}_{ref}$ Position for a Slider Set Point of 0.8
(Random Instance)
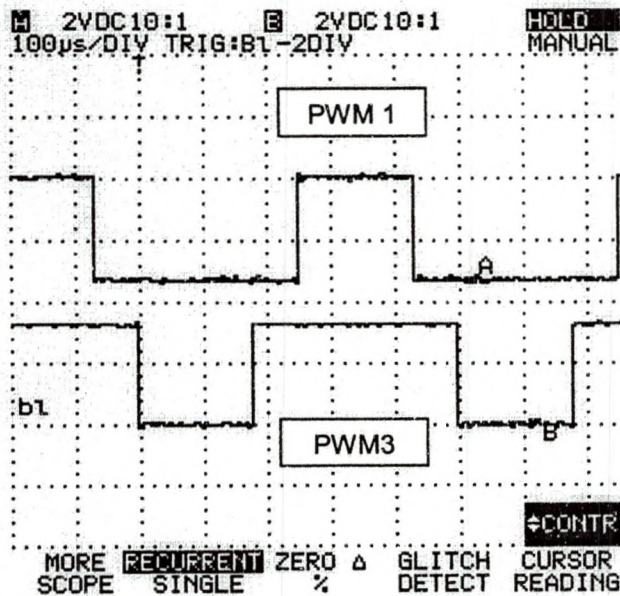
Figure 6.7 DSP PWM1 and PWM3 for a $\overline{V}_{ref}$ Position for a Slider Set Point of 0.8
(Another Random Instance)
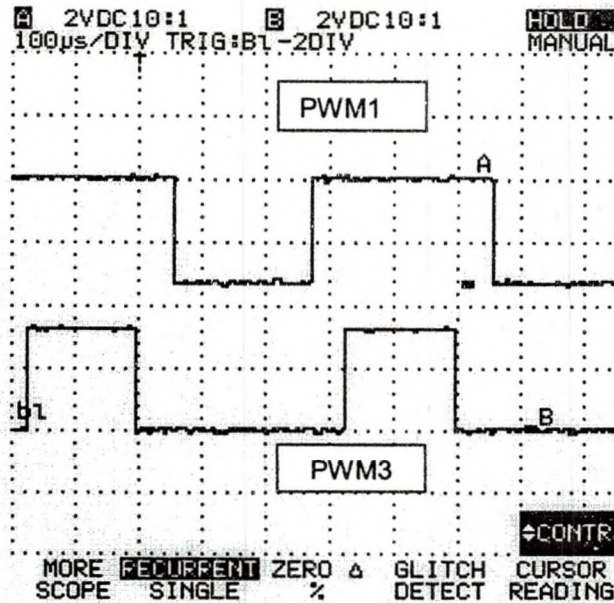
Figure 6.8: DSP PWM1 and PWM3 for a $\vec{V}_{ref}$ Position for a Slider Set Point of 0.8
(Still Another Random Instance)

Figure 6.9 shows the PWM1 signal superimposed on the low-pass-filtered (200Hz cut-off frequency) PWM1 signal. As mentioned earlier the low-pass-filtered PWM1 signal is a phase "a" voltage (duty ratio) waveform. It refers to the duty ratio of PWM1 signal [33]. It is called the duty ratio waveform because this waveform was obtained by averaging (equation (4.30)) the duty ratio waveform (PWM waveforms of Figure 4.13).
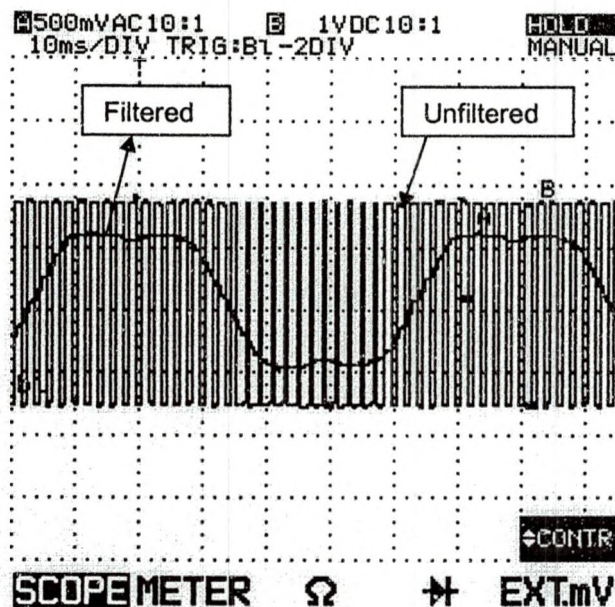
Figure 6.9: DSP PWM1 Superimposed on Low-pass-filtered (200Hz cut-off frequency) PWM1 Signal at a Slider Set Point of 0.8

Figure 6.10 shows the same low-pass-filtered PWM1 signal of Figure 6.9 with all its parameters. The duty ratio waveform's fundamental frequency is 16.6Hz (at slider setpoint 0.8). It can be seen that the phase voltage is not purely sinusoidal, due to the presence of harmonics of triplen orders [40]. The triplen harmonics occur a frequencies 49.8 Hz (16.6 Hz x 3 =49.8 Hz), 99.6 Hz, 149.4…and so on. Since the duty ratio waveform was low-pass filtered with a cut-off frequency of 200Hz, the triplen harmonics are present up to 200Hz.
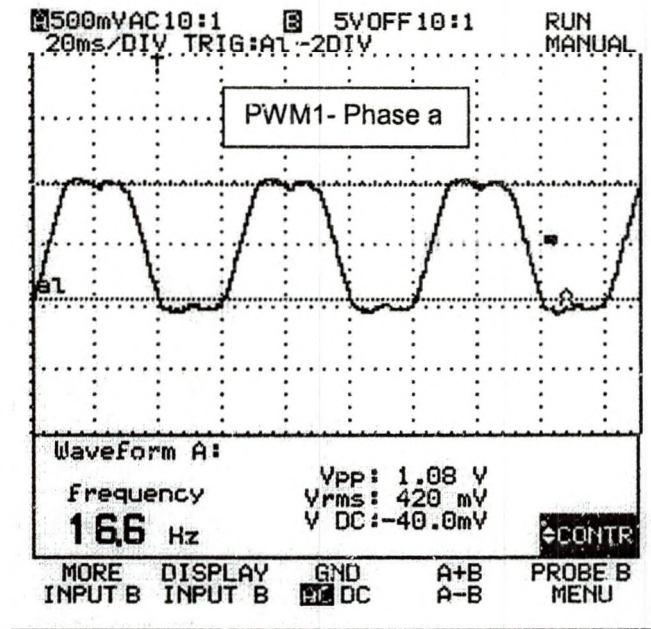
Figure 6.10: DSP Phase "a" (PWM1) Duty Ratio Waveform With All its Measurements for a Slider Set Point of 0.8

Figure 6.11 shows the three-phase duty ratio waveforms (PWM1, PWM3 and PWM5 signals). Keeping the cut-off frequency at 200Hz excluded the switching frequency (2 KHz) harmonics and its multiples. The waveforms in Figure 6.11 are similar to the duty ratio plots from MATLAB™ (Figure 4.14), VisSim-DSP (Figure 5.8) and VisSim-PC (Figure 5.8).

Figure 6.11: DSP Three Phase Duty Ratio (PWM1, PWM3, PWM5) Low Pass Filtered with Cutt-off Frequency of 200Hz for a Slider Setpoint of 0.8

To recover the fundamental waveform (fundamental frequency = 16.6 Hz) of PWM1, it was Low-pass-filtered with a 30Hz cut-off frequency. The resulting sinusoid, duty ratio and PWM1 signal are shown in Figure 6.12.
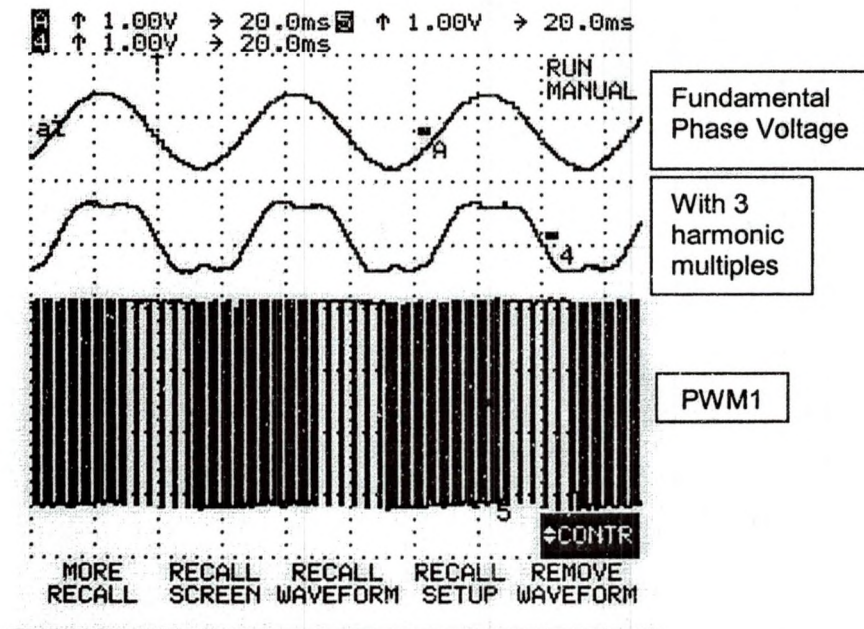
Figure 6.12: DSP PWM1 Signal With Fundamental Frequency (LP 30Hz) and Duty Ratio (LP 200Hz) for a Slider Setpoint of 0.8

Figure 6.13 shows the fundamental frequency phase-voltage waveform (PWM1) with all its parameters. Figure 6.14 shows the three-phase PWM1, PWM3 and PWM5 fundamental frequency phase-voltage waveforms.
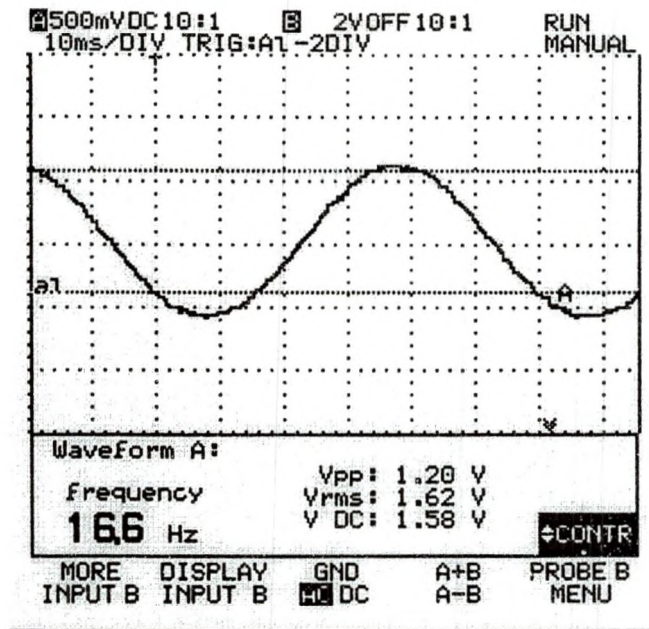
Figure 6.13: DSP PWM1 Fundamental Frequency (LP 30Hz) Component for a Slider Setpoint of 0.8
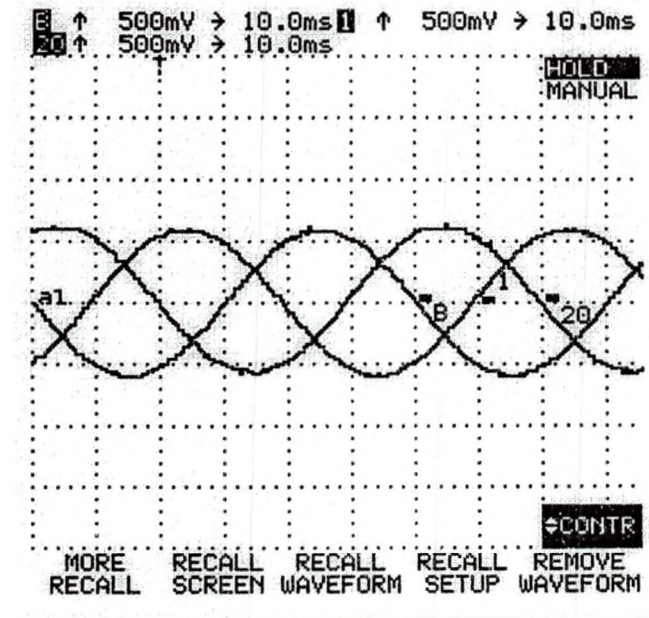
Figure 6.14:DSP Three-phase Fundamental Phase-Voltage (LP 30Hz) for a Slider Set point of 0.8

Figure 6.15 shows the three-phase duty ratio waveforms with phase "c" waveform (PWM5 signal) distorted by high frequency components. This waveform was obtained by increasing the cut-off frequency of the PWM5 signal from 200Hz to 1500Hz (which is closer to the switching frequency (2KHz)).

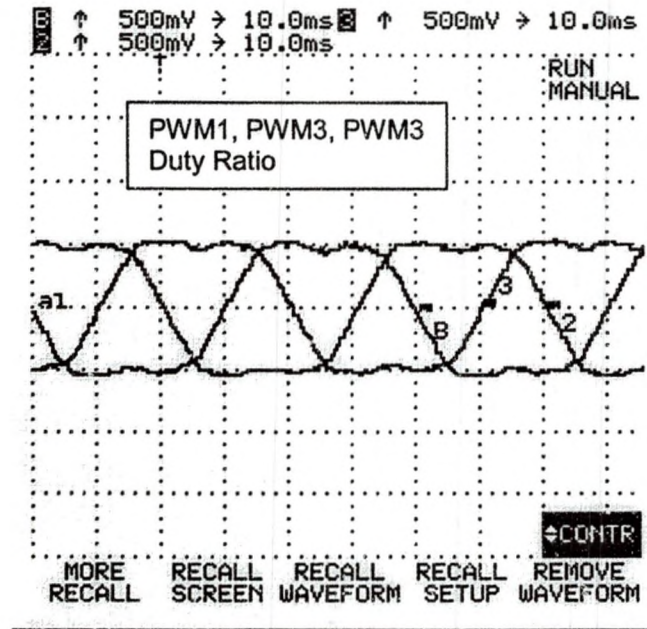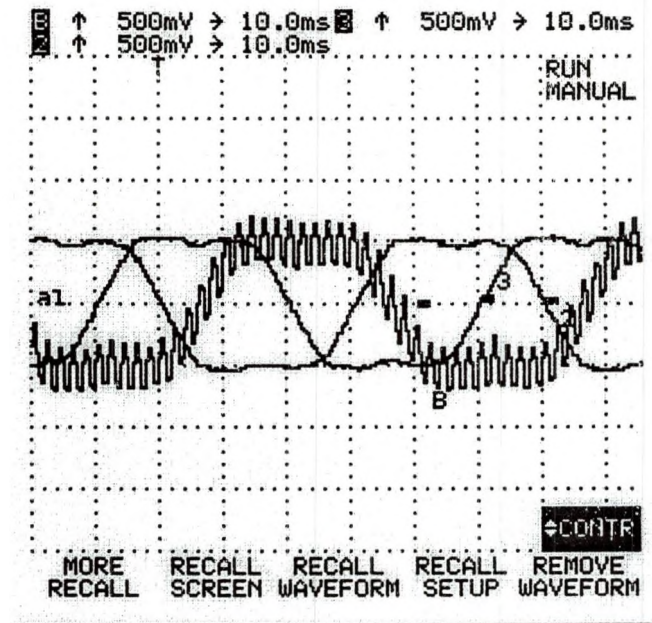

Figure 6.15:DSP Three Phase Duty Ratio With PWM5 Low Pass Filtered at Cut-off Frequency of 1.5KHz for a Slider Set point of 0.8

When the cut-off frequency was further increased beyond the switching frequency, the duty ratio waveform became more distorted, as shown in Figure 6.16 (cut-off frequency 3KHz) and Figure 6.17 (cut-off frequency 30 KHz). At a 30 KHz cut-off frequency, the high frequency switching harmonics and its multiples are included in the duty ratio waveform. This results in the pulse train shown in Figure 6.17.
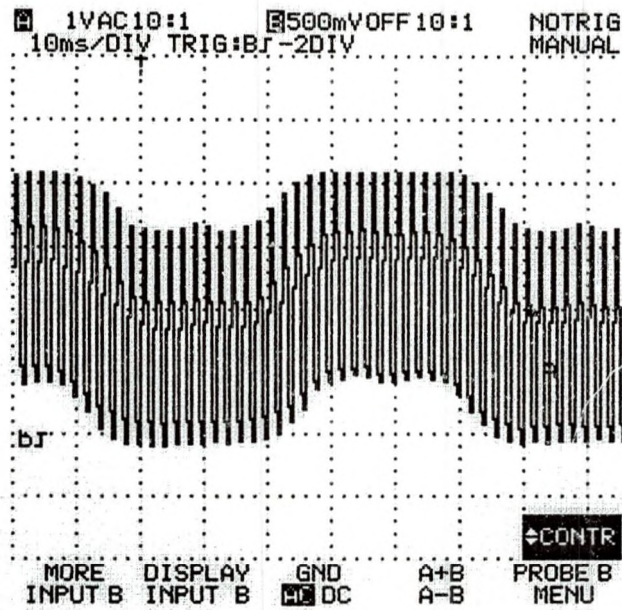
Figure 6.16: DSP PWM5 Signal of Figure 6.15 Low Pass-Filtered at Cut-off Frequency of 3KHz for a Slider Setpoint of 0.8
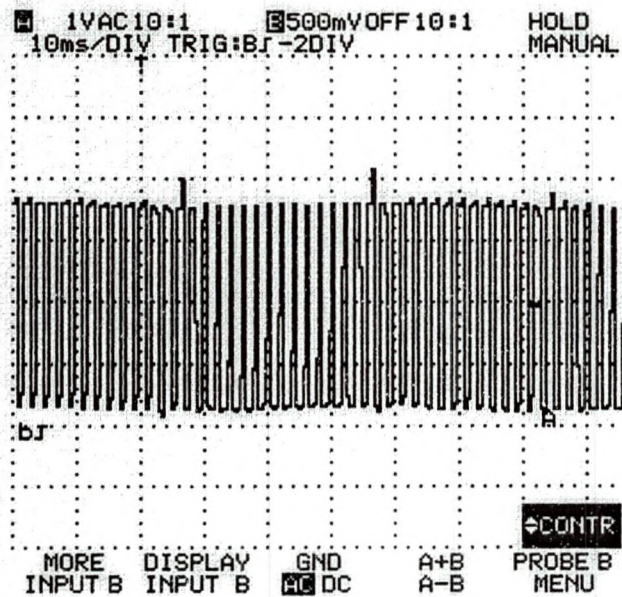
Figure 6.17: DSP PWM5 Signal of Figure 6.15 Low Pass-Filtered at Cut-off Frequency of 30KHz for a Slider Setpoint of 0.8

From the above observations it is noted that the duty ratio waveforms (PWM1, PWM3, PWM5) are infested with triplen order and high frequency switching harmonics. Low-pass-filtering the duty ratio waveform at a cutoff frequency of 200Hz removed the high frequency switching harmonics leaving the low frequency triplen order harmonics (Figure 6.10). The fundamental frequency line-voltage waveform was obtained by taking the difference between PWM1 and PWM3 waveforms, as shown in Figure 6.18. The triplen order harmonics cancel each other leaving a nearly pure sinewave. However the high switching frequency harmonics do not cancel this way, rather they are removed by the motor's inductances. Reference [28] shows that for a purely resistive load, the line voltage waveform appears to be noisy. It will be shown later (from motor input measurements) that for an inductive load the line voltage automatically appears to be free from high frequency noise. The motor winding's inductances act as a low pass filter and remove the high frequency switching components, leaving the triplen order harmonics in the phase voltage waveforms. These triplen harmonics do not affect the line-voltage, so it (line-voltage) is a pure sinusoidal [40], as shown by the observed waveforms in Figure 6.18. The line-voltage's immunity from high and low frequency harmonics explains why three phase inverters are popular for motor drives. Figure 6.19 shows the fundamental frequency (16.6Hz) line-voltage (PWM1-PWM3) waveform with it's measurements.
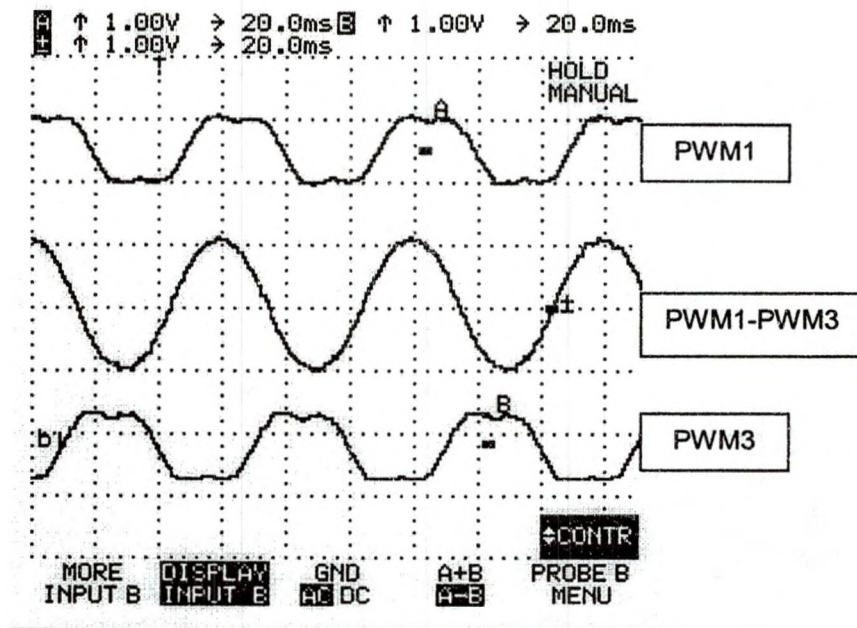
Figure 6.18:DSP Duty Ratio and Line_Voltage Waveforms for a Slider Set point of 0.8
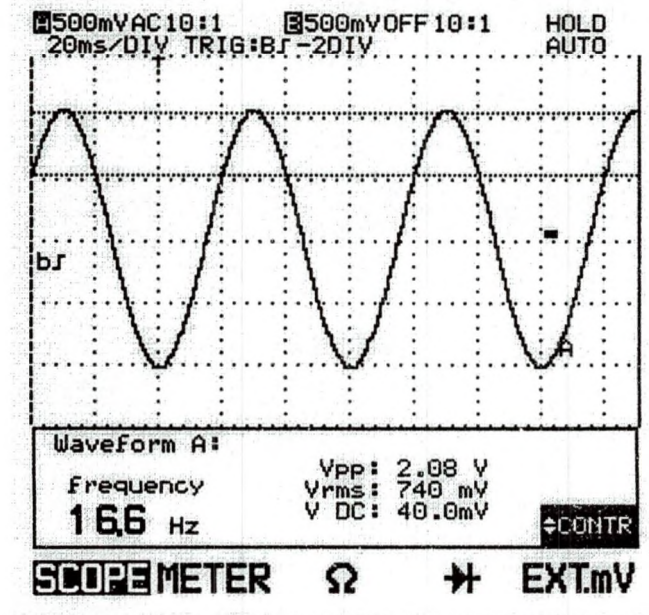
Figure 6.19: Closed-up Version of Fundamental Frequency Line Voltage Waveform of Figure 6.18

Figure 6.20 shows unfiltered PWM1, PWM3 and PWM1-PWM3 signals. It can be seen that PWM1 and PMW3 signals have positive pulses only but PWM1-PWM3 signal has negative and positive pulses (as also shown in Figure 5.15).
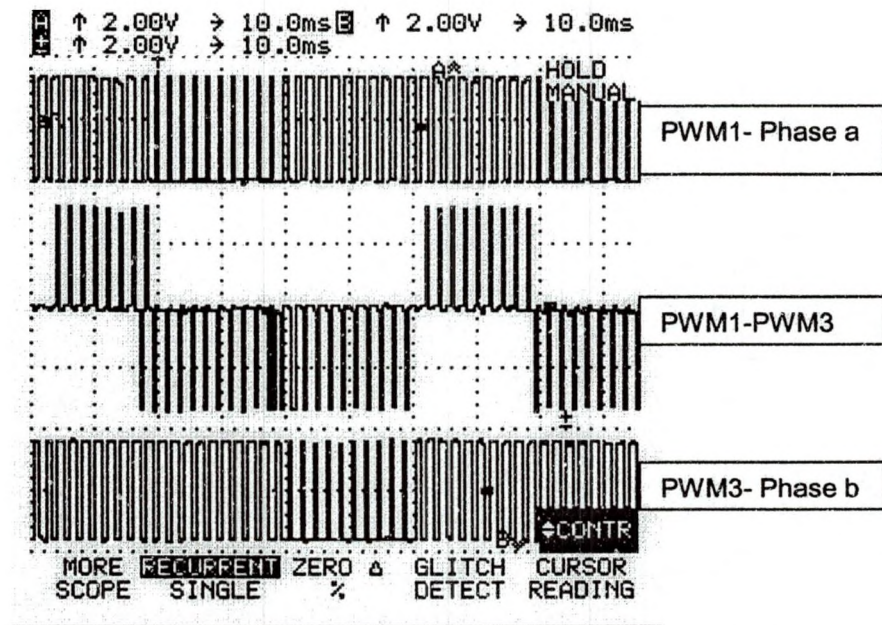
Figure 6.20: DSP PWM1, PWM3, PWM1-PWM3 Signals for a Slider Set point of 0.4

Figure 6.21 shows the PWM1-PWM3 waveform superimposed with low-pass-filtered PWM1-PWM3 waveform (cut-off frequency of 30Hz) to recover its fundamental frequency component.
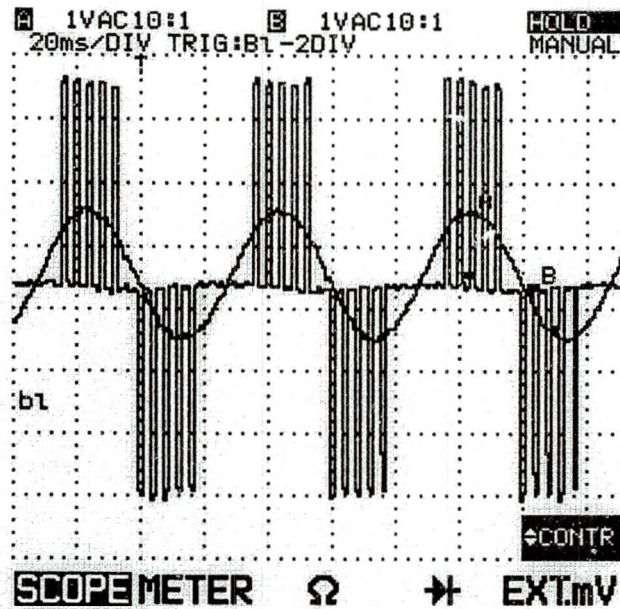
Figure 6.21: DSP Filtered and Unfiltered PWM1-PWM3 Waveforms for a Slider Setpoint of 0.8

Figure 6.22 is the close-up version of the fundamental frequency

waveform shown in Figure 6.21, showing all the measured values. For a slider

set point of 0.8, the fundamental component frequency is 16.6Hz and the peak-

to-peak amplitude is 2.12 Volts AC. In Figure 6.19 the same waveform was

obtained by filtering the PWM1 and PWM3 waveforms first and then subtracting

the PWM3 from PWM1.
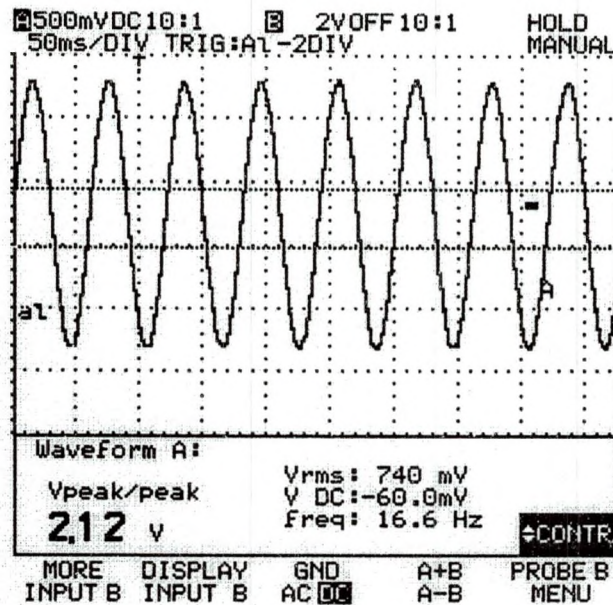
Figure 6.22: Close-up Version of the Fundamental Frequency Component Waveform of Figure 6.21

To understand how the slider setpoint affects the DSP's PWM output, PWM1-PWM3 filtered and unfiltered waveforms were observed again with a slider set point of 0.4, as shown in Figures 6.23 and 6.24. It can be seen that reducing the slider setpoint from 0.8 to 0.4, reduced the fundamental frequency from 16.6Hz to 8.33 Hz and the fundamental amplitude from 2.12 to 1.06 Volts AC. Therefore the slider set point varies both the fundamental frequency and amplitude of the output voltage waveform to maintain a contant V/Hz profile. Also note that from Figures 6.4 and 6.5 we concluded that changes in the slider set point affect the duty cycle of the switches. That is, for example, increasing the slider set point from 0.2 to 0.8, increases the duty cycle (the on time) of the switching PWM signals.

```
A  1VAC10:1      B  1VAC10:1          HOLD
 20ms/DIV TRIG:A1 -2DIV               MANUAL
```
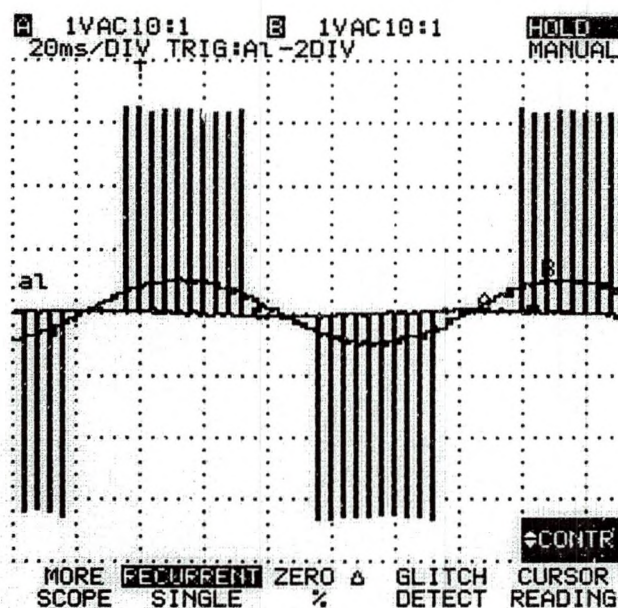
Figure 6.23: DSP Filtered and Unfiltered PWM1-PWM3 Waveforms for a Slider Setpoint 0.4


```
A500mVDC10:1     B  2VOFF10:1          HOLD
 50ms/DIV TRIG:A1 -2DIV                MANUAL

Waveform A:
                        Vrms:  360  mV
 Vpeak/peak             V DC:-60.0mV
                        freq:  8.33 Hz
 1.06 V
```
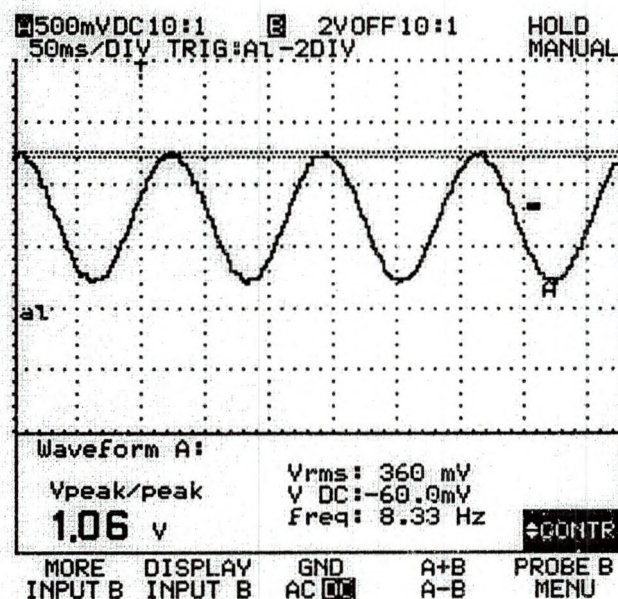
Figure 6.24:Close-up Version of the Fundamental Frequency Component Waveform of Figure 6.23

The measured parameters of the fundamental line-voltages (PWM1-PWM3) for slider set points of 0.4 and 0.8 are tabulated in Table 6.1. The filtered (LP 30Hz) PWM1-PWM3 waveform is the line voltage waveform. These results

match with MATLAB™ plots (Figure 4.15) , VisSim™ PC simulations (Figure 5.8) and DSP real time (Figure 5.8) plots. For a larger slider set point value of 0.8 the fundamental frequency component has a larger amplitude and frequency.

Table 6.1: SVPWM Line-Voltage (PWM1-PWM3) Waveform Measurements at DSP output

Slider Set point	Pulse Amplitude (Volts)	Fundamental Component			
		Volts peak- to- peak	Period (msec)	Frequency (Hz)	V/Hz Profile
0.4	3.44	1.04	120	8.33	0.06
0.8	3.44	2.2	60	16.6	0.07

Figure 6.25 shows the three-phase PWM signals for about nine switching time periods.
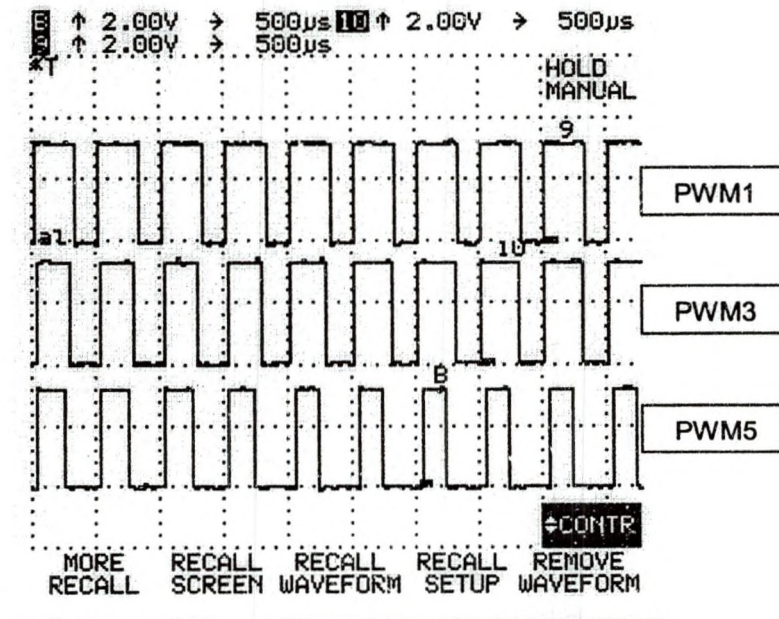
Figure 6.25: DSP Three phase (PWM1, PWM3, PWM5) PWM Waveforms for About Nine Switching Period for a Slider Setpoint of 0.8

Figure 6.26 shows the three-phase PWM signals for one switching time period. This waveform resembles the theoretical PWM waveforms shown in Figure 5.15.
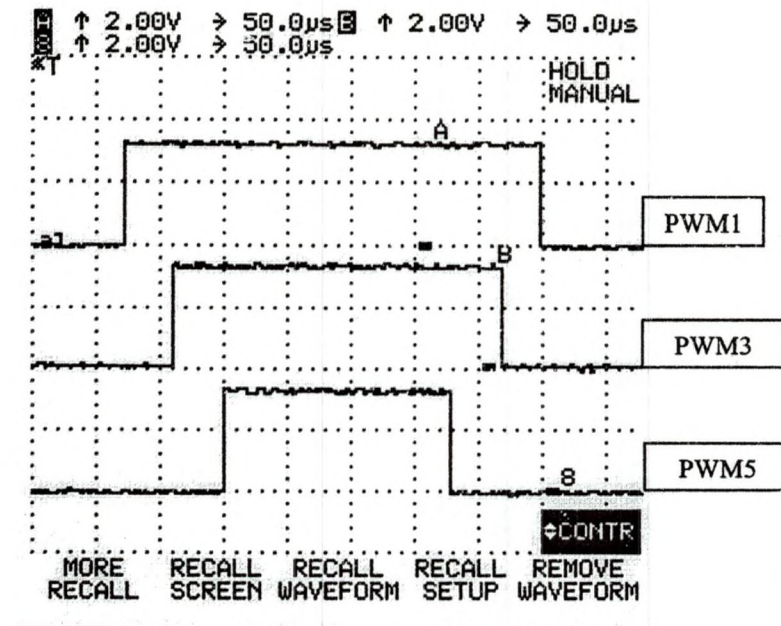
Figure 6.26: DSP Three-phase (PWM1,PWM3, PWM5) PWM Waveform for one Switching Period for a Slider Set Point of 0.8

Figures 6.27 through 6.29 show PWM1, PWM3 and PWM1-PWM3 PWM signals for one switching time period at three instances. The PWM1, PWM3 and PWM1-PWM3 do match the illustration of Figure 5.15 (Space Vector PWM and its Corresponding Line-to-line Pulses). Next, the input voltages and currents to the three-phase induction motor are observed.
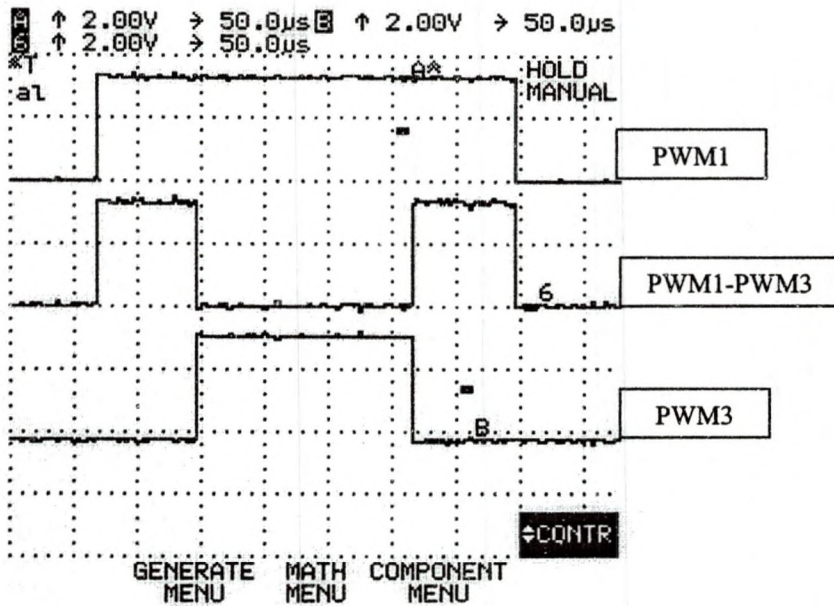
Figure 6.27:DSP Three-phase (PWM1, PWM3, PWM1-PWM3) PWM Waveform for one Switching Period for a Slider Set Point of 0.8
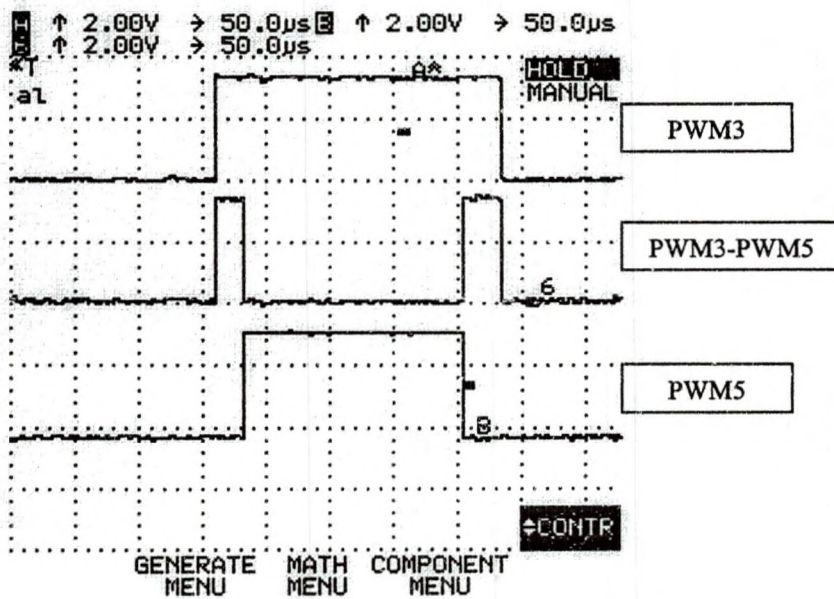
Figure 6.28:DSP Three-phase (PWM3, PWM5, PWM3-PWM5) PWM Waveform for one Switching Period for a Slider Set Point of 0.8
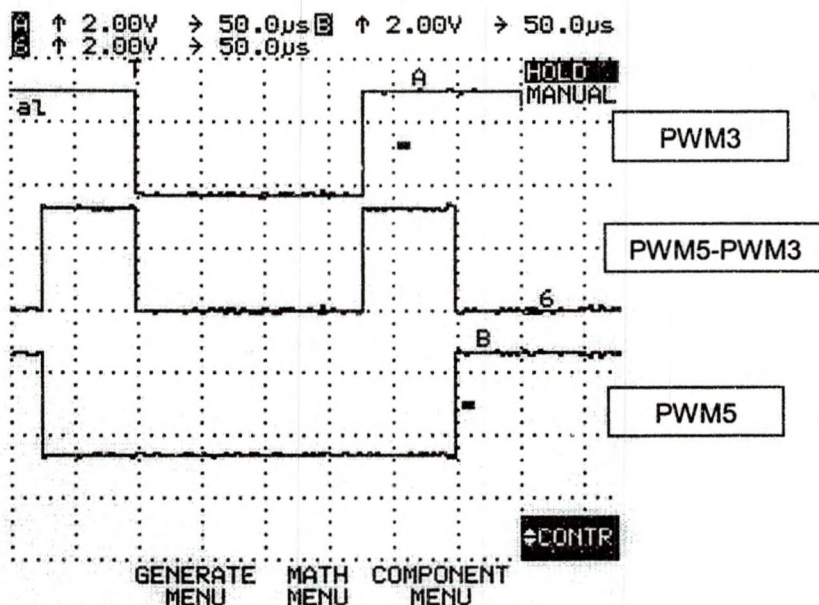
Figure 6.29:DSP Three-phase (PWM1, PWM5, PWM5-PWM1) PWM Waveform for one Switching Period for a Slider Set Point of 0.8

Motor Input Voltages And Currents Observation (Fluke 99B Scopemeter)

In the following experiment, the voltage and current waveforms were observed at the motor input. Figure 6.30 shows the three-phase PWM (PWM1, PWM3, PWM5) waveforms for several switching time periods at a slider set point of 0.8 and a variac input of 138 Volts AC. This waveform resembles the DSP output of Figure 6.25, but the amplitude of the pulses are different. The amplitudes of the pulses are same as the DC bus voltage.
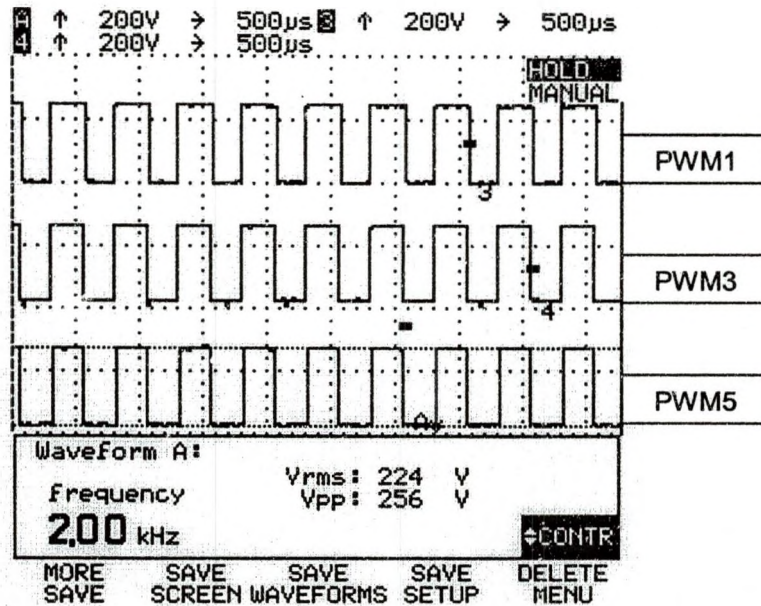
Figure 6.30:Motor Input PWM1, PWM3, PWM5 Signals for Several Switching Period for a Slider Set point of 0.8 and Variac Input of 138 Volts AC

Figure 6.31 shows the same waveform of Figure 6.30 for one switching time period. The signal for one switching time period resembles the theoretical PWM waveforms shown in Figure 5.15 and the DSP PWM output waveforms shown in Figure 6.26.
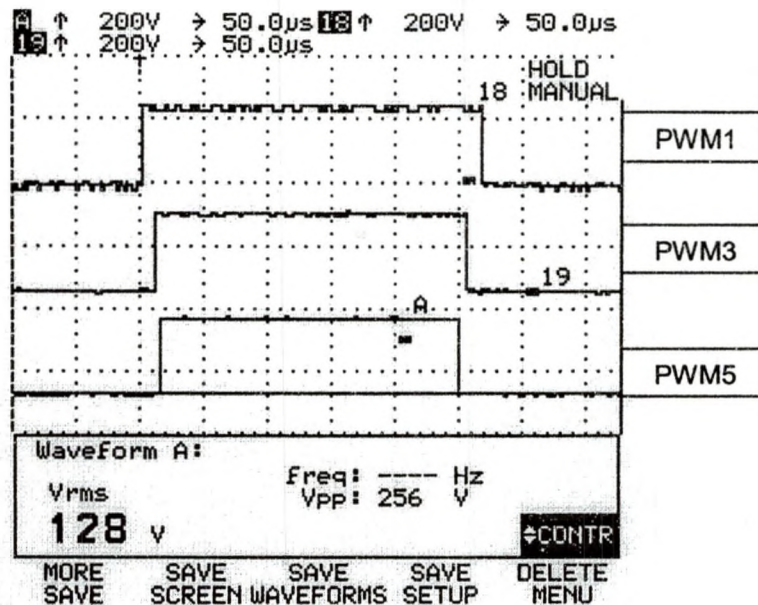
Figure 6.31:Motor Input PWM1, PWM3, PWM5 Signals for one Switching Time Period for a Slider Set Point of 0.8 and Variac Input of 138 Volts AC

Figure 6.32 shows the three-phase (PWM1-PWM3, PWM3-PWM5, PWM5-PWM1) line voltage waveforms for several switching time periods. It can be seen that similar to that of Figure 5.15 , here (at a different instant) V_{ab} and V_{ca} waveforms are positive pulse trains and V_{bc} waveform is a negative pulse train.
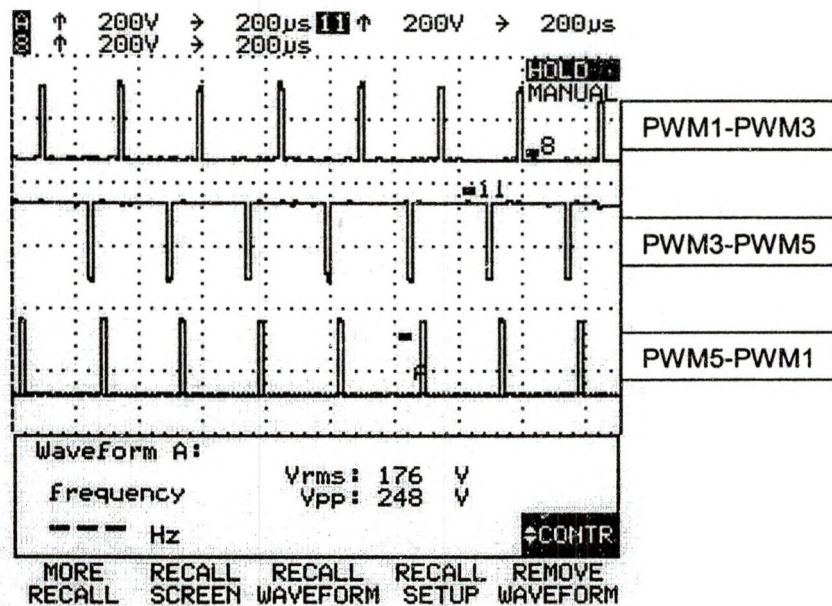
Figure 6.32: Motor Input PWM1-PWM3, PWM3-PWM5, PWM5-PWM1 Signals for a Slider Setpoint of 0.8 and Variac Input of 138 Volts AC

Figure 6.33 shows the line-voltage (PWM1-PWM3,) and phase voltage (PWM1, PWM3) waveforms for a much larger time domain. These waveforms resemble the DSP output signals of Figure 6.20. The inverter switches exactly follow the command signal (PWM waveform) of the DSP.
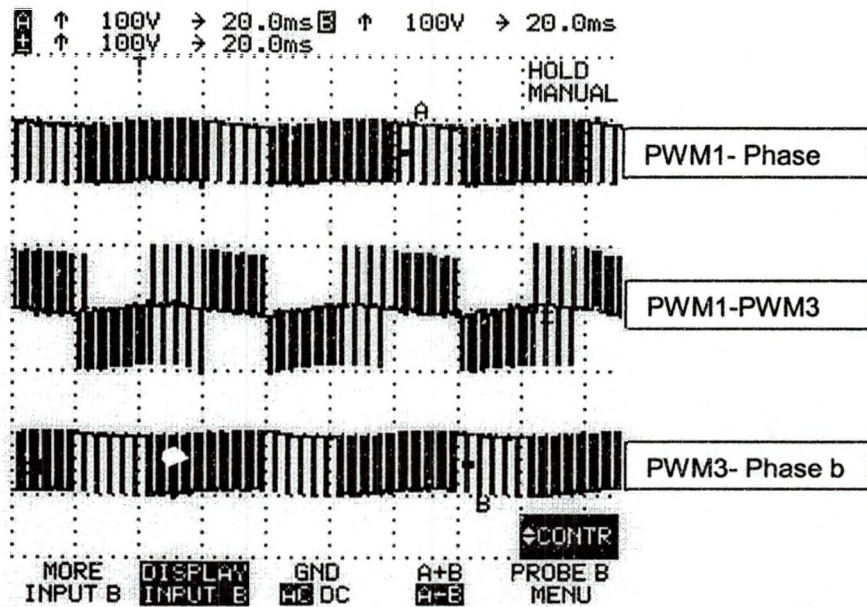
Figure 6.33:Motor Input Line Voltage (PWM1-PWM3) and Phase voltage (PWM1, PWM3) Pulses for a Slider Set Point of 0.8 and Variac Input of 70 Volts AC

Figure 6.34 shows the PWM1 signal and its low-pass-filtered (200Hz cut-off frequency) version at the motor input. As mentioned earlier, the low-pass-filtered PWM1 signal is phase "a" voltage waveform. Phase "a" voltage waveform is also referred to as the duty ratio of the PWM1 signal [33]. This waveform also resembles the duty ratio waveform of the DSP output (Figures 6.9 through 6.11). The result agrees with the MATLAB™ simulation (Figure 4.14), VisSim™ PC simulation (Figure 5.7) and with the DSP real time simulation (Figure 5.7).
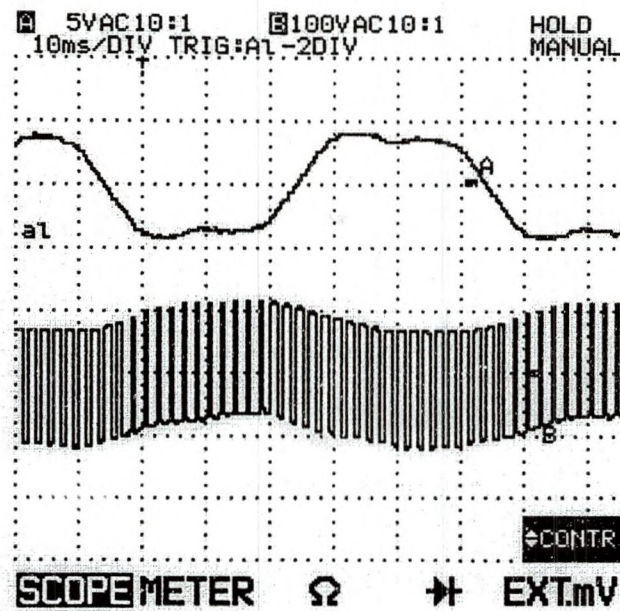
Figure 6.34: Motor Input Phase "a" Voltage Pulse Train and Duty Ratio Waveform for a Slider Set Point of 0.8 and Variac Input of 70 Volts AC

Figures 6.35 to 6.38 show the fundamental line-voltage (V_{ab}) waveform superimposed on the PWM (PWM1-PWM3) line-voltage waveform at the motor input for four combinations of variac inputs and slider set points. Figures 6.39 to 6.42 are the close-up versions of the fundamental frequency waveforms of Figures 6.35 to 6.38.
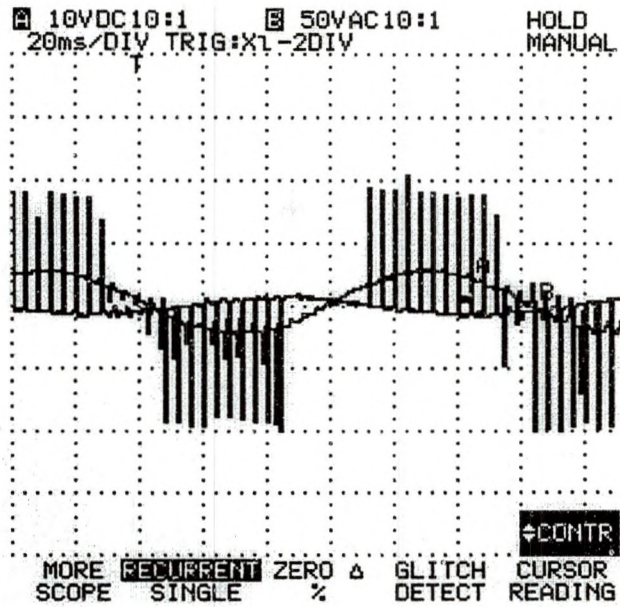
Figure 6.35: Motor Input Line Voltage (V$_{ab}$) Pulses and its Fundamental Waveforms for a Slider Set point of 0.4 and Variac Input of 70 Volts AC
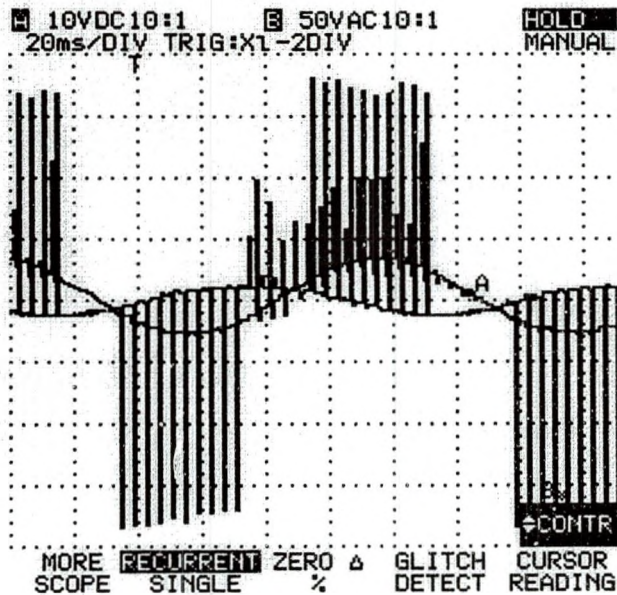
Figure 6.36:Motor Input Line Voltage (V$_{ab}$) Pulses and its Fundamental Waveforms for a Slider Set Point 0.4 and Variac Input of 138 Volts AC
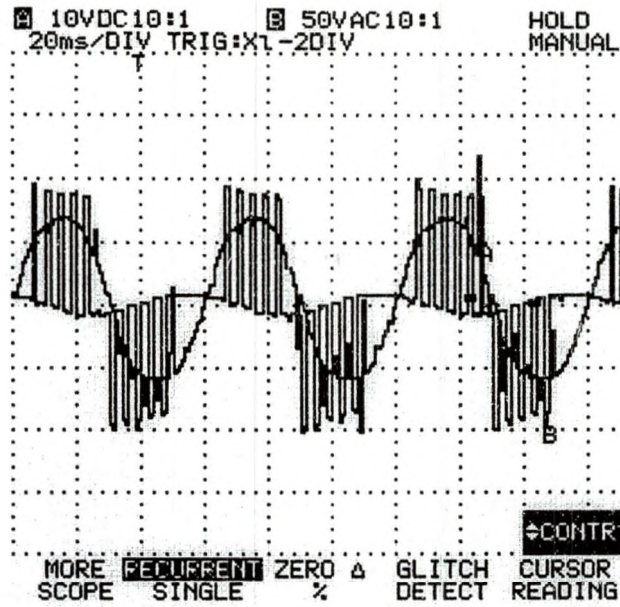
Figure 6.37: Motor Input Line Voltage (V_{ab}) Pulses and its Fundamental Waveforms for a Slider Set Point of 0.8 and Variac Input of 70 Volts AC
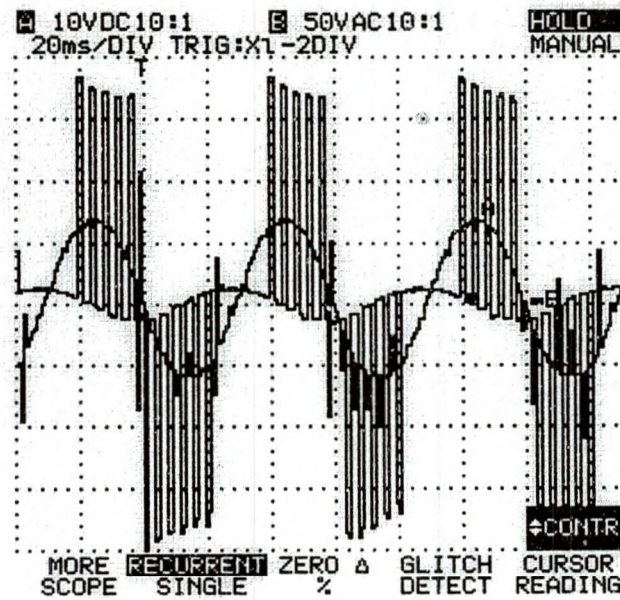
Figure 6.38:Motor Input Line Voltage (V_{ab}) Pulses and its Fundamental Waveforms for a Slider Set Point of 0.8 and Variac Input of 138 Volts AC
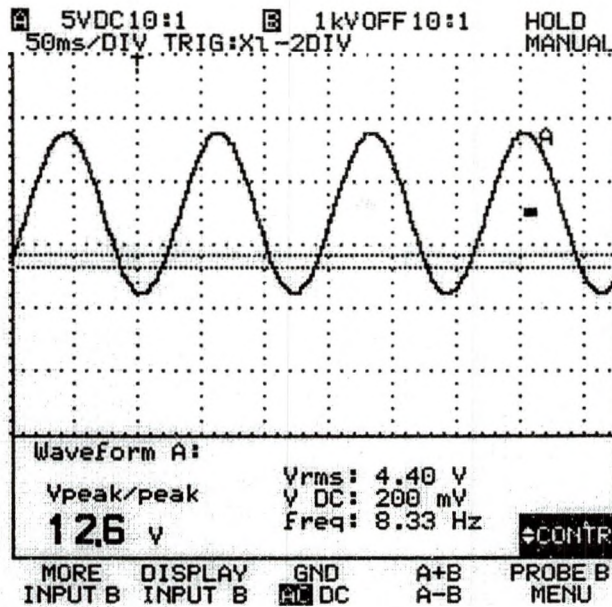
Figure 6.39: Close-up Fundamental Line-Voltage (V_{ab}) Waveform of Figure 6.35 for a Slider Set Point 0.4 and Variac Input of 70 Volts AC
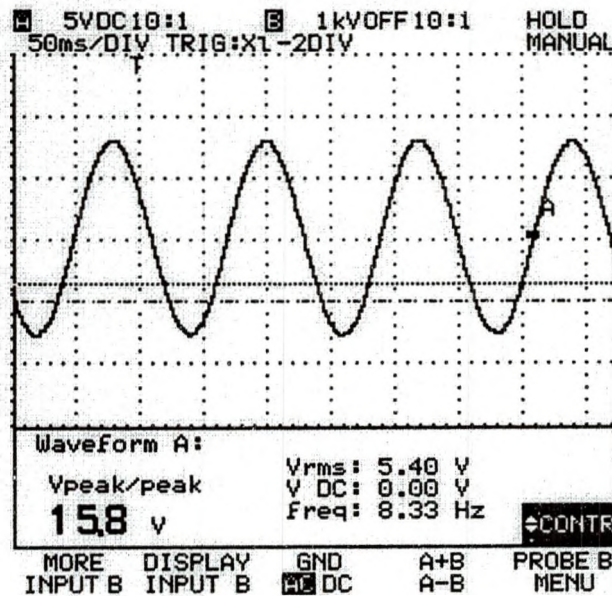
Figure 6.40:Close-up Fundamental Line-Voltage (V_{ab}) Waveform of Figure 6.36 for Slider Set Point 0.4 and Variac Input of 138 Volts AC
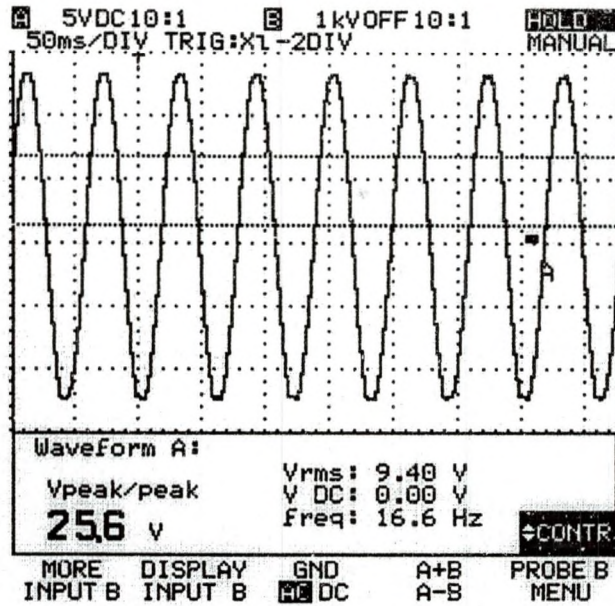
Figure 6.41: Closed-up Fundamental Line-Voltage (V_{ab}) Waveform of Figure 6.37 for a Slider Set Point of 0.8 and a Variac Input of 70 Volts AC
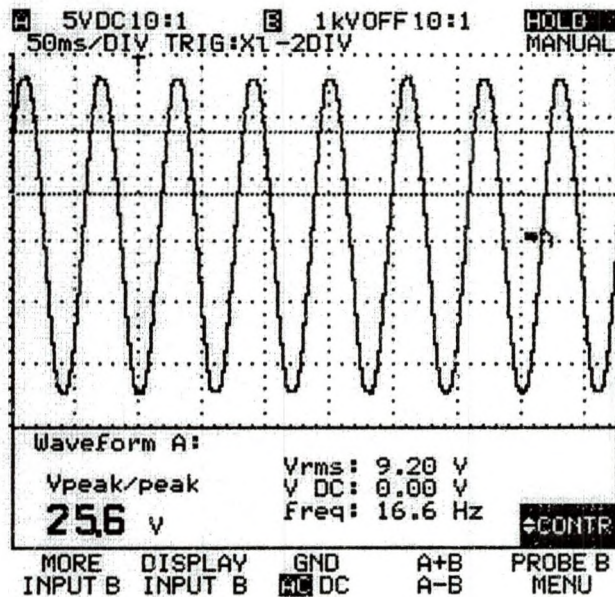
Figure 6.42: Closed-up Fundamental Line-Voltage (V_{ab}) Waveform of Figure 6.38 at Slider Set Point 0.8 Variac Input of 138 Volts AC

Figures 6.43 to 6.46 show the filtered and unfiltered current waveforms observed across the phase "a" current sensing resistor (input to the motor) for four combinations of variac inputs and slider setpoints.
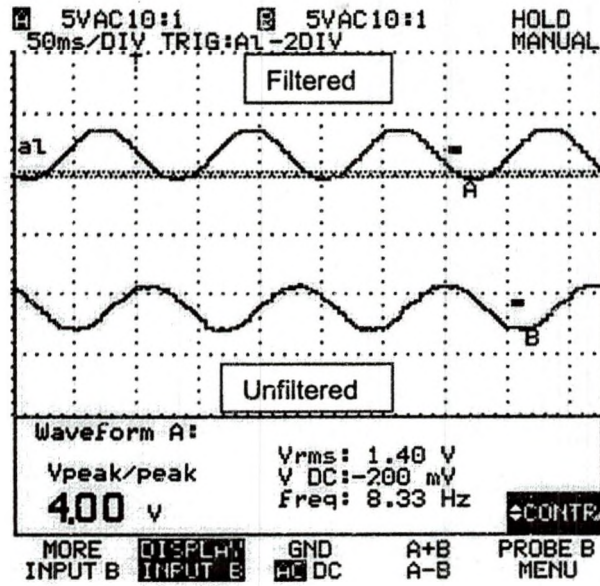
Figure 6.43:Motor Input Phase "a" Current Waveform for a Slider Setpoint of 0.4 and Variac Input of 70 Volts AC

Figure 6.44:Motor Input Phase "a" Current Waveform for a Slider Set Point of 0.4 and Variac Input of 138 Volts AC

Figure 6.45: Motor Input Phase "a" Current Waveform for a Slider Set 0.8 and Variac Input of 70 Volts AC
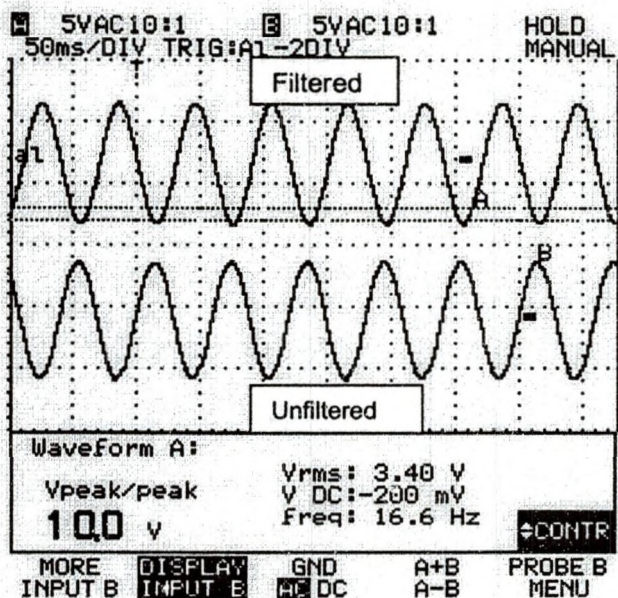
Figure 6.46: Motor Input Phase "a" Current Waveform at slider setpoint of 0.8 of and Variac Input of 138 Volts AC

All the measured parameters at the motor input are tabulated in Table 6.2.

The motor's RPM is higher for larger slider set points. Motor's speed is adjusted

by changing the slider set point which in turn controls the fundamental output frequency applied to the motor. The DSP, based on the slider setpoint value adjusts the fundamental frequency output to the DMC1500, thus adjusting the motor's speed. The fundamental frequency of the line-voltage determines the motor's speed. As the fundamental frequency is increased, the fundamental voltage is also increased proportionally to maintain the constant V/Hz profile. This relationship must be maintained to prevent overheating the motor yet it must be large enough to enable the motor to develop sufficient torque [44]. This is indicated by the observed waveforms shown from Figures 6.35 to 6.38. Table 6.2 shows the recorded values. Analysis shows that for a constant 70 Volts

Table 6.2: Measurements at Motor Input

Slider Set point		0.4		0.8	
Variac Input (Volts AC)		70	138	70	138
Bus Voltage (Volts DC)		95	189.5	93.3	188.7
RPM (Rev/Min)		499	509	1008	1013
Pulse (Volts DC)		96	190	96	190
Fundamental	Phase "a" Current (Amps AC p-to-p)	0.67	1.47	0.8	1.67
	Line Voltage (V_{ab} -Volts AC)	12.9	15.8	25.5	25.5
	Frequency (Hz)	8.33	8.33	16.6	16.6
	V/Hz (V_{ab}/Frequency)	0.77	0.95	0.77	0.77

AC variac input, increasing the slider set point by100% (from 0.4 to 0.8), increases the fundamental frequency by 100%, increases the fundamental line

voltage amplitude by 98% , increases fundamental phase current amplitude by 19.4 % and increases the RPM by 102%.

On the other hand keeping the slider set point constant and increasing the variac input by almost 100% has literally no effect on the motor's speed. For example keeping a constant slider setpoint at 0.4 and increasing variac input by 97% increases the fundamental line-voltage frequency by 0%, increases the fundamental line voltage amplitude by 22. 4%, increases the fundamental phase current by 119.4% and increases the speed by 2%. Although the phase-a current increased by 119.4% (measured across the current sensing resistor), the speed increased only by 2%. From equation (4.53) it can be seen that the magnetizing current (I_m) is the ratio of the stator voltage to stator winding inductance (L_m). The dramatic increase in current (I_m or phase-a current) should be the consequence of an increase in the fundamental voltage. However the fundamental voltage increased only by 22.4 %. Therefore what could have caused the current (I_m) to increase by 119.4% ? This indicates that speed is controlled by the fundamental frequency of the line-voltage and not the bus voltage (which is controlled by the variac input). At a constant slider setpoint of 0.4 (8.33 Hz fundamental frequency), increasing the DC bus voltage from 96 Volts DC to 170 Volts DC resulted in an increase in fundamental voltage from 12.9 to 15.8 Volts AC. Since the fundamental frequency is constant as it is controlled by the slider setpoint value the V/Hz profile increased slightly from 0.77 V/Hz to 0.95 V/Hz.

Voltage And Current Harmonic Distortion At Motor Input (Fluke 41)

The following observations were made at the motor input with Fluke 41 Power Harmonics Analyzer's current and voltage probes. The Fluke scopemeter showed that the observed fundamental line voltage and phase current waveforms (from Figures 6.39 to 6.46) were clean sinusoids. To verify that, harmonics analysis of the PWM output waveforms at the motor inputs were carried out. Figures 6.47 through 6.50 show that the phase current waveform is significantly free from harmonics for various combinations of slider set points and variac inputs. This agrees with the unfiltered waveforms of Figures 6.43 through 6.46. Only odd harmonics exist for the variac input of 138 V AC. Apparently, a higher bus voltage has an effect of attenuating even order harmonics. The induction motor has a natural low pass filtering characteristic that blocks the high frequency components. The low frequency components (triplen harmonics) were also absent in the phase-a current because the line-voltages (stator) were free from triplen harmonics. This agrees with line voltage waveforms of Figures 6.39 through 6.41.
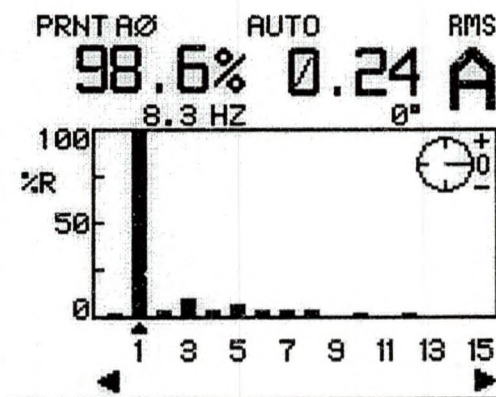
Figure 6.47: Motor Input Phase "a" Current Waveform Harmonic Spectra Slider for a Slider Set Point of 0.4 and a Variac Input of 70 Volts AC
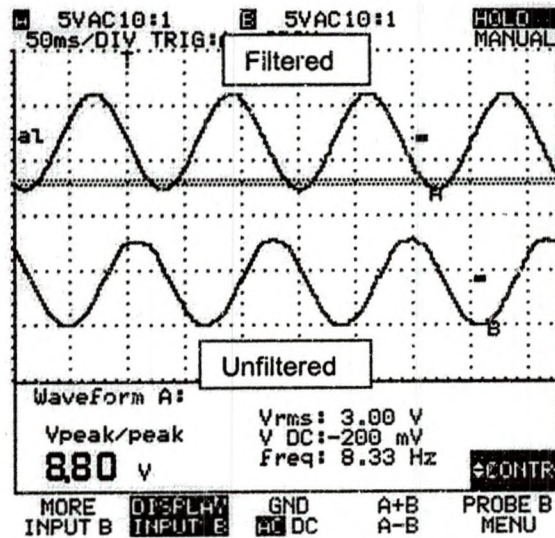
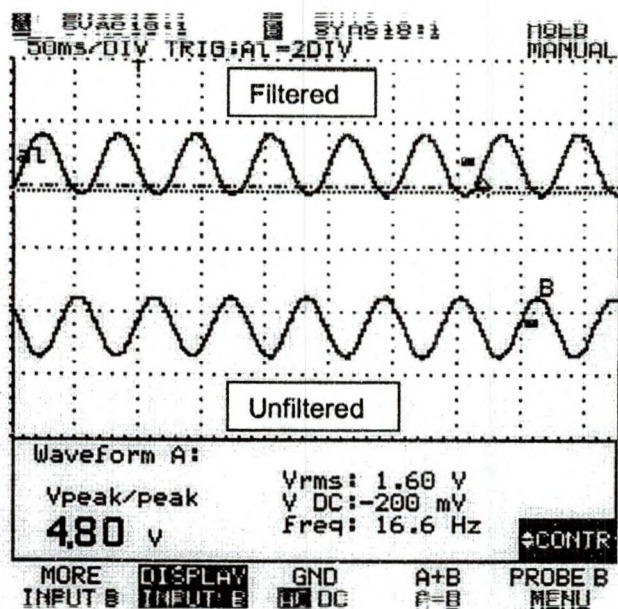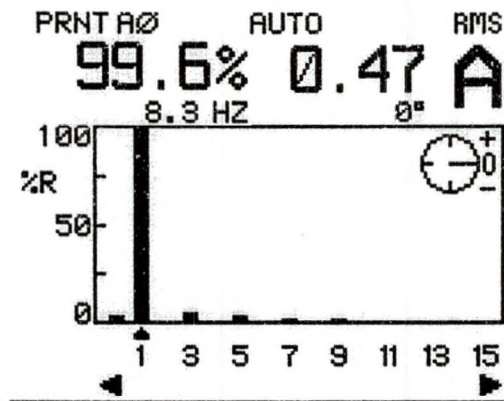Figure 6.48: Motor Input Phase "a" Current Waveform Harmonic Spectra for a Slider Set point of 0.4 and a Variac Input of 138 Volts AC
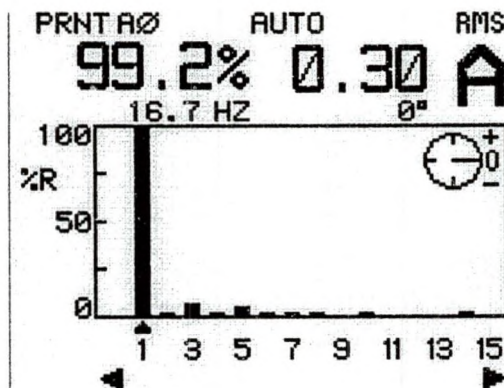
Figure 6.49: Motor Input Phase "a" Current Waveform Harmonic Spectra Slider at Slider Set point of 0.8 and Variac Input of 70 Volts AC
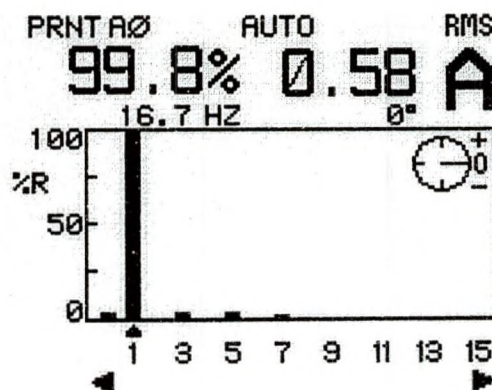
Figure 6.50: Phase "a" Current Waveform Harmonic Spectra Slider at Slider Set point 0.8 and Variac Input of 138 Volts AC

Figures 6.51 to 6.54 show the observed phase "a" voltage harmonics for various slider set points and variac inputs. The phase voltage has a very large magnitude of DC component (100%), about 30 % third harmonic magnitude and a small magnitudes of fifth and ninth harmonics.
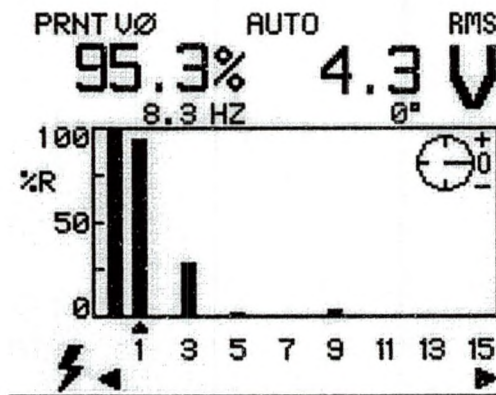
Figure 6.51: Motor Input Phase "a" Voltage Waveform Harmonic Spectra for a Set Point of 0.4 and a Variac Input of 70 Volts AC
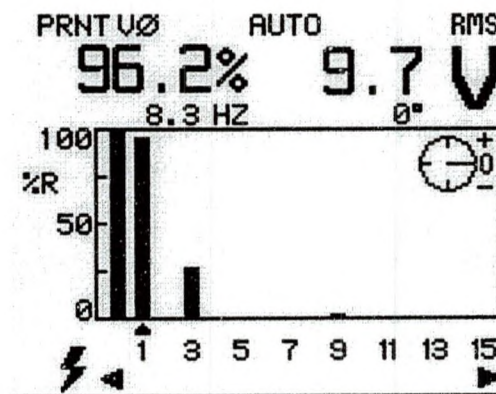
Figure 6.52: Motor Input Phase "a" Voltage Waveform Harmonic Spectra for a Slider Set Point of 0.4 and a Variac Input of 138 Volts AC

PRNT VØ　　AUTO　　RMS

96.9%　10.9 V

16.7 HZ　　Ø°
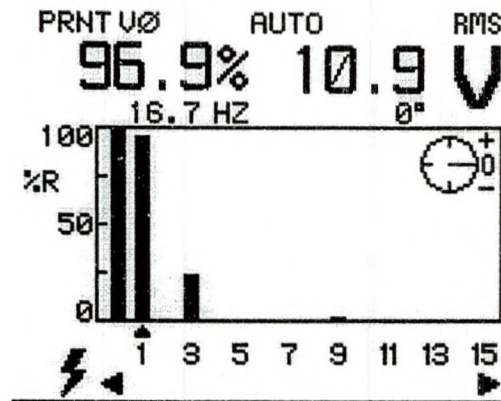
Figure.6.53: Motor Input Phase "a" Voltage Waveform Harmonic Spectra for a Slider Set Point of 0.8 and Variac Input of 70 Volts AC

PRNT VØ　　AUTO　　RMS

97.4%　22 V

16.7 HZ　　Ø°
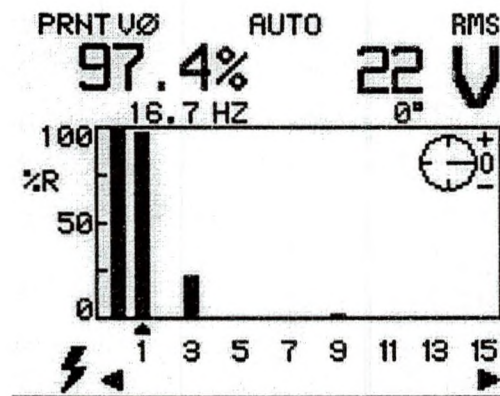
Figure 6.54: Motor Input Phase "a" Voltage Waveform Harmonic Spectra for a Slider Set Point of 0.8 and Variac Input of 138 Volts AC

Figures 6.55 to 6.58 show the observed line-voltage (V_{ab}) harmonics for various slider set points and variac inputs. The observation indicates that the line voltage is almost free from high content triplen order harmonics. This agrees with the waveforms of Figures 6.39 to 6.42. The phase voltage harmonics and the triplen harmonics (Figure 6.18) are cancelled-out in the line voltage waveform. As can be seen from Figures 6.51 and 6.55, the line voltage amplitude is $\sqrt{3}$x the phase voltage due to the three-phase relationship.
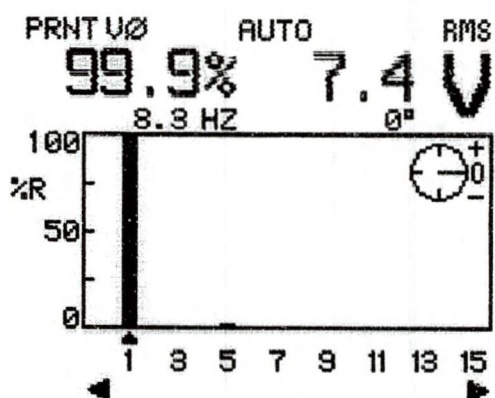
Figure 6.55: Motor Input Line Voltage (V_{ab}) Waveform Harmonic Spectra for a Slider Set Point of 0.4 and a Variac Input of 70 Volts AC
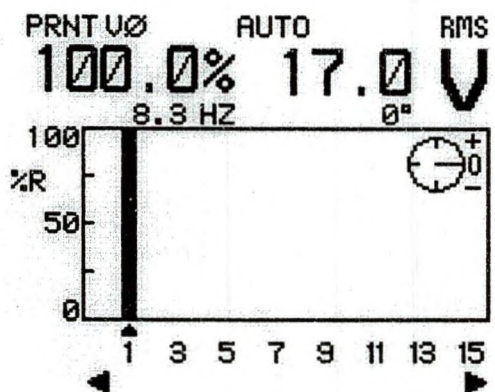
Figure 6.56:Motor Input Line Voltage (V_{ab}) Waveform Harmonic Spectra for a Slider Set Point of 0.4 and a Variac Input of 138 Volts AC
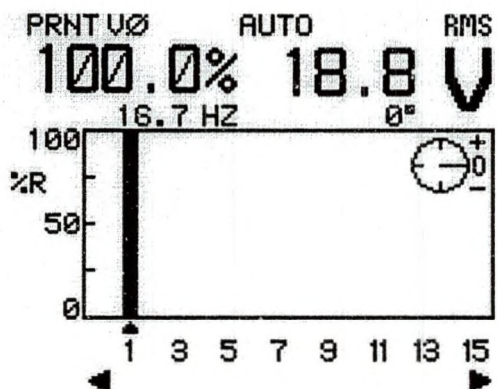
Figure 6.57: Motor Input Line Voltage (V_{ab}) Waveform Harmonic Spectra for a Slider Set Point of 0.8 and Variac Input of 70 Volts AC
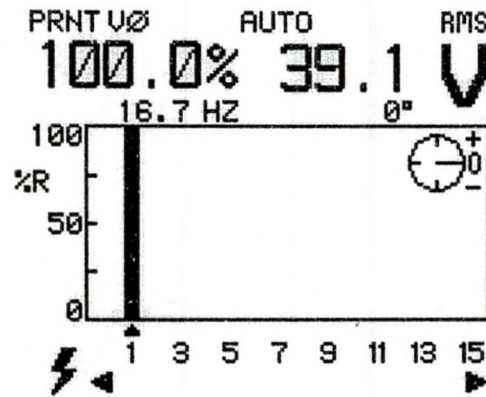
Figure 6.58:Motor Input Line Voltage (V_{ab}) Waveform Harmonic Spectra for a Slider Set Point of 0.8 and Variac Input of 138 Volts AC

Figures 6.59 and 6.60 show the observed line voltage (V_{ab}) harmonics, phase current "a" harmonics, line voltage waveform, phase current waveform, THDs and other measured parameters for slider set point of 0.8 and a variac input of 138V AC. The observation indicates that the line voltage has 0.9% THD-R and the phase current has 6.6% THD-R at slider set point of 0.8 and a variac input of 138V AC. THD-R represents the ratio of the harmonic components of voltage (or current) to the total voltage (or current), including the fundamental and all harmonics.
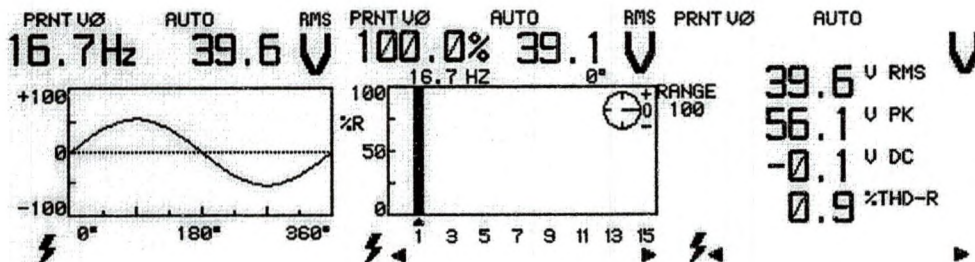
Figure 6.59: Motor Input Line Voltage (V_{ab}) Waveform, Harmonic Spectra and Harmonic Distortion
(Variac input = 138 V_{AC} and Slider Set point of 0.8)
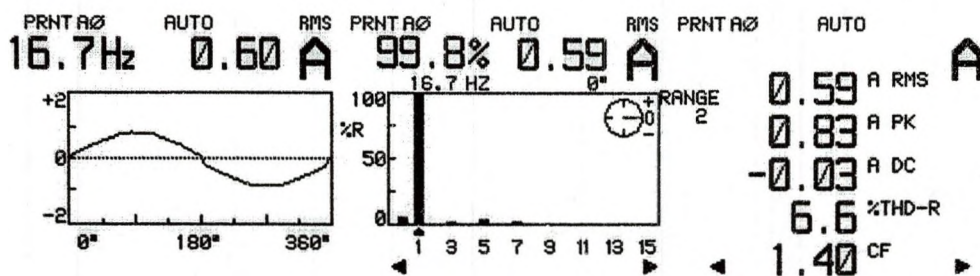
Figure 6.60: Motor Input Phase "a' Current Waveform, Harmonic Spectra and Harmonic Distortion
(Variac input = 138 V_{AC} and Slider Set point = 0.8)

Complete Phase Current Measurement

Figures 6.61 through 6.64 show the observed phase "a" current

harmonics, and their respective fundamental component amplitudes, THDs and

other measured parameters for various combinations of slider set points and

variac inputs. The observation (THD-F) indicates that the phase current

harmonics distortion is highest (16.9%) at a slider setpoint of 0.4 and variac input

of 70V AC and lowest (6.9%) at a slider setpoint of 0.8 and variac input of 138V.

THD-F represents the ratio of the harmonic components of voltage (or current) to

the voltage (or current) of the fundamental alone.
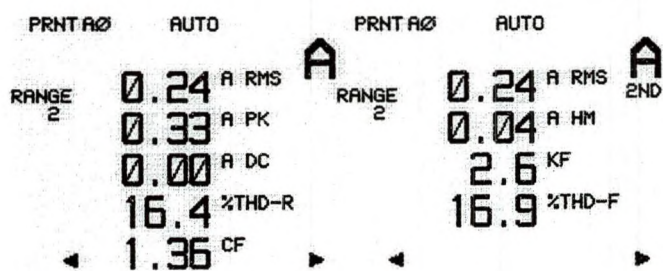
Figure 6.61: Motor Input Phase "a' Current Waveform Measured Parameters
(Variac input = 70 V_{AC} and Slider Set point = 0.4)
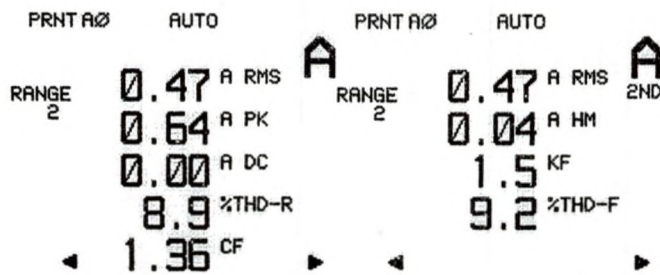
Figure 6.62: Motor Input Phase "a' Current Waveform Measured Parameters
(Variac input = 138 V_AC and Slider Set point = 0.4)
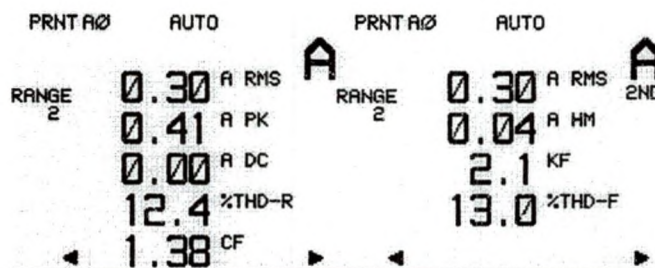
Figure 6.63: Motor Input Phase "a' Current Waveform Measured Parameters
(Variac input = 70 V_AC and Slider Set point = 0.8)
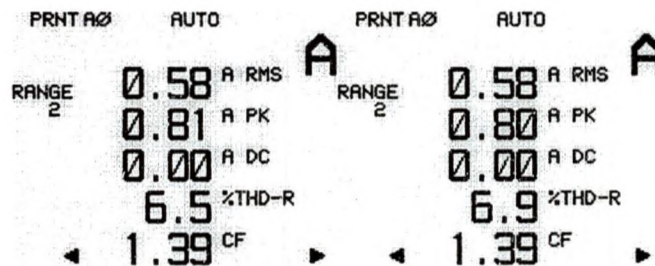
Figure 6.64: Motor Input Phase "a' Current Waveform Measured Parameters
(Variac input = 138 V_AC and Slider Set point = 0.8)

Complete Line Voltage (V_ab) Measurement

Figures 6.65 thru 6.68 show the observed line voltage (V_ab) harmonics and

their respective fundamental component amplitudes, THDs and other measured

parameters for various combinations of slider set points and variac inputs. The

observation (THD-F) indicates that the line-voltage harmonics distortion is highest (3.4%) at a slider setpoint of 0.4 and variac input of 70V AC and lowest (0.9%) at at slider setpoint of 0.8 and variac input of 138V.
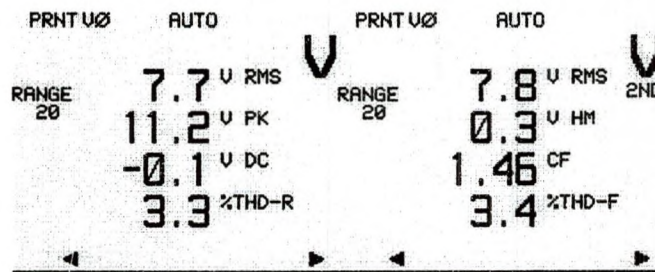
Figure 6.65: Motor Input Line Volltage (V$_{ab}$) Waveform Measured Parameters
(Variac input = 70 V$_{AC}$ and Slider Set point = 0.4)
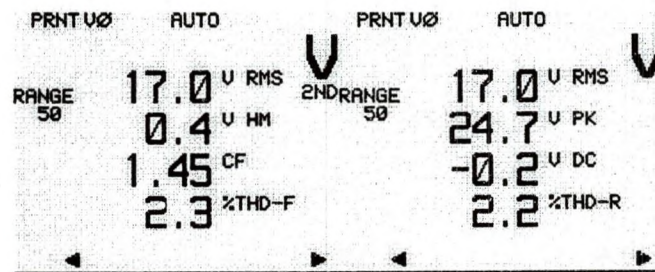
Figure 6.66:Motor Input Line Volltage (V$_{ab}$) Waveform Measured Parameters
(Variac input = 138 V$_{AC}$ and Slider Set point = 0.4)
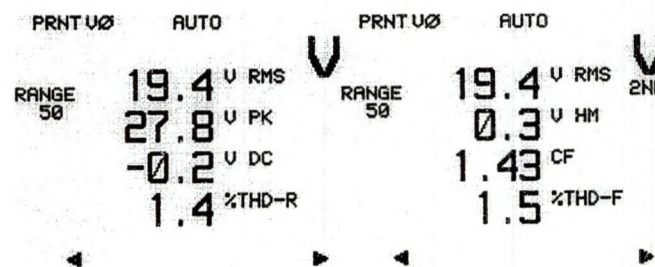
Figure 6.67:Motor Input Line Volltage (V$_{ab}$) Waveform Measured Parameters
(Variac input = 70 V$_{AC}$ and Slider Set point = 0.8)

PRNT UØ   AUTO   PRNT UØ   AUTO

RANGE 100   **39.4** U RMS   2ND RANGE 100   **39.5** U RMS

0.4 U HM   **55.9** U PK

1.42 CF   **-0.2** U DC

0.9 %THD-F   **0.9** %THD-R
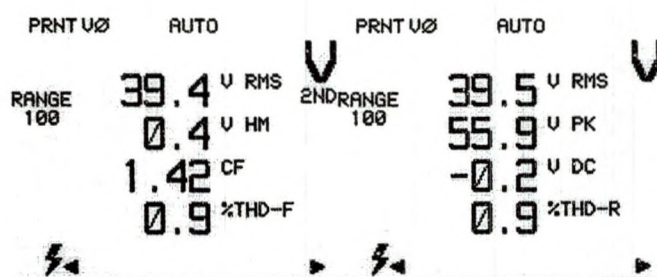
Figure 6.68: Motor Input Line Volltage (V_{ab}) Waveform Measured Parameters
(Variac input = 138 V_{AC} and Slider Set point = 0.8)

CHAPTER 7

CONCLUSIONS AND RECOMMENDATIONS

7.1 The Square Wave Inverter

The square wave inverter discussed in chapter 2 generates a very high level of harmonics that are hard to get rid of. The square wave's switching frequency is very low so it produces only low frequency switching noise. Its major drawback is that its waveform is rich with a high level of lower order odd harmonics. Current and voltage harmonics can cause such problems as excessive heat in wiring, connections, motors, and in transformers and can cause inadvertent tripping of circuit breakers [83]. The harmonics also can propagate and interfere with the normal operations of other equipment or devices. This can cause an erratic behavior in biomedical devices such as pacemakers and thus pose a human safety hazard. The selective harmonic elimination technique discussed in section 3.8 may be used effectively in square wave inverter to eliminate the dominant harmonics. For example, once the hard-to-filter third and fifth harmonics are removed from the spectra a low pass filter will easily recover the fundamental frequency component. It is easy to build a square wave inverter.

7.2 Pulse Width Modulation (PWM) Technique

Sine Wave PWM powered inverters dicussed in chapter 3 produce waveforms that are compatible with power distribution companies' waveforms,

and therefore operate on any equipment without interference or overheating. At every switching time period, the sine wave PWM inverters deliver energy to the load equivalent to what would have been delivered by the modulating (desired) waveform. Over one switching time period the average voltage applied to the load is proportional to the amplitude of the modulating signal (assumed constant) during this period [25]. The higher the switching frequency, the smaller the switching time period and the better the quality of the power delivered to the load (lower THD). However, the switching frequency is limited by the switching losses and EMI problems

Bipolar Versus Unipolar PWM Waveform

The bipolar PWM inverter switching frequency is 2x lower than the unipolar PWM inverter switching frequency. Therefore the control circuitry required to build the bipolar PWM inverter is much simpler and cheaper than the unipolar PWM inverter. The bipolar PWM inverter needs only one modulating waveform to generate the PWM waveform and it is more suitable for single phase inverters. The unipolar PWM switching requires more than one modulating waveform. To be more economical and practical, the unipolar PWM switching is more suitable for three-phase inverters. However, the bipolar PWM switching sine wave may not be as smooth as a the unipolar PWM switching sinewave because of its slower switching rate. A high-end low pass filter may be required at the output to match the quality of the unipolar PWM switching output waveform. Therefore selecting a bipolar or unipolar PWM inverter depends on cost and quality of the needed power.

Selective Harmonic Elimination PWM

The selective harmonic elimination PWM technique discussed in section 3.8 is suitable for eliminating certain harmonics. The selective harmonic elimination PWM technique is similar to bipolar PWM switching technique but it does not require a carrier wave to generate a PWM waveform. In the selective harmonic elimination technique, the PWM waveform is generated by a set of pre-calculated switching angles. In the PWM waveform shown in Figure 1.2 the hard-to-filter third and fifth harmonics can be eliminated with only two switching angles ($\alpha = 23.62°$ and $\beta = 33.3°$) per quadrant. For example, once the hard-to-filter third and fifth harmonics are removed from the spectra, a low pass filter will easily recover the fundamental frequency component. As the number of switching angles per quadrant increases, more harmonic multiples at the output voltage waveform can be removed. The artificial neural network technique discussed in section 3.9 integrates low switching losses (due to low frequency switching), efficient control of the fundamental output voltage as well as eliminates the selected set of harmonics. The piecewise-linear strategy eliminates the requirement for high computing powers. However, increasing the α_n's increases the number of switching actions per quarter cycle. This increases switching losses and reduces the average output voltage. Figure 3.16 indicates the relationship between notch angles and the fundamental frequency amplitude. Therefore, there is a compromise and the reference [1] method has eliminated all the non-triplen harmonics up to the 29th. The selective harmonic elimination technique offers a better voltage utilization and lower switching frequencies [11].

However, when this technique is used with variable frequency/amplitude inverter, complicated control hardware is required to store and to access the large number of switching angles [11].

7.3 Space Vector PWM (SVPWM)

SVPWM technique discussed in section 4.3 is relatively simple and more efficient than the sine wave PWM technique. $\vec{V}_{ref}$, the rotating vector, is the desired three-phase output voltage of the inverter, mapped to the complex plane. When the desired waveform is a balanced three-phase voltage waveform, then $\vec{V}_{ref}$ becomes a rotating vector with a frequency and amplitude equal to that of the desired three-phase voltage waveform.

SVPWM method provides a more efficient use of the DC supply voltage than the sine wave PWM method. The magnitude of each of the six active-state space vectors is $\frac{2}{3}V_{DC}$. In steady state operation, when approximating a three-phase balanced sinusoid, $\vec{V}_{ref}$'s radius is constant and less than $\frac{2}{3}V_{DC}$. For this reason the $\vec{V}_{ref}$'s locus is a circle inscribed within a hexagon with a radius of $\frac{1}{\sqrt{3}}V_{DC}$ (Figure 4.16). The locus of $\vec{V}_{ref}$ for sine wave PWM is a circle with a radius $\frac{1}{2}V_{DC}$. With the SVPWM technique (Figure 4.16) the maximum inverter output voltage is 90.6% of the inverter capability compared to the sine wave PWM, which is only 78.5% efficient. With SVPWM method (compared to sine wave PWM method) the percentage of the inverter capability is increased by 15.4%.

Equation (4.25) shows that given the reference vector components (V_α and V_β) as the inputs for the SVPWM system the outputs are the on times need to approximate $\overline{V}_{ref}$. The rotation of $\overline{V}_{ref}$ in sector 1 and the corresponding three-phase PWM waveform patterns were shown in Figure 5.12. In a switching time period, every position of $\overline{V}_{ref}$ results in a unique set of three-phase PWM patterns. Figure 7.1 shows the hexagon and the three-phase PWM patterns in all the sectors as $\overline{V}_{ref}$ rotates 360° [20].
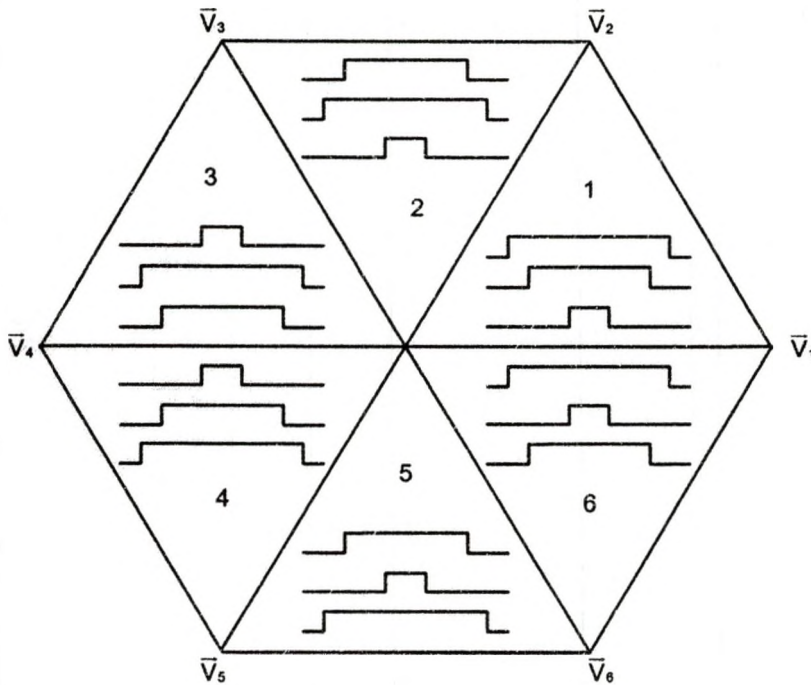
Figure 7.1: Hexagon of SVPWM in All Sectors

Experimentation

The observations at the DSP output and motor input indicate that the motor input voltage waveforms are the exact waveforms that the DSP give out, but on a larger scale. The amplitude of PWM pulses at the motor input are the same as the DC bus voltage. From Figure 6.18, the DSP Duty Ratio and

Line Voltage (V_{ab}) output waveforms, it can be concluded that the duty ratio (phase voltage) waveform is distorted with triplen harmonics. Figures 6.51 to 6.54 show the phase "a" voltage waveform harmonic spectra at the motor input. The motor input phase "a" voltage waveform harmonic spectra show that it (motor input phase "a" voltage) has a very high level of DC component, about 30% 3rd order harmonic and a low level of 9th harmonic. However these harmonics do not affect the line-voltage. The harmonics spectra of the line voltage (Figures 6.55 to 6.58) show that the line voltage is free from low order harmonics up to 15th order. However the line-voltage waveform contains the high switching frequency harmonics, as seen from the line-voltage pulses shown in Figure 6.33

It can be seen from the observed phase voltage waveforms at the motor input that the inverter generates only pulses that have high harmonic content (Figures 6.51 to 6.54). However, in Figure 6.59, the observed fundamental line voltage (V_{ab}) waveform, its harmonic spectra and THD-R (0.9%) at the motor input, show that the inverter fundamental line-voltage is free from high content low order harmonics. It seems like the motor recognizes only the fundamental line voltage waveforms, therefore the phase current is a sinusoid. In the line voltage the triplen harmonics cancel and the high frequency switching harmonics are attenuated by the motor's inductances. The current waveform's (Figures 6.43 thru 6.46) switching harmonics are mainly suppressed by the low-pass characteristic of the machine inductances. The distortion in the current becomes smaller when the commanded voltage is sampled more accurately, that means

the sampling period becomes smaller and sampling frequency increases.

The VisSim's slider set-points control the amplitude and frequency of the fundamental frequency component that drives the motor. For a bigger slider set point value of 0.8 the fundamental frequency output has a higher amplitude and frequency. The increase in frequency makes the motor run faster. The increase in frequency is accompanied by an increase in amplitude to maintain the constant V/Hz profile.

7.4 Grounding And Shielding

The output of the inverter phase voltages contains a very high level of switching harmonics. The output from the power transistors was connected to the motor using four feet of cable. There were very high levels of conducted and radiated spurs. To solve this problem, an output filter sufficient to meet the conducted emission standards could be used, but it is very costly, therefore it is recommended to use shielded power cables and solid grounding. The single phase AC line input of the drive carries a substantial RF noise primarily because it comprises the return path for the common-mode RF current. This can be solved with the installation of an RFI filter. This coupled with a screened cable provides a low impedance return path for the RF current [82].

Inadequate grounding and shielding of the motor cable can be the major source of radiated spur. The screening material too plays a part in curbing the radiated emission. Some drive manufacturers have recommended specialized cables using one or more braided copper shields. Measurements of control techniques have consistently shown that low-cost steel-wire armoured cable, as

is widely used in the UK, gives equally good results. The reason for this appears to be that although the steel wire is a less effective shield (impedance is higher than for the copper braid), the losses in this frequency range are higher so that the actual current flowing in the shield is less. The cable is terminated by an impedance far removed from its characteristic impedance, so it is strongly resonant at some frequencies. The loss caused by the steel wire gives a useful degree of damping [82].

7.5 Recommendations

Various PWM Techniques

In this thesis the square wave technique, the six-step mode and PWM techniques (sine wave PWM, SVPWM, harmonic elimination PWM) were discussed. Different techniques generate different waveshapes that have different harmonic spectra and fundamental component amplitude. There are references that talk about the fundamental component amplitude and the harmonic profiles of various AC waveform generation techniques. However, more references that compare and document the various AC waveform generation and PWM techniques would be helpful. There is a need to provide a complete documentation of various AC waveform technique based on experimental results. This type of documentation will be a valuable reference among the power electronics researchers.

Closed-loop V_s/f Control

In section 4.10 it was noted that a simple open-loop V_s/f (or V/Hz) system is not suitable to accurately control the speed with the presence of a load. As

load increases the slip speed increases. To rectify this, a slip compensation strategy can be included for speed control. Thus, the result is a closed-loop V/Hz system with a speed sensor as shown in Figure 4.21. The open-loop motor speed control that was implemented in this thesis should be extended to a closed-loop speed control system.

APPENDIX A: MATLAB SOURCE CODE

Space Vector Duty Ratio Waveform (Phase voltage plot)

```
%Magnitute of reference vector
Vref=1;

% sectors phase a
theta1=0:.01/pi:pi/3;
theta2=pi/3:.01/pi:2*pi/3;
theta3=2*pi/3:.01/pi:pi;
theta4=pi:.01/pi:4*pi/3;
theta5=4*pi/3:.01/pi:5*pi/3;
theta6=5*pi/3:.01/pi:2*pi;

%phase a voltages
Va1=0.5*Vref*sqrt(3)*cos(theta1-pi/6);
Va2=0.5*3*Vref*cos(theta2);
Va3=0.5*sqrt(3)*Vref*cos(theta3+pi/6);
Va4=0.5*sqrt(3)*Vref*cos(theta4-pi/6);
Va5=0.5*3*Vref*cos(theta5);
Va6=0.5*sqrt(3)*Vref*cos(theta6+pi/6);

% sectors phase b
thet1=2*pi/3:.01/pi:pi;
thet2=pi:.01/pi:4*pi/3;
thet3=4*pi/3:.01/pi:5*pi/3;
thet4=5*pi/3:.01/pi:2*pi;
thet5=0:.01/pi:pi/3;
thet6=pi/3:.01/pi:2*pi/3;

%phase b voltages
Vb1=0.5*Vref*sqrt(3)*cos(thet1-pi/6-2*pi/3);
Vb2=0.5*3*Vref*cos(thet2-2*pi/3);
Vb3=0.5*sqrt(3)*Vref*cos(thet3+pi/6-2*pi/3);
Vb4=0.5*sqrt(3)*Vref*cos(thet4-pi/6-2*pi/3);
Vb5=0.5*3*Vref*cos(thet5-2*pi/3);
Vb6=0.5*sqrt(3)*Vref*cos(thet6+pi/6-2*pi/3);

% sectors phase c
the1=4*pi/3:.01/pi:5*pi/3;
the2=5*pi/3:.01/pi:2*pi;
the3=0:.01/pi:pi/3;
the4=pi/3:.01/pi:2*pi/3;
the5=2*pi/3:.01/pi:pi;
the6=pi:.01/pi:4*pi/3;
```

```
% phase c voltages
Vc1=0.5*Vref*sqrt(3)*cos(the1-pi/6-4*pi/3);
Vc2=0.5*3*Vref*cos(the2-4*pi/3);
Vc3=0.5*sqrt(3)*Vref*cos(the3+pi/6-4*pi/3);
Vc4=0.5*sqrt(3)*Vref*cos(the4-pi/6-4*pi/3);
Vc5=0.5*3*Vref*cos(the5-4*pi/3);
Vc6=0.5*sqrt(3)*Vref*cos(the6+pi/6-4*pi/3);

%plot phase voltages
plot(theta1,Va1,'--b',theta2,Va2,'--b',theta3,Va3,'--b',theta4,Va4,'--b',theta5,Va5,'--
b',theta6,Va6,'--b');
hold on
plot(thet1,Vb1,'g:',thet2,Vb2,'g:',thet3,Vb3,'g:',thet4,Vb4,'g:',thet5,Vb5,'g:',thet6,Vb
6,'g:');
plot(the1,Vc1,'-r',the2,Vc2,'-r',the3,Vc3,'-r',the4,Vc4,'-r',the5,Vc5,'-r',the6,Vc6,'-r');
%clf;
axis([0 2*pi -2 2]);
grid on;
ylabel('phase voltage amplitude');
xlabel('\omegat');
set(gca,'XTick',0:pi/3:2*pi);
set(gca,'XTickLabel',{'0','pi/3','2pi/3','pi','4pi/3','5pi/3','2*pi'});
text(.1,1.6,'Phase Voltages Of The Inverter Output');
title('text(.1,1.6,'Square wave 50% duty cycle') ;
```

Three –Phase Line Voltage plot

```
%Magnitute of reference vector
Vref=1;

% sectors phase a
theta=0:.01/pi:2*pi;

%phase a voltages
Vab=sqrt(3)*Vref*sin(theta+pi/3);
Vbc=sqrt(3)*Vref*sin(theta+pi/3-2*pi/3);
Vca=sqrt(3)*Vref*sin(theta+pi/3-4*pi/3);

%plot phase voltages
plot(theta,Vab,'--b');
hold on
plot(theta,Vbc,'g:');
plot(theta,Vca,'-r');
hold off
```

```
%clf;
axis([0 2*pi -2 2]);
grid on;
ylabel('line-to-line voltage amplitude');
xlabel('\omegat');
set(gca,'XTick',0:pi/3:2*pi);
set(gca,'XTickLabel',{'0','pi/3','2pi/3','pi','4pi/3','5pi/3','2*pi'});
text(.1,1.6,'line-to-line Voltages Of The Inverter Output');
title('text(.1,1.6,'Square wave 50% duty cycle') ;
```

APPENDIX B: DUTY RATIO DERIVATION

Finding the inverse of :

$$\begin{bmatrix} V_\alpha \\ V_\beta \end{bmatrix} \frac{T_{PWM}}{2} = \frac{2}{3} V_{DC} \begin{bmatrix} \cos\left[(n-1)60^\circ\right] & \cos(n60^\circ) \\ \sin\left[(n-1)60^\circ\right] & \sin(n60^\circ) \end{bmatrix} \begin{bmatrix} T_n \\ T_{n+1} \end{bmatrix}$$

The inverse is

$$\begin{bmatrix} T_n \\ T_{n+1} \end{bmatrix} = \frac{T_{PWM}}{2} \cdot \frac{3}{2V_{DC}} \begin{bmatrix} \cos\left[(n-1)60^\circ\right] & \cos(n60^\circ) \\ \sin\left[(n-1)60^\circ\right] & \sin(n60^\circ) \end{bmatrix}^{-1} \begin{bmatrix} V_\alpha \\ V_\beta \end{bmatrix}$$

$$= \frac{3T_{PWM}}{4V_{DC}} \frac{\begin{bmatrix} \sin(n60^\circ) & -\cos(n60^\circ) \\ -\sin\left[(n-1)60^\circ\right] & \cos\left[(n-1)60^\circ\right] \end{bmatrix} \begin{bmatrix} V_\alpha \\ V_\beta \end{bmatrix}}{\sin(n60^\circ)\cos\left[(n-1)60^\circ\right] - \sin(n60^\circ)\cos\left[(n-1)60^\circ\right]}$$

$\{\text{using the trig identity} : \sin(\theta \pm \phi) = \sin\theta\cos\theta \pm \cos\theta\sin\theta\}$

$\sin(n60^\circ)\cos\left[(n-1)60^\circ\right] - \sin(n60^\circ)\cos\left[(n-1)60^\circ\right] = \sin(n60^\circ - (n-1)60^\circ)$

$= \sin 60^\circ = \dfrac{\sqrt{3}}{2}$

therefore

$$\begin{bmatrix} T_n \\ T_{n+1} \end{bmatrix} = \frac{3T_{PWM}}{4V_{DC}} \frac{\begin{bmatrix} \sin(n60^\circ) & -\cos(n60^\circ) \\ -\sin\left[(n-1)60^\circ\right] & \cos\left[(n-1)60^\circ\right] \end{bmatrix} \begin{bmatrix} V_\alpha \\ V_\beta \end{bmatrix}}{\dfrac{\sqrt{3}}{2}}$$

$$\begin{bmatrix} T_n \\ T_{n+1} \end{bmatrix} = \frac{T_{PWM}}{V_{DC}} \cdot \frac{\sqrt{3}}{2} \begin{bmatrix} \sin(n60^\circ) & -\cos(n60^\circ) \\ -\sin\left[(n-1)60^\circ\right] & \cos\left[(n-1)60^\circ\right] \end{bmatrix} \begin{bmatrix} V_\alpha \\ V_\beta \end{bmatrix}$$
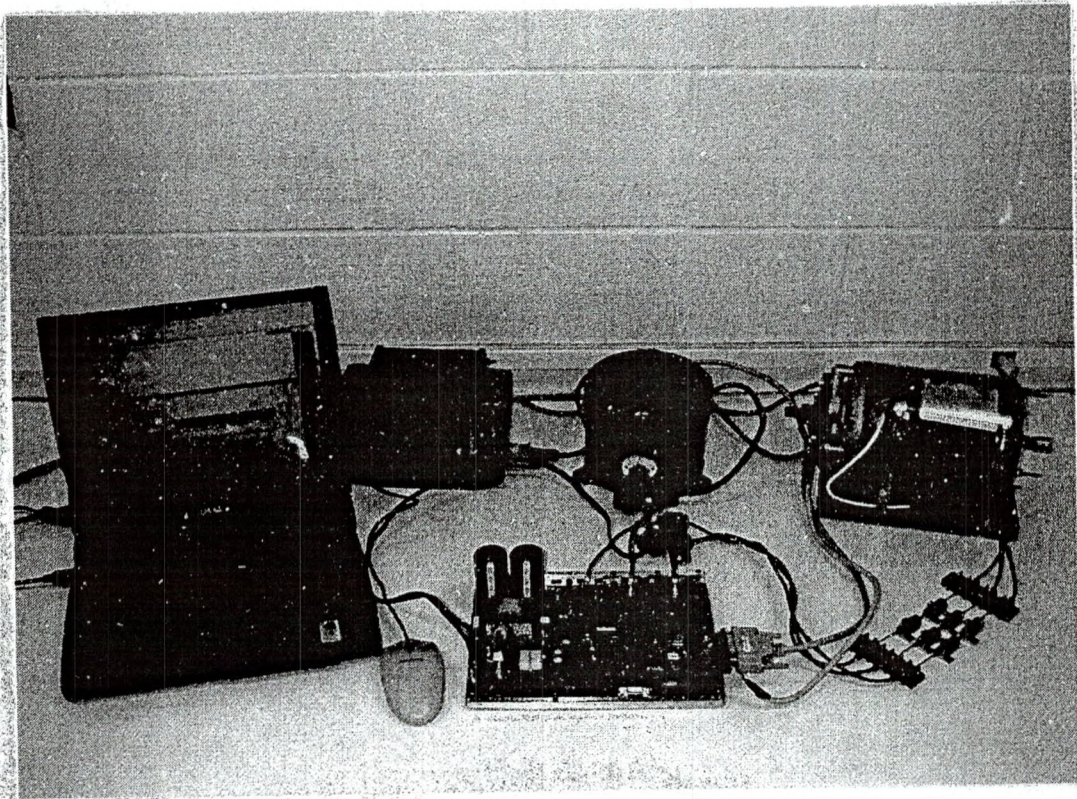
APPENDIX D: PICTURE OF eZdsp and DMC1500
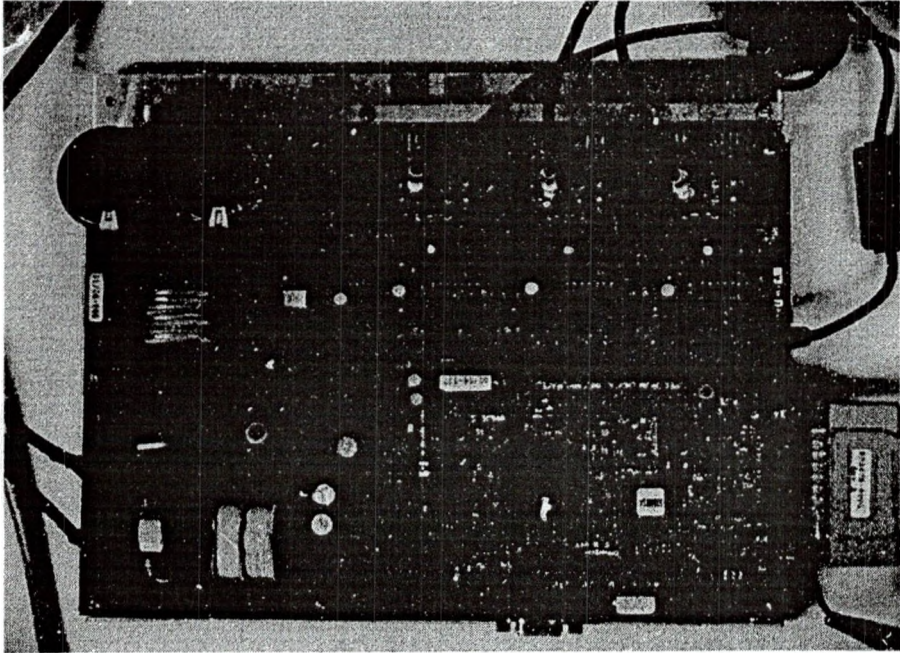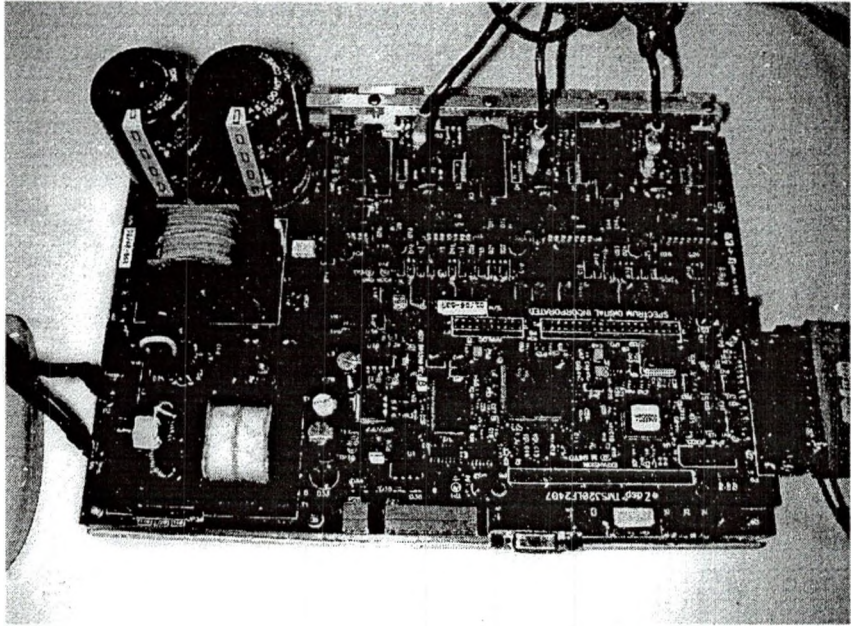
APPENDIX E: PICTURE of eZdsp
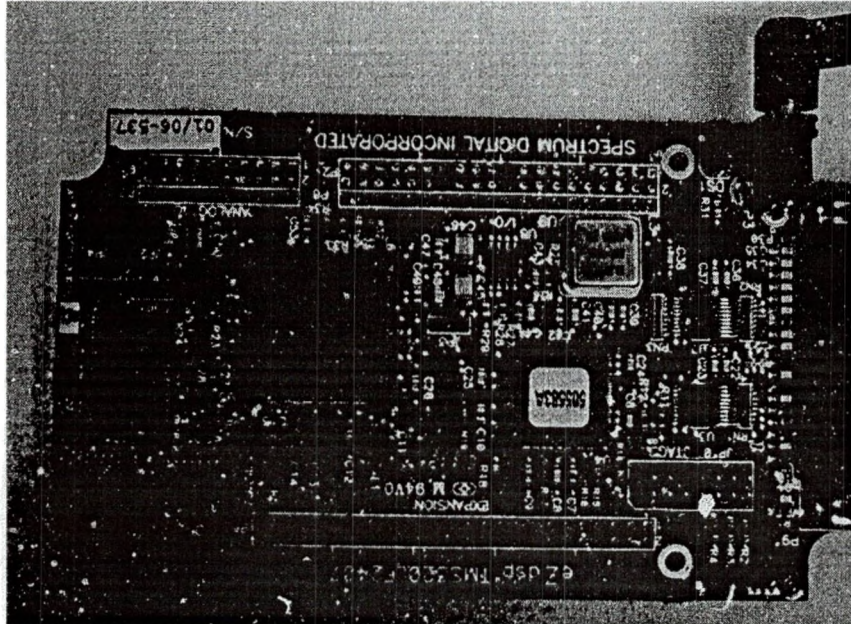
FRONT VIEW

BACK VIEW

APPENDIX F: PICTURE OF TMS320LF2407 (DSP)
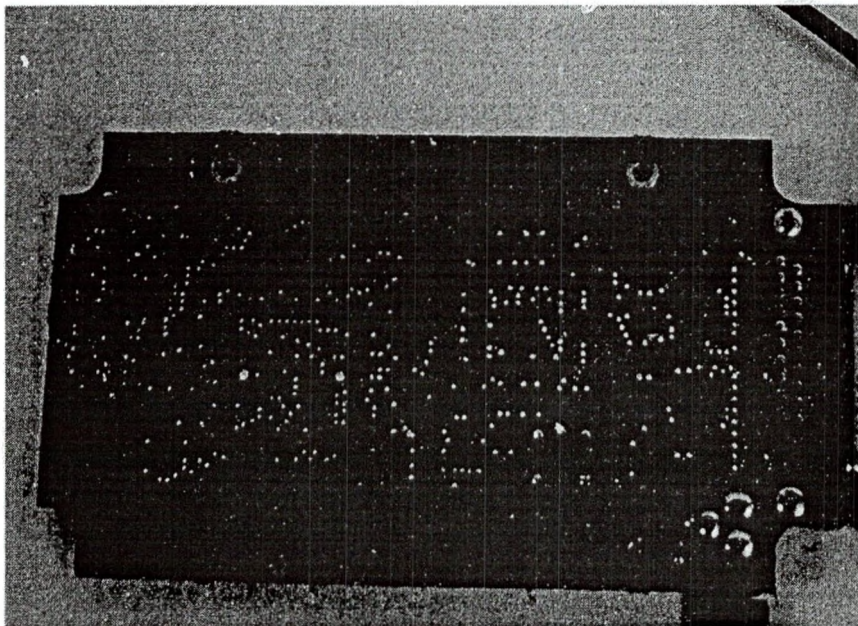
APPENDIX G: CURRENT WAVEFORM HARMONICS OBSERVED ACROSS
THE CURRENT SENSING RESISTORS

Variac = 70 V$_{AC}$
Slider = 0.4

Variac = 138 V$_{AC}$
Sider = 0.4

Variac = 70 V$_{AC}$
Slider = 0.8

Variac = 138 V$_{AC}$
Slider = 0.8
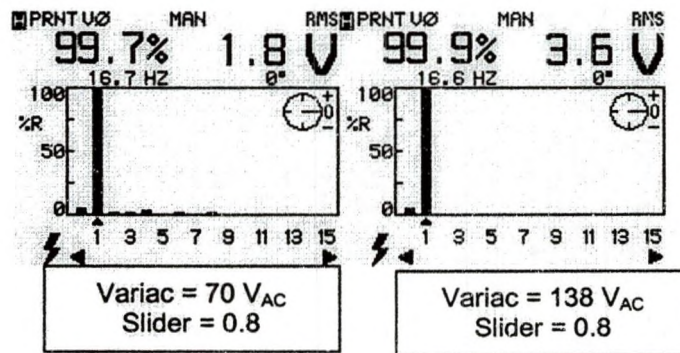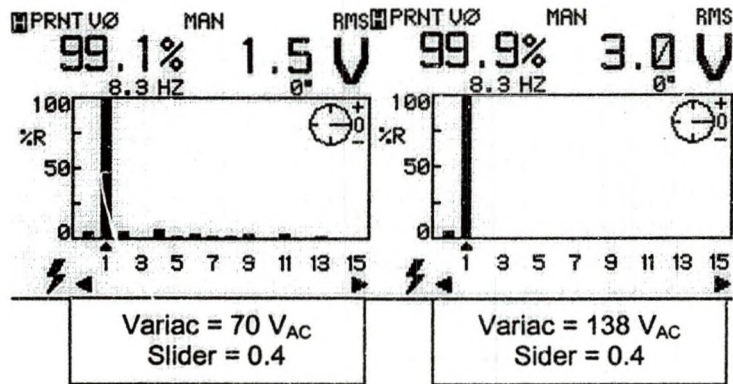
APPENDIX H: MEASURING INSTRUMENTS AND EQUIPMENT

1) Fluke 99B scopemeter series II 100Mhz (9444 200 99003, No DM6640235)

2) Fluke 41 power harmonics analyzer (6050018)

3) Fluke 45 dual display multimeter (5310062)

4) Philips Oscilloscope (Pm3335/40, DQ005076)

5) Dell Laptop Inspiron 4000, OS Windows 2000

6) Isolation transformer, 115V/115V, Triad N-59M (10366424)

7) Variable auto transformer (Variac), Tenma, Input 117V/ouput 130V

8) Three-phase induction motor, 3/4hp, Emerson, Model P55AZET-220, CAT 2758244

9) $2 \times 3\Omega$ 25 watts 1% resistors

10) Safety glasses

11) Low Pass Filter/High Pass Filter, Waveteck Rockland, Model 852, Dual HI/LO Filter, IBM 656819A
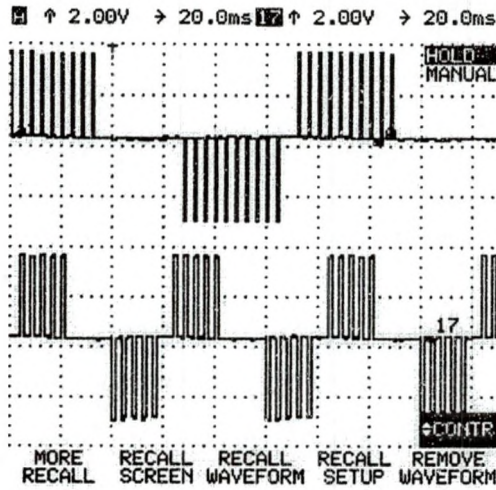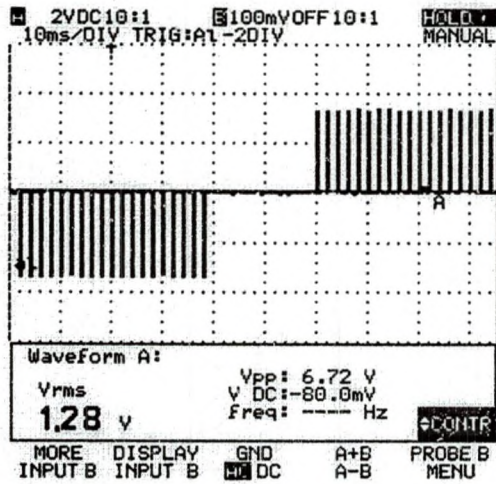
Slider setpoint =0.8

Slider setpoint =0.4
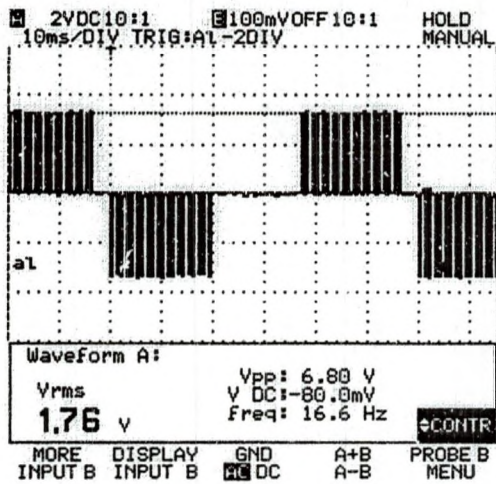
Slider setpoint =0.8
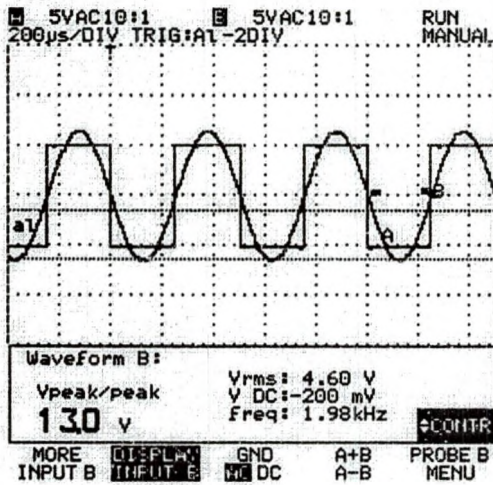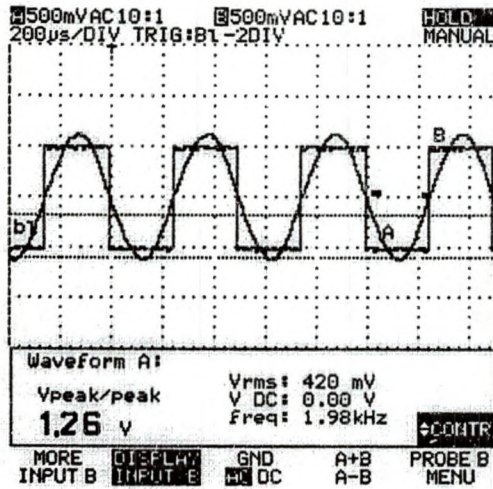
APPENDIX K: PHASE "A" VOLTAGE PULSES AND ITS FUNDAMENTAL
WAVEFORM AT MOTOR INPUT.
VARIAC INPUT: 138V AC AND SLIDER SET POINT: 0.8
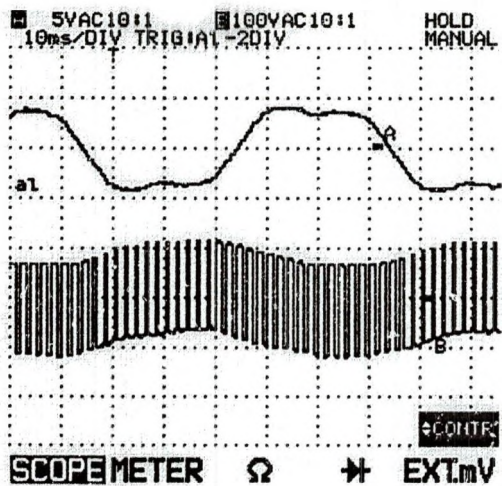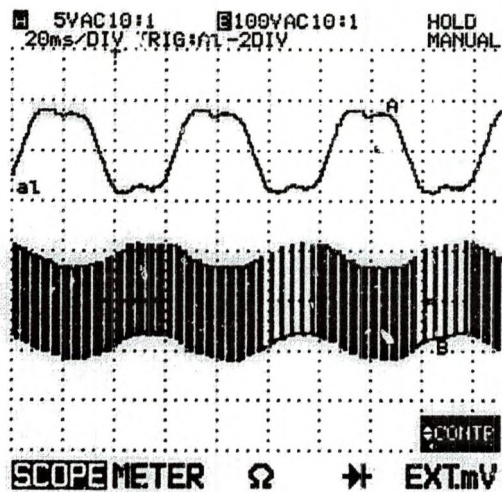
APPENDIX L: LINE VOLTAGE PULSES AND ITS FUNDAMENTAL WAVEFORM AT MOTOR INPUT.
SLIDER SET POINT: 0.4
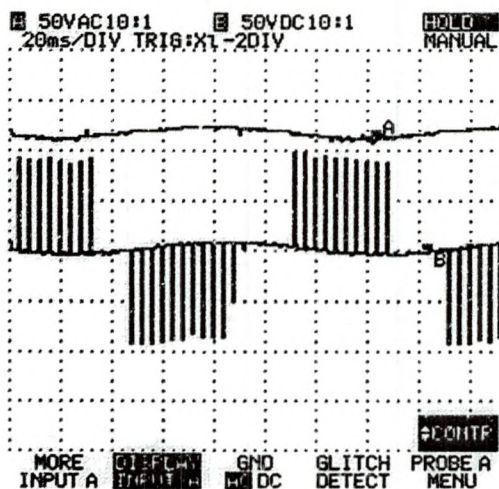
variac input =70V AC
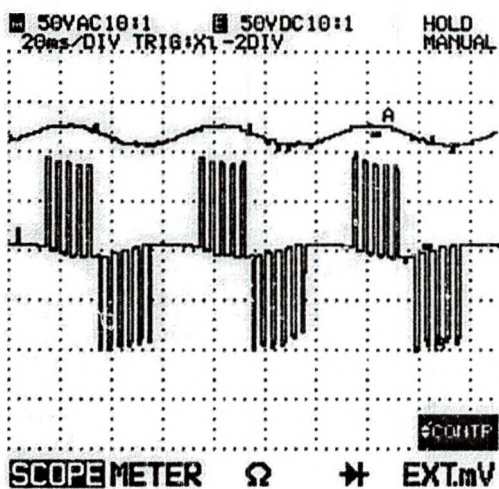
variac input =138V AC

APPENDIX M: LINE VOLTAGE PULSES AND ITS FUNDAMENTAL
WAVEFORM AT MOTOR INPUT.
SLIDER SET POINT: 0.8
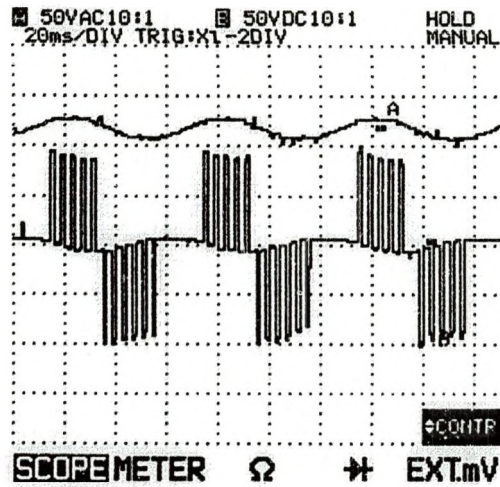
variac input
=70V AC
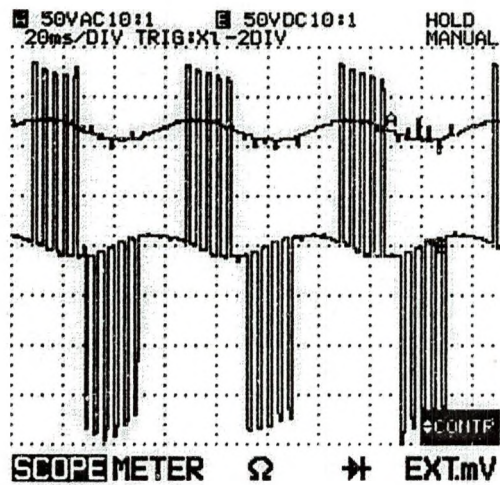
variac input
=138V AC

APPENDIX N:PWM-PHASE-A (DUTY RATIO) WAVEFORM AT THE DSP OUTPUT FOR A SLIDER SETPOINT OF 0.4
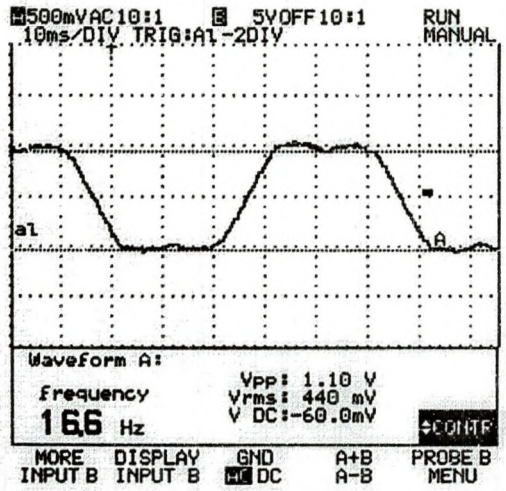
LOW PASS FILTER CUT-OFF
200HZ
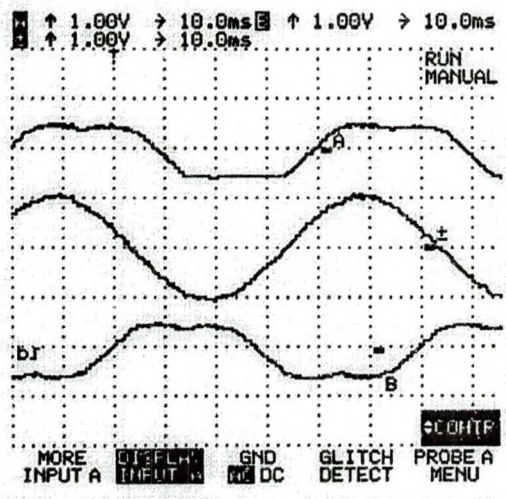
PWMA- Phase a

PWM Phase a-b

PWM - Phase b

LOW PASS FILTER CUT-OFF
200HZ

APPENDIX 0: PHASE AND LINE VOLTAGE PULSES AT MOTOR INPUT.
(SLIDER SET POINT: 0.8 AND VARIAC INPUT 70 V AC)
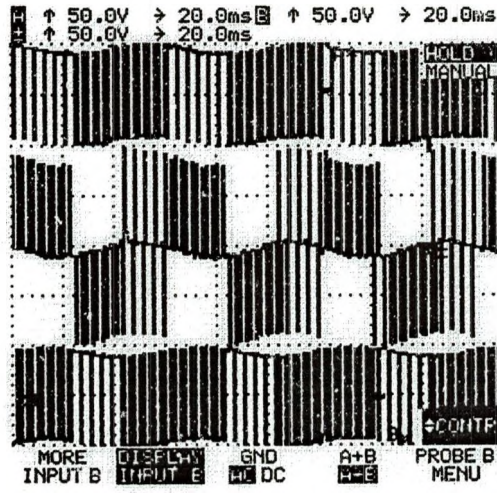
APPENDIX P: THE OVERALL BLOCK DIAGRAM OF CLOSED-LOOP SPEED CONTROL [30]
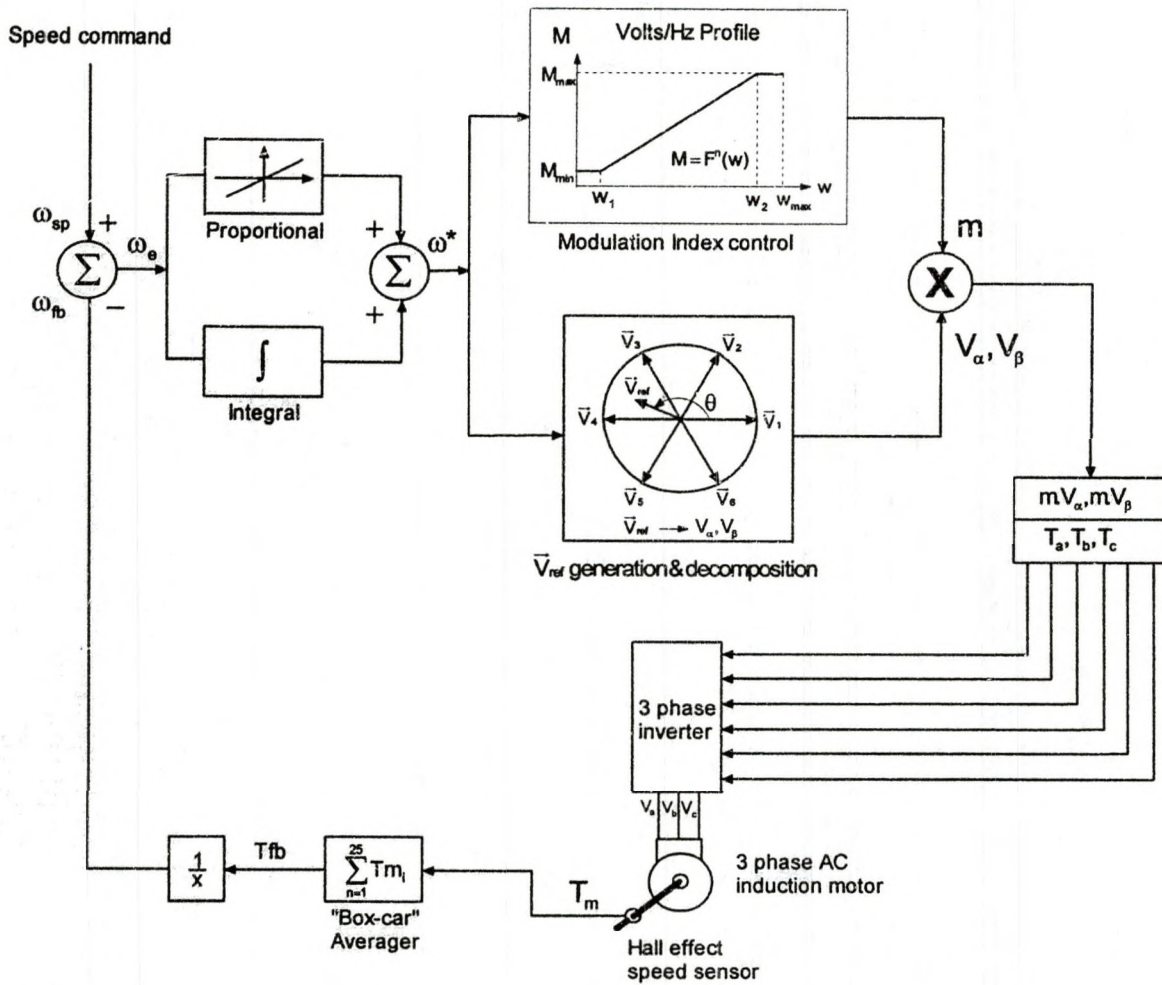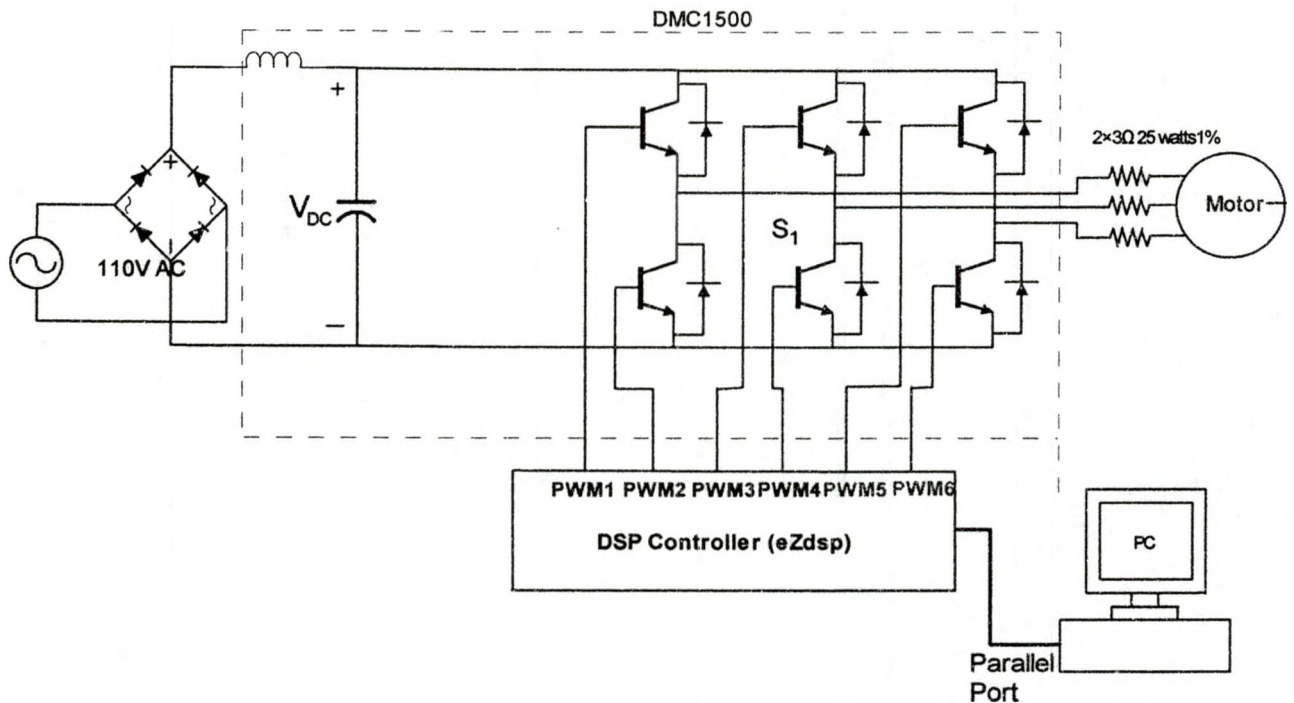
Figure 6.69 shows a schematic of a small section on DMC1500. The DC

bus section accepts the single phase AC voltage input from the variac and

converts it to DC voltage, then filters and smoothes the waveform. On average,

DC bus voltage is approximately $\sqrt{2}$ times the variac input. For a variac input of

70V AC and 138 V AC, the observed DC bus voltages were 99V DC and 195 V

DC. The DC bus voltage is delivered to the final section of the drive, called the

inverter by the chopping action of the switches. This section inverts the DC

voltage to three-phase AC, but in a variable voltage and frequency output [42].

Power transistors act as power switches to turn the DC bus voltage on and off at

specific intervals determined by precalculated duty ratios $(T_1, T_2 ... T_7)$ and space

vectors $(\vec{V}_1, \vec{V}_2, ... V_7)$. In so doing, the inverter actually creates a variable three-

phase AC voltage and frequency output. The drive's output doesn't exactly

replicate the three-phase AC sine waveform, rather it supplies negative and positive voltage pulses that are a constant magnitude in height [42] equal to $\sqrt{2}$ times the variac input. This is what is seen in Figures 6.35 through 6.38. Since the pulse's magnitude depends on the variac input, a higher pulse magnitude is observed for 138 Volts AC input compared to 70 Volts AC input. In Figures 6.35 to 6.38 it seems like the fundamental waveform positive-half is created by a positive series of pulses and the negative-half is created by a negative series of pulses. This alternating of positive and negative pulses creates the fundamental frequency output. These pulse trains carry in them the fundamental frequency component plus high frequency components. That is why a low pass filter allows only the fundamental frequency to pass through. The current waveforms in Figures 6.43 through 6.46 appear to be sinusoidal even without a low pass filter. This indicates that motor inductances act as a natural low pass filter, blocking high frequency components (switching frequency and its multiples), allowing only the low frequency fundamental components to pass through.

REFERENCES

[1]   M. Mohaddes, P. G. McLaren, and A. M. Gole, "Control of Optimal PWM Voltage Source Inverter Using Sigmoid and Piecewise Linear Artificial Neural Networks," in *Proc. 1998 Graduate Student Conf.* [Online]. Available: http://www.ee.umanitoba.ca/~gradcon/ gradcon98/proceed /epdocs/sessb/mohaddes.pdf

[2]   A. Levy, "Understanding DC-AC Inverter Technology," Technology Dynamics Inc., Bergenfield, NJ, May 2000. [Online]. Available: http://www.theallpower.com/tech/understanding_p1.htm

[3]   J. R. Espinoza, G. Joos, J. I. Guzman, L. A. Moran, and R. P. Burgos, "Selective Harmonics Elimination and Current/Voltage Control in Current/Voltage Source Topologies: A Unified Approach," *IEEE Trans. Industrial Electronics*, vol. 48, No. 1, February 2000.

[4]   Z. Salam, "DC to AC Conversion (Inverter)", FKE, UTM Skudai, JB. [Online]. Available: http://encon.fke.utm.my/notes/inverter.pdf

[5]   H. Ogiwara and M. Nakaoka, "Instantaneous Current-Controlled Zero-Current Soft Switching Inverter using B-SITs," *IEE Proc. Electr. Power Appl.*, vol. 148, No. 1, January 2001.

[6]   J. Paramesh and A. V. Jouanne, "Use of Sigma-Delta Modulation to Control EMI from Switch-Mode Power Supplies," *IEEE Trans. Industrial Electronics*, vol. 48, No. 1, February 2001.

[7]   I. Panahi, Z. Yu, and M. Arefeen, "Generate Advanced PWM Signals Using DSP," Texas Instruments, Digital Control Applications Group, 12203 S.W.Freeway, M/S 723, Stafford, TX 7747, May 1998. [Online]. Available:http://www.elecdesign.com/1998/may0198/dsp/0501dsp.shtml

[8]   S. Sirisukprasert, "Optimized Harmonic Stepped-Waveform For Multilevel Inverter," MSc thesis, Virginia Polytechnic Institute and State University, Blacksburg, Virginia, September 15, 1999. [Online]. Available: http://www.ee.iitb.ernet.in/uma/~sableraj/title.pdf

[9]   N. Mohan, T. M. Undeland, and W. P. Robbins, *Power Electronics, Converters, Applications and Design*, New York: John Wiley & Sons, Inc., 1995.

[10]   J. W. Nilsson and S. A. Riedel, *Electric Circuits*, Reading, MA: Addison-Wesley Publishing Company, 1996.

[11]   M. Boost and P. D. Ziogas, "State Of The Art PWM Techniques: A Critical Evaluation," *in Proc.1986 IEEE Power Electronics Specialists Conference*, pp. 425-433.

[12]   W. Dankoff, "Inverters: How To Choose An Inverter For An Independent Power System," Dankoff Solar Products Technical, 2001. [Online]. Available: www.dankoffsolar.com/reference/choosing_inverters.html

[13]   M. K. Darwish, Power Electronics Research, Department of Electronic and Computer Engineering, Brunel University. [Online] Available: www.brunel.ac.uk/~eestmkd/RR.html

[14]   D. W. Hart, *Introduction to Power Electronics*, Upper Saddle River,

NJ: Prentice Hall, Inc.,1997.

[15]   A. M. Trzynadlowski, *Introduction to Modern Power Electronics*,

New York: John Wiley & Sons, Inc.,1995.

[16]   I. Campos, B. Pineda, J. A. De La Cruz, and F. Ruiz, "An Enhanced

Model For UPS Inverters," in *Instrumentation and Development*, vol. 3 No

10, pp. 49-52 1998. [Online]. Available: http://somi.cinstrum.unam.mx:90

/i&d/pdfv3n10/Artic8.pdf

[17]   Analog Devices Inc.,"Implementing Space Vector Modulation with the

ADMC401," application note: AN401-17, January 2000. [Online].

Available: www.analog.com/marketSolutions/motorControl/application

Code/admc401/pdf/svpwm.pdf

[18]   Analog Devices Inc., "Reference Frame Conversions with the ADMC401,"

application note: AN401-11, January 2000. [Online]. Available:

http://www.analog.com/marketSolutions/motorControl/applicationCode/ad

mc401/pdf/refframe.pdf

[19]   J Holtz, "Modulation for Electronic Power Conversion," *in Proc. 1994*

IEEE, vol. 82, No. 8, pp. 1194–1214. [Online]. Available: www.ema.uni

-wuppertal.de/paper/pwmproc.pdf

[20]   Texas Instruments Europe, "Field Oriented Control of 3-Phase AC-Motors

of 3-Phase AC-Motors," literature number: BPRA073, February 1998.

[Online]. Available: http://www-s.ti.com/sc/psheets/bpra073/bpra073.pdf

[21]   M. M. Bech and R. Teodorescu, "Control of AC Machines (FP8-3),"

Aalborg University, Institute of Energy Technology. [Online]. Available:

http://www.iet.auc.dk/~mmb/undervisning/ee8-acmotor/1mm_oh.pdf

[22] S. Buso, "Digital Control of Three-Phase DC/AC-Converters: Space Vector Modulation," University of Padova, September 1999. [Online] Available: http://www.dsce.fee.unicamp.br/~antenor/pdffiles/lez2.pdf

[23] N. Mohan, *Electric Drives-An Integrative Approach*, MNPERE, 2001.

[24] R, Valentine, *Motor Control Electronics Handbook*, New York: McGraw-Hill, 1998.

[25] A. M. Gole, "Sinusoidal Pulse Width Modulation," 2001. [Online]. Available: http://www.ee.umanitoba.ca/programs/undergrad/c24437/ power%20electronics%202001/pwm.pdf

[26] J, Vithayathil, *Power Electronics Principles and Applications*, New York: McGraw Hill, 1995

[27] Z. Yu, "Space-Vector PWM WithTMS320C24x/F24x Using Hardware and Software Determined Switching Patterns," Texas Instrument Application Report SPRA52, March 1999. [Online]. Available: http://www-s.ti.com/sc /psheets/spra524/spra524.pdf

[28] M. Copeland, "Space Vector Modulation and Overmodulation with an 8-bit Microcontroller," Infineon Technology, AP0836,1999. [Online] Available: http://www.infineon.com/cmc_upload/migrated_files/document _files/Application_Notes/ap083601.pdf

[29] V. H. Prasad, "Analysis and Comparison of Space Vector Modulation for Three-Leg and Four-Leg Voltage Source Inverter Schemes" MS

Thesis, Virginia Polytechnic Institute and State University. May 15, 1997. [Online]. Available: http://scholar.lib.vt.edu/theses/available/etd-2798-12 16/unrestricted/title pdf

[30]   M. S. Arefeen, D Figoli, and Z. Yu, "Multiple Motor Control Using a Single DSP," Texas Instrument Inc., 2000. [Online]. Available: http://www. powerpulse.net/powerpulse/archive/pdf/aa_011700c.pdf

[31]   J. W. Kelly, E. G. Strangas and J. M. Miller, "Multi-phase Inverter Analysis," in *Electrical Machines and Drives Conference, 2000. IEMDC 2001. IEEE International 2001,* pp. 147 – 155.

[32]   Texas Instrument, "Sensorless Variable Speed 3-Phase AC Induction Motor with Closed Loop Speed Control," application Report: SPRU443, July 2001. [Online]. Available: http://dspvillage.ti.com/pdfs/spru443.pdf

[33]   Visual Solutions Inc., VisSim/TI C2000 Rapid Prototyper User's Guide, Version 4.5, 3rd ed., 2000.

[34]   Visual Solutions Inc., VisSim/T User's Guide, Version 4.5, 3rd ed., 2000.

[35]   L. Lecoz, "Evolution of Industrial Motor Control, Mitsubishi Electric," Europe B.V., Travellers Lane, Hatfield, Hertfordshire, AL10 8XB, UK, 2001. [Online]. Available: www.mdece.com/M16C62/app_notes/Motor_ Control_Tutorial.pdf

[36]   Adept Scientific. [Online]. Available: www.adeptscience.co.uk/products /mathsim/vissim/c2000.html

[37]   O. Ustun, M. Yilmaz, and R. N. Tuncay, "Simulation of Power Electronic Circuits Using VisSim Software: A Study On Toolbox Development,

"Istanbul Technical University, Electrical and Electronic Engineering Faculty, Electrical Engineering Department, Masiak, Istanbul 80626, Turkey, 2000. [Online] Available: http://www.vissim.com/apps/SimofP owElCircuitsUsingVisSim.pdf

[38] Spectrum Digital Incorporated, eZdsp LF2407 Technical Reference, DSP Development Systems, 2000. [Online] Available: http://www.spectrum digital.com/technical/pdfs/eZdsp2407.pdf

[39] Spectrum Digital Incorporated, DMC1500 Technical Reference, DSP Development Systems, 2000. [Online] Available: http://www.spectrum digital.com/technical/pdfs/dmc1500.pdf

[40] T. Wiangtong, W. Sangchai, and P. Lumyong, "FPGA-Based IC Design for 3-Phase PWM Inverter with Optimized Space Vector Modulation Schemes," Mahanakorn University of Technology Bangkok Thailand, 2000. [Online] Available: http://www.ee.mut.ac.th/research/ 2000/C_ISCAS_01E.pdf

[41] Z. Mihailovic, "Modeling and Control Design of VSI-fed Pmsm Drive Systems with Active Load," MS Thesis, Virginia Polytechnic Institute and State University, Blacksburg, Virginia, June 26, 1998. [Online] Available: http://scholar.lib.vt.edu/theses/available/etd-031899-212402/

[42] D. Polka, "Motions Fundamental Control," Motion Control ABB Inc., Automation Drives & Power Products Group, 16250 West Glendale New Berlin, WI 53151, September, 1999. [Online] Available: http://www.isa. org/isaolp/journals/pdf/motion/990937.pdf

[43]   S. J. Fedigan and C. P. Cole, "A Variable-Speed Sensorless Drive System
       for Switched Reluctance Motors," application report SPRA600, Texas
       Instrument, DSPS Research and Development Center, October, 1999.
       [Online] Available: http://www-s.ti.com/sc/psheets/spra600/spra600.pdf

[44]   UNICO, INC., AC Equals DC, 2000. [Online] Available: http://www.
       unicous.com/html/acdc.html.

[45]   J. W. Kolar, "Space Vector Based Current Control of a Six-Switch
       PWM Rectifier," Interactive Power Electronics Seminar (iPES), 2002.
       [Online] Available: http://www.ipes.ethz.ch/ipes/Raumzeiger/e_RZ4.html,

[46]   P. M. Darmstadt, "A new speed-control method for induction
       motors," University of Technology, Department of Power Electronics and
       Drives Landgraf-Georg-Str. 4, D-64283 Darmstadt. [Online] Available:
       www.srt.tu-darmstadt.de/pub/general/publicat/speed.pdf

[47]   J. Yao, "Programmable DSP Applications in Motor Control," Wisconsin
       Electric Machines and Power Electronics Consortium (WEMPEC), 2000,
       October 27). [Online] Available: www.lsi.usp.br/~gucerezo/DSP%20wit
       h%20FPGAs/1

[48]   ST Microelectronics, A Reference Guide For Motor Control. [Online]
       Available: http://us.st.com/stonline/products/promlit/pdf/brmotor-1000.pdf

[49]   S. Hadi, "Three-phase Systems," [Online] Available: http://people.msoe
       edu/~saadat/3-phaseCkt.pdf

[50]   A. A. Henri Jr., "Three-phase Induction Motors," [Online] Available:
       www.uno.edu/~halciato/3521/induction_motor_reference/page1.htm

[51] Analog Devices, "Constant Volts/Hertz Operation for Variable Speed Control of Induction Motors V/F Controller on the ADMC401," AN401-24, January 2000. [Online]. Available: www.analog.com/marketSolutions/ motorControl/applicationCode/admc401/pdf/VbyF401.pdf

[52] Analog Devices, "Control of Induction Motors," E-learning Resources in Microelectronics. [Online] Available: www.bolton.ac.uk/technology/mind /paderborn/motors/induction/induiction-motor.html#general

[53] Reid Technology, "The Sine Wave Advantage," [Online] Available: www.reidtechnology.co.nz/sinewave.html

[54] E. Gurdjian and C. Maxwell, "Inverter Technology," [Online] Available: www.rvtechstop.com/articles/Invtech2-s.pdf

[55] E. Josephson, "What's an inverter," December 1992/January 1993. [Online] Available: www.humboldt1.com/~michael.welch/hp32-22.pdf

[56] Solid State Controls, Inc., "A Comparison of Ferroresonant and PWM Inverter Technologies," [Online] Available: www.solidstatecontrolsinc .com/techhpapers/papers/compferro.html

[57] B. Buyukbozkirli and H. Chrifi-Alaoui, "An Alternative Pulse-Width Modulation Scheme for Automotive Inverters," May 2001. [Online] Available: www.mth.msu.edu/Graduate/msim/MSIMProjectReports /MCP3.May.2001.report.pdf

[58] S. J. Chapman, "Electric Machinery Fundamentals," 3rd ed., fundamentals. [Online] Available: www.mhhe.com/engcs/electrical/chapman/ /PWM.pdf

[59] Voltech™, "Making Measurements on PWM Drive," Voltech Power

Analysis, Reference Sheet 009. [Online]. Available: www.voltech.com/ Downloads/86165_01.pdf.

[60] Hsin-Chu, "ASI Tested on Pulse Width Modulation (PWM) of ANPEC," Advantech Semiconductor Inc.,October 2000. [Online] Available: http://www.asit.com.tw/en_news/upload/891005_01.doc

[61] ITT Industries, "Basic principle," [Online] Available: http://www.flygtus com/119023.asp

[62] S. Pekarek and T. Skvarenina, "PWM Inverter," November 1998. [Online]. Available: http://www.ece.msstate.edu/~hagler/Nov1998/08/BEGIN.HTM# INDEX

[63] R. E. Locher, "Introduction to Power Supply," National Semiconductor, Application Note 556, November 1988. [Online]. Available: http://www. national.com/an/AN/AN-556.pdf

[64] Advanced Controls and Drives, "Harmonic Generation in Solid State AC Motor Controls," Benshaw Technical Notes, TN0020-01. [Online]. Available: www.benshaw.com/service/Technical_Notes/TN0020.pdf

[65] General Cable, "Variable Speed Drive Cables," [Online]. Available: www.generalcable.co.nz/Products/Energy/varible.HTM

[66] N. Yadlapalli, "Implementation of a Novel Soft-switching Inverter for Switched Reluctance Motor Drives," MSc. Thesis, Virginia Polytechnic Institute and State University, Virginia, Blacksburg, July 14, 1999. [Online]. Available: http://scholar.lib.vt.edu/theses/available/etd-071499-192601/unrestricted/navetd1.pdf

[67] S. Barna, "Solid State Switches," 2001. [Online]. Available: http://power
      .eng.mcmaster.ca/szabados/courses/4pk4/notes/switches.pdf

[68] Rockwell Automation Reliance Electric, "Drive Carrier Frequency,"
      [Online]. Available: www.reliance.com/pdf_elements/d7720.pdf

[69] G. Ledwich, "Pulse Width Modulation (PWM) Basic," Power Designers,
      1998 [Online]. Available: www.powerdesigners.com/InfoWeb/ design_
      center/articles/PWM/pwm.shtm#anchor

[70] B.J Farahani and A. Keyhani, "Space Vector PWM Modulation
      Technique," The Ohio State University Electrical Engineering Department,
      Columbus Ohio 43210, 2001. [Online]. Available:eewww.eng.ohio-state
      .edu/ ems/Abstracts/BaharAbs2.html

[71] M. Stäble, "Using A DSP For Digital Motor Control Brings Benefits To
      Designers," [Online]. Available: www.neon.co.uk/campus/articles/texas
      /ti%20autumn%2000.htm

[72] M. Krempfel, "Sinusoidal Filters for Frequency Converters: Optimum
      Compatibility For Man And Machine," Dipl.-Ing. Siemens Matsushita,
      Munich. [Online]. Available: www.compliance-club.com/archive1/
      951215.htm

[73] Spectrum Digital Inc., Product FAQ, April 26, 2001. [Online]. Available:
      www.spectrumdigital.com/technical/pdfs/faq.pdf

[74] Texas Instruments, "Digital Signal Processing Solution for AC Induction
      Motor," Application Note BPRA043. [Online]. Available: www-s.ti.com/
      sc/ psheets/bpra043/bpra043.pdf

[75]   Z. Yu and D. Figoli, "AC Induction Motor Control Using Constant V/Hz Principle/Space Vector PWM with TMS320C240," Application Report SPRA284a, Digital Signal Processing Solutions, April 1998. [Online] Available: focus.ti.com/docs/apps/catalog/resources/appnoteabstract jhtml?abstractName=spra284a

[76]   Texas Instruments, TMS320C2xx/C24x Code Composer User's Guide, SPRU490, October 2000. [Online]. Available: www-s.ti.com/sc/psheets/ spru490/spru490.pdf

[77]   F. Wang, "Sine-Triangle vs. Space Vector Modulation for Three-Level PWM Voltage Source Inverters," in *2000 IEEE Industry Applications Conf.*, vol.4, pp. 2482 -2488.

[78]   R. W. Erickson and O. A. Al-Naseem, "A New Family of Matrix Converters," Colorado Power Electronics Center, University of Colorado, Boulder, CO 80309-0425, USA. [Online]. Available: ece-www.colorado .edu/~rwe/papers/IECON01.pdf

[79]   Energy Efficiency and Renewable Energy Clearinghouse (EREC), "Inverters," P.O. Box 3048, Merrifield, VA 22116. [Online]. Available: www.eren.doe.gov/consumerinfo/refbriefs/bb8.html

[80]   University of Glamorgan, School of Electronics, DSP glossary. [Online]. Available: http://www.eit.glam.ac.uk/cepe/glossary.htm

[81]   Xantrex Technology, "Modified Sine wave and Sine wave Waveforms," April 9, 1999. [Online]. Available: www.traceengineering.com/technical/ tech_notes/tn6.html

[82] C. Hargis, Control Techniques Ltd. "EMC of Variable Speed Drives," [Online]. Available: www.complianceclub.com/EMC%20of%%20Speed %20Drives.htm

[83] Bangor Hydro, Common Power Quality Terms, [Online]. Available: www.bhe.com/residential/quality_terms.cfm

[84] K. Oguchi, A. Kawaguchi, T. Kubota and Nobukazu, "A Novel Six-Phase Inverter System with 60-Step Output Voltages for High-Power Motor Drives," *IEEE Trans on Industry Applications*, vol. 35, No. 5, September/ October 1999.

[85] Electronics Tutorial, "Harmonic Trap Filter," [Online]. Available: www.electro nics-tutorials.com/filters/trap-filter.htm

[86] Motion Village, "What is Pulse Modulation?," [Online]. Available: www.motionvillage.com/

[87] Mathworld, "Square Wave," [Online]. Available: wolfram.com/ SquareWave.html

[88] Visual Solution Incorporated. [Online]. Available: http://www.vissim.com/

[89] Drives World, A Crash Course on Drives Power Topologies. [Online]. Available: www.execpc.com/~hgmurphy/DRVTYPES.HTM

[90] DrivesMag. [Online]. Available: www.drivesmag.com/index_home.html.

[91] Prices Effective, "What's The Harm in Harmonics," October 1, 2001 [Online]. Available: www.powerware.ca/images/CanadianSP_6.pdf

[92] Benshaw Advanced Controls and Drives, "Introduction To Drives Motor Background Volts/Hz Relationship," [Online]. Available: www.benshaw.

com/service/VFD/Chapter1.pdf

[93]   H. W. Van Der Broeck, H. C. Skudenly, and G. V. Stanke, "Analysis and
          Realization of a Pulsewidth Modulator Based on Voltage Space Vectors,"
          IEEE Trans Industry Applications, vol. 24, No. 1, January /February 1988.

[94]   R. Teodorescu, F. Blaabjerg, J. K. Pedersen, P Enjeti, and E. Cengelci,
          "Space Vector Modulation Applied to Modular Multilevel Converters,"
          [Online]. Available: www.iet.auc.dk/~ret/multilevel/Pcim99.PDF

[95]   T. Kato, "Precise PWM Elimination Analysis of Inverter for Selected
          Harmonic Elimination," Department of Electrical Engineering, Doshisha
          University, Kyoto, 602, Japan.

[96]   J. Hyeong, C. H. Choi, and D. S. Hyun, "A New Simplified Space-Vector
          PWM Method for Three-Level Inverters," *IEEE Trans. Power Electronics*,
          vol. 16, No. 4, July 2001.

[97]   Pennsylvania State University, "DC-AC converters: Inverter circuits,"
          [Online]. Available: hegel.ee.psu.edu/ee497d/alllectures/node32.html

[98]   H. A. Toliyat and H. Xu, "A Novel Direct Torque Control (DTC)
          Method for Five-Phase Induction Machines," in *IEEE Applied Power
          Electronics Conference and Exposition 2000, Fifteenth Annual*, vol 1, pp.
          162 -168 vol.1. [Online]. Available: http://ee.tamu.edu/~empelab/papers
          /apec'00-xu.pdf

[99]   J. Mahdavil, A. M. Ranjbarl, and H. A. Toliyat, "Extension of PWM
          Space Vector Technique for Multilevel Current-Controlled Voltage
          Source Inverters," 1999. [Online]. Available: http://ee.tamu.edu/~

empelab/papers/iecon'99-mahdavi.pdf

[100] G. Oriti, A. L. Julian, and T. A. Lipo, "A New Space Vector Modulation Strategy for Common Mode Voltage Reduction, 1997. [Online]. Available: www.wempec.org/users/lipo/1997pub/giovana_pesc97.pdf

[101] A. M. Hava, R. J. Kerkman, and T. A. Lipo, " Simple Analytical and Graphical Tools for Carrier Based PWM Methods," in *Power Electronics Specialists Conference, 1997. PESC '97 Record., 28th Annual IEEE,* vol 2, pp. 1462-1471. [Online]. Available: www.powerdesigners.com/Info Web/ design_center/articles/ hava_pesc97.pdf

[102] A. M. Hava, S. K. Sul, R. J. Kerkman, and T. A. Lipo, "Dynamic Overmodulation Characteristics of Triangle Intersection PWM Methods" in *Industry Applications Conference, 1997. Thirty-Second IAS Annual Meeting, Conference Record of the 1997 IEEE,* vol 2, pp. 1520-1528. [Online]. Available: www.powerdesigners.com/InfoWeb/design_ center/articles/ hava_ias97.pdf

[103] H. Xu, H. A. Toliyat, "Implementing Rotor Field Orientated Control and Direct Torque Control of Five-Phase Induction Motor Using TMS320C32 DSP," 2000. [Online]. Available: www.ti.com/sc/docs/ general /dsp/festproceedings/fest2000/tamu003.pdf

[104] H. A. Toliyat, "Analysis and Simulation of Five-Phase Variable-Speed Induction Motor Drives Under Asymmetrical Connections," *IEEE Trans. Power Electronics,* vol. 13, No. 4, 1998. [Online]. Available: http://ee.tamu.edu/~empelab/power_tran98.pdf